THE ANTIMICROBIAL RESISTOME OF PEROMYSCUS AND THEIR ENVIRONMENT: IMPLICATIONS FOR PUBLIC HEALTH

by

JESSE C. THOMAS IV

(Under the Direction of Travis C. Glenn)

ABSTRACT

Contamination of the environment by heavy metals is a widespread and rapidly increasing global issue. Common sources of heavy metal pollution include coal-fired power plants, mining and industrial wastes, vehicle emissions, and agriculture. Elevated metal levels have been observed in urban topsoils, runoff, rivers, and coastal zones, despite national regulatory standards limiting the maximum contaminant levels. Furthermore, because metals and metal-containing compounds can persist in the environment and bioaccumulate in living tissues, they can provide a long-term selective pressure on bacteria. In addition, current evidence suggests that heavy metals can indirectly co-select antibiotic resistance in bacteria, an issue that presents serious public health concerns. Resistance determinants are frequently located on mobile genetic elements (e.g. integrons, transposons, and plasmids), which can rapidly be disseminated among phylogenetically diverse microorganisms via horizontal gene transfer. Therefore, the biological processes that drive the co-selection of antibiotic resistance following

exposure to heavy metals may also facilitate the spread of multi-resistant human pathogens. In this context, the microbiome of wild animals, particularly those from areas near sources of contamination, provide interesting models for examining the prevalence of antimicrobial resistance.

In this dissertation, I investigate the influence of heavy metals on the microbiome of wild *Peromyscus* and their environment. In the first study, I explore how heavy metals in the environment influence the structure, diversity, and co-abundance of soil microbial communities (archaea, bacteria, fungi) using a combination of Illumina based 16S rRNA gene and ITS amplicon sequencing and network-based analysis. I also examine the co-occurrence of heavy metal and antibiotic resistance, and investigate the potential co-selection of antimicrobial resistance using predictive functional profiling. In the second study, I explore how exposures to heavy metals may modulate the co-occurrence of heavy metal and antibiotic resistance, co-selection of antimicrobial resistance, and host dysbiosis in the gut microbiota of wild *Peromyscus* using a combination of Illumina based 16S rRNA gene sequencing, predictive functional profiling, and network-based analysis. In the third study, I examine how exposures to heavy metals and a ciprofloxacin treatment differentially affect the abundance and diversity of the gut microbiota of captive *Peromyscus leucopus* using Illumina-based 16S rRNA gene sequencing. I also examine the co-selection of antibiotic resistance in gut microbiota following heavy metal exposures using predictive functional profiling and network-based analysis.

INDEX WORDS: antibiotics, fungi, heavy metals, microbiome, *Peromyscus*, resistome, soil, 16S rDNA sequencing

THE ANTIMICROBIAL AND HEAVY METAL RESISTOME OF WILD PEROMYSCUS AND THEIR ENVIRONMENT: IMPLICATIONS FOR PUBLIC HEALTH

by

JESSE C. THOMAS IV

BS, Florida Agricultural & Mechanical University, 2009

MS, Florida Agricultural & Mechanical University, 2012

A Dissertation Submitted to the Graduate Faculty of The University of Georgia in Partial Fulfillment of the Requirements for the Degree

DOCTOR OF PHILOSOPHY

ATHENS, GEORGIA

2017

THE ANTIMICROBIAL RESISTOME OF WILD PEROMYSCUS AND THEIR ENVIRONMENT: IMPLICATIONS FOR PUBLIC HEALTH

by

JESSE C. THOMAS IV

Major Professor:	Travis C. Glenn
Committee:	Olin Rhodes
	J Vaun McArthur
	Erin K. Lipp

Electronic Version Approved:

Suzanne Barbour
Dean of the Graduate School
The University of Georgia
August 2017

DEDICATION

This is dedicated to my sons. When you came into my life you guys inspired me to go farther and work harder than I ever thought was possible…to my parents and my sister who always motivated me to keep climbing, and showed unwavering support through my long journey…to my Grandma T who always gave me books to read (she had the entire Encyclopedia Britannica)…to Grandpa…his nickname for me was Professor...as if he already knew where I'd be…to all my grandparents, and family who sacrificed so I could be at this moment in time…this is for you.

ACKNOWLEDGEMENTS

First, all thanks to God. I followed the path you led before me. I experienced many trials and tribulations along the way, and during my lowest moments, when I thought I might give up it was through my own faith that I was able to come through the proverbial storm. I want to thank Gene for giving me the once in a life time opportunity to work with him, and support me over the past four years. It still amazes me at how it all happened, and it seems like it was yesterday we were on the phone talking about the projects you wanted me to help you with. I want to thank Travis for always being there to talk about school and personal matters, for always being honest. Not only are you an excellent advisor but you are also a fantastic mentor and a friend. I learned many things from your wisdom. Travis also gave me enough room to grow and learn on my own, while providing a careful guide. I want to thank J Vaun for all the talks we had, his palpable enthusiasm, for challenging my abilities to look at experimental design, and for always believing in my abilities. I want to thank Erin for challenging my ability to integrate microbial ecology with environmental health, and for giving me a chance to excel in the newly developed EHS doctoral program. I thank the rest of the EHS faculty (Luke, Marsha, Mary Alice, Anne Marie, Dr. Yu, Dr. Wang) for molding me into a researcher that thinks about complex environmental and public health issues. I want to thank Haoguang and Betsy for making my time in EHS warm and pleasant, and for always being there to answer my one million questions. Of course, I also want to extend a special thanks to my lab mates who made every day interesting. Troy thanks for listening

to all of my crazy ideas…Natalia thanks for reading over my stuff and giving me the thumbs up (or down) on all of my R plots, and for listening to my very bad Spanish. Thanks to Pat and Swarnali for always being friendly and helpful, and giving me great feedback. I also want to thank my many colleagues in the Department of Environmental Health Science (especially John Finger, Bei Gao, Jincheng Wang, David Brew, Keri Lydon, Keri Kemp, Jason Westrich, and Ade), the Georgia Genomics Facility (especially Jeff Wagner and Roger Nilsen), Dr. Claire de La Serre and her lab, the Peromyscus Genetic Stock Center (Vimala Kaza, Janet Crossland and Hippokratis Kiaris), and the Savannah River Ecology Laboratory (especially Dr. John Seaman, Dr. Jim Beasley, Matt Hamilton, Erin Abernathy, and Angela Lindell) for assistance with sampling and data collection. I want to thank all my friends from back home (especially Brandon, Devin, Corey), and those I met at UGA in GAPS (Wes, Jordan, Kevin, Ian, Zerotti, Justin, Tasha, Malcolm and others). Lastly, I want to thank my counselor Dr. Kipp Matthews for helping me navigate through all of my daily struggles, as a father and a doctoral student, talking with me and providing me with the necessary tools and strategies to overcome life's many challenges. And for those that supported me over the years that I may have missed thank you! Funding to support this work was provided by the Area Completions Project of Savannah River Nuclear Solutions, the Department of Energy under Award Number DE-FC09-07SR22506 to the University of Georgia Research Foundation.

TABLE OF CONTENTS

Page

LIST OF TABLES

Page

LIST OF FIGURES

Page

LIST OF FREQUENTLY USED ACRONYMS

1. AB – Ash Basins
2. AMR – Antimicrobial resistance
3. ARGs – Antibiotic resistance genes
4. CAP – Canonical analysis of principal coordinates
5. DbRDA – Distance based redundancy analysis
6. DISTLM – Distance linear modeling
7. GI - Gastrointestinal
8. GIs – Genomic islands
9. HGT – Horizontal gene transfer
10. HMR – Heavy metals and radionuclides
11. HMs – Heavy metals
12. KO – KEGG Orthologs
13. MGE – Mobile genetic element
14. MIC – Minimum inhibitory concentration
15. MRGs – Metal resistance genes
16. NGS – Next generation sequencing
17. NMDS – Non-metric multidimensional scaling plot
18. OTUs – Operational Taxonomic Unit
19. PAIs – Pathogenicity islands

20. PB – Pond B

21. PCR - Polymerase chain reaction

22. REIs – Resistance islands

23. SMS – Shotgun metagenomic sequencing

24. TB – Tim's Branch

25. UR – Upper Three Runs

CHAPTER 1

INTRODUCTION AND LITERATURE REVIEW

Natural and anthropogenic sources of heavy metals

Broadly defined, heavy metals are inorganic chemical hazards that consist mainly of high atomic weigh metals, including metalloids such as arsenic, that have the capacity to induce toxicity at low levels of exposure (Wuana et al., 2011). They are naturally occurring elements found in the Earth's crust and thus cycle throughout the environment in varying concentrations. The weathering of parent material and other pedogenetic processes contribute to the natural geochemical cycle of metals in soils (Alloway, 2012). Volcanic eruptions can also emit heavy metals into the surrounding air, which are preferentially associated with airborne particulate matter. Once in the atmosphere, heavy metal-laden aerosols are transported by the wind, and ultimately deposited into the environment where they remain at low background levels (Abdu, 2010). However, human activities have greatly accelerated nature's slowly occurring geochemical cycles, and unlocked previously sequestered sources of heavy metals from stable matrices, releasing them in concentrations that increase elemental background levels (Shivakumar et al., 2012). Anthropogenic activities such as a coal burning, petroleum combustion, mining and smelting operations, industrial processes, and agricultural use of metal-containing products have greatly increased potential human exposure. Heavy metals are ubiquitous and persistent environment pollutants; they have been identified in domestic, agricultural, pharmaceutical, and industrial effluents, rural and urban soils, and as

components of airborne particulate matter (Wuana et al., 2011). Consequently, several studies over the last few decades have emphasized the increasing ecological and global public health concerns associated with contamination of the environment by heavy metals.

Heavy metals and their role in biological systems

Several heavy metals are trace elements, or micronutrients that provide small, but critical, quantities for various biochemical and physiological functions in living organisms. The heavy metals that are considered essential micronutrients for maintaining optimal health in a variety of organisms include: chromium (Cr), cobalt (Co), iron (Fe), magnesium (Mg), manganese (Mn), molybdenum (Mo), nickel (Ni), selenium (Se), vanadium (V), and zinc (Zn) (Alloway, 2013). Many essential heavy elements have major structural and functional roles as constituents and/or activators for several key enzymes. For instance, copper has very diverse biological roles and is essential for maintaining the integrity of skin, blood vessels, as well as epithelial and connective tissues in the body (Osredkar and Sustar, 2011). Cuproenzymes (copper containing proteins) are essential in catalyzing several reactions in the immune and nervous systems; while multi-copper oxidases are important in iron metabolism (Chan and Rennert, 1980; Prohaska and Lukasewycz, 1990; Kaplan et al., 1996; Collins et al., 2010; Alloway, 2013). Copper is also involved in redox systems, scavenging of free radicals, and is an important constituent in more than 12 metalloenzymes in plants and animals, including: catalase, super oxidase dismutase (SOD), cytochrome c oxidase, ascorbate oxidase,

polyphenol oxidase, ferroxidases, monoamine oxidase, dopamine β-monooxygenase and electro-transfer proteins in plants (Alloway, 2013; Hansch and Mendel, 2009).

As stated above, several heavy metals have important biological roles as trace nutrients. Chromium (Cr^{3+}) is another essential nutrient that is necessary for normal carbohydrate, lipid, and protein metabolism (Pechova and Pavlata, 2007). Chromium is an important constituent of the glucose tolerance factor (GTF), a dinicotinic acid-glutathiome complex that acts as a biological modifier of insulin action (Sumrall and Vincent, 1997; Pechova and Pavlata, 2007). Iron, one of the most abundant elements on Earth, is essential for various oxidation-reduction reactions, DNA and protein synthesis; and cell growth and differentiation (Jomova et al., 2011; Abbaspour et al., 2014). Zinc is also essential for a myriad of regulatory, structural, and enzymatic proteins and is required for normal reproductive, neurological, and immune system functioning (Frederickson et al., 2000; Hänsch and Mendel, 2009; Alloway, 2013).

Diets with inadequate supplies of these micronutrients can result in a myriad of trace metal deficiencies, syndromes, and diseases (Brown et al., 2001; Fraga, 2005). Conversely, excessive concentrations of metals, even at low doses, have been demonstrated to be highly toxic (Lars Järup, 2003; Duruibe et al., 2007; Zheng et al., 2010). Excess heavy metal ions can cause deleterious effects in organisms by disrupting metabolic functions, inhibiting growth (and yield), causing physiological stress, and even death (Jaishanskar et al., 2014). Heavy metals have been shown to bioaccumulate in vital organs and fatty tissues of livestock and fish; as well as food crops (Vinodhini and Narayanan, 2008; Vinodhini and Narayanan, 2008; Zhuang et al., 2009). They can also replace or mimic essential minerals in living organisms (Bridges and Zalups, 2005).

Eukaryotes possess and share a variety of homeostatic mechanisms that are crucial in regulating the bioavailable concentrations of heavy metals. Glutathiones, metallothioniens and plant-derived phytochelatins, a class of cysteine-rich, heavy metal-binding protein molecules, allow them to bind to, sequester, and preferentially discriminate non-essential heavy metals from essential ones (Vatamaniuk et al., 2001; Cobbett and Goldsbrough, 2002; Perales-Vela, 2006). However, when these mechanisms are compromised due to poor diet or excessive heavy metal intake, certain organisms may be unable maintain the optimal range of metal ions (Alloway, 2013).

Heavy metals and bacteria

Similar to larger organisms, certain metals (e.g., Co, Cu, Zn, Ni) are essential to microorganisms because they provide important co-factors for mellatoproteins and enzymes (Nies, 1999; Alloway, 2013). Microorganisms such as bacteria can acquire essential metals from the environment by excreting siderophores or using siderophores produced by other bacteria. These chelating agents scavenge metal ions in nutrient poor environments, and form soluble metal complexes that can be readily transported into the cell (Neilands, 1995; Ahmed and Holmström, 2014; Behnsen and Raffatellu, 2016).

The introduction of heavy metals in relatively high concentrations can elicit considerable modifications to microbial communities and their activities. Heavy metals can exert an inhibitory action on microorganism by blocking essential functional groups, displacing essential metal ions, or modifying the active conformations of various enzymes (Jansen et al., 1994). However, microbial communities and even strains of bacteria within the same species can display considerable differences in their sensitivity

to metal toxicity (JanK0wska et al., 2006; de Lima e Silva et al., 2012; EL-Sherbiny and M.E., 2014). These discrepancies may be the result of differences in community structure, innate tolerance to metals by certain species or whole communities, or acquisition of resistance via lateral gene transfer. Nonetheless, heavy metal minimum inhibitory concentrations (MICs) for model bacterial strains such as *Pseudomonas*, *Salmonella* and *Ralstonia mellidurans,* among others, have been established (Hassen et al., 1998; Nies, 1999; Mergeay et al., 2003; Nishino et al., 2007; Khan et al., 2016).

Heavy metal resistance in bacteria

In general, there are six primary mechanism of heavy metal resistance, which include: 1) bacteria extracellular barrier, 2) active transport of metal ions (efflux), 3) extracellular sequestration, 4) intracellular sequestration, 5) reduction of metal ions and 6) enzymatic detoxification (Bruins et al., 2000; Tanaka et al., 2004; Baker-Austin et al., 2006). Several heavy metal resistance determinants (chromosomal or plasmid-borne genes) located on mobile genetic elements (MGEs) (e.g. transposons, integrons, and gene cassettes) have been identified in bacteria. Such resistance determinants include *mer* (mercury resistance), *czc* (cobalt, zinc and cadmium resistance), *cnr* (cobalt and nickel resistance), and *chr* (chromate resistance) (Dressler et al., 1991). In fact, there are reports of resistance genes to many toxic ions of heavy metals, including Ag^{+}, AsO_2^{-}, AsO_4^{3-}, Cd^{2+}, Co^{2+}, CrO_4^{2-}, Cu^{2+}, Hg^{2+}, Ni^{2+}, Sb^{3+}, TeO_3^{2-}, Tl^{+}, and Zn^{2+} (Amiard-Triquet and Rainbow, 2011).

While resistance systems have been found mostly on plasmids, more recent studies of bacterial genomes using next generation sequencing (NGS) have revealed

homologues to metal resistance determinants that exist chromosomally (Lim and Cooksey, 1993; Silver and Phung, 1996; Parsley et al., 2010; Monsieurs et al., 2011; Peña-Montenegro and Dussán, 2013). These metal-resistance genes confer resistances to many of the same heavy metal cations and oxyanions as do plasmids. Several examples exist of bacterial chromosomes containing resistance systems for metals. For example, in *Cupriavidus metallidurans* the *copABCD* determinant on chromosome 2, which encodes periplasmic proteins involved in copper resistance, was found to be required for full resistance to gold particles (Wiesemann et al., 2013). Another study on methicillin-resistant *Staphylococcus aureus* (MRSA) determined that structures of staphylococcal cassette chromosome mec (*SCCmec*) contained genes conferring resistance to metals such cadmium (*cadDX*) and arsenic (*arsRBC* and *arsDARBC*), copper (*copB*), and zinc (*crzC*) (Li et al., 2011).

Of the various heavy metal resistance systems in bacteria, the energy–dependent efflux of toxic metal ions is perhaps the most well-studied. Many of these efflux systems are composed of ATPases, whereas others are chemiosmotic cation/proton antiporters (Silver, 1996; Lee et al., 2007; Takahashi et al., 2012; Chacón et al., 2014). For example, the *Ars* (arsenic) resistance operon contains three genes (*arsA*, *arsB*, and *arsC*) which compose the arsenic resistance efflux system (Branco et al., 2008). Bacteria can use alternatively the two-component ATPases, *ArsA* and *ArsB*, or a single polypetide (*ArsB*) functioning as a chemiosmotic transporter for arsenite and antimonite (Silver, 1996; Li and Rosen, 2000; Castillo and Saier Jr., 2010). The third gene, *arsC*, encodes the arsenate reductase (*ArsA*) that reduces intracellular arsenate [As (V)] to arsenite [As (III)], the preferred substrate of the efflux system (Castillo and Saier Jr., 2010). Efflux pump

systems are enormously important, as they allow bacteria to transport metal ions from the cytoplasm across the periplasmic space to the outside of the cell.

Heavy metals can co-select antibiotic resistance in bacteria

Recent studies have demonstrated that widespread heavy metal contamination in the environment may facilitate the proliferation of antibiotic resistance via coselection of antibiotic resistance genes (ARGs) and metal resistance genes (MRGs). Coselection mechanisms refer to the indirect but shared regulatory responses to metal and antibiotic exposure (Baker-Austin et al., 2006). Among the co-selection mechanisms that appear in resistance systems are cross-resistance, whereby different resistance determinants confer resistance to both antibiotics and metals simultaneously via a common pathway; and co-resistance whereby resistance determinants are physically linked on the same genetic element (Baker-Austin et al., 2006; Seiler and Berendonk, 2012). Several studies have examined heavy-metal and antibiotic co-resistance by *in vitro* screening of isolates obtained from environmental sources with metal contaminants. Stepanauskas et al. (2006) exposed naïve freshwater bacterioplankton to various concentrations of metals (Cd and Ni) or antibiotics (tetracycline and ampicillin), providing the first experimental evidence that exposure to both stressors could select for multiresistant organisms. Since then, there have been several *in vitro* studies that have examined bacteria co-resistance. For example, Yamina *et al*. (2012) screened 13 heavy metal resistant bacteria isolated from wastewater and determined the minimum inhibitory concentration (MIC) for chromium, cadmium, zinc, and lead. In addition, they also examined co-resistance to multiple antibiotics including cefalotin, gentamycin, kanamycin, amikacin, doxycycline, and nalidixic acid. It

was demonstrated that over 60% of isolates displayed resistance to multiple heavy metals and antibiotics. Culture-independent studies have also examined co-resistance in model bacteria. Nishino *et al*. (2007) screened multi-drug resistant (MDR) *Salmonella enterica* and isolated a plasmid containing baeR, which codes for BaeSR, a two-component regulatory that contains efflux proteins ArcD and MdtABC. It was demonstrated that when BaeR was overexpressed there was an increase in multidrug and metal resistance (zinc and copper) via the drug efflux systems. Similar studies on *E. coli* have also examined the drug resistance systems in the BaeSR regulon, and more recently it was established that it's associated efflux proteins MdtABC, MdtD, and Spy (a periplasmic protein) are involved in zinc detoxification (Wang and Frieke, 2013). Holt *et al*. (2007) screened multi-drug resistant (MDR) *S. enterica* serovar Typhi using whole-genome sequencing and found several plasmids with IncHI1 backbones including the plasmid pHCM1 which has genes conferring streptomycin and mercury resistance transcriptionally linked.

Pathogenicity islands: virulence and metal resistance determinants

Heavy metal resistance genes have been routinely identified on within a myriad of highly virulent strains of bacteria. These resistance genes allow pathogens to sense and remove heavy metals, such as copper, an essential co-factor in mammalian immune defenses. Copper is used by macrophages for killing pathogens within phagosomes (Reva and Bezuidt, 2012). Resistance determinants are often linked to pathogenesis via mobile genetic elements (e.g. integrons, transposons, and insertion sequences) (Stokes and Gillings, 2011). These elements form the assembly units involved in the formation of

genomic islands (GIs), discrete DNA segments which mediate the horizontal transfer of genes encoding various proteins that confer virulence and antimicrobial resistance (AMR) (Juhas et al., 2009; Bellanger, 2014). The genomes of pathogenic bacteria often contain a type of GI called pathogenicity islands (PAIs) which are associated with genes encoding a plethora of virulence factors (Schmidt and Hensel, 2004; Che et al., 2014). For instance, Shiga-toxin producing *Escherichia coli* (STEC) serogroups (e.g. O157, O111, O26, and O103) contain well characterized PAIs such as the locus of enterocyte effacement (LEE), which contains the enterocyte attachment-effacing gene (eae) and secretory proteins (Ju et al., 2014). Pathogenic *E. coli* serogroups have also been shown to contain plasmid genomic islands containing a wide range of genes encoding virulence factors, as well as resistances to multiple antibiotics and heavy metals (Losada et al., 2016). These resistance elements can be rapidly disseminated within a community conferring virulence to other recipient bacteria, including commensals, via horizontal transmission (Dyar et al., 2012).

Antimicrobial resistance islands: antibiotics and heavy metals

While PAIs have important roles in the dissemination of virulence genes and the spread of pathogens, antimicrobial resistance islands (REIs) have a similar importance in facilitating the emergence of multi-drug resistant pathogens (Post et al., 2010; Kim et al., 2013; Yoon et al., 2014; Ashton et al., 2015). The widespread and over-use of antimicrobials in clinical settings is recognized as the driving force for the selection of resistant bacteria. However, intrinsic antimicrobial resistance is a naturally occurring phenomenon that predates antibiotic chemotherapy (Cox and Wright, 2013). It is

estimated that the resistome, the collection of all genetic elements that contribute to the inhibition of toxic molecules, is as ancient as bacterial metabolism (>3 billion years) (Gaze et al., 2013). Successive selection events, driven by exposure to different antimicrobials can lead to the enrichment of bacteria that are resistant to multiple antimicrobial agents. Indeed, much like PAIs there is considerable evidence that resistance islands containing several resistance genes clustered within a single genetic locus can be transferred horizontally, or even translocated (e.g. plasmid-encoded genes being shuffled into the chromosome) (Stokes and Gillings, 2011; Yoon et al., 2014). The megaplasmid pMOL30 discovered in *C. metallidurans* strain CH34, contained two large putative resistance islands (CMGI-30a and CMGI-30b) comprising multiple genes involved in cadmium, zinc, cobalt, lead, copper, and mercury resistance (Mergeay et al., 2009). Acinetobacter baumannii, a serious nosocomial pathogen that has rapidly spread worldwide, was shown to contain >9 antibiotic resistance islands harboring genes conferring resistance to both metals and antibiotics (Krizova et al., 2011; Šeputienė et al., 2012). Liu et al. (2012) completed a comparative genomic analysis of *A. baumannii* clinical isolates, and discovered a novel genomic island (GIBJ4) in the drug-sensitive strain BJ4 carried metal resistance genes inserted in the position where AbaR-like RIs would normally reside. Furthermore, they discovered that *A. baumannii* contained resistance determinants present outside the RIs. Wu et al. (2015) reported a novel staphylococcal cassette chromosome *mec* (SCC*mec*) composite island containing heavy metal and antibiotic resistance-related genes in *Staphylococcus aureus* isolat*e*, BA01611. The SCC*mec* island is a mobile genetic element containing the *mecA* gene, which encodes antibiotic-binding proteins such as PBP 2a. (Wielder et al., 2002). This

resistance island can be exogenously acquired by methicillin-susceptible *Staphylococcus aureus* (MSSA) and lead to the dissemination of methicillin-resistance among other coagulase-negative staphylococci (CoNS). The emergence of methicillin-resistant *Staphylococcus aureus* (MRSA) strains has become of the most important global health threats of the 21st century (Stefani et al., 2012).

The gut microbiome

The microbiome consists of an enormous collection of microorganisms (fungi, protozoa, bacteria, archaea, bacteriophages, and viruses of eukaryotes) that has co-evolved on and within the bodies of humans and animals (Hoffman et al., 2015; Llyod-Price et al., 2016). Microorganisms greatly outnumbers host cell, with estimates ranging into the trillions, creating a complex, dynamic and highly competitive ecosystem (Hoffman et al., 2015). The microbiome and its gene products aid in many processes, including: digestion, cognitive development, immune response, pathogen resistance, intra-host communication, homeostasis and energy production (Lu et al., 2014). Moreover, the microbiome can be significantly influenced by host genetics, early life history, diet, and environment factors (Phillips, 2009; Turnbaugh et al., 2009; Neu et al., 2011; Bonder et al., 2016; Snijders et al., 2016).

The microbiota associated with the gastrointestinal tract (the 'gut microbiome') is comparatively more diverse than other body sites, excluding the oral cavity, and also harbors the greatest density of microorganisms (Chakraborti et al., 2015; Hoffmann et al., 2015; Shriener et al., 2015). The gut microbiome has many important roles in health and in disease. For example, studies using germ-free (GF) murine models, have revealed the

importance of the gut microbiome in shaping host immune homeostasis via modulation of host antigen presenting cells (APCs). These cells (e.g., dendritic cells and intestinal macrophages) are located in close proximity to gut microbiota; providing protection against infection while maintaining immune tolerance to gut commensals (Wu and Wu, 2012). Studies of obesity and various metabolic syndromes have examined GF and high-fat diet mice to understand how certain microbiota may affect energy harvesting. Current evidence suggests that differences in the ratio of *Bacteroidetes* and *Firmicutes*, particularly those leaning toward more *Firmicutes*, can affect the fermentation activity of short-chain fatty acids (e.g. butyrate, propionate, and acetate) and ultimately the genesis of obesity (Parekh et al., 2015; Chakraborti et al., 2015). Other studies have suggested that fecal microbiota transplantation, whereby fecal material from a donor is administered to a recipient with a condition (e.g. inflammatory bowel disease, obesity, metabolic syndrome, and functional gastrointestinal disorders), not only alter the recipient's gut microbial composition but may also confer a health benefit (Gupta et al., 2016).

Antibiotics and gut dysbiosis

As mentioned previously, the gut microbiome can be influenced by a variety of factors. Environmental insults, in particular, such as antibiotics have also been demonstrated to strongly correlate with perturbations in gut microbiota, as well as increased host susceptibility to various inflammatory and infectious diseases (Breton et al., 2013; Lu et al., 2014; Zhang et al., 2015; Gao et al., 2017). Gut commensals normally promote resistance and colonization by pathogenic species, however, disruptions in these communities may promote infection of the host by bona fide or opportunistic pathogens

(Bäumler and Sperandio, 2016). For example, Ng et al. (2013) demonstrated that the gut pathogens *Salmonella* Typhimurium and *Clostridium difficile*, can exploit microbiota-liberated mucosal carbohydrates during their expansion in the gut, following disruption of the 'normal' microbiota with oral antibiotics. More recently, studies have indicated that gut disturbances (dysbiosis) may not always coincide with an increase in pathogen susceptibility. For example, a study by Fehlbaum et al. (2016) demonstrated that *Clostridium difficile* (CD) spores successfully colonized continuous fermentation models mimicking the elderly colon in treatments not containing antibiotics. In treatments with metronidazole, CD numbers were decreased below the detection limit. Upon cessation of the antibiotic treatment, however, after 2 days, CD displayed a rapid recurrence. Similarly, Iizumi showed that while orally administered antibiotics (ciprofloxacin and penicillin) disturbed the intestinal microbiota in C57/BL6 mice, colonization susceptibility to the pathogens *Campylobacter jejuni* and *Acinetobacter baumannii* was not significantly increased.

Heavy metals and gut dysbiosis

Similar to the aforementioned studies, heavy metals have been shown to have potential roles in pathogen susceptibility and dysbiosis. Heavy metals can have a profound impact on microbial diversity, metabolic profiles of the host at the functional level, and increased levels of metal-resistant species. For example, oral lead exposure was shown to cause drastic changes in the gut microbiota of rats (Sadykov et al., 2009). The relative abundance of *Escherichia coli* increased dramatically, proportionally to the amount of lead dose received (up to 1,000-fold) (Sadykov et al., 2009). Fazeli et al.

(2011) demonstrated that cadmium could not only induce dysbiosis in the GI tract of mice, but opportunistic gut pathogens such as *E. coli* and *Klebsiella* were less sensitive to heavy metal exposure compared to other commensals. Breton et al. (2013) provided evidence that non-absorbed heavy metals could have a significant impact on the gut microbiota of mice, particularly *Lactobacilacae* and *Erysipelotricaceacae* (mainly due to changes in *Turicibacter* spp).

The gut resistome: a reservoir for antimicrobial resistant diseases

Growing antimicrobial resistance is a global public health crisis that is not restricted to human medical settings. Resistances to frontline antibiotics such as fluoroquinolones, third- and fourth generation cephalosporins, and carbapenams, as well as multidrug resistance has led to the rise of multi-resistant pathogens (Magiorakos et al., 2012; Woolhouse and Ward, 2013; Tang et al., 2014). In general, there are three major pathways for resistance-driving chemicals to enter the environment: 1) municipal and industrial wastewater; 2) land spreading of animal manure and sewage sludge; and 3) aquaculture (Singer et al., 2016). Urban centers contain a myriad of non-point sources of pollution that may drive resistance, including: household effluent, drainage water, industrial waste, and traffic-related emissions (Singer et al., 2016). Furthermore, antimicrobials are frequently used in livestock production which can generate large amounts of animal waste that may contain AMR bacteria (Woolhouse and Ward, 2013). This waste is often applied to crops, where it leaches from the soil during rain events, and contaminates water bodies while contributing to the dissemination of AMR genes (Woolhouse and Ward, 2013). Similarly, the application of biosolids in agricultural

settings can cause an increase in soil heavy metal concentrations, and thus indirectly co-select AMR bacteria (Silveira et al., 2003; Munir and Xagoraraki et al., 2011; Singer et al., 2016).

Given the enormous density of microbiota in the gut ecosystem and its capacity to be altered by the external environment, there are ample opportunities for the horizontal exchange of AMR resistance genes between pathogens and commensals. Increasingly over the last 75 years, MGEs containing antibiotic resistance genes (ARGs) have been observed within the guts of animals (wild and domesticated), and humans (Zhu et al., 2012; Radhouani et al., 2014; Carroll et al., 2015; Pal et al., 2016). Previous studies have indicated that diverse ARGs are present in gut microbiota of young infants soon after birth, even without exposure to antibiotic therapy (Lee et al., 2014; Vaz et al., 2014; Moore et al., 2015). Biocide and heavy metal resistance genes were also identified in human microbiomes, however, compared to external environments the relative abundance and diversity was lower (Pal et al., 2016).

Furthermore, although wild animals do not naturally come into contact with antimicrobials; they have been observed to be reservoirs of AMR bacteria. For example, wild boar and red deer were observed to contain methicillin-resistant strains of *Staphylococcus*, *Bacillus* and *Enterococcus* (Meyer et al., 2014). Antibiotic resistant pathogens such as *E. coli* have also been observed in wild herring and yellow-legged gulls (Bonnedahl and Järhult, 2014). In any case, in regions where humans increasingly encroach on wild habitats, there is further potential for the spread of AMR bacteria between animal vectors and humans. This may be especially true in habitats that already affected by anthropogenic pollution. Hence the transmission of AMR resistant bacteria

and their genes from wildlife is an important factor to consider when surveilling zoonotic diseases and human health risks.

Methods for studying the gut microbiome

The 16S ribosomal RNA (rRNA) gene is a well-established and widely used molecular marker for studying the phylogeny and taxonomy of bacteria from complex environments (e.g. microbiomes, terrestrial and aquatic habitats). The 16S rRNA gene sequence is a region in bacteria approximately 1,550 base pairs (bp) long and is composed of highly conserved and variable regions. The sequence is long enough and contains enough genetic polymorphisms that it can be exploited to mark evolutionary distance and relatedness of bacterial species (Clarridge, 2004). Complementary universal primers, target the conserved regions of the 16S rRNA gene, and allow the polymerase chain reaction (PCR) amplification of the nine hypervariable regions. Recently, the V4-V6 subregions of the 16S rRNA gene have been demonstrated to be optimal for achieving superior phylogenetic resolution for bacteria, although others such as the V2-V3 subregions are also highly suitable (Chakravorty et al., 2007; Klindworth et al., 2013; Yang et al., 2016). Selection of the most efficient hypervariable region is still highly contentious. Traditionally, after PCR amplifying genomic DNA and purifying 16S rDNA amplicons, strategies such as molecular cloning and DNA fingerprinting were utilized, followed by sequencing on a capillary electrophoresis Sanger sequencer (Liang et al., 2008; Székely et al., 2009). Although this method provided long read lengths, the number of sequences obtained was quite low and thus prohibited a true estimation of microbial diversity. The arrival of next-generation sequencing (NGS) technologies created a boon

for microbial studies, allowing researchers across broad fields to study many samples in multiplex at the depth of millions of sequences at significantly reduced costs (Nature Methods, 2008; Glenn, 2011). Although, 16S amplicon sequencing has its own inherent limitations such as reduced taxonomic resolution and PCR bias; the availability of large curated 16S databases, flexibility, and lower costs make it a popular option for many researchers (Poretsky et al., 2014).

Our current strategy was developed for the Illumina platform. It involves PCR amplifying genomic DNA to generate unique combinatorically-tagged 16S rDNA amplicons, followed by a second-round PCR reaction to add sequencing adapters, pooling, and sequencing on a single MiSeq run. The quadruple-indexing strategy provides two important benefits. First, it allows hundreds of uniquely tagged samples to be pooled into one sequencing reaction. Secondly, following de-multiplexing each unique sample can be extracted for subsequent bioinformatics and statistical analyses. Moreover, while the 16S rRNA is a powerful tool for exploring microbial communities, its utility is limited when attempting to discern a community's functional capabilities. Data from 16S analyses can be used to in computational tools such as PICRUSt (phylogenetic investigation of communities by reconstruction of unobserved states) to predict gene families and estimate a composite metagenome, but it provides only indirect evidence of function (Manichanh et al., 2008; Langille et al., 2013).

In addition to 16S amplicons, methods such as shotgun metagenomics sequencing (SMS) have also been utilized to explore microbial communities from many diverse environments (Poretsky et al., 2014; Villanueve et al., 2014; Andersen et al., 2016). Unlike 16S rRNA gene sequencing, shotgun metagenomics does not carry the inherent

bias of PCR amplicon based approaches. Whereas amplicon sequencing relies on the amplification of bacterial DNA, in SMS genomic DNA is sequenced directly from the environment. Typically, genomic DNA is sheared either enzymatically or mechanically, to create fragments of a target size. The DNA ends are repaired and ligated with adapters and then sequenced. The advantages of this are two-fold: 1) direct sequencing of environmental DNA can provide superior taxonomic resolution; and 2) SMS provides direct surveillance of functional attributes of a microbial community (i.e., DNA from functional genes are sequenced directly, rather than being inferred). There are a few disadvantages of this technique and they include: 1) costs can prohibitive; 2) it is non-specific and thus captures the metagenomes of other organisms (i.e., eukaryotes); and 3) the results are highly dependent on sequencing depth (Poretsky et al., 2014; Jovel et al., 2016). Shotgun metagenome approaches can be improved by using more targeted methods. For example, sequence capture probes can be used to extract and enrich target DNA (e.g. 16S rRNA genes, ARGs and MRGs, etc.) (Grover et al., 2012; Faircloth et al., 2015; Dapprich et al., 2016). These probes hybridize to target genomic DNA that shares ~≥80% sequence similarity thereby permitting sufficient coverage of sequence diversity within genomic and gene families. Furthermore, enriched libraries can also be sequence-tagged and pooled with other samples (e.g. 16S rRNA gene amplicons) prior to next-generation sequencing. Therefore, one can survey thousands of bacteria and genes within an entire microbial community both simultaneously and in multiplex (Faircloth, 2012). A comparison of these techniques used in microbiome and resistome studies is provided in Table 1.

Overview of Dissertation

In this dissertation, I focus on the role of environmental heavy metal exposures on modulating antimicrobial resistance and dysbiosis in the gut microbiome. Firstly (above), I review heavy metals: their sources, physiological impacts on organisms including humans and then begin focusing on bacteria. I examine how bacteria are able to tolerate and resist metal toxicity, the role of heavy metals in the indirect co-selection of antibiotic resistance, and the modes that allow AMR to proliferate within microbial communities via horizontal gene transfer. I also briefly review current literature that examines the role of antibiotics and heavy metals in the microbiome, particularly regarding pathogen susceptibility and dysbiosis. Secondly, I discuss the microbial communities and their predicted resistome from heavy metal contaminated soils at the Savannah River Site (SRS). Thirdly, I investigate the role environmental heavy metal contamination may have in modulating the gut microbiota of wild *Peromyscus* trapped at the SRS. Fourthly, I examine microbial and AMR co-occurrence patterns between the contaminated soil environments and wild Peromyscus. And finally, I examine how direct exposures to a suite of environmentally relevant heavy metals and ciprofloxacin may affect the microbiome of captive *Peromyscus*, their resistome, and host inflammatory status.

References

Abbaspour, N., Hurrell, R., & Kelishadi, R. (2014). Review on iron and its importance for human health. *Journal of Research in Medical Sciences: The Official Journal of Isfahan University of Medical Sciences*, *19*(2), 164–174.

Alloway, B. J. (2013). Sources of heavy metals and metalloids in soils. In B. J. Alloway (Ed.), *Heavy Metals in Soils* (pp. 11–50). Springer Netherlands. https://doi.org/10.1007/978-94-007-4470-7_2

Amiard-Triquet, C., Rainbow, P. S., & Romeo, M. (2011). *Tolerance to Environmental Contaminants*. CRC Press.

Baker-Austin, C., Wright, M. S., Stepanauskas, R., & McArthur, J. V. (2006). Co-selection of antibiotic and metal resistance. *Trends in Microbiology*, *14*(4), 176–182. https://doi.org/10.1016/j.tim.2006.02.006

Bäumler, A. J., & Sperandio, V. (2016). Interactions between the microbiota and pathogenic bacteria in the gut. *Nature*, *535*(7610), 85–93. https://doi.org/10.1038/nature18849

Behnsen, J., & Raffatellu, M. (2016). Siderophores: more than stealing iron. *mBio*, *7*(6), e01906-16. https://doi.org/10.1128/mBio.01906-16

Bonnedahl, J., & Järhult, J. D. (2014). Antibiotic resistance in wild birds. *Upsala Journal of Medical Sciences*, *119*(2), 113–116. https://doi.org/10.3109/03009734.2014.905663

Branco, R., Chung, A.-P., & Morais, P. V. (2008). Sequencing and expression of two arsenic resistance operons with different functions in the highly arsenic-resistant

strain Ochrobactrum tritici SCII24T. *BMC Microbiology*, *8*, 95. https://doi.org/10.1186/1471-2180-8-95

Brown, K. H., Wuehler, S. E., & Peerson, J. M. (2001). The importance of zinc in human nutrition and estimation of the global prevalence of zinc deficiency. *Food and Nutrition Bulletin*, *22*(2), 113–125. https://doi.org/10.1177/156482650102200201

Bruins, M. R., Kapil, S., & Oehme, F. W. (2000). Microbial resistance to metals in the environment. *Ecotoxicology and Environmental Safety*, *45*(3), 198–207. https://doi.org/10.1006/eesa.1999.1860

Carroll, D., Wang, J., Fanning, S., & McMahon, B. J. (2015). Antimicrobial resistance in wildlife: implications for public health. *Zoonoses and Public Health*, *62*(7), 534–542. https://doi.org/10.1111/zph.12182

Castillo, R., & Saier, M. H. (2010). Functional promiscuity of homologues of the bacterial ArsA ATPases. *International Journal of Microbiology*, *2010*, e187373. https://doi.org/10.1155/2010/187373

Chacón, K. N., Mealman, T. D., McEvoy, M. M., & Blackburn, N. J. (2014). Tracking metal ions through a Cu/Ag efflux pump assigns the functional roles of the periplasmic proteins. *Proceedings of the National Academy of Sciences of the United States of America*, *111*(43), 15373–15378. https://doi.org/10.1073/pnas.1411475111

Chan, W. Y., & Rennert, O. M. (1980). The role of copper in iron metabolism. *Annals of Clinical and Laboratory Science*, *10*(4), 338–344.

Che, D., Hasan, M. S., & Chen, B. (2014). Identifying pathogenicity islands in bacterial pathogenomics using computational approaches. *Pathogens*, *3*(1), 36–56. https://doi.org/10.3390/pathogens3010036

Cobbett, C., & Goldsbrough, P. (2002). Phytochelatins and metallothioneins: Roles in heavy metal detoxification and homeostasis. *Annual Review of Plant Biology*, *53*(1), 159–182. https://doi.org/10.1146/annurev.arplant.53.100301.135154

Collins, J. F., Prohaska, J. R., & Knutson, M. D. (2010). Metabolic crossroads of iron and copper. *Nutrition Reviews*, *68*(3), 133–147. https://doi.org/10.1111/j.1753-4887.2010.00271.x

Dressler, C., Kües, U., Nies, D. H., & Friedrich, B. (1991). Determinants encoding resistance to several heavy metals in newly isolated copper-resistant bacteria. *Applied and Environmental Microbiology*, *57*(11), 3079–3085.

Duruibe, J. O., Ogwuegbu, M. O. C., Egwurugwu, J. N., & others. (2007). Heavy metal pollution and human biotoxic effects. *International Journal of Physical Sciences*, *2*(5), 112–118.

EL-Sherbiny, G. M., & E, S. M. (2014). Antimicrobial susceptibility, heavy metals tolerance and plasmid curing of *Shigella* species isolated from El- Dakahlia, Egypt. *American Journal of Microbiological Research, American Journal of Microbiological Research*, *2*(6), 211–216. https://doi.org/10.12691/ajmr-2-6-7

Engen, P. A., Green, S. J., Voigt, R. M., Forsyth, C. B., & Keshavarzian, A. (2015). The Gastrointestinal Microbiome. *Alcohol Research: Current Reviews*, *37*(2), 223–236.

Fazeli, M., Hassanzadeh, P., & Alaei, S. (2011). Cadmium chloride exhibits a profound toxic effect on bacterial microflora of the mice gastrointestinal tract. *Human & Experimental Toxicology*, *30*(2), 152–159. https://doi.org/10.1177/0960327110369821

Fraga, C. G. (2005). Relevance, essentiality and toxicity of trace elements in human health. *Molecular Aspects of Medicine*, *26*(4), 235–244. https://doi.org/10.1016/j.mam.2005.07.013

Gao, B., Chi, L., Mahbub, R., Bian, X., Tu, P., Ru, H., & Lu, K. (2017). Multi-Omics reveals that lead exposure disturbs gut microbiome development, key metabolites, and metabolic pathways. *Chemical Research in Toxicology*, *30*(4), 996–1005. https://doi.org/10.1021/acs.chemrestox.6b00401

Gupta, S., Allen-Vercoe, E., & Petrof, E. O. (2016). Fecal microbiota transplantation: in perspective. *Therapeutic Advances in Gastroenterology*, *9*(2), 229–239. https://doi.org/10.1177/1756283X15607414

Hoffmann, A. R., Proctor, L. M., Surette, M. G., & Suchodolski, J. S. (2016). The Microbiome: The trillions of microorganisms that maintain health and cause disease in humans and companion animals. *Veterinary Pathology*, *53*(1), 10–21. https://doi.org/10.1177/0300985815595517

Iizumi, T., Taniguchi, T., Yamazaki, W., Vilmen, G., AlekseyenK0, A. V., Gao, Z., … Blaser, M. J. (2016). Effect of antibiotic pre-treatment and pathogen challenge on the intestinal microbiota in mice. *Gut Pathogens*, *8*, 60. https://doi.org/10.1186/s13099-016-0143-z

Jaishankar, M., Tseten, T., Anbalagan, N., Mathew, B. B., & Beeregowda, K. N. (2014). Toxicity, mechanism and health effects of some heavy metals. *Interdisciplinary Toxicology*, *7*(2), 60–72. https://doi.org/10.2478/intox-2014-0009

JanK0wska, K., Olańczuk-Neyman, K., & Kulbat, E. (2006). The sensitivity of bacteria to heavy metals in the presence of mineral ship motor oil in coastal marine sediments and waters. *Polish Journal of Environmental Studies*, *15*(6). Retrieved from http://www.academia.edu/download/42462776/The_sensitivity_of_bacteria_to_heavy_met20160209-23813-1al4oc2.pdf

Jansen, E., Michels, M., Til, M. van, & Doelman, P. (1994). Effects of heavy metals in soil on microbial diversity and activity as shown by the sensitivity-resistance index, an ecologically relevant parameter. *Biology and Fertility of Soils*, *17*(3), 177–184. https://doi.org/10.1007/BF00336319

Järup, L. (2003). Hazards of heavy metal contamination. *British Medical Bulletin*, *68*(1), 167–182. https://doi.org/10.1093/bmb/ldg032

Jomova, K., & ValK0, M. (2011). Importance of iron chelation in free radical-induced oxidative stress and human disease. *Current Pharmaceutical Design*, *17*(31), 3460–3473. https://doi.org/10.2174/138161211798072463

Kaplan, J., & O Halloran, T. V. (1996). Iron metabolism in eukaryotes: Mars and Venus at it again. *Science; Washington*, *271*(5255), 1510.

Khan, Z., Rehman, A., Hussain, S. Z., Nisar, M. A., Zulfiqar, S., & ShaK0ori, A. R. (2016). Cadmium resistance and uptake by bacterium, *Salmonella enterica* 43C,

isolated from industrial effluent. *AMB Express*, *6*. https://doi.org/10.1186/s13568-016-0225-9

Kim, D. H., Choi, J.-Y., Kim, H. W., Kim, S. H., Chung, D. R., Peck, K. R., … K0, K. S. (2013). Spread of carbapenem-resistant acinetobacter baumannii global clone 2 in Asia and Abar-type resistance islands. *Antimicrobial Agents and Chemotherapy*, *57*(11), 5239–5246. https://doi.org/10.1128/AAC.00633-13

Lee, G. C., Reveles, K. R., Attridge, R. T., Lawson, K. A., Mansi, I. A., Lewis, J. S., & Frei, C. R. (2014). Outpatient antibiotic prescribing in the United States: 2000 to 2010. *BMC Medicine*, *12*, 96. https://doi.org/10.1186/1741-7015-12-96

Lee, S., Kim, Y.-Y., Lee, Y., & An, G. (2007). Rice P1B-Type Heavy-Metal ATPase, OsHMA9, Is a Metal Efflux Protein. *Plant Physiology*, *145*(3), 831–842. https://doi.org/10.1104/pp.107.102236

Li, J., & Rosen, B. P. (2000). The linker peptide of the ArsA ATPase. *Molecular Microbiology*, *35*(2), 361–367. https://doi.org/10.1046/j.1365-2958.2000.01696.x

Li, S., SK0v, R. L., Han, X., Larsen, A. R., Larsen, J., Sørum, M., … Ito, T. (2011). Novel types of staphylococcal cassette chromosome mec elements identified in clonal complex 398 Methicillin-Resistant *Staphylococcus aureus* strains▽. *Antimicrobial Agents and Chemotherapy*, *55*(6), 3046–3050. https://doi.org/10.1128/AAC.01475-10

Liu, Y., Li, Y., Liu, K., & Shen, J. (2014). Exposing to cadmium stress cause profound toxic effect on microbiota of the mice intestinal tract. *PLOS ONE*, *9*(2), e85323. https://doi.org/10.1371/journal.pone.0085323

Lloyd-Price, J., Abu-Ali, G., & Huttenhower, C. (2016). The healthy human microbiome. *Genome Medicine*, *8*, 51. https://doi.org/10.1186/s13073-016-0307-y

Lu, K., Abo, R. P., Schlieper, K. A., Graffam, M. E., Levine, S., Wishnok, J. S., … Fox, J. G. (2014). Arsenic exposure perturbs the gut microbiome and its metabolic profile in mice: an integrated metagenomics and metabolomics analysis. *Environmental Health Perspectives*. https://doi.org/10.1289/ehp.1307429

Madhusoodanan, J., Seo, K. S., Remortel, B., Park, J. Y., Hwang, S. Y., Fox, L. K., … Gill, S. R. (2011). An enterotoxin-bearing pathogenicity island in *Staphylococcus epidermidis*▽. *Journal of Bacteriology*, *193*(8), 1854–1862. https://doi.org/10.1128/JB.00162-10

Magiorakos, A.-P., Srinivasan, A., Carey, R. B., Carmeli, Y., Falagas, M. E., Giske, C. G., … Monnet, D. L. (2012a). Multidrug-resistant, extensively drug-resistant and pandrug-resistant bacteria: an international expert proposal for interim standard definitions for acquired resistance. *Clinical Microbiology and Infection*, *18*(3), 268–281. https://doi.org/10.1111/j.1469-0691.2011.03570.x

Magiorakos, A.-P., Srinivasan, A., Carey, R. B., Carmeli, Y., Falagas, M. E., Giske, C. G., … Monnet, D. L. (2012b). Multidrug-resistant, extensively drug-resistant and pandrug-resistant bacteria: an international expert proposal for interim standard definitions for acquired resistance. *Clinical Microbiology and Infection*, *18*(3), 268–281. https://doi.org/10.1111/j.1469-0691.2011.03570.x

Mergeay, M., Monchy, S., Vallaeys, T., Auquier, V., Benotmane, A., Bertin, P., … Wattiez, R. (2003). Ralstonia metallidurans, a bacterium specifically adapted to

toxic metals: towards a catalogue of metal-responsive genes. *FEMS Microbiology Reviews*, *27*(2–3), 385–410.

Messerschmidt, A. (1997). *Multi-Copper Oxidases*. World Scientific.

Meyer, C., Heurich, M., Huber, I., Krause, G., Ullrich, U., & Fetsch, A. (2014). The importance of wildlife as reservoir of antibiotic-resistant bacteria in Bavaria--first results. *Berliner Und Munchener Tierarztliche Wochenschrift*, *127*(3–4), 129–134.

Monsieurs, P., Moors, H., Houdt, R. V., Janssen, P. J., Janssen, A., Coninx, I., … Leys, N. (2011). Heavy metal resistance in *Cupriavidus metallidurans* CH34 is governed by an intricate transcriptional network. *BioMetals*, *24*(6), 1133–1151. https://doi.org/10.1007/s10534-011-9473-y

Moore, A. M., Ahmadi, S., Patel, S., Gibson, M. K., Wang, B., Ndao, I. M., … Dantas, G. (2015). Gut resistome development in healthy twin pairs in the first year of life. *Microbiome*, *3*, 27. https://doi.org/10.1186/s40168-015-0090-9

Munir, M., & Xagoraraki, I. (2011). Levels of antibiotic resistance genes in manure, biosolids, and fertilized soil. *Journal of Environmental Quality*, *40*(1), 248–255. https://doi.org/10.2134/jeq2010.0209

Neilands, J. B. (1995). Siderophores: Structure and function of microbial iron transport compounds. *Journal of Biological Chemistry*, *270*(45), 26723–26726. https://doi.org/10.1074/jbc.270.45.26723

Neu, J., & Rushing, J. (2011). Cesarean versus Vaginal Delivery: Long term infant outcomes and the Hygiene Hypothesis. *Clinics in Perinatology*, *38*(2), 321–331. https://doi.org/10.1016/j.clp.2011.03.008

Nies, D. H. (1999). Microbial heavy-metal resistance. *Applied Microbiology and Biotechnology*, *51*(6), 730–750.

Osredkar, J., & Sustar, N. (2011). Copper and zinc, biological role and significance of copper/zinc imbalance. *J. Clinic. Toxicol. S*, *3*, 1.

Parekh, P. J., Balart, L. A., & Johnson, D. A. (2015). The Influence of the Gut Microbiome on Obesity, Metabolic Syndrome and Gastrointestinal Disease. *Clinical and Translational Gastroenterology*, *6*(6), e91. https://doi.org/10.1038/ctg.2015.16

Pechova, A., & Pavlata, L. (2007). Chromium as an essential nutrient: a review. *VETERINARNI MEDICINA-PRAHA-*, *52*(1), 1.

Perales-Vela, H. V., Peña-Castro, J. M., & Cañizares-Villanueva, R. O. (2006). Heavy metal detoxification in eukaryotic microalgae. *Chemosphere*, *64*(1), 1–10. https://doi.org/10.1016/j.chemosphere.2005.11.024

Post, V., White, P. A., & Hall, R. M. (2010). Evolution of AbaR-type genomic resistance islands in multiply antibiotic-resistant Acinetobacter baumannii. *Journal of Antimicrobial Chemotherapy*, *65*(6), 1162–1170. https://doi.org/10.1093/jac/dkq095

Prohaska, J. R., & Lukasewycz, O. A. (1990). Effects of copper deficiency on the immune system. In A. Bendich, M. Phillips, & R. P. Tengerdy (Eds.), *Antioxidant Nutrients and Immune Functions* (pp. 123–143). Springer US. https://doi.org/10.1007/978-1-4613-0553-8_11

Radhouani, H., Silva, N., Poeta, P., Torres, C., Correia, S., & Igrejas, G. (2014). Potential impact of antimicrobial resistance in wildlife, environment and human health. *Frontiers in Microbiology*, *5*. https://doi.org/10.3389/fmicb.2014.00023

Rengel, Z. (1999). Heavy Metals as Essential Nutrients. In *Heavy Metal Stress in Plants* (pp. 231–251). Springer Berlin Heidelberg. https://doi.org/10.1007/978-3-662-07745-0_11

Sadykov, R., Digel, I., Artmann, A. T., Porst, D., Linder, P., Kayser, P., … Zhubanova, A. (2009). Oral lead exposure induces dysbacteriosis in rats. *Journal of Occupational Health*, *51*(1), 64–73.

Schmidt, H., & Hensel, M. (2004). Pathogenicity islands in bacterial pathogenesis. *Clinical Microbiology Reviews*, *17*(1), 14–56. https://doi.org/10.1128/CMR.17.1.14-56.2004

Schwarz, K., & Mertz, W. (1959). Chromium(III) and the glucose tolerance factor. *Archives of Biochemistry and Biophysics*, *85*, 292–295.

Seiler, C., & Berendonk, T. U. (2012). Heavy metal driven co-selection of antibiotic resistance in soil and water bodies impacted by agriculture and aquaculture. *Frontiers in Microbiology*, *3*. https://doi.org/10.3389/fmicb.2012.00399

Šeputienė, V., Povilonis, J., & Sužiedėlienė, E. (2012). Novel variants of AbaR resistance islands with a common backbone in *Acinetobacter baumannii* isolates of European clone II. *Antimicrobial Agents and Chemotherapy*, *56*(4), 1969–1973. https://doi.org/10.1128/AAC.05678-11

Shivakumar, D., Srikantaswamy, S., Sreenivasa, S., & Kiran, B. M. (2012). Speciation and geochemical behaviour of heavy metals in industrial area soil of Mysore City,

India. *Journal of Environmental Protection*, *3*(10), 1384–1392. https://doi.org/10.4236/jep.2012.310157

Silveira, M. L. A., Alleoni, L. R. F., & Guilherme, L. R. G. (2003). Biosolids and heavy metals in soils. *Scientia Agricola*, *60*(4), 793–806. https://doi.org/10.1590/S0103-90162003000400029

Singer, A. C., Shaw, H., Rhodes, V., & Hart, A. (2016). Review of antimicrobial resistance in the environment and its relevance to environmental regulators. *Frontiers in Microbiology*, *7*. https://doi.org/10.3389/fmicb.2016.01728

Snijders, A. M., Langley, S. A., Kim, Y.-M., Brislawn, C. J., Noecker, C., Zink, E. M., … Mao, J.-H. (2016). Influence of early life exposure, host genetics and diet on the mouse gut microbiome and metabolome. *Nature Microbiology*, *2*, 16221. https://doi.org/10.1038/nmicrobiol.2016.221

Stefani, S., Chung, D. R., Lindsay, J. A., Friedrich, A. W., Kearns, A. M., Westh, H., & MacKenzie, F. M. (2012). Methicillin-resistant *Staphylococcus aureus* (MRSA): global epidemiology and harmonization of typing methods. *International Journal of Antimicrobial Agents*, *39*(4), 273–282. https://doi.org/10.1016/j.ijantimicag.2011.09.030

Tang, S. S., Apisarnthanarak, A., & Hsu, L. Y. (2014). Mechanisms of β-lactam antimicrobial resistance and epidemiology of major community- and healthcare-associated multidrug-resistant bacteria. *Advanced Drug Delivery Reviews*, *78*, 3–13. https://doi.org/10.1016/j.addr.2014.08.003

Vaz, L. E., Kleinman, K. P., Raebel, M. A., Nordin, J. D., LaK0ma, M. D., Dutta-Linn, M. M., & Finkelstein, J. A. (2014). Recent Trends in Outpatient Antibiotic Use in Children. *Pediatrics*, *133*(3), 375–385. https://doi.org/10.1542/peds.2013-2903

Wielders, C. L. C., Fluit, A. C., Brisse, S., Verhoef, J., & Schmitz, F. J. (2002). mecA gene is widely disseminated in *Staphylococcus aureus* population. *Journal of Clinical Microbiology*, *40*(11), 3970–3975. https://doi.org/10.1128/JCM.40.11.3970-3975.2002

Wiesemann, N., Mohr, J., Grosse, C., Herzberg, M., Hause, G., Reith, F., & Nies, D. H. (2013). Influence of copper resistance determinants on gold transformation by Cupriavidus metallidurans strain CH34. *Journal of Bacteriology*, *195*(10), 2298–2308. https://doi.org/10.1128/JB.01951-12

Wu, Z., Li, F., Liu, D., Xue, H., & Zhao, X. (2015). Novel Type XII staphylococcal cassette chromosome mec harboring a new cassette chromosome recombinase, CcrC2. *Antimicrobial Agents and Chemotherapy*, *59*(12), 7597–7601. https://doi.org/10.1128/AAC.01692-15

Yamina, B., Tahar, B., & Marie Laure, F. (2012). Isolation and screening of heavy metal resistant bacteria from wastewater: a study of heavy metal co-resistance and antibiotics resistance. *Water Science & Technology*, *66*(10), 2041. https://doi.org/10.2166/wst.2012.355

Yoon, S. H., Park, Y.-K., & Kim, J. F. (2015). PAIDB v2.0: exploration and analysis of pathogenicity and resistance islands. *Nucleic Acids Research*, *43*(Database issue), D624–D630. https://doi.org/10.1093/nar/gku985

Zhang, S., Jin, Y., Zeng, Z., Liu, Z., & Fu, Z. (2015). Subchronic exposure of mice to cadmium perturbs their hepatic energy metabolism and gut microbiome. *Chemical Research in Toxicology*, *28*(10), 2000–2009. https://doi.org/10.1021/acs.chemrestox.5b00237

Zheng, N., Liu, J., Wang, Q., & Liang, Z. (2010). Health risk assessment of heavy metal exposure to street dust in the zinc smelting district, Northeast of China. *Science of The Total Environment*, *408*(4), 726–733. https://doi.org/10.1016/j.scitotenv.2009.10.075

Zhu, Y.-G., Johnson, T. A., Su, J.-Q., Qiao, M., Guo, G.-X., Stedtfeld, R. D., … Tiedje, J. M. (2013). Diverse and abundant antibiotic resistance genes in Chinese swine farms. *Proceedings of the National Academy of Sciences*, *110*(9), 3435–3440. https://doi.org/10.1073/pnas.1222743110

Zhuang, P., McBride, M. B., Xia, H., Li, N., & Li, Z. (2009). Health risk from heavy metals via consumption of food crops in the vicinity of Dabaoshan mine, South China. *Science of The Total Environment*, *407*(5), 1551–1561. https://doi.org/10.1016/j.scitotenv.2008.10.061

Table 1-1. Techniques used to survey microbial communities and their resistome.

Approach	Advantages	Limitations	References
Shotgun metagenomics sequence	• Scalability • Superior taxonomic resolution • Can be used to directly assess functional metagenomes	• Large amounts of non-target sequences • Requires large amounts of sequencing • Cost	Poretsky et al., 2014; Jovel et al., 2016
Sequence capture/targeted metagenome sequencing	• Useful for directly targeting metagenomes and resistance genes (the '1%') • Characterize thousands of loci in multiplex • Easily adapted for NGS	• Potential probe-target hybridization inefficiencies • Coverage on desired targets can vary on their design • Requires deeper sequencing • Cost	Carpenter et al., 2013; Gasc et al., 2016; Dapprich et al., 2016
PCR	• Useful surveying microbial communities • Useful for rapid detection and monitoring of resistance genes • Flexible and relatively inexpensive • Can be multiplexed	• Detection sensitivity is limited to the primers utilized • Cannot effectively screen resistance genes of large whole communities • Cannot be used to identify unknown genes or organisms	Poirel et al. 2011; Bartram et al. 2011; Roschanski et al. 2014
Functional Metagenomics	• Ability to isolate novel	• Obtaining expression of all resistance gene	McGarvey et al. 2012; Su et al. 2014; Forseberg et

(host/vector system screening)	antimicrobial genes • Clones can be used to identify phylogenetic origins of original bacteria • Can be subject to pooling and massively parallel sequencing • Can use targeted approach for specific genes of interest	can be biased in surrogate cloning host (e.g *E. coli*) • Host may be intrinsically resistant to certain antimicrobials • Screening clone libraries against multiple antimicrobial agents may require significant time	al. 2012; Amos et al. 2014.
DNA microarray	• Ability to identify and characterize thousands of target loci in parallel on a single array • Probes can be genes or even genomes • High specificity • Highly customizable	• Requires *a priori* knowledge of regions of interest • Can only detect regions for which probes have been designed • Can be costly	Card et al., 2013; Dally et al., 2013; Lu et al., 2014
Whole genome sequencing	• Well-suited for identification of resistance mechanisms in pathogens • Well-suited for surveillance and studying evolution of resistance in real-time	• Not suited surveying the genomes of mixed communities • Can be costly	Köser et al., 2014; Kwong et al., 2015; Allard, 2016

	• Extremely useful in drug discovery		
Minimum inhibitory concentration (MIC) screening	• Ability to screen pure isolates for antimicrobial susceptibility against multiple drugs simultaneously • Can be scaled for massively parallel high throughput screening	• Subject to culture bias • Pre-made plates can be very expensive • Not well-suited for mixed communities	Wiegand et al., 2008; Sarker et al., 2007; Bulik et al., 2010

CHAPTER 2

THE MICROBIAL RESISTOME OF HEAVY METAL CONTAMINATED SOILS AT THE SAVANNAH RIVER SITE (SRS) [†]

[†]Thomas, J. C. IV, T. J. Kieran, J. C. Seaman, J. Beasley, J V. McArthur, O. E. Rhodes Jr., and T. C. Glenn. Submitting to Environmental Microbiology.

Abstract

Soil environments represent a significant reservoir of microbial diversity and source of antimicrobial resistance (AMR). Contaminants such as heavy metals may contribute to dissemination of AMR by enriching resistance gene determinants via coselection mechanisms. Hence, understanding how microbial communities are influenced by heavy metals and how these changes manifest in heightened AMR is an important global health issue. In the present study, the diversity and composition of bacterial and fungal communities in soils collected from four areas with varying contaminant profiles (relatively pristine, heavy metal contaminated, radionuclides contaminated, and heavy metal + radionuclide contaminated) at the Savannah River Site (SRS), South Carolina were evaluated using a combination of 16S rRNA gene and ITS amplicon sequencing on an Illumina MiSeq. We obtained 6,078,406 high quality (Q≥20) 16S rRNA gene sequences, revealing a core microbiome consisting of 8 phyla shared between 95% of the sequences. Metal concentrations and carbon to nitrogen (C:N) ratio were the most important factors determining the microbial community structure. Contaminated sites at the SRS showed significantly decreased species richness compared to the reference site (Upper Three Runs). In addition, using PICRUSt to infer a predicted resistome from our 16S data, we found that the contaminated sites displayed small, but significantly higher relative abundance of several predicted genes related to heavy metal and antibiotic resistance including *corC* and *ycnj* (copper resistance); *smvA* (antimicrobial resistance); *yebQ* (multidrug efflux); *mmr* (methylenomycin A resistance); and *nixA* (nickel transport).

Introduction

Over the past century, heavy metal contamination of soils resulting from anthropogenic activities (e.g. industry and agriculture) has rapidly become one of the most serious environmental concerns (Arao et al., 2010; Wuana et al., Okieimen, 2011; Gonçalves Jr et al., 2014). Industrialization and technological advancements in the modern era have only exacerbated the issue of heavy metal pollution, facilitating the release of large quantities of heavy metals (HMs) into the environment. Consequently, governmental agencies such as the Environmental Protection Agency (EPA) have been tasked with establishing a regulatory framework that oversees both the implementation and enforcement of laws (e.g. Comprehensive Environmental Response Compensation and Liability Act or CERCLA) pertaining to the maximum permissible concentrations of heavy metals allowed to enter the environment (Wuana and Okieimen, 2011; Yap et al., 2012). Nonetheless, in certain circumstances, depending on the legacy of contamination, heavy metals in soils may already exceed recommended limits, presenting a significant risk to living organisms including humans.

Heavy metals and radionuclides (HMRs) such as Cd, Co, Cr, Ni, Sr, U, Zn, can chelate to organic matter within the soil interface, and persist for exceedingly long periods of time (Xu et al., 2016). In organisms, HMRs can interfere with a variety of physiological processes such as: (1) the alteration of enzyme specificity; (2) disruption of cellular functions; (3) impairment of DNA structural integrity; and (4) displacement of essential trace metals. Heavy metals concentrations can also magnify or bioaccumulate at higher trophic levels within a food chain (Wang and Chen; 2006; Xu et al., 2016). Therefore, due to the widespread and ubiquity of heavy metals pollution in soils, their

propensity to exhibit toxicity within most living organisms through various exposure routes, and their non-degradable nature, there has been considerable interest to study the extent at which these environmental hazards inflict damage on ecosystems.

Soil microbial communities have important roles in the maintenance of soil quality, particularly in terms of biogeochemical cycling and the promotion of plant growth. In addition, surveys of microbial communities may provide sensitive indicators of environmental HMR pollution (Sun et al., 2012). Heavy metals and radionuclides have long been established as stressors that can potentially affect the diversity, structure, and function of indigenous soil microbial communities (Kavamura and Esposito, 2010; Xie et al., 2016). However, bacterial and fungal populations can display varying sensitivities to HMRs depending on the in concentration and bioavailability. Rajapaksha et al. (2004) first reported that the addition of heavy metals can differentially affect the soil respiration activity of bacteria and fungi. Stefanowicz et al. (2006) and later Azarbad et al. (2013) found that the functional diversity of bacteria from contaminated soils decreased with increasing metal concentrations, whereas in fungi it slightly increased. Gołębiewski et al. (2014) found that soils contaminated with Zn possessed significantly different communities and decreased microbial diversity compared to soils contaminated with Cr and lower levels of Pb and Zn. Yin et al. (2015) reported significant changes in the structure, composition, and function of microbial communities across a gradient of increasing heavy metal contamination. In contrast, other works have shown that microbial diversity can increase in HM contaminated soils as the community stabilizes over long periods (Hong et al., 2015; Bourceret et al., 2016). Nevertheless, the presence of HMR contaminants is not always the primary driver of microbial community structure

due to the influence of other edaphic properties (e.g pH, C/N ratio, water, etc.) (Chodak et al. (2013; Bourceret et al., 2016). Therefore, determining the degree to which HMs can affect soil microbial communities remains challenging.

Heavy metal resistance in soil bacterial communities

Several studies have indicated that while bacteria in the phyla Proteobacteria (*Geobacter* spp*., Shewenella* spp*.,* etc) and Firmicutes (*Clostridia* spp., *Sedimentibacter* spp.) display HMR tolerance, others such as Verrucomicrobia may experience decreases with increasing pollution (Burkhardt et al., 2011; Azarbad et al., 2015). Gołębiewski et al. (2014) found that while the bacterial diversity of soils differed with respect to the type of HMR contaminants present, all samples shared a core microbiome consisting of taxa such as *Sphingomonas*, *Candidatus Solibacter*, and *Flexibacter*. Furthermore, in bacteria, genetic determinants for metal resistance are typically found on plasmids with class 1 integrons and transposons (Pal et al., 2015). Such resistances are achieved by several mechanisms such as: (1) exclusion by barriers (e.g. production of biofilms), (2) extracellular and intracellular sequestration, (3) and enzymatic reduction or transformation of HMRs. In addition, many of these genetic determinants are known to co-select antibiotic resistance, which has important implications regarding drug therapies (Sieler and Berendonk, 2012; Wales and Davies, 2015).

Heavy metal resistance in saprotrophic and ectomycorrhizal fungi in soils

Studies on saprotrophic and ectomycorrhizal fungi in soils have revealed a variety of resistance determinants that allow fungi to immobilize HMRs and reduce bioavailability. Fungi can (1) perform extracellular metal sequestration via the binding of metals to fungal siderophores or secretion of chelating agents such as oxalates; (2) bind

metals to cell wall and associated components (e.g. mycelium, fungal vacuole, cytoplasm etc.), and (3) reduce HMRs uptake by intracellular chelation or sequestration via metal-binding oligopeptides and metallothioneins (Gadd et al., 2005; Fomina., 2005). Furthermore, heavy metal tolerance is extensive among the major fungal divisions Ascomycota and Basidiomycota. For example, species within the genus *Aspergillus*, *Penicillium*, *Phoma*, *Alternaria*, *Peyronellaea*, *Fusarium* among many others have been exploited for bioremediation and even bioleaching efficiency (Anahid et al., 2011; Li et al., 2012; Iram et al., 2013; Fazil et al., 2015).

Specific aims and hypotheses

Previous studies on the relationship between HMR contamination and microbial communities at the Savannah River Site (SRS) have mainly focused a limited number of 16S rRNA gene clones or the selective enrichment of bacteria on media containing various HMRs present at the site (e.g. Cr, Cd, Ni, U, etc.) (Ye, 2007; Tuckfield and McArthur, 2008). These studies revealed that soils are co-dominated by highly diverse members from the phyla *Proteobacteria* and *Acidobacteria*, containing several metal-, and/or sulfate-reducing genera capable of immobilizing HMRs (Ye, 2007). However, to our knowledge, few studies have focused on the role of HMR contaminants on the co-occurrence of bacterial and fungal communities, or examined putative functional links to antibiotic/heavy metal resistance (AMR) using next generation sequencing (NGS).

Hence, the purpose of the present study was to first determine if HMR contamination has a measurable and significant influence on the diversity and structure of bacterial and fungal communities. Furthermore, we were interested in whether HMRs can contribute to the potential enrichment of the soil bacterial resistome. We focused on four

SRS sites with varying levels of HMR contamination. We hypothesized that areas with elevated HMR concentrations would (1) influence the composition, diversity, and co-occurrence of bacterial and fungal communities; and (2) display significantly higher frequencies of predicted metal/antibiotic resistance genes compared to the reference site.

Methods

Study areas

The Savannah River Site (SRS) (33º00'N and 81º41W) is an approximately 800-km^2 former nuclear weapons production facility situated along the Savannah River in the upper coastal plain of South Carolina near Aiken, SC**.** The SRS is characterized as having humid, subtropical weather (Garten et al., 2000). Historically, the Savannah River Site (SRS, Aiken, SC) served as the Department of Energy (DOE) production and refinement facility for nuclear materials. As part of its mission between the 1950 through 1980s the SRS operated five nuclear reactors, nine coal-fueled power stations, a heavy-water extraction planet, nuclear fuel and target fabrication areas, waste management facilities, and additional research and administrative facilities located across the site landscape (Seaman et al., 2007). Over the years, a combination of routine operations, improper disposal practices, and incidental spills contributed to the release of organic and inorganic waste into the environment. Some of the most widespread contaminants included heavy metals, metalloids, and radionuclides which were stored in massive storage tanks, discharged to unlined seepage basins, or buried in shallow trenches (Seaman et al., 2007). In 1989, the site was officially listed on EPA's National Priorities List (NPL) due to

chemical (HMRs and solvents) and radionuclide contamination of on-site groundwater (Agency for Toxic Substances and Disease Registry, 2007).

In this study, we collected soils from four locations with habitats consisting of mixed hardwood and pine forest; three contaminated sites, and a reference site located on the Savannah River Site (SRS) (Figure 2-1). The contaminated sites included an area with elevated metal and metalloid concentrations (D-area coal-fly ash basin; AB), an area with only radionuclide contamination (Pond B; PB), and an area with both metals and radionuclide contamination (Tim's Branch; TB). Soils from the D-area ash coal-fly basins are contaminated with coal combustion waste (CCW) containing a range of metals and metalloids such as arsenic (As), chromium (Cr), cadmium (Cd), copper (Cu), iron (Fe), nickel (Ni), selenium (Se), and Zinc (Zn) (Agency for Toxic Substances and Disease Registry, 2007; Tannenbaum and Beasley, 2016). Pond B is a reservoir that was originally constructed as a secondary cooling system for nuclear production at R Reactor until it was decommissioned in 1964 (Sugg et al., 1995). Between 1961-1964 R Reactor discharged several radionuclides (e.g. ^{3}H, ^{137}Cs, ^{90}Sr, americium-241, cerium-244, and plutonium-239, 240) into Pond B as effluents. Tim's Branch is a second-order stream that receives contamination from an eroding former discharge settling pond, Steed Pond (Seaman et al., 1999). Steed Pond received up to 44,000 kg of depleted and natural uranium (U), as well as similar quantities of Ni from an aluminum-clad nuclear reactor, between 1954 and 1985 (Seaman et al., 1999). Tim's branch soils are contaminated with aluminum (Al), Cu, Cr, Zn, lead (Pb), and depleted U (Tannenbaum and Beasley, 2016). Upper Three Runs Creek (UR) a 40-km waterway that empties into the Savannah River, was used as the reference location in this study. It is the only major tributary at SRS that

has not received any thermal, chemical, or radioactive (Agency for Toxic Substances and Disease Registry, 2007).

Sample Collection and Processing

Briefly, 15g of topsoil (0 – 20-cm depth) samples were collected near GPS points previously used in a study conducted by Tannenbaum and Beasley (2016) using a 70% ethanol-sterilized garden shovel (Figure 2-1). Soil collection was staggered, with collections taking place within 10 -15 m of contaminated water bodies (Cole, 2001). All samples were placed on ice until eventual storage at -20 °C. Soil heavy metals analysis was conducted using the EPA Method 3052 with modifications (Wu et al., 1996) (Supplemental Information). All digestions were analyzed for extractable arsenic (As), cobalt (Co), copper (Cu), chromium (Cr), nickel (Ni), strontium (Sr), uranium (U), and zinc (Zn) using an inductively coupled plasma mass spectrometer (ICP-MS). Edaphic factors such as total phosphorus, total carbon, total nitrogen, and pH were analyzed using custom protocols developed by the University of Georgia Stable Isotope Ecology Laboratory. Soil total phosphorus, was conducted using acid-persulfate digestion (Nelson, 1987). Micro-Dumas combustion analysis was used for total carbon and total nitrogen analysis (Hauck, 1982; Kirsten, 1983). Soil pH was measured using a pH analyzer placed in a 1:1 mixture of soil and a 0.01 M calcium chloride solution.

DNA isolation, PCR amplification, and Illumina Sequencing of 16S rRNA and ITS amplicons

DNA was extracted from 0.5g of soil using a MoBio PowerSoil DNA isolation kit (MoBio, Carlsbad, CA, 92010, USA) and purified by a magnetic-based size selection method using SeraMag Speed Beads (Thermo-Fisher Scientific, Asheville, NC, 28804,

USA) according to the manufacturer's protocol. PCR libraries for bacterial 16S were generated using the S-D-Bact-041-b-S-17 (5'-CCTACGGGNGGCWGCAG-3') forward and S-D-Bact-0785-a-A-21 (5'-GACTACHVGGGTATCTAATCC-3') reverse primer pair (Klindworth et., 2012), which amplify an approximately 444bp fragment. Modifications to the primer sets (8 forward + 12 reverse) were done according to Taggimatrix protocol, which included fusions with universal 5' iTru sequences containing up to 96 combinations of unique internal tags (Glenn et al., 2016). DNA from each sample was PCR amplified using the 16S-iTru fusions in 25-µl reactions using the KAPA HiFi Hotstart PCR kit (KAPA Biosystems, Wilmington, MA, 01887, USA). The PCR amplification protocol was as follows: 95°C for 3 minutes, followed by 30 cycles of 95°C for 1 min, 55°C for 30 s, and 72°C for 30 s with a final elongation step of 72°C for 5 min. PCR was performed using an T100 Thermal Cycler (BioRad, Hercules, CA, 945477, USA) and amplicons were visualized using 1.5% gel electrophoresis.

Similarly, for fungi, we used Taggimatrix to generate primers for the internal transcribed spacer region (ITS), a universal locus for fungi. We selected the primer pairs ITS3_KYO2 (5'-GATGAAGAACGYAGYRAA-3') and ITS4 (5'-TCCTCCGCTTATTGATATGC-3') to amplify the ITS2 region (327.2 bp) (Toju et al., 2012; Steilow et al., 2015). DNA from each sample was PCR amplified using the ITS-iTru fusions in 25-µl reactions using the KAPA HiFi Hotstart PCR kit (KAPA Biosystems, Wilmington, MA, 01887, USA). The PCR amplification protocol was as follows: 95°C for 10 minutes, followed by 35 cycles of 94°C for 20 s, 55°C for 30 s, and 72°C for 30 s with a final elongation step of 72°C for 5 min.

All PCRs were performed using an T100 Thermal Cycler (BioRad, Hercules, CA, 945477, USA) and amplicons were visualized using 1.5% gel electrophoresis. Final PCR products were purified then quantified using a Qubit Fluorometer (Thermo-Fisher Scientific, Asheville, NC, 28804, USA) set to broad range sensitivity and diluted to a final concentration of 2 ng/µl using sterile nuclease free water. The diluted PCR amplicons were used in a second PCR reaction containing the TruSeq Illumina P5 and P7 Primers. The PCR amplification was the same as above however modified with fewer cycles (5). The quadruple-indexed libraries were purified a final time using the magnetic-bead size selection method and pooled based on the number of desired reads. PCR products were then sent to the Georgia Genomics Facility (http://dna.uga.edu) for sequencing on an Illumina MiSeq using an Illumina PE300 kit (Illumina, San Diego, CA, 92122CA, USA).

Demultiplexing and Quality Filtering

All Fastq conversion and demultiplexing were conducted using bcl2fastq (Illumina, v1.8.4) and processed to remove low quality reads (FastX toolkit). Paired-end sequencing reads were imported into Geneious v10.0 (Biomatters Limited, NJ, USA), set as paired-reads with an expected insert size and trimmed to remove Illumina adapters using default settings. Paired-end sequencing reads were then merged using the FLASH v1.2.9 plugin (Magoc and Salzberg, 2011). The software package Mr_Demuxy v1.2.0 (https://pypi.python.org/pypi/Mr_Demuxy/1.2.0) was utilized to de-multiplex the merged reads into individual combinatorially tagged FASTQ files. Sequences were filtered based on size (≥ 400 bp) and quality scores (≥Q20).

Soil Bacterial and Archaeal 16S rDNA sequence analysis

Sequencing reads were imported into the phylogenetic software package QIIME v1.9.1 (MacQiime v1.91 package: http://www.wernerlab.org/software/macqiime, Caporaso et al., 2010) for OTU (Operational Taxonomic Unit) generation, multi-leveled taxonomic classification, and diversity estimates. Briefly, samples were sorted using the *add_qiime_labels.py* script. Afterward, bacterial OTUs were selected using the *pick_open_reference_otus.py* workflow, using the Greengenes v13_8 16S reference database (http://greengenes.secondgenome.com/, DeSantis et al., 2006) and VSEARCH OTU picking strategy (Rognes et al., 2016). Taxonomy was defined using default settings of ≥97% similarity to reference sequences. In addition, we also utilized deblurring, a novel sub-operational-taxonomic approach (sOTU) to Illumina-based 16S amplicon sequencing. Deblur uses error profiles to denoise Illumina data, and is capable of differentiating amplicons by a single base pair. Deblur was used to perform a higher resolution inspection of the bacterial community (https://github.com/biocore/deblur, Amir et al., 2017).

Metagenome functional prediction with PICRUSt

The software PICRUSt (Languille et al., 2013) was applied to make gene content predictions using the Greengenes v. 13_5 reference database respectively (Supplemental Information). We were primarily interested in KEGG orthologs corresponding to HM resistance and multi-drug efflux, since prior studies have suggested they can be co-selected (Baker-Austin et al., 2006; Pal et al., 2015). A total of 37 KEGG orthologs were selected by manually searching the KEGG database (Table 1).

Soil Fungal ITS sequence analyses

Raw reads were initially combined using QIIME's *add_qiime_labels.py* script, then processed through PIPITS' funits pipeline (https://github.com/hsgweon/pipits) to extract the ITS2 region. The output from this was then processed using UCHIME in order remove potentially chimeric fungal sequences (Edgar et al., 2011). Finally, quality-filtered reads were clustered into OTUs using a VSEARCH open-reference workflow, and the UNITE database from January 31, 2016 (Nilsson et al., 2015).

Network analysis using SparCC

Phylum level OTU tables containing absolute counts from 16S sequences (archaea, bacteria) and fungal ITS sequences were merged, and then prepared for all downstream network analyses. SparCC was utilized to represent co-abundance and co-exclusion networks from all microbiota as it examines the absolute abundance of taxa. SparCC is a python based script that uses a permutation-based approach (100 repetitions) to generate (pseudo) p-values from correlations for all taxa. A network plot was generated for each soil sampling region in Cytoscape 3.5, and correlation magnitudes ≥ 0.6 (indicating strong co-abundant relationships) and ≤ -0.6 (indicating strong co-exclusion relationships) were plotted (Yueng et al., 2015).

Statistical analyses and data visualization

We used linear regression to compare metals present in the soil among different sites using JMP Pro 13 (SAS, Cary, NC USA). Trace elements were log-transformed, when necessary, to meet assumptions of normality. *Post-hoc* multiple comparisons were made using t-tests to further examine site differences in trace elements.

Within-sample (alpha) diversity was evaluated and visualized in QIIME v1.91 and the Phyloseq package using various metrics (Chao1, ACE, Fisher's Alpha, Shannon-Wiener, and Simpson) (McMurdie and Holmes, 2014). Alpha diversity of communities found in soil samples was computed using the *core_diversity_analyses.py* workflow with a sequencing depth set to 15,000 sequences. To test for the significant variation in taxonomic richness across the four sampling sites, we used the non-parametric Kruskal-Wallis test (Kruskal & Wallis, 1952) with the False Discovery Rate (FDR) correction (Stielow et al., 2011) as implemented in the *compare_alpha_diversity.py* script.

We used QIIME v1.91 to test for the significant variation in the frequency of individual OTUs across the four sites, using Kruskal-Wallis test with FDR correction for multiple comparisons, and the Monte Carlo simulated non-parametric t-test for pair-wise comparisons, as implemented in the *group_significance.py* script. Hierarchical clustering based on complete linkage was used to examine the similarity between samples, and similarity of profile analysis (SIMPROF) was used to test the significance of clusters (Clarke et al., 2008). Bray-Curtis distances between samples (beta diversity) were computed and visualized using PRIMER 7.0 software with PERMANOVA+ add-on (Primer-E, United Kingdom; Bray & Curtis, 1957). This dissimilarity matrix was used to generate a non-metric multi-dimensional scaling plot (nMDS) based on 999 permutations, which was followed by canonical analysis of principle coordinates (CAP) for testing our *a priori* hypotheses (e.g. site) (Kruskal, 1964; Anderson and Willis, 2003). Distance based redundancy analysis (dbRDA) plots were generated to visualize the direction and magnitude of the relationship between edaphic properties and HMs and the microbiota associated with the soil environments (Legendre and Anderson, 1999).

Differences in microbial community structure and composition between the four sampling sites were tested using permutational multivariate analysis of variance (PERMANOVA) on log-transformed Bray-Curtis dissimilarity values (Anderson et al., 2005). For the PERMANOVA analysis soil sampling location was a fixed effect. We used a type I partial sum of squares design and Monte Carlo sampling permutated 999 times over residuals under a full model.

The final output from PICRUSt was imported into Statistical Analysis of Metagenomic Profiles (STAMP) to examine pathways KEGG orthologs (KO) and (Parks et al., 2014). Multiple comparison analyses were conducted using a Kruskal-Wallis test with the FDR correction (Storey, 2014). Two group comparisons were conducted using a Welch's t-test with FDR correction (Satterthwaite, 1946).

Results

General characteristics of the soil samples

Soil samples displayed significant differences with respect to edaphic properties including water content, acidity, total P content, and C:N ratio (Table 2-1). Soils from Upper Three Runs were the most acidic, highest C and N, the second highest water content, and the third most total phosphorus. The Pond B soils were the least acidic, exhibited the highest water content, and lowest total P, C, and N. Soils from Tim's Branch had a significantly lower pH compared to the soils from Pond B and Ash Basins. Tim's Branch soils also exhibited the lowest water content of all the soils, and second highest total P, C, N. The soils from Ash Basins exhibited the second highest pH, second lowest water content, highest total P, and third highest C and N.

Metal concentrations in soils

Soil heavy metal concentrations from the four sampling sites are provided in Table 2-1. Pairwise comparisons varied depending on the type of HM, however generally, metals such as Sr [AB: up to 176.27 mg/kg (40.43 ± 49.24 mg/kg), TB: up to 37.90 mg/kg (25.05 ± 13.10 mg/kg)), and Co (AB: up to 18.17 mg/kg (4.53 ± 5.10 mg/kg), TB: up to 12.99 mg/kg (5.71 ± 3.38 mg/kg)] were significantly higher ($P < 0.05$) in soil samples from AB and TB, compared to PB and UR (Supplemental Information).

Soil archaeal and bacterial communities

After completing all quality filtering steps, denoising, and chimera removal in Geneious and QIIME, a dataset of 6,078,406 high quality (Q≥20) 16S rRNA gene sequences with an average read length of 458.2 ± 18.6 bp were obtained for further analyses. Analyses were performed on rarefied data using an even sampling depth of 15,000 reads per sample. A total of 311,376 OTUs (16655.36 ± 8030.35 OTUs/sample) were identified spanning 3 archaeal phyla (15 orders, 17 families) and 51 bacterial phyla (574 orders, and 559 families) (Figure 2-2). In terms of archaea, the two dominant phyla included Crenarchaeota (0.35% ± 0.40%) and Euryarchaeota (0.15% ± 0.14%). Within those phyla we identified two dominant archaeal classes from the soils, Methanomicrobia (0.096% ± 0.108%) and MGBA (0.037% ± 0.048%). In addition, we also identified a core microbiome consisting of 8 bacterial phyla (i.e. Acidobacteria, Actinobacteria, Bacteriodetes, Firmicutes, Planctomycetes, Proteobacteria, TM7, Verrucomicrobia, WPS-2) shared between 95% all the sequences analyzed in the study. In terms of relative abundance, the dominant phyla (sequences with an abundance >1%) across the four soil

sites were Proteobacteria (27.24% ± 0.02%), Acidobacteria (22.00% ± 0.04%), Actinobacteria (14.83% ± 0.02%), Planctomycetes (11.65% ± 0.01%), Verrucomicrobia (4.25% ± 0.01%), Bacteroidetes (3.00% ± 0.01%), Chloroflexi (1.85% ± 0.01%), TM7 (1.32% ± 0.00%) and Firmicutes (1.02% ± 0.01%). Compared with samples from UR, soils from AB and TB displayed significantly higher ($p < 0.05$) abundances of several bacterial orders including Rhodospirillales (Alphaproteobacteria), Solirubrobacterales (Actinobacteria), Bacillales (Firmicutes), Sphingobacteriales (Bacteroidetes), and Chthoniobacterales (Verrucomicrobia). Similarly, samples from Pond B also displayed significant differences from UR soils in several bacterial orders, but also others including Rhizobiales (Alphaproteobacteria), Pseudomanadales (Gammaproteobacteria), Burkholderiales (Betaproteobacteria), and Saprospirales (Bacteroidetes). However, much like soil samples from UR, PB soils were significantly lower ($p < 0.05$) in Bacillales (Firmicutes) compared to AB and TB. Furthermore, deblurring revealed that the most abundant phylotypes that could be assigned to a genus were *Rhodoplanes* (Alphaproteobacteria) (3.20% ± 0.01%), *Candidatus Solibacter* (2.84% ± 0.01%) (Acidobacteria), *Mycobacterium Celatum* (1.94% ± 0.00%), *Pseudomonas* (Gammaproteobacteria) (1.77% ± 3.52%), and *Candidatus Xiphinematobacter* (1.38% ± 0.01%).

Soil fungal community composition

Our fungal pipeline was similar to our bacterial one with slight modifications. After completing all quality filtering steps, dereplicating, extracting ITS2 regions using PIPITS, and chimera removal in UCHIME a dataset of 796,739 high quality (Q≥20) ITS

sequences with an average read length of 185.3 ± 37.8 bp were obtained for further analyses. Analyses were performed on rarefied data using an even sampling depth of 15,000 reads per sample. A total of 7,157 OTUs (636.56 ± 271.53 OTUs/sample) were identified spanning three fungal phyla across all the soil environments: Ascomycota (41.58% ± 2.57%), Basidiomycota (37.67% ± 6.35%), Zygomycota (4.50% ± 2.57%), Rozellomycota (0.85% ± 0.71%), Glomeromycota (0.42% ± 0.37%), and Chytridiomycota (0.08% ± 0.05%) (Figure 2-3). Furthermore, we identified a core microbiome of soil habitats shared between 95% of the sequences including species in the Ascomycota phylum (*Oidiodendron maius*, *Penicillium adametzii*, *Chaetosphaeriaceae* spp., *Trichoderma koningiopsis*, *Talaromyces calidicanius*, *Penicillium humicoloides*), Basidiomycota (*Cryptococcus podzolicus*), and Zygomycota (*Mortierella humilis*). The soil environments displayed significant differences ($P < 0.05$) between a myriad of fungal species (Figure 2-3). Compared to UR, soils from PB were significantly higher in *Hebeloma sacchariolens*, *Thelephoraceae* spp., and *Cenocccum geophilum*, as well as several others. Pairwise comparisons between UR and TB revealed significant differences in taxa such as *Russula atropurpurea*, *Wilcoxina mikolae*, *Sphaerosporella* spp., and others. In addition, pairwise comparisons between UR and AB revealed significant differences in taxa such as *Russula vesca*, *Geoglossum difforme*, *Cryptoccoccus podzolicus*, and several others.

Soil environments with elevated heavy metal contamination display significantly reduced bacterial species richness, but enriched fungal diversity

Generally, soil samples from TB and AB displayed the lowest diversity, while those from PB and UR had the highest diversity across all diversity metrics (Figure 2-4). In addition, when performing pairwise group comparisons there were significant differences in Chao1 and Faith's phylogenetic diversity when comparing the sites with the highest heavy metal contamination (AB or TB) with either PB or UR (non-parametric test with *compare_alpha_diversity.py*, $P < 0.05$) for all default QIIME diversity metrics (Supplemental Information). There were no significant differences in Chao1 or Faith's phylogenetic diversity between PB compared to UR, or TB compared to AB. The pattern for fungal communities appeared to be inversely related to the bacterial diversity, as soil samples from AB and TB displayed significantly higher fungal diversity than either PB or UR ($P < 0.05$) (Figure 2-5).

Drivers of bacterial community structure

Multivariate analyses based on the Bray-Curtis distances between 16S profiles for the four sites revealed that the sampling region had a significant effect on the observed OTUs between samples (PERMANOVA, Pseudo-F= 10.75, P= 0.001) (Table 2-2). Unconstrained nMDS plots based on a Bray-Curtis dissimilarity matrix were overlaid with SIMPROF based cluster analysis data to examine overall similarity between sites in multi-dimensional space (Figure 2-6). The nMDS plots displayed that overall the similarity between all soil groups was approximately 40% with many differences in within-group variability. Because group differences can potentially be masked by high variability and high correlation structure among unrelated variables we also applied

canonical analysis of principal coordinates (CAP) (Anderson and Willis, 2003) (Figure 2-7). The results of the CAP ordination demonstrated that both the first squared canonical correlation (σ_1^2= 0.9549) and second squared canonical correlation (σ_1^2= 0.9301) were large, indicating that the soil bacterial OTUs correlated strongly with both canonical axes. Our canonical analysis of principal coordinates (CAP) also showed that the bacterial communities clustered away from each other using location as the primary factor (our '*a priori hypothesis*'), with a slight overlap between samples from TB and AB (Figure). Vectors overlaid on the CAP plot indicated that phosphorus, Sr, Co, Ni, Cu, Zn, As were more influential in shaping bacterial communities in TB and AB soils, while moisture content and pH were more influential in bacterial communities in PB soils. Lead was more influential in shaping bacterial communities in UR soils.

To further identify the key drivers of soil bacterial community structure for the soils collected from the four sites at the SRS, we also performed a distance-based linear model (DistLM), which is an extension of distance-based redundancy analysis (dbRDA). We were specifically interested in the fitting the edaphic properties (soil pH, moisture content, total phosphorus, and C:N ratio) as well as the soil heavy metal concentrations to the dbRDA ordination. Our DistLM analysis revealed that pH, C:N ratio, Co, Ni, As, Zn, Sr, and PB explained 40% (R^2 sequential) of the observed total variation in the composition of the bacterial community in the soils (Table 2-3). Using these factors the primary and secondary axes of the dbRDA explains 28.5% of the total variation, and 70.5% of the fitted variation (Figure 2-8). In general, the longer vectors for soil moisture content and C:N ratios suggest these variables are strongly correlated with the bacterial community structure at PB. The vectors for moisture content and zinc suggest these

variables are strongly correlated with the community structure at UR. The soils from AB and TB were more strongly correlated with HMs, especially strontium, however there were some exceptions. Cobalt was more influential in community structure in TB soils, while zinc and lead were larger factors in AB soils.

Drivers of fungal community structure

Multivariate analyses based on the Bray-Curtis distances between ITS profiles, indicated the sampling region had significant effect on the observed OTUs between samples (PERMANOVA, Pseudo-F= 6.2608, P= 0.001) (Table 2-4). Unconstrained nMDS plots revealed that overall the similarity between all soil groups was approximately 20% with many differences in within-group variability (Figure 2-9). Canonical analysis of principal coordinates was again applied and results of the CAP ordination demonstrated the fungal communities from the four sites were highly correlated with both canonical axes: axis 1 (σ_1^2= 0.9431) and axis 2 (σ_1^2= 0.8955). Our canonical analysis of principal coordinates (CAP) indicated that fungal communities clustered away from each other using location as the primary factor (our '*a priori hypothesis*'), with communities from TB and AB displaying very slight overlap (Figure 2-10).

Lastly, we also applied a constrained ordination method (dbRDA) to determine if the fungal communities were driven by the same environmental factors as the bacterial communities. Both dbRDA axes collectively explained 19.2% of the total variation, and 53.9% of the fitted variation (Figure 2-11). Our DistLM analysis revealed that total phosphorus, pH, moisture, Cr, Co, Ni, Cu, Zn, As, Sr, Pb, U, and C:N explained approximately 35.6% (R^2 sequential) of the observed total variation in fungal community

structure (Table 2-5). In general, fungal communities from UR and TB appeared to be influenced by metals such as As and U, while those from PB were more influenced by cobalt. Finally, fungal communities from TB appeared to be more strongly influenced by the soil moisture.

Co-abundance of archaeal, bacterial and fungal communities

SparCC was utilized to explore co-abundance relationships between microbial OTUs (at the phylum level) detected in the soils from the four sampling regions. Over 400 significant relationships were observed in total. A co-abundance network for each site was plotted including all observed microbial phyla (Figure 2-11, 2-12, 2-13). Our comparisons revealed several positive associations between OTUs within the same domain across all sites, however positive correlations between OTUs in different domains appeared to be site-specific. For example, soil samples from UR show very strong interactions between Acidobacteria and Proteobacteria with Basidiomycetes ($r= 0.819$, $P= 0.04$; $r= 0.792$, $P= 0.02$) (Table 2-6). In samples from PB there were strong interactions between Plantomycetes and Ascomycota ($r= 0.652$, $P= 0.01$) (Table 2-7). Soil samples from TB displayed strong interactions between Crenarchaeota and Acidobacteria ($r = 0.771$, $P= 0.01$) (Table 2-8). Finally, samples from AB the phyla Actinobacteria and Basidiomycetes ($r= 0.654$); as well as Armatimonadetes and Zygomycota ($r= 0.615$, $P= 0.01$) displayed strong interactions (Table 2-9).

Inferring soil environmental metagenomes using PICRUSt

The mean weighted nearest sequenced taxon index (NSTI), which measures the prediction accuracy of PICRUSt, of our 75 soil samples was 0.17 ± 0.02. We were initially interested in examining the proportion of sequences for various KEGG pathways.

The pathways that demonstrated significant differences among all sites are provided in Table 2-10. In addition, we were specifically interested in pathways that might be potentially beneficial to bacteria in environments under heavy metal stress. The relative abundance of the predicted pathway "Cell Communication" (P= 1.10e-6, FDR corrected) was highest in soils from AB and TB (Figure 2-16). In addition, two pathways, "Membrane Transport" (P= 8.23-3, FDR corrected) and "Xenobiotic Biodegradation and Metabolism" (P= 8.04e-3, FDR corrected) were highest in samples from TB (Figure 2-17; 2-18).

We also examined the relative abundance of predicted genes for metal and antibiotic resistance (Figure 2-19). In general, we detected a number of predicted genes across all of the sites, however, the proportion of sequences for certain genes relative to each site was not easily discernable visually. Hence, a heatmap was utilized to see distinctions between each site (Figure 2-20). In addition, we performed a non-parametric Kruskal-Wallis test to identify differences in the selected KEGG orthologs (KOs) between all four sites. We found significant differences in the relative abundance of sequences for 28 of the 35 selected KEGG orthologs ($P < 0.01$, FDR corrected) (Table 2-11). Pair-wise comparisons using Welch's t-test between HM contaminated sites (AB, TB, PB) and the reference site revealed that there were significant differences in the relative abundance of multiple KOs. Two predicted genes related to antibiotic and heavy metal resistance genes, emrB (K07644) and cusS (K07644) respectively, were significantly enriched in soils from AB and PB compared to the reference site (UR) (Figure 2-20; 2-21). Interestingly, the soil samples from TB contained the greatest number of predicted genes compared to the reference site (UR) (Figure 2-22). Predicted

genes corresponding to copper resistance (K14166; K06189) and antibiotic resistance (K07788, K07789) among several others were significantly enriched in TB soils. In addition, in order to determine the OTUs that contributed the largest proportion of predicted genes from the soils from each of the four sites we utilized PICRUSt's predict metagenome contributions script. We observed that bacterial taxa such as *Ktedonobacteraceae*, *Solibacteracea*, *Pseudomonas viridiflava*, *Pseudomonas* spp., *Spingomonadales*, *Bradyrhizobiaceae*, and *Spartobacteria* contributed the greatest number of metal and antibiotic resistance genes. A table of specific OTU contributions to each KO term was also generated (Supplemental File).

Discussion

Bacterial and fungal diversity were inversely correlated with respect to HM contamination

In our study, heavy metal contamination within the SRS is distributed non-uniformly, and is largely confined to various hotspots, such as near the effluent channels for waste water at D-Area (AB), within the floodplain of Tim's Branch (TB), or the sediments of Pond B (PB). Our results generally supported our hypothesis that HMs would impact the soil community structure and microbial diversity, as all the contaminated sites (in order: AB, TB, PB) had lower diversity indices compared to the reference site (UR). We also observed significant differences in fungal community diversity. Specifically, the fungal diversity from AB and TB were higher than either UR or PB. Heavy metals are known to affect bacteria and fungi in soil differently. In fact, several studies have reported that when bacterial functional diversity decreases, fungal

diversity can increase with respect to increasing metal concentrations in the soil (Rajapaksha et al., 2004; Stefanowicz et al., 2008).

Microbial community structure is influenced by heavy metals

Our DistLM and dbRDA analysis revealed strong correlations between edaphic properties and the metal concentrations with the bacterial communities present in the soils. A moderate fraction of the total variation (40%) in the SRS soils was explained by C:N ratio, Co, Ni, As, Zn, Sr, and Pb. Previous studies on soils suggest that pH is one of the primary predictors of bacterial community structure (Fierer and Jackson et al., 2006; Lauber et al., 2009; Wu et al., 2013). However, despite significance differences in soil pH between the four SRS sites, other edaphic factors as well as HMs appeared to be stronger drivers of bacterial community structure. It should be noted that although the results were significant and supported our hypothesis (i.e. HMs would predict the structure of bacterial communities) the data should be viewed with caution as it does not directly imply causality. For instance, despite the fitted model in the dbRDA plot displaying a large percentage of explained variation in the soil using the edaphic properties and HMs data provided, the total percent variation explained was very low. This suggests that there are confounding factors not measured in this study which could also contribute to soil bacterial community structure and diversity. Additional factors known to influence the communities includes soil depth, soil type, salinity, porosity, sulfur, nitrogen, trace minerals, temperature, dead organic matter (DOM), and presence of fungi and plants (Wieland et al., 2001; Zhou et al., 2002; Guan et al., 2013; Dotaniya and Meena, 2015; Kaiser et al., 2016). Furthermore, we observed that factors such as HMs and/or edaphic properties had more modest effects on the fungal community structure. It is possible that

the soil fungal communities are less sensitive to variations in edaphic factors or the presence of metals compared to bacteria. Lastly, our SparCC analyses suggest that the presence of HMs as well as other edaphic factors may have important roles in shaping the co-abundance and co-exclusion relationships between microbial OTUs from different domains. The ability to resolve co-occurrence patterns between the predominant soil microbiota is an important strategy for studying the ecology of these communities with respect to environmental factors.

Heavy metal contamination may enrich soil resistome

Lastly, we evaluated the capacity of the contaminated soils as reservoirs of metal and antibiotic resistance. Soils are heterogeneous habitats that are known to contain extremely large genetic diversity at very small spatial scales (Nesme and Simonet, 2015). Thus, soils have the capacity to support the rapid exchange of genetic material via horizontal gene exchange (HGT) from other bacteria. This soil 'resistome' containing the gene products of millions of bacteria is speculated to be a large source of resistance gene determinants. Also, because previous studies have indicated that antibiotic resistance can be indirectly co-selected through exposures to HMs we hypothesized that microbes in soil environments with HM contaminants would display significantly enriched metal resistance (MRGs) and antibiotic (ARGs) resistance genes. To that end, we utilized PICRUSt to infer a functional metagenome. Although correlations between environmental HMs and microbial relative abundance suggest a potential role of HMs in shaping overall community structure and diversity we thought examining the functional metagenome might better illuminate the community's physiological response to the contaminants, and hence whether the HMs had a true biological effect.

Our predictive functional profiling results displayed the same prediction accuracy as the original Langille et al. (2013) study (NSTI = 0.17 ± 0.02), which demonstrated a strong correlation between inferred metagenomes using 16S rDNA sequences and shotgun metagenome data from soils. Although, caution must be taken when using predictive functional profiling, our results indicate a strong association between the presence of HMs and several pathways and genes we hypothesized would be enriched. For example, the "Cell Communication" pathway (P= 1.10e-6, FDR corrected) is linked to capacity of certain microbes such as *Pseudomonas* spp. or *E. coli* to synthesize biofilms, a strategy that protects bacteria from environmental stress and antimicrobials. The "Membrane Transport" category includes several microbial pathways such as the ATP-binding cassette (ABC) transporters and bacterial secretion systems that enable the active transport of a wide variety of substrates including lipids, sugars, heavy metals, and drugs (Davidson and Chen, 2004). These transporters are also important in regulating virulence factors (Davidson and Chen, 2004). The "Xenobiotic Biodegradation and Metabolism" category contains several pathways for the degradation of pesticides, drugs, polyaromatic hydrocarbons (PAHs) and other potential environmental insults. These three pathways were all significantly enriched from the sites with heavy metal burden.

In addition, we hypothesized the sites with higher HM concentrations in the soils would display an enriched number of predicted MRGs and ARGs. Our results indicated that many of the selected genes were present in all of the soil samples, particularly emrB (multidrug efflux), cusR (copper and silver resistance), and HME family (heavy metal efflux) genes which had relative abundances of between 10 and 15 percent. These results are not particularly surprising given that antibiotic resistance occurs naturally in soils. In

addition, the heavy metal efflux (HME) gene has several metal resistance homologs in the larger resistance nodulation division (RND) superfamily, and are widespread in a myriad of bacteria. These resistance systems can also be highly specialized and only occur in a few taxa (Nies et al., 2003). Our results also indicated that although the occurrence of predicted resistance genes was widespread, the sites with chronic HM contamination displayed small but significant differences in certain genes such as corC and ycnj (copper resistance); smvA (antimicrobial resistance); yebQ (multidrug efflux); mmr (methylenomycin A resistance); nixA (nickel transport) and several others. Lastly, our predicted metagenome contributions illustrated that our selected resistance genes were presence in a variety of soil bacteria such as *Ktedonobacteraceae*, *Pseudomonas* spp*., Solibacteraceae*, *Bradyrhizobiaceae*, *Spartobacteria*, *Koribacteraceae*, *Acidobacteria*, and several others that are known to possess tolerance toward heavy metals (Sangwan et al., 2004; Barns et al., 2007; Delmont et al., 2015; Pitondo-Silva et al., 2016).

Conclusion

In summary, our study demonstrated strong associations between the microbial community in soils at the SRS, and the presence of chronic HM contamination. We found that bacterial and fungal communities are differentially affected by edaphic factors and HM contamination. Finally, our study demonstrates that heavy metals may have an important role in shaping the functional community, particularly in terms of bacterial-derived AMR. Our results indicated that antibiotic and heavy metal resistance is ubiquitous and widespread even in relatively pristine environments. Moreover, the

intrinsic resistance of soil communities could be potentially magnified in the presence of HM contamination as illustrated by the small but significantly higher relative abundance of predicted resistance genes at contaminated SRS sites (Figure 2-16). Because the soil environment is an important reservoir for antimicrobial resistance determinants (ARGs and MRGs) it represents an ecosystem with significant public and environmental health implications. This is especially true if anthropogenic activities can accelerate the enrichment and dissemination of antimicrobial resistance.

Acknowledgments

We thank our colleagues in the Department of Environmental Health Science, the Georgia Genomics Facility and Savannah River Ecology Laboratory for assistance with sampling and data collection. This research was supported by a contract from the US Department of Energy through Cooperative Agreement number DE-FC09-07SR22506 with the University of Georgia Research Foundation.

Disclaimer

United States Government or any agency thereof. The views and opinions of authors expressed herein do not necessarily state or reflect those of the United States Government or any agency thereof.

References

Aiken, South Carolina. "Evaluation of off-site groundwater and surface water contamination at the Savannah River Site (DOE)," 2007. https://pdfs.semanticscholar.org/cf1b/9e3bf81b26cf0fb83b113966e3d1c3912516.pdf.

Amir, Amnon, Daniel McDonald, Jose A. Navas-Molina, Evguenia Kopylova, James T. Morton, Zhenjiang Zech Xu, Eric P. Kightley, et al. "Deblur Rapidly Resolves Single-Nucleotide Community Sequence Patterns." *mSystems* 2, no. 2 (April 21, 2017): e00191-16. doi:10.1128/mSystems.00191-16.

Anahid, S., S. Yaghmaei, and Z. Ghobadinejad. "Heavy Metal Tolerance of Fungi." *Scientia Iranica* 18, no. 3 (June 2011): 502–8. doi:10.1016/j.scient.2011.05.015.

Anderson, Marti J. "Permutational Multivariate Analysis of Variance." *Department of Statistics, University of Auckland, Auckland* 26 (2005): 32–46.

Anderson, Marti J., and Trevor J. Willis. "Canonical analysis of principal coordinates: a useful method of constrained ordination for ecology." *Ecology* 84, no. 2 (February 2003): 511–25. doi:10.1890/0012-9658(2003)084[0511:CAOPCA]2.0.CO;2.

Arao, Tomohito, Satoru Ishikawa, Masaharu Murakami, Kaoru Abe, Yuji Maejima, and Tomoyuki Makino. "Heavy Metal Contamination of Agricultural Soil and Countermeasures in Japan." *Paddy and Water Environment* 8, no. 3 (September 1, 2010): 247–57. doi:10.1007/s10333-010-0205-7.

Arey, J. Samuel, John C. Seaman, and Paul M. Bertsch. "Immobilization of Uranium in Contaminated Sediments by Hydroxyapatite Addition." *Environmental Science & Technology* 33, no. 2 (January 1, 1999): 337–42. doi:10.1021/es980425+.

Ayangbenro, Ayansina Segun, and Olubukola Oluranti Babalola. "A New Strategy for Heavy Metal Polluted Environments: A Review of Microbial Biosorbents." *International Journal of Environmental Research and Public Health* 14, no. 1 (January 2017). doi:10.3390/ijerph14010094.

Azarbad, Hamed, Maria Nikliska, Ryszard Laskowski, Nico M. van Straalen, Cornelis A. M. van Gestel, Jizhong Zhou, Zhili He, Chongqing Wen, and Wilfred F. M. Röling. "Microbial Community Composition and Functions Are Resilient to Metal Pollution along Two Forest Soil Gradients." *FEMS Microbiology Ecology* 91, no. 1 (January 1, 2015): 1–11. doi:10.1093/femsec/fiu003.

Baker-Austin, C., Wright, M. S., Stepanauskas, R., & McArthur, J. V. "Co-selection of antibiotic and metal resistance." *Trends in Microbiology*, *14*, no. 4 (April, 1, 2006): 176–182. doi:/10.1016/j.tim.2006.02.006

Baldrian, Petr. "Effect of Heavy Metals on Saprotrophic Soil Fungi." In *Soil Heavy Metals*, 263–79. Soil Biology 19. Springer Berlin Heidelberg, 2010. doi:10.1007/978-3-642-02436-8_12.

Barns, Susan M., Elizabeth C. Cain, Leslie Sommerville, and Cheryl R. Kuske. "Acidobacteria Phylum Sequences in Uranium-Contaminated Subsurface Sediments Greatly Expand the Known Diversity within the Phylum." *Applied and Environmental Microbiology* 73, no. 9 (May 1, 2007): 3113–16. doi:10.1128/AEM.02012-06.

Bourceret, Amélia, Aurélie Cébron, Emilie Tisserant, Pascal Poupin, Pascale Bauda, Thierry Beguiristain, and Corinne Leyval. "The Bacterial and Fungal Diversity of an Aged PAH- and Heavy Metal-Contaminated Soil Is Affected by Plant Cover

and Edaphic Parameters." *Microbial Ecology* 71, no. 3 (April 1, 2016): 711–24. doi:10.1007/s00248-015-0682-8.

Bray, J. Roger, and J. T. Curtis. "An Ordination of the Upland Forest Communities of Southern Wisconsin." *Ecological Monographs* 27, no. 4 (February 1, 1957): 325–49. doi:10.2307/1942268.

Brofft, Jennifer E., J. Vaun McArthur, and Lawrence J. Shimkets. "Recovery of Novel Bacterial Diversity from a Forested Wetland Impacted by Reject Coal." *Environmental Microbiology* 4, no. 11 (November 1, 2002): 764–69. doi:10.1046/j.1462-2920.2002.00337.x.

Chen, Ming, Piao Xu, Guangming Zeng, Chunping Yang, Danlian Huang, and Jiachao Zhang. "Bioremediation of Soils Contaminated with Polycyclic Aromatic Hydrocarbons, Petroleum, Pesticides, Chlorophenols and Heavy Metals by Composting: Applications, Microbes and Future Research Needs." *Biotechnology Advances* 33, no. 6, Part 1 (November 1, 2015): 745–55. doi:10.1016/j.biotechadv.2015.05.003.

Chodak, Marcin, Marcin Gołębiewski, Justyna Morawska-Płoskonka, Katarzyna Kuduk, and Maria Niklińska. "Diversity of Microorganisms from Forest Soils Differently Polluted with Heavy Metals." *Applied Soil Ecology* 64 (February 1, 2013): 7–14. doi:10.1016/j.apsoil.2012.11.004.

Clarke, K. Robert, Paul J. Somerfield, and Raymond N. Gorley. "Testing of Null Hypotheses in Exploratory Community Analyses: Similarity Profiles and Biota-Environment Linkage." *Journal of Experimental Marine Biology and Ecology*,

Marine ecology: A tribute to the life and work of John S. Gray, 366, no. 1 (November 15, 2008): 56–69. doi:10.1016/j.jembe.2008.07.009.

Russell G. Cole (2001) Staggered nested designs to identify hierarchical scales of variability, New Zealand Journal of Marine and Freshwater Research, 35:5, 891-896, DOI: 10.1080/00288330.2001.9517051

Congeevaram, Shankar, Sridevi Dhanarani, Joonhong Park, Michael Dexilin, and Kaliannan Thamaraiselvi. "Biosorption of Chromium and Nickel by Heavy Metal Resistant Fungal and Bacterial Isolates." *Journal of Hazardous Materials* 146, no. 1–2 (July 19, 2007): 270–77. doi:10.1016/j.jhazmat.2006.12.017.

Davidson, Amy L., and Jue Chen. "ATP-Binding Cassette Transporters in Bacteria." *Annual Review of Biochemistry* 73, no. 1 (2004): 241–68. doi:10.1146/annurev.biochem.73.011303.073626.

Delmont, Tom O., A. Murat Eren, Lorrie Maccario, Emmanuel Prestat, Özcan C. Esen, Eric Pelletier, Denis Le Paslier, Pascal Simonet, and Timothy M. Vogel. "Reconstructing Rare Soil Microbial Genomes Using in Situ Enrichments and Metagenomics." *Frontiers in Microbiology* 6 (2015). doi:10.3389/fmicb.2015.00358.

Dotaniya, M. L., and V. D. Meena. "Rhizosphere Effect on Nutrient Availability in Soil and Its Uptake by Plants: A Review." *Proceedings of the National Academy of Sciences, India Section B: Biological Sciences* 85, no. 1 (March 1, 2015): 1–12. doi:10.1007/s40011-013-0297-0.

Epelde, Lur, Anders Lanzén, Fernando Blanco, Tim Urich, and Carlos Garbisu. "Adaptation of Soil Microbial Community Structure and Function to Chronic

Metal Contamination at an Abandoned Pb-Zn Mine." *FEMS Microbiology Ecology* 91, no. 1 (January 1, 2015): 1–11. doi:10.1093/femsec/fiu007.

Fierer, Noah, and Robert B. Jackson. "The Diversity and Biogeography of Soil Bacterial Communities." *Proceedings of the National Academy of Sciences of the United States of America* 103, no. 3 (January 17, 2006): 626–31. doi:10.1073/pnas.0507535103.

Fomina, M. A., I. J. Alexander, J. V. Colpaert, and G. M. Gadd. "Solubilization of Toxic Metal Minerals and Metal Tolerance of Mycorrhizal Fungi." *Soil Biology and Biochemistry* 37, no. 5 (May 1, 2005): 851–66. doi:10.1016/j.soilbio.2004.10.013.

Gadd, Geoffrey M. "Microorganisms in Toxic Metal-Polluted Soils." In *Microorganisms in Soils: Roles in Genesis and Functions*, edited by Professor Dr Ajit Varma and ProfessorDr Francois Buscot, 325–56. Soil Biology 3. Springer Berlin Heidelberg, 2005. doi:10.1007/3-540-26609-7_16.

Guan, Xiangyu, Jinfeng Wang, Hui Zhao, Jianjun Wang, Ximing Luo, Fei Liu, and Fangqing Zhao. "Soil Bacterial Communities Shaped by Geochemical Factors and Land Use in a Less-Explored Area, Tibetan Plateau." *BMC Genomics* 14 (November 22, 2013): 820. doi:10.1186/1471-2164-14-820.

Hong, Chen, Yanxiao Si, Yi Xing, and Yang Li. "Illumina MiSeq Sequencing Investigation on the Contrasting Soil Bacterial Community Structures in Different Iron Mining Areas." *Environmental Science and Pollution Research* 22, no. 14 (July 1, 2015): 10788–99. doi:10.1007/s11356-015-4186-3.

Iram, Shazia, Ayesha Zaman, Zaiba Iqbal, and Rabia Shabbir. "Heavy Metal Tolerance of Fungus Isolated from Soil Contaminated with Sewage and Industrial

Wastewater." *Polish Journal of Environmental Studies* 22, no. 3 (2013). http://www.pjoes.com/pdf/22.3/Pol.J.Environ.Stud.Vol.22.No.3.691-697.pdf.

Izah, Sylvester, Iniobong Inyang, Tariwari Angaye, and Ifeoma Okowa. "A Review of Heavy Metal Concentration and Potential Health Implications of Beverages Consumed in Nigeria." *Toxics* 5, no. 1 (December 22, 2016): 1. doi:10.3390/toxics5010001.

Jie, Shiqi, Mingming Li, Min Gan, Jianyu Zhu, Huaqun Yin, and Xueduan Liu. "Microbial Functional Genes Enriched in the Xiangjiang River Sediments with Heavy Metal Contamination." *BMC Microbiology* 16 (2016): 179. doi:10.1186/s12866-016-0800-x.

Jose, Jiya, Rajesh Giridhar, Abdulaziz Anas, P. A. Loka Bharathi, and Shanta Nair. "Heavy Metal Pollution Exerts Reduction/Adaptation in the Diversity and Enzyme Expression Profile of Heterotrophic Bacteria in Cochin Estuary, India." *Environmental Pollution*, Nitrogen Deposition, Critical Loads and Biodiversity, 159, no. 10 (October 2011): 2775–80. doi:10.1016/j.envpol.2011.05.009.

Kaiser, Kristin, Bernd Wemheuer, Vera Korolkow, Franziska Wemheuer, Heiko Nacke, Ingo Schöning, Marion Schrumpf, and Rolf Daniel. "Driving Forces of Soil Bacterial Community Structure, Diversity, and Function in Temperate Grasslands and Forests." *Scientific Reports* 6 (September 21, 2016): srep33696. doi:10.1038/srep33696.

Kavamura, Vanessa Nessner, and Elisa Esposito. "Biotechnological Strategies Applied to the Decontamination of Soils Polluted with Heavy Metals." *Biotechnology Advances* 28, no. 1 (January 2010): 61–69. doi:10.1016/j.biotechadv.2009.09.002.

Kruskal, Joseph B. “Multidimensional Scaling by Optimizing Goodness of Fit to a Nonmetric Hypothesis.” *Psychometrika* 29, no. 1 (1964): 1–27.

Kruskal, William H., and W. Allen Wallis. “Use of Ranks in One-Criterion Variance Analysis.” *Journal of the American Statistical Association* 47, no. 260 (December 1, 1952): 583–621. doi:10.1080/01621459.1952.10483441.

Lauber, Christian L., Micah Hamady, Rob Knight, and Noah Fierer. “Pyrosequencing-Based Assessment of Soil pH as a Predictor of Soil Bacterial Community Structure at the Continental Scale.” *Applied and Environmental Microbiology* 75, no. 15 (August 1, 2009): 5111–20. doi:10.1128/AEM.00335-09.

Legendre, Pierre, and Marti J. Anderson. “Distance-Based Redundancy Analysis: Testing Multispecies Responses in Multifactorial Ecological Experiments.” *Ecological Monographs* 69, no. 1 (1999): 1–24.

Li, Hai-Yan, Dong-Wei Li, Cai-Mei He, Zuo-Ping Zhou, Tao Mei, and Hong-Mei Xu. “Diversity and Heavy Metal Tolerance of Endophytic Fungi from Six Dominant Plant Species in a Pb–Zn Mine Wasteland in China.” *Fungal Ecology*, The Secret World of Endophytes, 5, no. 3 (June 2012): 309–15. doi:10.1016/j.funeco.2011.06.002.

Li, Xian-Zhi, Christopher A. Elkins, and Helen I. Zgurskaya. *Efflux-Mediated Antimicrobial Resistance in Bacteria: Mechanisms, Regulation and Clinical Implications*. Springer, 2016.

Magoč, Tanja, and Steven L. Salzberg. “FLASH: Fast Length Adjustment of Short Reads to Improve Genome Assemblies.” *Bioinformatics (Oxford, England)* 27, no. 21 (November 1, 2011): 2957–63. doi:10.1093/bioinformatics/btr507.

McMurdie, Paul J., and Susan Holmes. "Phyloseq: An R Package for Reproducible Interactive Analysis and Graphics of Microbiome Census Data." Edited by Michael Watson. *PLoS ONE* 8, no. 4 (April 22, 2013): e61217. doi:10.1371/journal.pone.0061217.

Nesme, Joseph, and Pascal Simonet. "The Soil Resistome: A Critical Review on Antibiotic Resistance Origins, Ecology and Dissemination Potential in Telluric Bacteria." *Environmental Microbiology* 17, no. 4 (April 1, 2015): 913–30. doi:10.1111/1462-2920.12631.

Nies, Dietrich H. "Efflux-Mediated Heavy Metal Resistance in Prokaryotes." *FEMS Microbiology Reviews* 27, no. 2–3 (June 1, 2003): 313–39. doi:10.1016/S0168-6445(03)00048-2.

Pal, Chandan, Johan Bengtsson-Palme, Erik Kristiansson, and D. G. Joakim Larsson. "Co-Occurrence of Resistance Genes to Antibiotics, Biocides and Metals Reveals Novel Insights into Their Co-Selection Potential." *BMC Genomics* 16 (November 17, 2015): 964. doi:10.1186/s12864-015-2153-5.

Parks, Donovan H., Gene W. Tyson, Philip Hugenholtz, and Robert G. Beiko. "STAMP: Statistical Analysis of Taxonomic and Functional Profiles." *Bioinformatics* 30, no. 21 (November 1, 2014): 3123–24. doi:10.1093/bioinformatics/btu494.

Perrin, Elena, Marco Fondi, Maria Cristiana Papaleo, Isabel Maida, Silvia Buroni, Maria Rosalia Pasca, Giovanna Riccardi, and Renato Fani. "Exploring the HME and HAE1 Efflux Systems in the Genus Burkholderia." *BMC Evolutionary Biology* 10 (June 3, 2010): 164. doi:10.1186/1471-2148-10-164.

Pitondo-Silva, André, Guilherme Bartolomeu Gonçalves, and Eliana Guedes Stehling. "Heavy Metal Resistance and Virulence Profile in Pseudomonas Aeruginosa Isolated from Brazilian Soils." *APMIS* 124, no. 8 (August 1, 2016): 681–88. doi:10.1111/apm.12553.

Rajapaksha, R. M. C. P., M. A Tobor-Kapłon, and E. Bååth. "Metal Toxicity Affects Fungal and Bacterial Activities in Soil Differently." *Applied and Environmental Microbiology* 70, no. 5 (May 2004): 2966–73. doi:10.1128/AEM.70.5.2966-2973.2004.

Rognes, Torbjørn, Tomáš Flouri, Ben Nichols, Christopher Quince, and Frédéric Mahé. "VSEARCH: A Versatile Open Source Tool for Metagenomics." PeerJ Preprints, September 6, 2016. doi:10.7287/peerj.preprints.2409v1.

Sandaa, Ruth-Anne, Vigdis Torsvik, Øivind Enger, Frida Lise Daae, Tonje Castberg, and Dittmar Hahn. "Analysis of Bacterial Communities in Heavy Metal-Contaminated Soils at Different Levels of Resolution." *FEMS Microbiology Ecology* 30, no. 3 (November 1, 1999): 237–51. doi:10.1111/j.1574-6941.1999.tb00652.x.

Sangwan, Parveen, Xiaolei Chen, Philip Hugenholtz, and Peter H. Janssen. "Chthoniobacter Flavus Gen. Nov., Sp. Nov., the First Pure-Culture Representative of Subdivision Two, Spartobacteria Classis Nov., of the Phylum Verrucomicrobia." *Applied and Environmental Microbiology* 70, no. 10 (October 2004): 5875–81. doi:10.1128/AEM.70.10.5875-5881.2004.

Seaman, J. C., B. B. Looney, and M. K. Harris. "Research in Support of Remediation Activities at the Savannah River Site." *Vadose Zone Journal* 6, no. 2 (May 1, 2007): 316–26. doi:10.2136/vzj2007.0044.

Seiler, Claudia, and Thomas U. Berendonk. "Heavy Metal Driven Co-Selection of Antibiotic Resistance in Soil and Water Bodies Impacted by Agriculture and Aquaculture." *Frontiers in Microbiology* 3 (December 14, 2012). doi:10.3389/fmicb.2012.00399.

Stefanowicz, Anna M., Maria Niklińska, and Ryszard Laskowski. "Metals Affect Soil Bacterial and Fungal Functional Diversity Differently." *Environmental Toxicology and Chemistry* 27, no. 3 (March 1, 2008): 591–98. doi:10.1897/07-288.1.

Stielow, J. B., C. A. Lévesque, K. A. Seifert, W. Meyer, L. Iriny, D. Smits, R. Renfurm, et al. "One Fungus, Which Genes? Development and Assessment of Universal Primers for Potential Secondary Fungal DNA Barcodes." *Persoonia* 35 (December 2015): 242–63. doi:10.3767/003158515X689135.

Storey, John D. "False Discovery Rate." In *International Encyclopedia of Statistical Science*, edited by Miodrag Lovric, 504–8. Springer Berlin Heidelberg, 2011. doi:10.1007/978-3-642-04898-2_248.

Sun, Melanie Y., Katherine A. Dafforn, Mark V. Brown, and Emma L. Johnston. "Bacterial Communities Are Sensitive Indicators of Contaminant Stress." *Marine Pollution Bulletin* 64, no. 5 (May 1, 2012): 1029–38. doi:10.1016/j.marpolbul.2012.01.035.

Tannenbaum, Lawrence V., and James C. Beasley. "Validating Mammalian Resistance to Stressor-Mediated Reproductive Impact Using Rodent Sperm Analysis." *Ecotoxicology (London, England)* 25, no. 3 (April 2016): 584–93. doi:10.1007/s10646-016-1617-y.

Teaf, Christopher M., Douglas J. Covert, Patrick A. Teaf, Emily Page, and Michael J. Starks. "Arsenic Cleanup Criteria for Soils in the US and Abroad: Comparing Guidelines and Understanding Inconsistencies." In *Proceedings of the Annual International Conference on Soils, Sediments, Water and Energy*, 15:10, 2010. http://scholarworks.umass.edu/soilsproceedings/vol15/iss1/10/.

Toju, Hirokazu, Akifumi S. Tanabe, Satoshi Yamamoto, and Hirotoshi Sato. "High-Coverage ITS Primers for the DNA-Based Identification of Ascomycetes and Basidiomycetes in Environmental Samples." *PLoS ONE* 7, no. 7 (July 12, 2012). doi:10.1371/journal.pone.0040863.

Tuckfield, R. Cary, and J. Vaun McArthur. "Spatial Analysis of Antibiotic Resistance Along Metal Contaminated Streams." *Microbial Ecology* 55, no. 4 (May 1, 2008): 595–607. doi:10.1007/s00248-007-9303-5.

Wales, Andrew, and Robert Davies. "Co-Selection of Resistance to Antibiotics, Biocides and Heavy Metals, and Its Relevance to Foodborne Pathogens." *Antibiotics* 4, no. 4 (November 13, 2015): 567–604. doi:10.3390/antibiotics4040567.

Wang, Jianlong, and Can Chen. "Biosorption of Heavy Metals by Saccharomyces Cerevisiae: A Review." *Biotechnology Advances* 24, no. 5 (September 2006): 427–51. doi:10.1016/j.biotechadv.2006.03.001.

Wang, YuanPeng, JiYan Shi, Hui Wang, Qi Lin, XinCai Chen, and YingXu Chen. "The Influence of Soil Heavy Metals Pollution on Soil Microbial Biomass, Enzyme Activity, and Community Composition near a Copper Smelter." *Ecotoxicology and Environmental Safety* 67, no. 1 (May 1, 2007): 75–81. doi:10.1016/j.ecoenv.2006.03.007.

Wieland, Gabriele, Regine Neumann, and Horst Backhaus. "Variation of Microbial Communities in Soil, Rhizosphere, and Rhizoplane in Response to Crop Species, Soil Type, and Crop Development." *Applied and Environmental Microbiology* 67, no. 12 (December 1, 2001): 5849–54. doi:10.1128/AEM.67.12.5849-5854.2001.

Wu, Yucheng, Jun Zeng, Qinghe Zhu, Zhenfa Zhang, and Xiangui Lin. "pH Is the Primary Determinant of the Bacterial Community Structure in Agricultural Soils Impacted by Polycyclic Aromatic Hydrocarbon Pollution." *Scientific Reports* 7 (January 4, 2017): srep40093. doi:10.1038/srep40093.

Wuana, Raymond A., and Felix E. Okieimen. "Heavy Metals in Contaminated Soils: A Review of Sources, Chemistry, Risks and Best Available Strategies for Remediation." Research article. *International Scholarly Research Notices*, 2011. doi:10.5402/2011/402647.

Xie, Yan, Jibiao Fan, Weixi Zhu, Erick Amombo, Yanhong Lou, Liang Chen, and Jinmin Fu. "Effect of Heavy Metals Pollution on Soil Microbial Diversity and Bermudagrass Genetic Variation." *Frontiers in Plant Science* 7 (May 31, 2016). doi:10.3389/fpls.2016.00755.

Xu, Xihui, Zhou Zhang, Shunli Hu, Zhepu Ruan, Jiandong Jiang, Chen Chen, and Zhenguo Shen. "Response of Soil Bacterial Communities to Lead and Zinc Pollution Revealed by Illumina MiSeq Sequencing Investigation." *Environmental Science and Pollution Research* 24, no. 1 (January 1, 2017): 666–75. doi:10.1007/s11356-016-7826-3.

Yamina, Benmalek, Benayad Tahar, and Fardeau Marie Laure. "Isolation and Screening of Heavy Metal Resistant Bacteria from Wastewater: A Study of Heavy Metal

Co-Resistance and Antibiotics Resistance." *Water Science & Technology* 66, no. 10 (November 15, 2012): 2041–48. doi:10.2166/wst.2012.355.

Ye, Qi. "Microbial Diversity Associated with Metal-and Radionuclide-Contamination at the DOE Savannah River Site (SRS), South Carolina, USA." uga, 2007. https://getd.libs.uga.edu/pdfs/ye_qi_200712_phd.pdf.

Yin, Huaqun, Jiaojiao Niu, Youhua Ren, Jing Cong, Xiaoxia Zhang, Fenliang Fan, Yunhua Xiao, et al. "An Integrated Insight into the Response of Sedimentary Microbial Communities to Heavy Metal Contamination." *Scientific Reports* 5 (September 22, 2015): srep14266. doi:10.1038/srep14266.

Zhou, Jizhong, Beicheng Xia, David S. Treves, L.-Y. Wu, Terry L. Marsh, Robert V. O'Neill, Anthony V. Palumbo, and James M. Tiedje. "Spatial and Resource Factors Influencing High Microbial Diversity in Soil." *Applied and Environmental Microbiology* 68, no. 1 (January 1, 2002): 326–34. doi:10.1128/AEM.68.1.326-334.2002.

Zhu, Jianyu, Jingxia Zhang, Qian Li, Tao Han, Jianping Xie, Yuehua Hu, and Liyuan Chai. "Phylogenetic Analysis of Bacterial Community Composition in Sediment Contaminated with Multiple Heavy Metals from the Xiangjiang River in China." *Marine Pollution Bulletin* 70, no. 1–2 (May 15, 2013): 134–39. doi:10.1016/j.marpolbul.2013.02.023.

Tables

Table 2-1. Means and standard deviations for heavy metal concentrations and edaphic factors in SRS soils.

HM (mg/kg) or edaphic factor	UR		AB		TB		PB	
	Mean	Stdev	Mean	Stdev	Mean	Stdev	Mean	Stdev
Cr 53	17.418	10.830	25.746	22.358	19.283	10.630	12.302	6.419
Co 59	2.742	1.267	4.553	5.099	5.707	3.375	1.522	0.388
Ni 60	6.644	4.430	9.753	11.641	8.987	6.414	5.317	3.951
Cu 63	7.489	5.921	11.654	16.183	7.230	3.539	4.217	2.601
Zn 66	21.995	14.370	25.074	23.550	20.767	10.892	11.639	3.441
As 75	26.633	2.482	27.325	4.881	25.987	1.590	24.798	1.645
Sr 88	14.464	9.333	40.343	49.245	25.051	13.099	5.920	2.946
Pb 208	21.480	14.750	16.422	11.031	18.587	9.102	7.740	4.879
U 238	1.611	0.878	2.108	1.381	6.285	13.773	1.029	0.306
Phosphorus (mg/g)	0.007	0.000	0.021	0.001	0.011	0.001	0.003	0.000
pH	3.983	0.031	4.273	0.042	4.337	0.006	4.377	0.025
Moisture (g)	22.000	0.000	8.333	0.577	7.000	0.000	29.333	0.577
Carbon (mg/g)	12.667	0.866	5.800	0.358	11.377	1.851	3.107	0.430
Nitrogen (mg/g)	0.477	0.038	0.313	0.021	0.580	0.104	0.113	0.015
C:N Ratio	26.784	0.467	18.572	0.005	19.683	0.519	27.823	0.152

Table 2-2. Effects of main factor assesed by PERMANOVA. The main factor represents site (Location) (Ash Basins, Pond B, Tim's Branch, Upper Three Runs). Values in table represent the F-ratio (F) and the level of significance ($p < 0.05$).

Source	df	SS	MS	Pseudo-F	P(perm)	Unique perms	P (Monte Carlo Test)
Location of site	3	11244	3748	10.75	**0.001**	999	**0.001**
Residuals	69	24056	667.64				
Total	72	126550					

Table 2-3. DISTLM results. Relative position of soil samples in the biplot is based on log-transformed Bray Curtis dissimilarities of archaeal/bacterial OTUs. Vectors indicate the weight and direction of those edaphic properties or heavy metals that were best predictors of soil bacterial composition as suggested by the results of the distance-based linear model (distLM). The dbRDA axes describe the percentage of the fitted or total variation explained by each axis while being constrained to account for group differences.

MARGINAL TESTS				
Variable	SS(trace)	Pseudo-F	P	Proportion of Varation Explained
P	4172.1	9.516	**0.001**	0.11819
pH	3759	8.4615	**0.001**	0.10649
Water	5332.3	12.633	**0.001**	0.15106
Carbon	3243.5	7.1838	**0.001**	0.091883
Nitrogen	3965.1	8.9841	**0.001**	0.11232
Cr	945.21	1.9534	**0.048**	0.026776
Co	2373.5	5.118	**0.001**	0.067238
Ni	983.13	2.034	0.061	0.02785
Cu	959.51	1.9838	0.057	0.027181
Zn	1109.6	2.3041	**0.03**	0.031432
As	1254.3	2.6156	**0.026**	0.035531
Sr	1664	3.5124	**0.005**	0.047139
Pb	1304.2	2.7238	**0.011**	0.036946
U	539.61	1.1022	0.252	0.015286
C:N	4940.8	11.555	**0.001**	0.13997
Res. Df: 71				

OVERALL BEST SOLUTIONS			
R^2	RSS	No. Variables	Selected Variables
0.4048	21010	9	pH, Carbon, Co, Ni, Zn, As Sr, Lead, C:N

Table 2-4. Effects of main factor assesed by PERMANOVA on fungal communities. The main factor represents site (Location) (Ash Basins, Pond B, Tim's Branch, Upper Three Runs). Values in table represent the F-ratio (F) and the level of significance ($p < 0.05$).

Source	df	SS	MS	Pseudo-F	P(perm)	Unique perms	P (Monte Carlo Test)
Location of site	3	26038	8679.5	6.2608	**0.001**	997	**0.001**
Residuals	63	87338	1386.3				
Total	66	1.13E+05					

Table 2-5. Relative position of soil samples in the biplot is based on log transformed Bray Curtis dissimilarities of fungal OTUs. Vectors indicate the weight and direction of those edaphic properties or heavy metals that were best predictors of soil bacterial composition as suggested by the results of the distance-based linear model (distLM). The dbRDA axes describe the percentage of the fitted or total variation explained by each axis while being constrained to account for group differences.

MARGINAL TESTS				
Variable	SS(trace)	Pseudo-F	P	Prop.
Phosphorus	7522.800	4.619	**0.001**	0.066
pH	6719.000	4.095	**0.001**	0.059
Moisture	7492.800	4.600	**0.001**	0.066
Cr	2897.900	1.705	**0.018**	0.026
Co	3081.800	1.816	**0.011**	0.027
Ni	2749.600	1.616	**0.030**	0.024
Cu	3072.000	1.810	**0.018**	0.027
Zn	2388.700	1.399	0.072	0.021
As	3171.400	1.871	**0.013**	0.028
Sr	3656.500	2.166	**0.003**	0.032
Pb	1984.000	1.158	0.253	0.018
U	3757.200	2.228	**0.003**	0.033
C:N	6558.700	3.991	**0.001**	0.058

OVERALL BEST SOLUTIONS			
R^2	RSS	No. Variables	Selected Variables
0.35631	72979	13	Phosphorus, Moisture, Co, Ni, Zn, As, Sr, Pb, U, C:N, Lead, C:N

Table 2-6. Significant SparCC correlations between OTUs of fungal and bacterial origins in UR soils.

OTU 1	OTU 2	corr	Pval
Actinobacteria	Proteobacteria	0.910	0.00
Chlamydiae	Verrucomicrobia	0.842	0.02
Acidobacteria	Basidiomycota	0.819	0.04
Proteobacteria	Basidiomycota	0.793	0.02
Basidiomycota	Zygomycota	0.788	0.00
Actinobacteria	Planctomycetes	0.769	0.00
Planctomycetes	Proteobacteria	0.734	0.00
Actinobacteria	WPS2	0.729	0.01
Planctomycetes	Basidiomycota	0.723	0.02
Acidobacteria	Proteobacteria	0.721	0.01
Chlamydiae	TM6	0.708	0.00
Actinobacteria	TM7	0.707	0.02
AD3	Chloroflexi	0.691	0.00
Planctomycetes	Zygomycota	0.657	0.05
Nitrospirae	Spirochaetes	0.657	0.00
Acidobacteria	Planctomycetes	0.649	0.00
Actinobacteria	Basidiomycota	0.608	0.00
Bacteroidetes	Verrucomicrobia	0.580	0.00
Chlorobi	OD1	0.568	0.03
Acidobacteria	Actinobacteria	0.538	0.00
Planctomycetes	WPS2	0.522	0.01
OP3	Spirochaetes	0.506	0.01
OD1	OP11	0.476	0.02
Acidobacteria	WPS2	0.473	0.05
Crenarchaeota	Parvarchaeota	0.445	0.03
Planctomycetes	TM7	0.441	0.03
Nitrospirae	WS4	0.425	0.03
Crenarchaeota	FCPU426	0.416	0.02
Elusimicrobia	Spirochaetes	0.409	0.02
Armatimonadetes	Zygomycota	0.408	0.01
Gemmatimonadetes	Proteobacteria	0.393	0.03
Chloroflexi	Nitrospirae	0.380	0.01
Elusimicrobia	Verrucomicrobia	0.377	0.01
BRC1	Spirochaetes	0.371	0.00
Actinobacteria	Armatimonadetes	0.363	0.00
Spirochaetes	WS4	0.360	0.01
BHI80139	Planctomycetes	0.339	0.00
Chloroflexi	OP11	0.337	0.04
BRC1	Nitrospirae	0.325	0.00

Armatimonadetes	Planctomycetes	0.324	0.01
Acidobacteria	Elusimicrobia	-0.328	0.02
OD1	SAR406	-0.344	0.03
Chlorobi	Rozellomycota	-0.346	0.03
Euryarchaeota	Gemmatimonadetes	-0.354	0.01
Acidobacteria	Spirochaetes	-0.356	0.01
Nitrospirae	Zygomycota	-0.358	0.05
Nitrospirae	Verrucomicrobia	-0.359	0.05
Armatimonadetes	Nitrospirae	-0.361	0.05
Elusimicrobia	Basidiomycota	-0.361	0.04
Chlamydiae	Chloroflexi	-0.379	0.00
Gemmatimonadetes	Spirochaetes	-0.385	0.00
Bacteroidetes	Spirochaetes	-0.387	0.00
OP3	TM7	-0.388	0.05
Chloroflexi	FCPU426	-0.405	0.00
Planctomycetes	WS4	-0.407	0.05
Spirochaetes	Basidiomycota	-0.410	0.05
OP3	Proteobacteria	-0.413	0.00
Armatimonadetes	Spirochaetes	-0.419	0.01
BRC1	WPS2	-0.426	0.05
Chlamydiae	Spirochaetes	-0.442	0.02
Nitrospirae	WPS2	-0.444	0.05
Spirochaetes	TM6	-0.445	0.04
Elusimicrobia	WPS2	-0.446	0.02
Actinobacteria	OP3	-0.454	0.03
Bacteroidetes	Nitrospirae	-0.466	0.01
Proteobacteria	Spirochaetes	-0.467	0.01
Chlorobi	Ascomycota	-0.492	0.00
Gemmatimonadetes	Verrucomicrobia	-0.500	0.02
OD1	Ascomycota	-0.506	0.00
Elusimicrobia	Planctomycetes	-0.528	0.04
OP3	Planctomycetes	-0.566	0.02
Actinobacteria	Spirochaetes	-0.632	0.04
Spirochaetes	WPS2	-0.666	0.04
Planctomycetes	Spirochaetes	-0.740	0.02

Table 2-7. Significant SparCC correlations between OTUs of fungal and bacterial origins in PB soils.

OTU 1	OTU 2	corr	pval
Acidobacteria	Planctomycetes	0.960	0.000
Actinobacteria	Planctomycetes	0.914	0.000
Planctomycetes	Proteobacteria	0.846	0.000
Acidobacteria	Bacteroidetes	0.844	0.000
Actinobacteria	Proteobacteria	0.833	0.000
Bacteroidetes	Planctomycetes	0.830	0.000
Planctomycetes	Verrucomicrobia	0.809	0.000
Planctomycetes	TM7	0.807	0.000
Acidobacteria	Actinobacteria	0.786	0.000
Actinobacteria	WPS2	0.767	0.000
Acidobacteria	Verrucomicrobia	0.763	0.000
Chlamydiae	Gemmatimonadetes	0.761	0.000
Gemmatimonadetes	Verrucomicrobia	0.761	0.000
Actinobacteria	Verrucomicrobia	0.759	0.000
Gemmatimonadetes	Planctomycetes	0.749	0.010
Acidobacteria	Proteobacteria	0.744	0.000
Actinobacteria	TM7	0.743	0.000
Chlamydiae	TM6	0.738	0.000
Acidobacteria	TM6	0.732	0.000
Bacteroidetes	TM7	0.727	0.010
Gemmatimonadetes	TM6	0.726	0.000
Basidiomycota	Zygomycota	0.725	0.000
Acidobacteria	TM7	0.711	0.000
Acidobacteria	Gemmatimonadetes	0.709	0.000
Chlamydiae	Planctomycetes	0.681	0.000
Planctomycetes	TM6	0.671	0.000
Acidobacteria	Chlamydiae	0.669	0.000
Bacteroidetes	Verrucomicrobia	0.656	0.010
Chlamydiae	Verrucomicrobia	0.654	0.000
Planctomycetes	Ascomycota	0.653	0.010
Bacteroidetes	Proteobacteria	0.649	0.000
Ascomycota	Rozellomycota	0.647	0.000
Actinobacteria	Bacteroidetes	0.634	0.000
Acidobacteria	Ascomycota	0.631	0.000
Chloroflexi	Rozellomycota	0.622	0.000
Proteobacteria	TM7	0.612	0.010
Bacteroidetes	TM6	0.609	0.000
AD3	Chloroflexi	0.605	0.000
Actinobacteria	Gemmatimonadetes	0.603	0.000

Proteobacteria	Verrucomicrobia	0.602	0.020
TM6	Verrucomicrobia	0.600	0.000
Chlamydiae	Proteobacteria	0.598	0.010
Proteobacteria	WPS2	0.597	0.010
Gemmatimonadetes	Basidiomycota	0.594	0.000
Verrucomicrobia	WPS2	0.584	0.000
Planctomycetes	WPS2	0.582	0.010
Gemmatimonadetes	Proteobacteria	0.569	0.010
Gemmatimonadetes	TM7	0.568	0.020
TM7	Basidiomycota	0.564	0.020
Chlamydiae	TM7	0.560	0.010
Planctomycetes	Basidiomycota	0.552	0.010
Chlorobi	Elusimicrobia	0.547	0.000
Bacteroidetes	Chlamydiae	0.543	0.000
TM6	TM7	0.542	0.040
Actinobacteria	Chlamydiae	0.530	0.010
Bacteroidetes	Ascomycota	0.516	0.030
TM7	Verrucomicrobia	0.513	0.030
Crenarchaeota	Euryarchaeota	0.508	0.000
Bacteroidetes	Gemmatimonadetes	0.507	0.020
TM7	Ascomycota	0.492	0.010
TM7	WPS2	0.490	0.010
Acidobacteria	Basidiomycota	0.486	0.020
Bacteroidetes	Basidiomycota	0.478	0.030
Acidobacteria	WPS2	0.463	0.040
Elusimicrobia	Verrucomicrobia	0.462	0.030
Elusimicrobia	TM7	0.453	0.000
Actinobacteria	Elusimicrobia	0.443	0.020
Actinobacteria	TM6	0.438	0.040
Elusimicrobia	TM6	0.429	0.040
Elusimicrobia	OD1	0.426	0.030
BHI80139	TM6	0.426	0.000
WPS2	Zygomycota	0.425	0.040
Crenarchaeota	AD3	0.423	0.010
Chlamydiae	Basidiomycota	0.406	0.050
Armatimonadetes	OP11	0.401	0.040
AD3	Chlorobi	0.398	0.020
Armatimonadetes	Ascomycota	0.393	0.040
TM6	Tenericutes	0.392	0.040
Euryarchaeota	Nitrospirae	0.391	0.030
Acidobacteria	BHI80139	0.389	0.010
BHI80139	Planctomycetes	0.352	0.040
Euryarchaeota	FCPU426	0.344	0.050
Deferribacteres	Firmicutes	0.338	0.000
Chlorobi	OP11	0.326	0.050

Deferribacteres	Glomeromycota	0.324	0.000
BHI80139	Ascomycota	0.308	0.030
Actinobacteria	Deferribacteres	-0.305	0.000
BHI80139	Nitrospirae	-0.315	0.020
Acidobacteria	Deferribacteres	-0.334	0.000
Chlorobi	Deferribacteres	-0.341	0.000
Deferribacteres	TM7	-0.343	0.000
Cyanobacteria	OP11	-0.345	0.050
Deferribacteres	Planctomycetes	-0.350	0.000
Chlamydiae	Nitrospirae	-0.378	0.040
Deferribacteres	TM6	-0.394	0.000
Chlorobi	Chytridiomycota	-0.401	0.050
Nitrospirae	TM6	-0.401	0.040
Cyanobacteria	TM6	-0.403	0.040
Nitrospirae	Proteobacteria	-0.406	0.030
Nitrospirae	Verrucomicrobia	-0.419	0.030
Euryarchaeota	TM6	-0.429	0.030
Euryarchaeota	Basidiomycota	-0.429	0.040
Euryarchaeota	WPS2	-0.440	0.050
Elusimicrobia	Glomeromycota	-0.441	0.050
Euryarchaeota	Ascomycota	-0.450	0.020
Actinobacteria	Nitrospirae	-0.459	0.000
Deferribacteres	Elusimicrobia	-0.463	0.000
Euryarchaeota	Bacteroidetes	-0.465	0.020
Bacteroidetes	Firmicutes	-0.466	0.030
Chlamydiae	Chloroflexi	-0.467	0.030
BHI80139	Firmicutes	-0.473	0.000
Bacteroidetes	Nitrospirae	-0.475	0.010
Nitrospirae	TM7	-0.476	0.050
Euryarchaeota	Verrucomicrobia	-0.477	0.020
AD3	Bacteroidetes	-0.486	0.040
Euryarchaeota	Proteobacteria	-0.488	0.000
Crenarchaeota	Acidobacteria	-0.496	0.010
Euryarchaeota	Actinobacteria	-0.497	0.000
Chlamydiae	Glomeromycota	-0.502	0.020
Euryarchaeota	Gemmatimonadetes	-0.502	0.000
Elusimicrobia	Firmicutes	-0.515	0.020
Crenarchaeota	Bacteroidetes	-0.516	0.010
Acidobacteria	Nitrospirae	-0.550	0.000
TM6	Glomeromycota	-0.557	0.010
Euryarchaeota	Planctomycetes	-0.573	0.000
Firmicutes	Ascomycota	-0.591	0.010
Euryarchaeota	Acidobacteria	-0.696	0.000

Table 2-8. Significant SparCC correlations between OTUs of fungal and bacterial origins in TB soils.

OTU 1	OTU 2	corr	pval
Acidobacteria	WPS2	0.903	0.000
Proteobacteria	WPS2	0.873	0.000
Acidobacteria	Proteobacteria	0.830	0.000
Planctomycetes	Proteobacteria	0.807	0.000
Actinobacteria	Proteobacteria	0.806	0.000
Planctomycetes	WPS2	0.794	0.000
Actinobacteria	WPS2	0.790	0.000
Acidobacteria	Planctomycetes	0.782	0.010
Crenarchaeota	Acidobacteria	0.771	0.000
Basidiomycota	Zygomycota	0.752	0.000
Acidobacteria	Cyanobacteria	0.746	0.000
Crenarchaeota	WPS2	0.744	0.000
Cyanobacteria	WPS2	0.737	0.000
Acidobacteria	Verrucomicrobia	0.730	0.000
Actinobacteria	Cyanobacteria	0.717	0.000
Ascomycota	Zygomycota	0.716	0.000
Ascomycota	Basidiomycota	0.716	0.000
Chlamydiae	Elusimicrobia	0.710	0.000
Chlamydiae	TM6	0.674	0.000
Chlorobi	Chloroflexi	0.661	0.000
Cyanobacteria	Proteobacteria	0.659	0.000
Planctomycetes	TM6	0.657	0.000
Actinobacteria	Planctomycetes	0.650	0.010
Acidobacteria	Actinobacteria	0.644	0.000
Cyanobacteria	TM7	0.631	0.000
Acidobacteria	TM7	0.622	0.000
Verrucomicrobia	WPS2	0.616	0.000
Cyanobacteria	Planctomycetes	0.616	0.000
Crenarchaeota	Cyanobacteria	0.612	0.000
Acidobacteria	TM6	0.605	0.010
Crenarchaeota	TM6	0.605	0.010
Crenarchaeota	Euryarchaeota	0.591	0.000
TM6	WPS2	0.586	0.000
Crenarchaeota	Planctomycetes	0.585	0.000
Proteobacteria	TM7	0.581	0.010
Gemmatimonadetes	Nitrospirae	0.578	0.000
Planctomycetes	Verrucomicrobia	0.578	0.020
Bacteroidetes	Verrucomicrobia	0.575	0.010
Chlamydiae	Verrucomicrobia	0.570	0.010

Bacteroidetes	Elusimicrobia	0.565	0.000
Nitrospirae	OD1	0.563	0.000
AD3	Actinobacteria	0.560	0.000
Actinobacteria	TM7	0.559	0.010
Proteobacteria	TM6	0.557	0.010
Chloroflexi	OD1	0.549	0.010
FCPU426	TM6	0.545	0.000
Crenarchaeota	TM7	0.534	0.010
Proteobacteria	Verrucomicrobia	0.530	0.050
FCPU426	Tenericutes	0.530	0.000
Chloroflexi	Firmicutes	0.530	0.030
Bacteroidetes	Chlamydiae	0.529	0.010
Chloroflexi	Nitrospirae	0.528	0.020
Glomeromycota	Rozellomycota	0.522	0.030
Armatimonadetes	FBP	0.518	0.020
Crenarchaeota	Proteobacteria	0.518	0.010
AD3	WPS2	0.517	0.020
TM6	Tenericutes	0.511	0.000
Crenarchaeota	Actinobacteria	0.509	0.010
Euryarchaeota	Chlamydiae	0.507	0.010
TM7	WPS2	0.506	0.020
Bacteroidetes	OD1	0.504	0.010
Euryarchaeota	Acidobacteria	0.490	0.000
Crenarchaeota	FCPU426	0.483	0.020
Glomeromycota	Zygomycota	0.480	0.000
Cyanobacteria	TM6	0.476	0.050
Bacteroidetes	Gemmatimonadetes	0.475	0.040
Tenericutes	Rozellomycota	0.473	0.000
Chlamydiae	Rozellomycota	0.472	0.040
Euryarchaeota	TM6	0.464	0.010
Euryarchaeota	FCPU426	0.460	0.000
OD1	Chytridiomycota	0.451	0.010
TM6	Rozellomycota	0.451	0.030
Ascomycota	Chytridiomycota	0.448	0.010
Verrucomicrobia	Rozellomycota	0.448	0.050
Fibrobacteres	Nitrospirae	0.447	0.000
TM6	Verrucomicrobia	0.443	0.040
Crenarchaeota	Verrucomicrobia	0.420	0.050
Chlorobi	OD1	0.418	0.040
Firmicutes	Chytridiomycota	0.416	0.040
TM6	TM7	0.413	0.050
OP11	Verrucomicrobia	0.412	0.020
OP11	TM6	0.405	0.020
Euryarchaeota	Verrucomicrobia	0.394	0.020
Gemmatimonadetes	WS3	0.389	0.030

Fibrobacteres	WS3	0.387	0.000
Gemmatimonadetes	OP3	0.384	0.030
WS2	WS3	0.376	0.000
FBP	Fibrobacteres	0.374	0.010
Armatimonadetes	BRC1	0.354	0.000
Fibrobacteres	Gemmatimonadetes	0.353	0.040
FBP	WS3	0.349	0.010
BRC1	FBP	0.347	0.000
Crenarchaeota	OP11	0.338	0.040
Armatimonadetes	WS3	0.332	0.050
Nitrospirae	OP3	0.316	0.020
OD1	OP3	0.303	0.040
Fibrobacteres	Kazan3B28	0.302	0.000
Chlamydiae	ZB3	-0.301	0.000
FCPU426	WS3	-0.302	0.030
Acidobacteria	WS2	-0.302	0.030
Verrucomicrobia	WS2	-0.302	0.050
Cyanobacteria	OP3	-0.316	0.020
Spirochaetes	Verrucomicrobia	-0.321	0.020
Fibrobacteres	Rozellomycota	-0.322	0.050
WS2	Rozellomycota	-0.324	0.020
NC10	TM6	-0.325	0.000
BRC1	TM6	-0.327	0.010
Acidobacteria	Kazan3B28	-0.328	0.000
BRC1	Firmicutes	-0.328	0.000
Planctomycetes	WS3	-0.329	0.050
TM6	WS2	-0.342	0.020
Actinobacteria	Fibrobacteres	-0.347	0.050
WPS2	WS2	-0.361	0.020
Crenarchaeota	FBP	-0.365	0.040
Crenarchaeota	Fibrobacteres	-0.368	0.010
Crenarchaeota	WS2	-0.376	0.000
Fibrobacteres	TM7	-0.376	0.020
Actinobacteria	WS3	-0.377	0.020
Fibrobacteres	TM6	-0.378	0.020
Proteobacteria	WS3	-0.395	0.040
Nitrospirae	Basidiomycota	-0.395	0.040
FBP	Rozellomycota	-0.397	0.050
FCPU426	Gemmatimonadetes	-0.398	0.050
Nitrospirae	WPS2	-0.399	0.050
OP3	Zygomycota	-0.404	0.010
Chlorobi	Cyanobacteria	-0.405	0.050
Cyanobacteria	Chytridiomycota	-0.407	0.050
AD3	Chytridiomycota	-0.410	0.030
FBP	Tenericutes	-0.412	0.000

Euryarchaeota	Chloroflexi	-0.412	0.040
Acidobacteria	Fibrobacteres	-0.413	0.050
Chloroflexi	WPS2	-0.414	0.040
Fibrobacteres	Verrucomicrobia	-0.414	0.050
Euryarchaeota	FBP	-0.417	0.030
Fibrobacteres	WPS2	-0.420	0.020
Acidobacteria	WS3	-0.425	0.040
Crenarchaeota	Nitrospirae	-0.438	0.040
FBP	TM6	-0.451	0.010
Armatimonadetes	FCPU426	-0.459	0.010
WPS2	WS3	-0.461	0.000
Cyanobacteria	OD1	-0.467	0.040
Cyanobacteria	WS3	-0.468	0.000
Acidobacteria	Nitrospirae	-0.469	0.020
Crenarchaeota	Gemmatimonadetes	-0.470	0.020
WPS2	Chytridiomycota	-0.472	0.000
Nitrospirae	Zygomycota	-0.474	0.010
Crenarchaeota	WS3	-0.476	0.000
TM7	WS3	-0.478	0.000
Armatimonadetes	Chlamydiae	-0.501	0.010
TM6	WS3	-0.504	0.000
Crenarchaeota	Chloroflexi	-0.505	0.010
Armatimonadetes	Elusimicrobia	-0.518	0.000
Armatimonadetes	TM6	-0.537	0.000
Cyanobacteria	Gemmatimonadetes	-0.578	0.030
Cyanobacteria	Nitrospirae	-0.579	0.000
FBP	FCPU426	-0.589	0.000
Chloroflexi	Cyanobacteria	-0.604	0.000
Acidobacteria	Chloroflexi	-0.625	0.010

Table 2-9. Significant SparCC correlations between OTUs of fungal and bacterial origins in AB soils.

OTU 1	OTU 2	corr	pval
Planctomycetes	Proteobacteria	0.848	0.000
Acidobacteria	Proteobacteria	0.761	0.010
Actinobacteria	Planctomycetes	0.753	0.000
Chlamydiae	FCPU426	0.748	0.000
Armatimonadetes	Planctomycetes	0.743	0.010
Chlamydiae	TM6	0.739	0.000
Actinobacteria	Proteobacteria	0.719	0.000
Planctomycetes	Verrucomicrobia	0.715	0.000
Acidobacteria	Planctomycetes	0.713	0.000
Chlamydiae	Elusimicrobia	0.711	0.000
Proteobacteria	Verrucomicrobia	0.680	0.010
BHI80139	Verrucomicrobia	0.677	0.000
Actinobacteria	Basidiomycota	0.655	0.000
Bacteroidetes	Verrucomicrobia	0.641	0.000
Crenarchaeota	Euryarchaeota	0.637	0.000
Acidobacteria	Actinobacteria	0.635	0.000
Acidobacteria	BHI80139	0.630	0.000
Acidobacteria	Verrucomicrobia	0.629	0.000
Elusimicrobia	Verrucomicrobia	0.625	0.010
Basidiomycota	Zygomycota	0.622	0.000
Armatimonadetes	Zygomycota	0.615	0.010
Planctomycetes	TM7	0.608	0.030
BHI80139	Proteobacteria	0.605	0.000
Ascomycota	Glomeromycota	0.601	0.020
Gemmatimonadetes	Verrucomicrobia	0.594	0.020
BHI80139	Planctomycetes	0.588	0.000
AD3	Chloroflexi	0.586	0.000
Proteobacteria	Basidiomycota	0.581	0.020
Nitrospirae	Spirochaetes	0.581	0.000
Acidobacteria	Elusimicrobia	0.577	0.020
Chlamydiae	WPS2	0.557	0.010
FCPU426	TM6	0.557	0.020
Acidobacteria	WPS2	0.556	0.050
Gemmatimonadetes	Proteobacteria	0.551	0.030
BHI80139	Elusimicrobia	0.547	0.000
Planctomycetes	Basidiomycota	0.545	0.020
Actinobacteria	Armatimonadetes	0.544	0.000
Armatimonadetes	Basidiomycota	0.539	0.040
BHI80139	WPS2	0.539	0.010

Armatimonadetes	Proteobacteria	0.537	0.020
Planctomycetes	WPS2	0.534	0.010
Bacteroidetes	Gemmatimonadetes	0.529	0.020
Acidobacteria	Basidiomycota	0.528	0.040
Acidobacteria	Armatimonadetes	0.527	0.010
Actinobacteria	TM7	0.522	0.020
BRC1	Nitrospirae	0.521	0.000
Chloroflexi	Nitrospirae	0.513	0.010
Elusimicrobia	Planctomycetes	0.511	0.040
OP11	TM7	0.511	0.010
Chlamydiae	Verrucomicrobia	0.506	0.020
Elusimicrobia	WPS2	0.490	0.020
BHI80139	Bacteroidetes	0.489	0.050
BRC1	Spirochaetes	0.487	0.000
Planctomycetes	Zygomycota	0.476	0.050
BRC1	WS4	0.474	0.010
Elusimicrobia	Basidiomycota	0.473	0.040
Elusimicrobia	TM6	0.471	0.020
OD1	OP11	0.469	0.020
Chlorobi	OD1	0.467	0.030
Actinobacteria	WPS2	0.464	0.010
Firmicutes	TM6	0.452	0.030
Cyanobacteria	TM7	0.448	0.020
Chloroflexi	OP11	0.444	0.040
Crenarchaeota	FCPU426	0.443	0.020
WS6	Glomeromycota	0.441	0.000
Verrucomicrobia	WPS2	0.438	0.040
Euryarchaeota	Nitrospirae	0.436	0.050
TM6	WPS2	0.432	0.030
Spirochaetes	WS4	0.419	0.010
Chlorobi	Chytridiomycota	0.412	0.040
Nitrospirae	WS4	0.397	0.030
FBP	Glomeromycota	0.396	0.050
GN02	Gemmatimonadetes	0.390	0.030
Crenarchaeota	Parvarchaeota	0.382	0.030
Parvarchaeota	TM6	0.381	0.020
Actinobacteria	BHI80139	0.379	0.050
Gemmatimonadetes	WS3	0.369	0.020
OP3	Spirochaetes	0.355	0.010
Parvarchaeota	FCPU426	0.352	0.020
FBP	WS2	0.335	0.000
NC10	Ascomycota	0.311	0.020
NC10	TM6	-0.309	0.000
Fibrobacteres	Chytridiomycota	-0.310	0.040
Cyanobacteria	WS3	-0.318	0.040

Parvarchaeota	FBP	-0.323	0.020
NC10	OD1	-0.325	0.000
BHI80139	NC10	-0.325	0.000
Chlamydiae	NC10	-0.334	0.000
Bacteroidetes	NKB19	-0.339	0.010
BHI80139	BRC1	-0.339	0.020
Spirochaetes	TM6	-0.342	0.040
Parvarchaeota	Ascomycota	-0.353	0.030
Euryarchaeota	GN02	-0.356	0.040
NKB19	Basidiomycota	-0.368	0.040
OP3	Planctomycetes	-0.368	0.020
Actinobacteria	Spirochaetes	-0.378	0.040
BRC1	Verrucomicrobia	-0.383	0.020
BRC1	WPS2	-0.383	0.050
Bacteroidetes	Ascomycota	-0.401	0.050
Crenarchaeota	WS2	-0.401	0.000
Euryarchaeota	WS3	-0.405	0.020
Parvarchaeota	Glomeromycota	-0.406	0.010
Chlamydiae	Spirochaetes	-0.412	0.020
BHI80139	Spirochaetes	-0.422	0.040
Planctomycetes	WS4	-0.422	0.050
Spirochaetes	WPS2	-0.423	0.040
Armatimonadetes	Nitrospirae	-0.423	0.050
Chlorobi	Rozellomycota	-0.424	0.030
Bacteroidetes	WS4	-0.426	0.040
Nitrospirae	Verrucomicrobia	-0.426	0.050
Elusimicrobia	Spirochaetes	-0.431	0.020
FBP	TM6	-0.431	0.020
Chlamydiae	FBP	-0.434	0.040
Actinobacteria	OP3	-0.434	0.030
Spirochaetes	Basidiomycota	-0.435	0.050
OD1	Glomeromycota	-0.436	0.030
TM7	Glomeromycota	-0.464	0.030
Nitrospirae	WPS2	-0.483	0.050
Crenarchaeota	Zygomycota	-0.483	0.020
Armatimonadetes	Spirochaetes	-0.485	0.010
Verrucomicrobia	WS4	-0.487	0.000
Crenarchaeota	Ascomycota	-0.495	0.030
Cyanobacteria	Rozellomycota	-0.497	0.030
Euryarchaeota	FBP	-0.498	0.000
BRC1	Gemmatimonadetes	-0.500	0.000
Nitrospirae	Zygomycota	-0.504	0.050
Acidobacteria	Spirochaetes	-0.504	0.010
OP3	Proteobacteria	-0.511	0.000
Euryarchaeota	Gemmatimonadetes	-0.515	0.010

BRC1	Bacteroidetes	-0.520	0.010
Euryarchaeota	Bacteroidetes	-0.520	0.040
Gemmatimonadetes	Spirochaetes	-0.551	0.000
Nitrospirae	Basidiomycota	-0.552	0.030
Planctomycetes	Spirochaetes	-0.555	0.020
Chlamydiae	Chloroflexi	-0.578	0.000
Bacteroidetes	Spirochaetes	-0.581	0.000
Bacteroidetes	Nitrospirae	-0.586	0.010
Spirochaetes	Verrucomicrobia	-0.587	0.000
Gemmatimonadetes	WS4	-0.606	0.000
Proteobacteria	Spirochaetes	-0.617	0.010
Chlorobi	Ascomycota	-0.624	0.000
Cyanobacteria	Glomeromycota	-0.630	0.000
Chloroflexi	FCPU426	-0.673	0.000
Crenarchaeota	Glomeromycota	-0.674	0.000
OD1	Ascomycota	-0.791	0.000

Table 2-10. KEGG Pathways with significant differences between bacterial communities of SRS soils as inferred by PICRUSt.

Observation Ids	p-values	p-values (corrected)	Effect size
Amino Acid Metabolism	0.018	0.021	0.146
Biosynthesis of Other Secondary Metabolites	0.000	0.001	0.267
Cancers	0.000	0.000	0.320
Carbohydrate Metabolism	0.002	0.003	0.229
Cardiovascular Diseases	0.000	0.000	0.330
Cell Communication	0.000	0.000	0.312
Cellular Processes and Signaling	0.012	0.017	0.158
Circulatory System	0.000	0.001	0.139
Endocrine System	0.000	0.000	0.210
Energy Metabolism	0.016	0.020	0.192
Enzyme Families	0.000	0.000	0.318
Excretory System	0.000	0.000	0.347
Genetic Information Processing	0.030	0.034	0.089
Glycan Biosynthesis and Metabolism	0.002	0.004	0.274
Immune System	0.000	0.000	0.432
Immune System Diseases	0.000	0.001	0.228
Infectious Diseases	0.000	0.000	0.310
Lipid Metabolism	0.004	0.007	0.166
Membrane Transport	0.005	0.008	0.186
Metabolic Diseases	0.000	0.000	0.416
Metabolism	0.000	0.000	0.389
Metabolism of Cofactors and Vitamins	0.000	0.000	0.433
Metabolism of Other Amino Acids	0.015	0.019	0.135
Metabolism of Terpenoids and Polyketides	0.003	0.006	0.192

Nervous System	0.014	0.019	0.165
Neurodegenerative Diseases	0.000	0.000	0.278
Nucleotide Metabolism	0.013	0.018	0.153
Poorly Characterized	0.004	0.007	0.252
Replication and Repair	0.025	0.029	0.106
Sensory System	0.000	0.000	0.291
Signal Transduction	0.000	0.000	0.294
Signaling Molecules and Interaction	0.000	0.000	0.385
Transcription	0.000	0.000	0.328
Translation	0.012	0.017	0.172
Transport and Catabolism	0.000	0.000	0.246

Table 2-11. Selected antibiotic and metal resistance KEGG Orthologs (KOs) with significant differences between bacterial communities in SRS soils as inferred by PICRUSt.

KO	Superfamily	Family	Gene	Type	Significance ($p < 0.05$)
K03446	MFS	DHA2	emrB	antibiotic	7.88E-06
K05557	MFS	DHA2	actVA1	antibiotic	1.43E-06
K06189	ABC	CorC	corC	metal	4.06E-05
K07156	ABC	CopC	copC	metal	2.34E-03
K07239	RND	HME	HME family	metal	3.63E-07
K07240	ABC	CHR	chrA	metal	1.12E-02
K07241	ABC	NIX	nixA	metal	1.23E-03
K07245	ABC	PCO	pcoD	metal	2.58E-03
K07644	RND	OmpR	cusS	metal	7.23E-05
K07664	RND	OmpR	baeR	antibiotic	5.49E-02
K07665	RND	OmpR	cusR	metal	2.50E-03
K07681	RND	NarL	vraS	antibiotic	2.30E-06
K07694	RND	NarL	vraR	antibiotic	2.36E-02
K07785	MFS	NRE	nrsD	metal	2.41E-02
K07786	MFS	DHA2	emrY	antibiotic	4.12E-01
K07787	ABC	OmpR	cusA	metal	5.89E-04
K07788	RND	MDT	mdtB	antibiotic	5.87E-04
K07789	RND	MDT	mdtC	antibiotic	5.55E-04
K07796	RND	OmpR	cusC	metal	7.83E-03
K07798	RND	OmpR	cusB	metal	1.71E-06
K07799	RND	MDT	mdtA	antibiotic	2.42E-03
K07803	RND	NtrC	zraP	metal	3.75E-03
K07810	RND	OmpR	cusF	metal	3.25E-06
K08160	MFS	DHA1	mdfA	antibiotic	1.61E-05
K08161	MFS	DHA1	mdtG	antibiotic	2.11E-03
K08162	MFS	DHA1	mdtH	antibiotic	2.87E-01
K08163	MFS	DHA1	mdtL	antibiotic	6.30E-01
K08164	MFS	DHA1	ybcL	antibiotic	3.59E-03
K08166	MFS	DHA2	mmR	antibiotic	5.19E-04
K08167	MFS	DHA2	smvA	antibiotic	1.72E-04
K08168	MFS	DHA2	tetB	antibiotic	5.37E-07
K08169	MFS	DHA2	yebQ	antibiotic	9.31E-04
K11629	RND	OmpR	bceS	antibiotic	2.46E-06
K11630	RND	OmpR	bceR	antibiotic	2.87E-06
K14166	ABC	NosL	Ycnj	antibiotic	1.54E-04

Figures

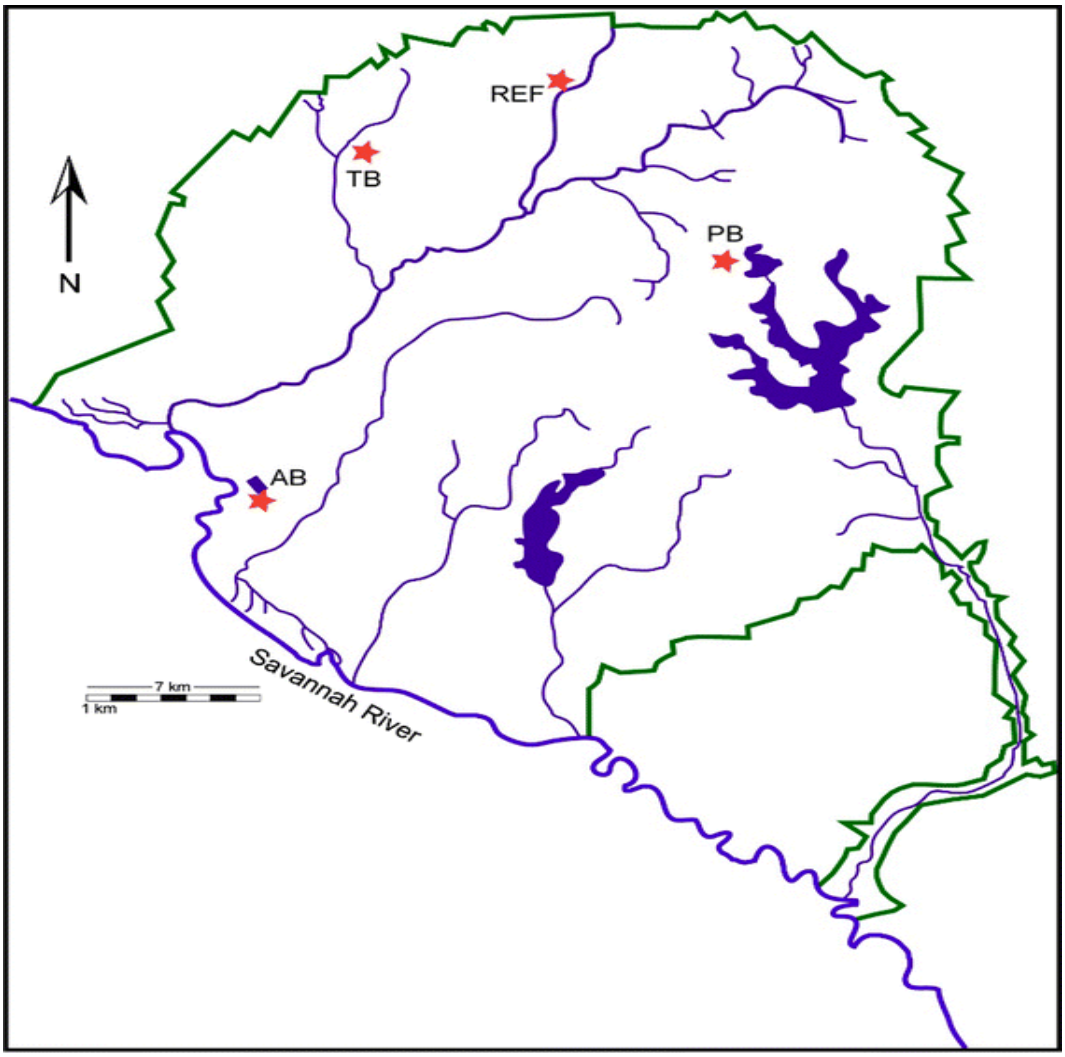

Figure 2-1. Map of the Savannah River Site, South Carolina, USA, depicting the distribution of the reference location (REF) and contaminated study areas, ash basin (AB), Pond B (PB), and Tim's Branch (TB) sampled for small mammals in spring 2014 (Tannebaum and Beasley, 2016).

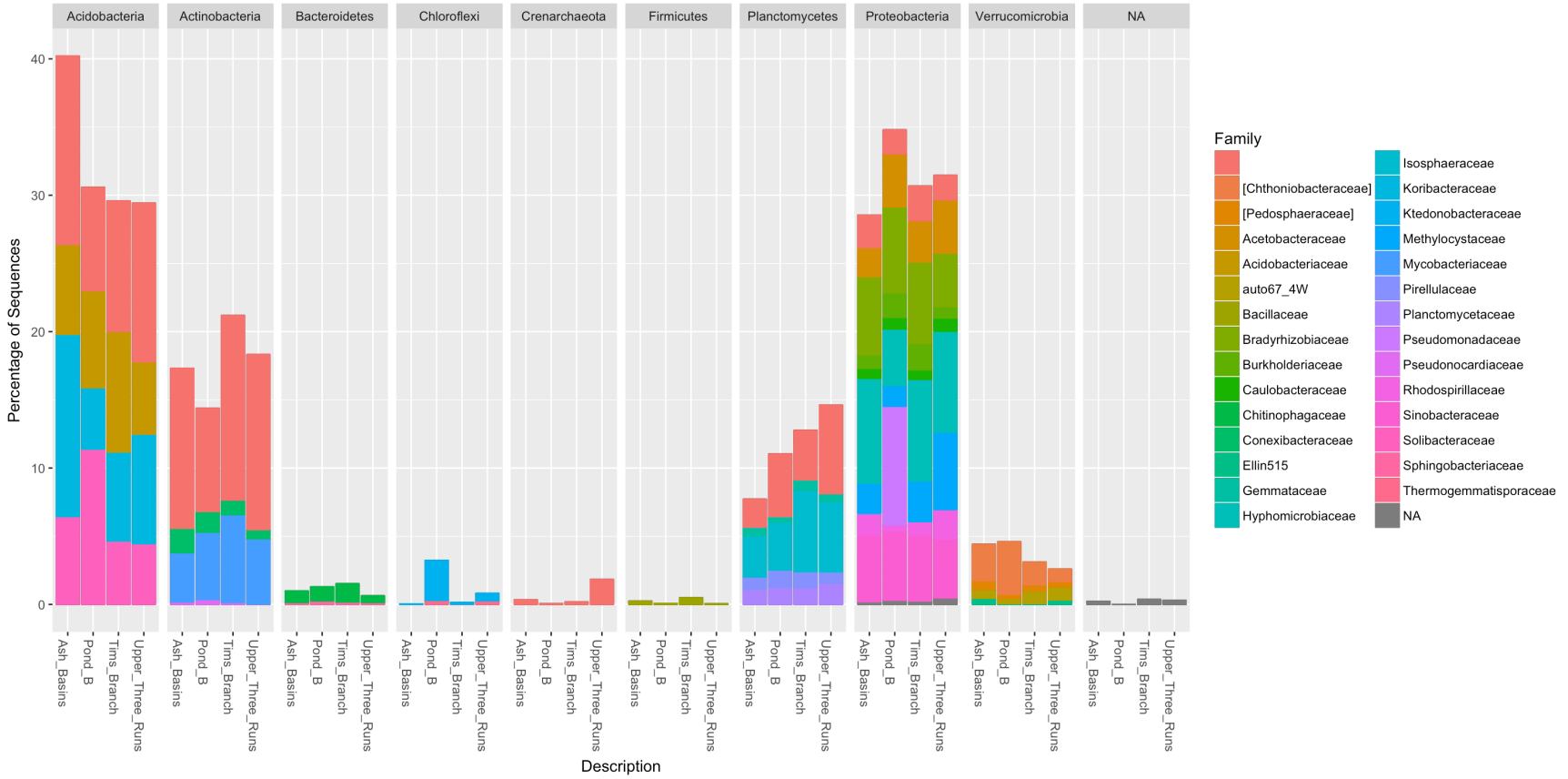

Figure 2-2. The relative abundance at the level of Phylum and corresponding families representing the 9 most abundant bacterial/archaeal OTUs (clustered at 97% similarity) in soil samples from the four sampling sites. Bacterial phyla are further expanded into respective families.

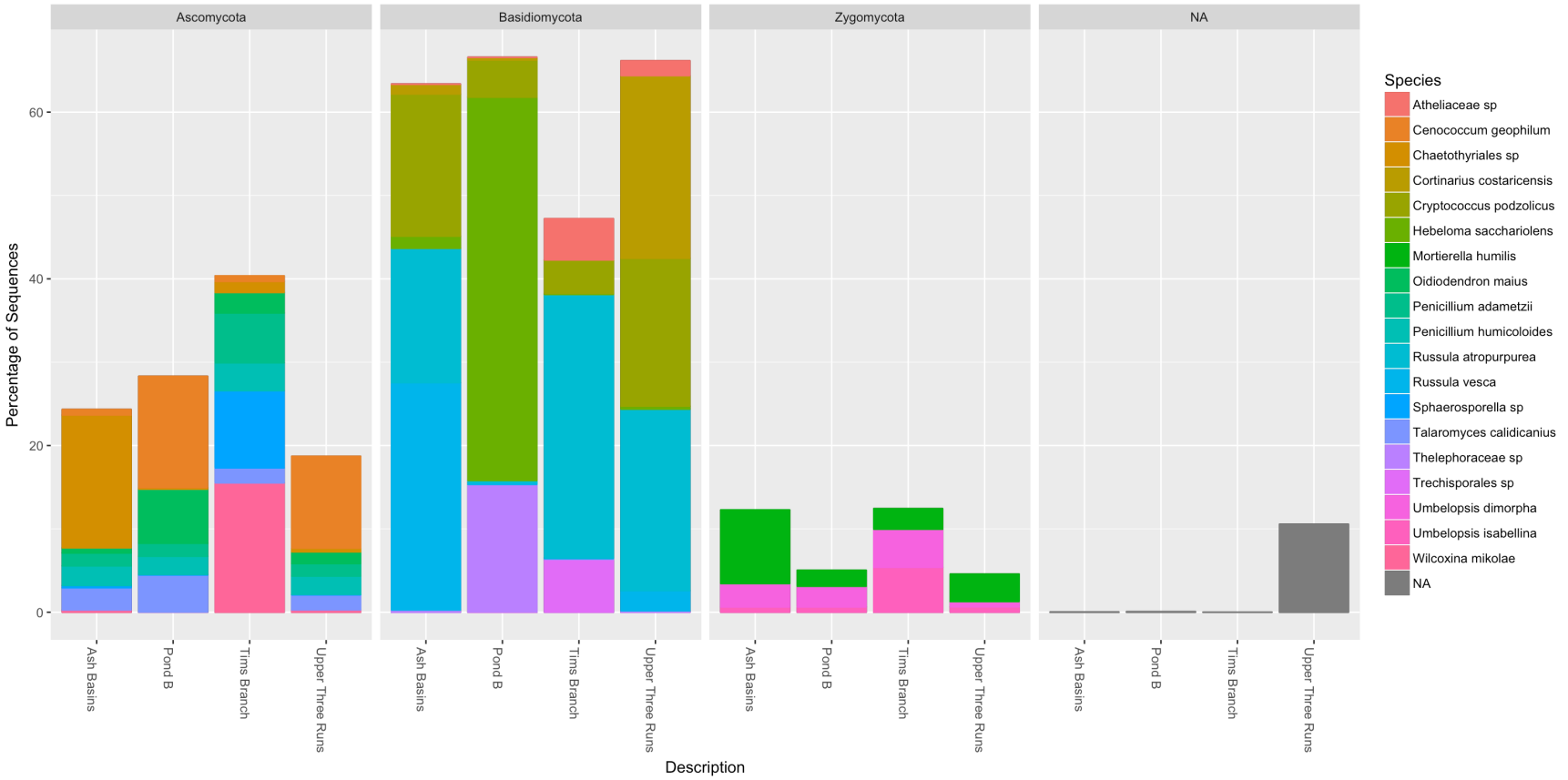

Figure 2-3. The relative abundance at the level of Phylum and corresponding families representing the 9 most abundant OTUs (clustered at 97% similarity) in soil samples from the four sampling sites. Fungal phyla are further expanded into respective families.

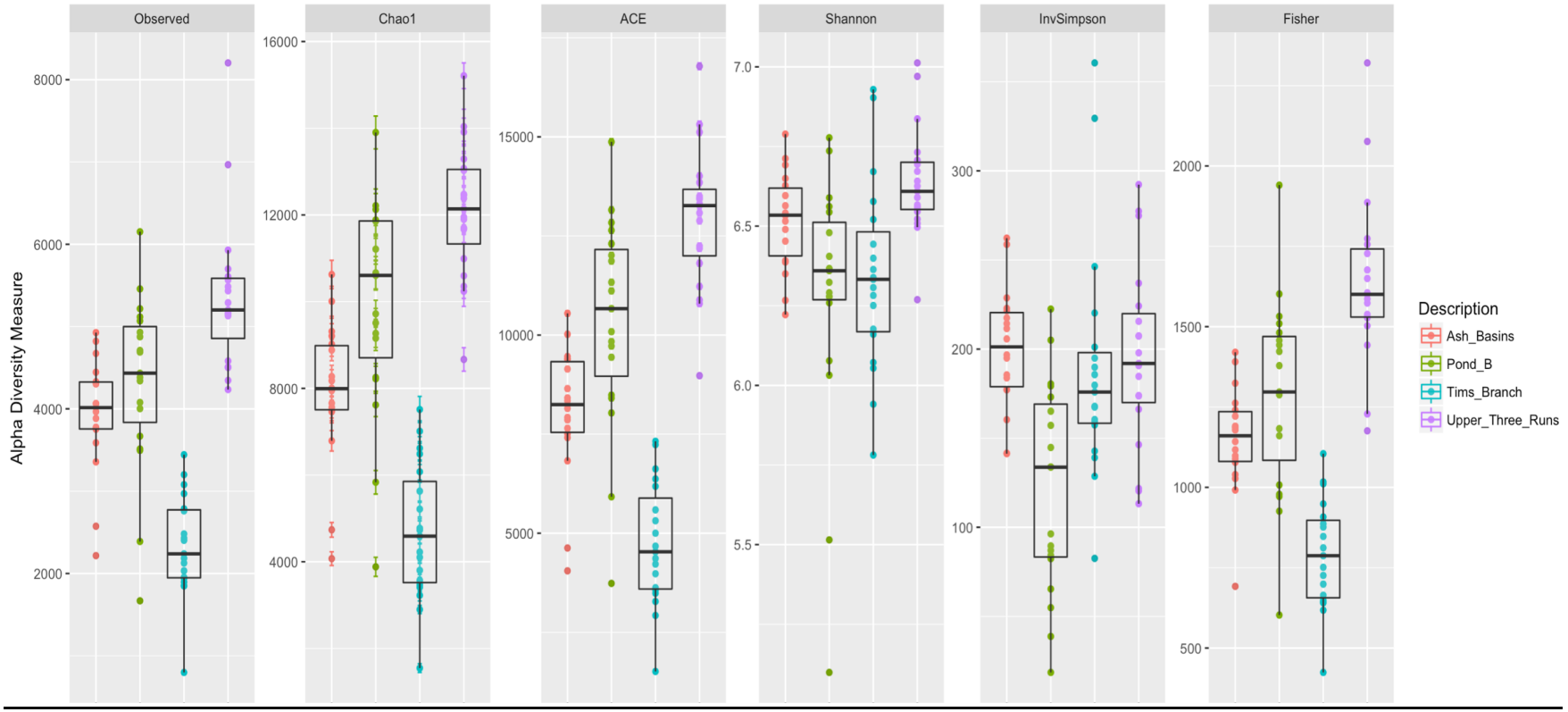

Figure 2-4. Alpha diversity measures soils at the four sampling sites (defined either by the number of bacterial/archaeal OTUs observed or by Chao1, ACE, Shannon, Inverse Simpson, and Fisher diversity measures).

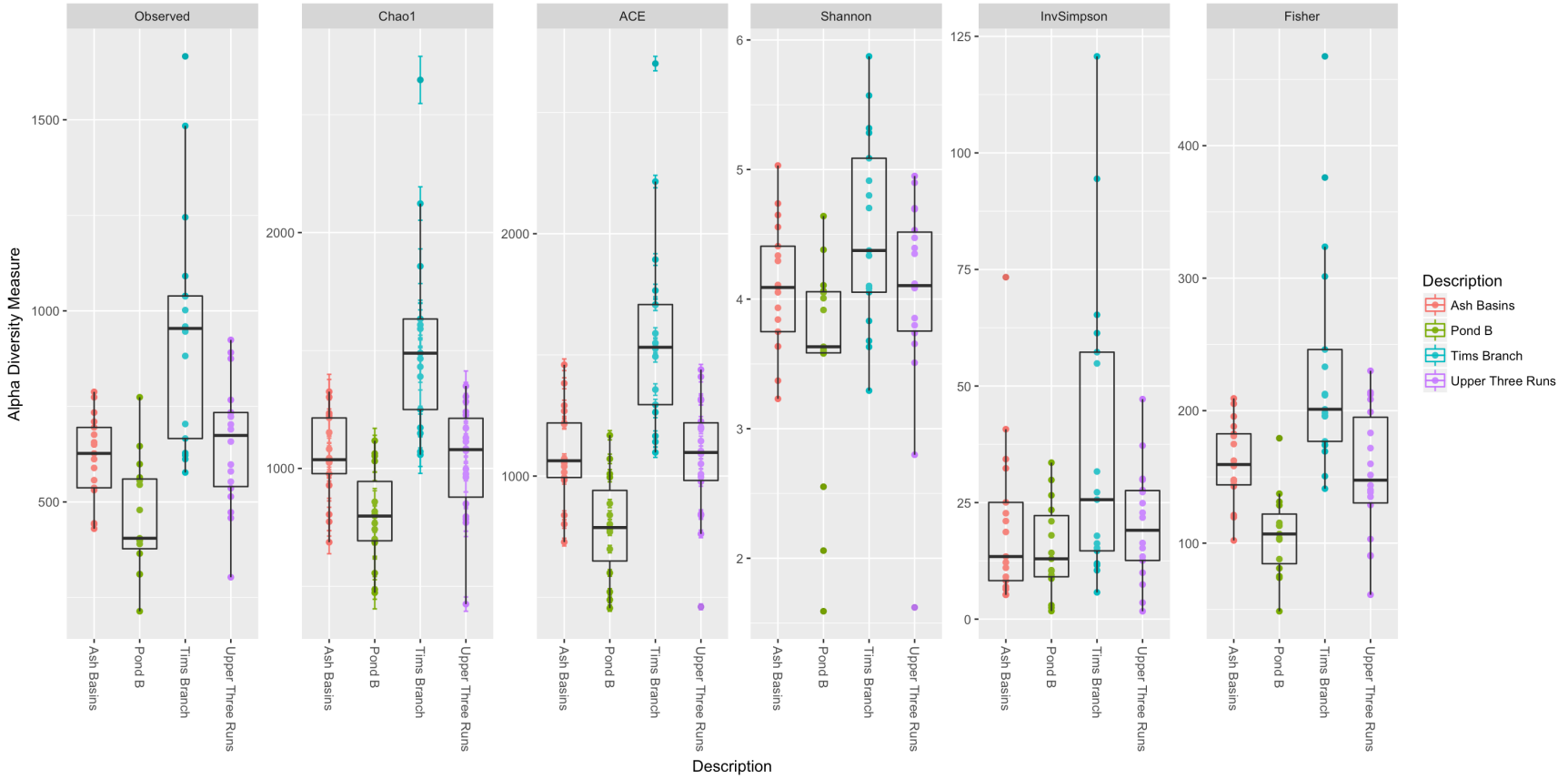

Figure 2-5. Alpha diversity measures for soils at the four sampling sites (defined either by the number of fungal OTUs observed or by Chao1, ACE, Shannon, Inverse Simpson, and Fisher diversity measures).

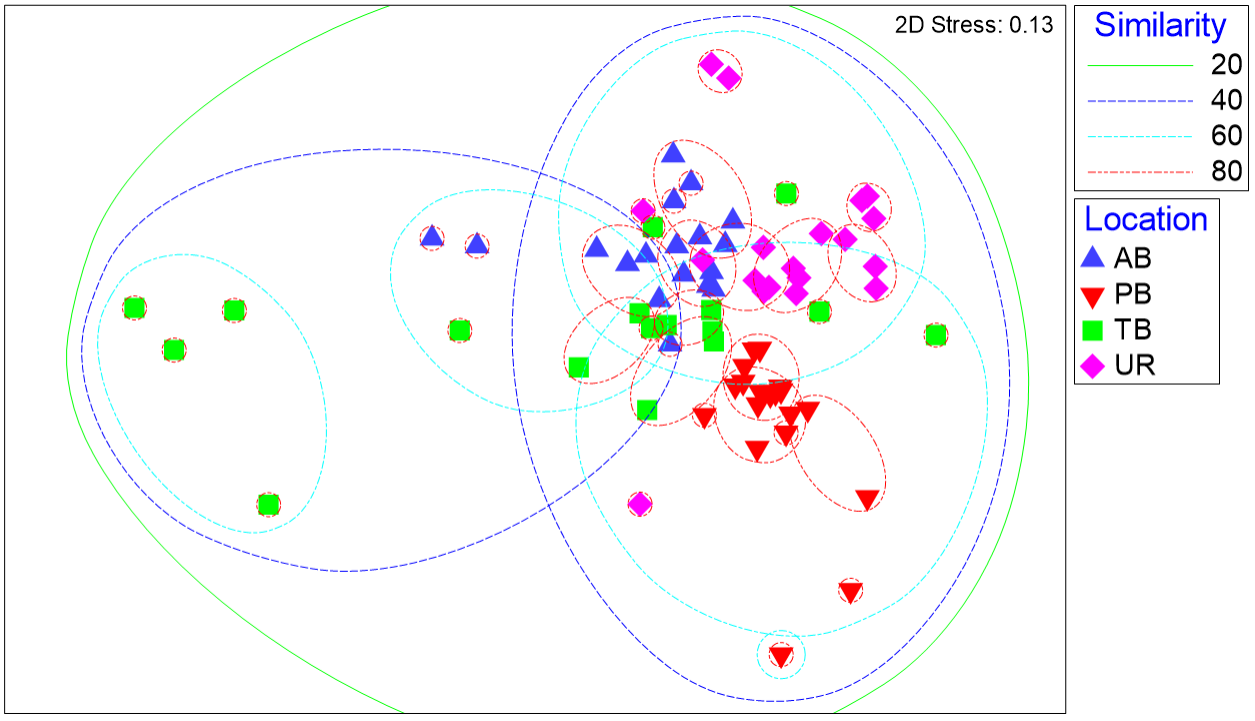

Figure 2-6. Non-metric multi-dimensional scaling plot of bacterial/archaeal OTU frequency after log-transformation, which reduces the influence of the most abundant OTUs. Dashed lines represent percent similarity of clusters using SIMPROF: green lines 20%, dashed blue lines 40%, dashed cyan lines 60%, dashed red lines 80%. Blue triangles represent soils from Ash Basins (AB); Red upside down triangles represent Pond B (PB) soils; Green squares represent Tim's Branch (TB) soils; pink diamonds represent Upper Three Runs (UR) soils. Stress value is 0.13.

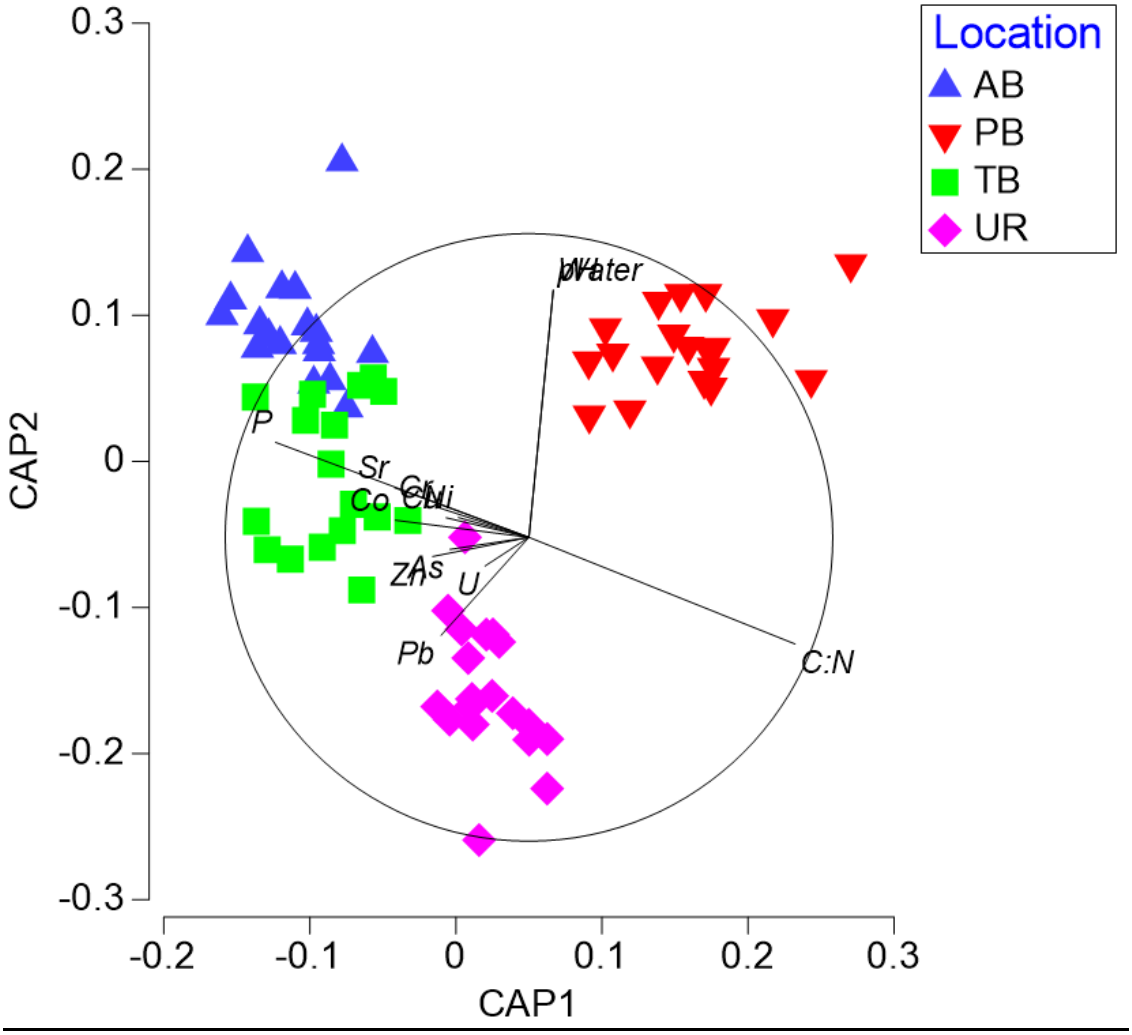

Figure 2-7. Canonical analysis of principal coordinates based on a Bray–Curtis dissimilarity matrix of log-transformed bacterial/archaeal OTU frequencies. Blue triangles represent soils from Ash Basins (AB); Red upside down triangles represent Pond B (PB) soils; Green squares represent Tim's Branch (TB) soils; pink diamonds represent Upper Three Runs (UR) soils.

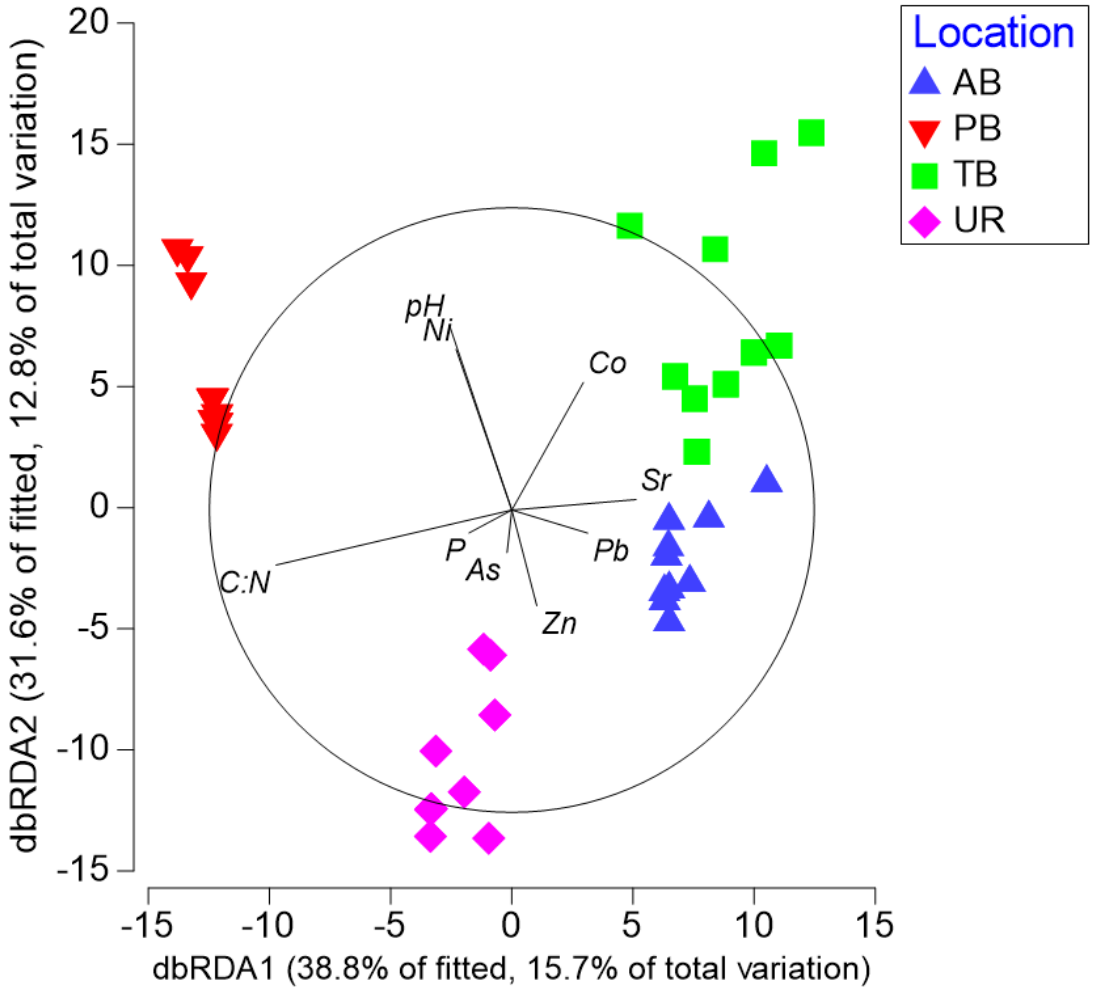

Figure 2-8. Distance-based redundancy analysis (dBRDA) representing raw Pearson correlations for habitat variables and bacterial/archaeal OTUs. Vectors are overlaid to represent the different HMs and edaphic factors most important to the modeling approach. Length and direction of vectors indicate the strength and direction of the relationship. Fitted variation refers to variance within the linear model created during the DistLM analysis. The total variation refers to the variance within the original data. Blue triangles represent soils from Ash Basins (AB); Red upside-down triangles represent

Pond B (PB) soils; Green squares represent Tim's Branch (TB) soils; pink diamonds represent Upper Three Runs (UR) soils.

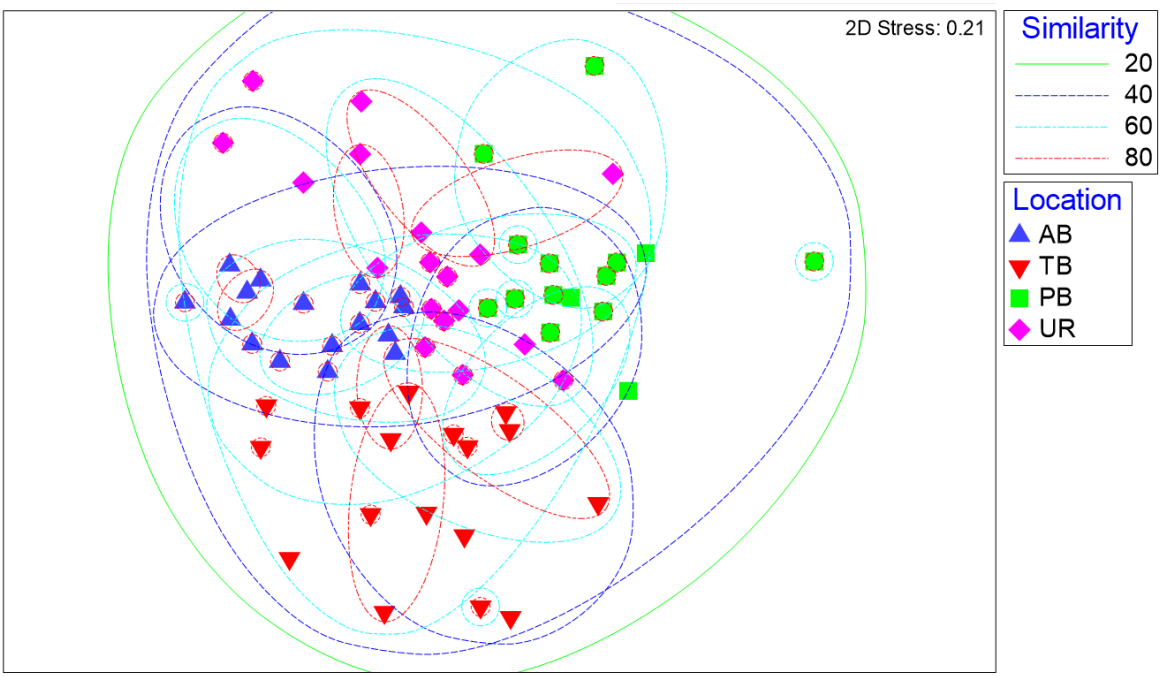

Figure 2-9. Non-metric multi-dimensional scaling plot of fungal OTU frequency after log-transformation, which reduces the influence of the most abundant OTUs. Dashed lines represent percent similarity of clusters using SIMPROF: green lines 20%, dashed blue lines 40%, dashed cyan lines 60%, dashed red lines 80%. Blue triangles represent soils from Ash Basins (AB); Red upside down triangles represent Pond B (PB) soils; Green squares represent Tim's Branch (TB) soils; pink diamonds represent Upper Three Runs (UR) soils. Stress value is 0.13.

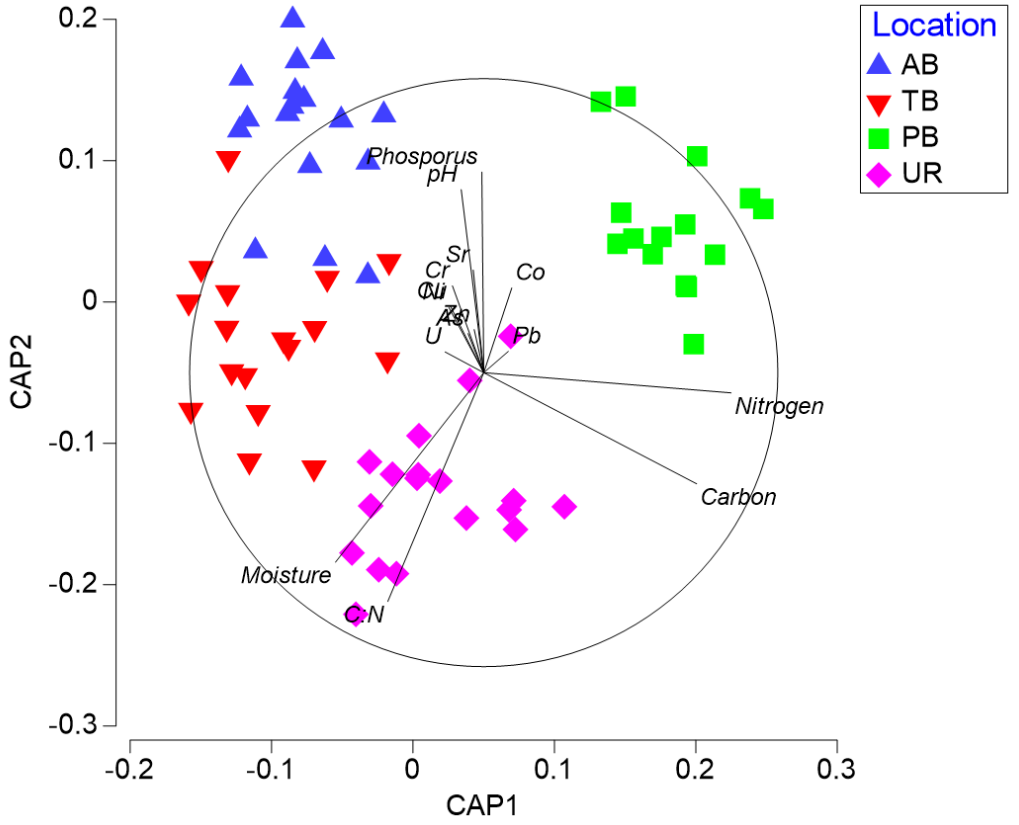

Figure 2-10. Canonical analysis of principal coordinates based on a Bray–Curtis dissimilarity matrix of log-transformed fungal OTU frequencies. Blue triangles represent soils from Ash Basins (AB); Red upside down triangles represent Pond B (PB) soils; Green squares represent Tim's Branch (TB) soils; pink diamonds represent Upper Three Runs (UR) soils.

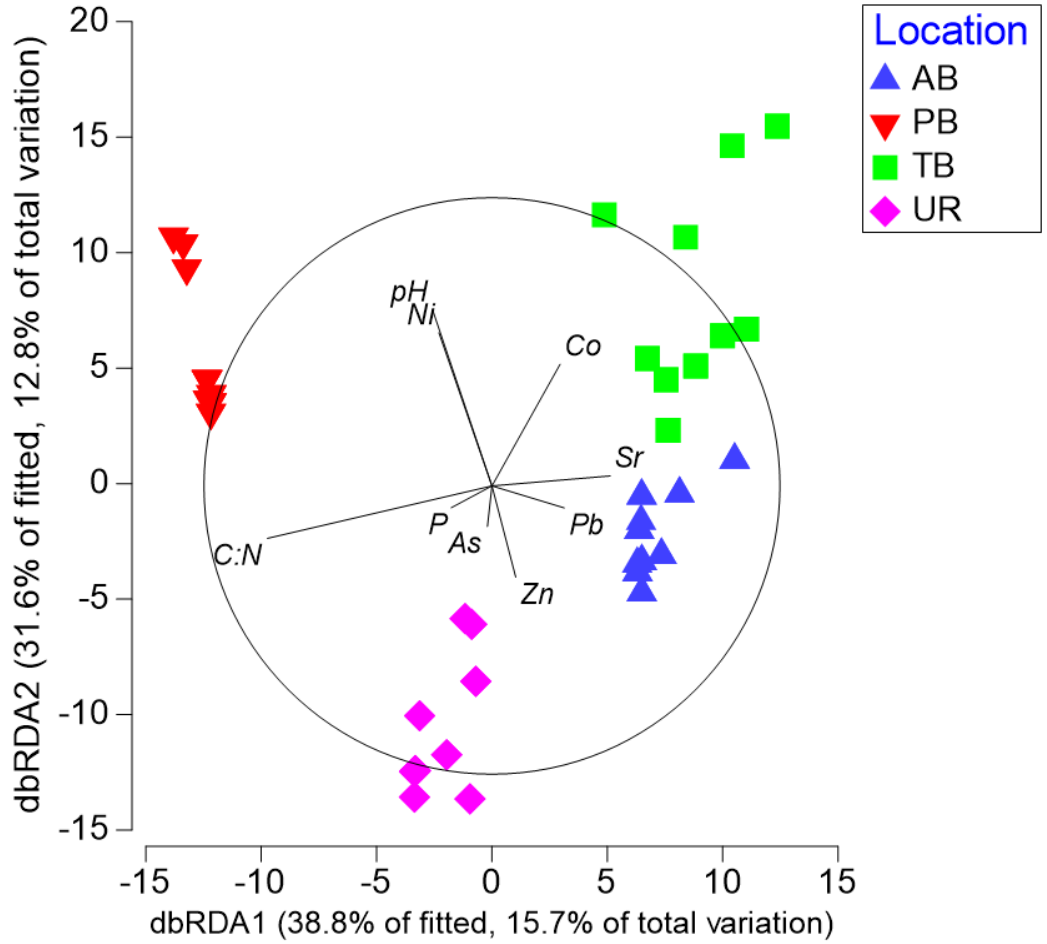

Figure 2-11. Distance-based redundancy analysis (dBRDA) representing raw Pearson correlations for fungal habitat variables. Vectors are overlaid to represent the different HMs and edaphic factors most important to the modeling approach. Length and direction of vectors indicate the strength and direction of the relationship. Fitted variation refers to variance within the linear model created during the DistLM analysis. The total variation refers to the variance within the original data. Blue triangles represent soils from Ash Basins (AB); Red upside down triangles represent Pond B (PB) soils; Green squares represent Tim's Branch (TB) soils; pink diamonds represent Upper Three Runs (UR) soils.

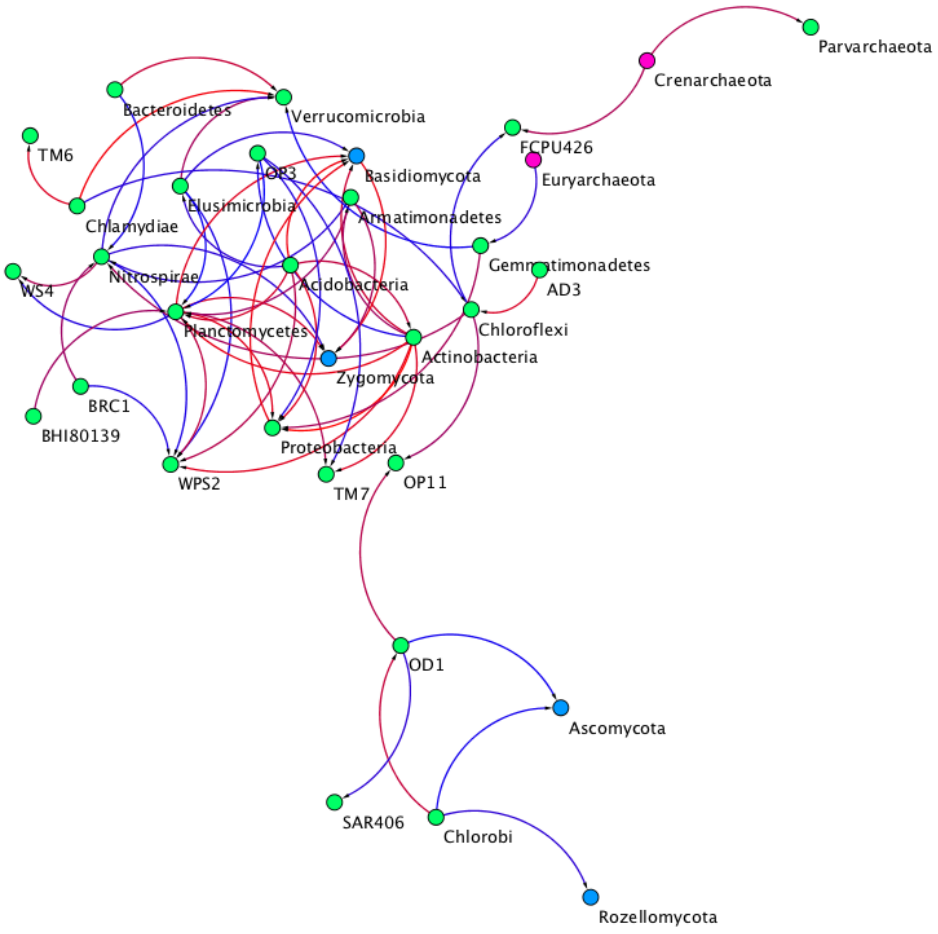

Figure 2-12. Network co-occurrence analysis of archaeal, bacterial, and fungal communities in UR soils. Each dot represents a microbial phylotype (an OTU clustered at 97%): pink dots represent archaea, green dots represent bacteria, blue dots represent fungi. Each connection represents a SparCC correlation with a magnitude >0.6 (positive correlation—red edges) or <−0.6 (negative correlation—blue edges) and statistically significant (P<0.05). Each node was labelled at the phylum level.

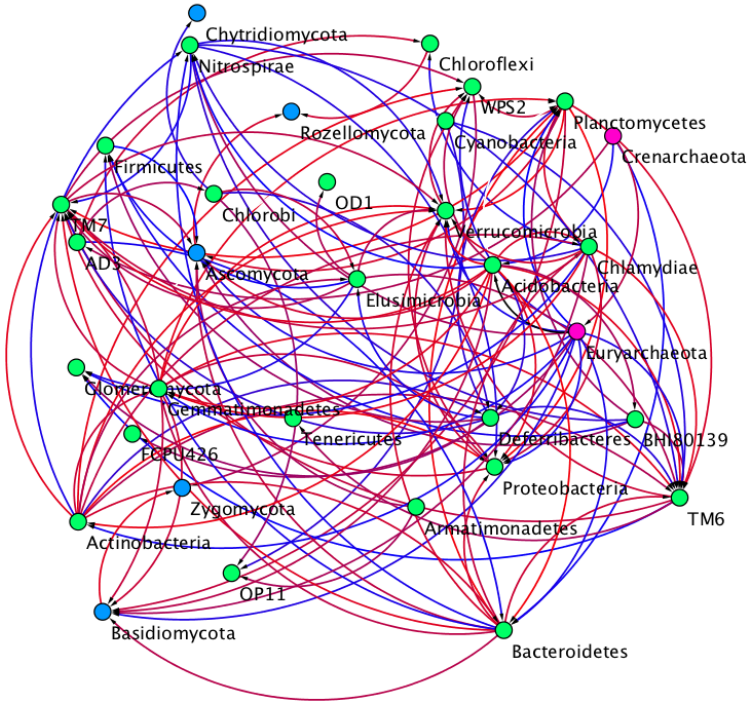

Figure 2-13. Network co-occurrence analysis of archaeal, bacterial, and fungal communities in PB soils. Each dot represents a microbial phylotype (an OTU clustered at 97%): pink dots represent archaea, green dots represent bacteria, blue dots represent fungi. Each connection represents a SparCC correlation with a magnitude >0.6 (positive correlation—red edges) or <−0.6 (negative correlation—blue edges) and statistically significant (P <0.05). Each node was labelled at the phylum level.

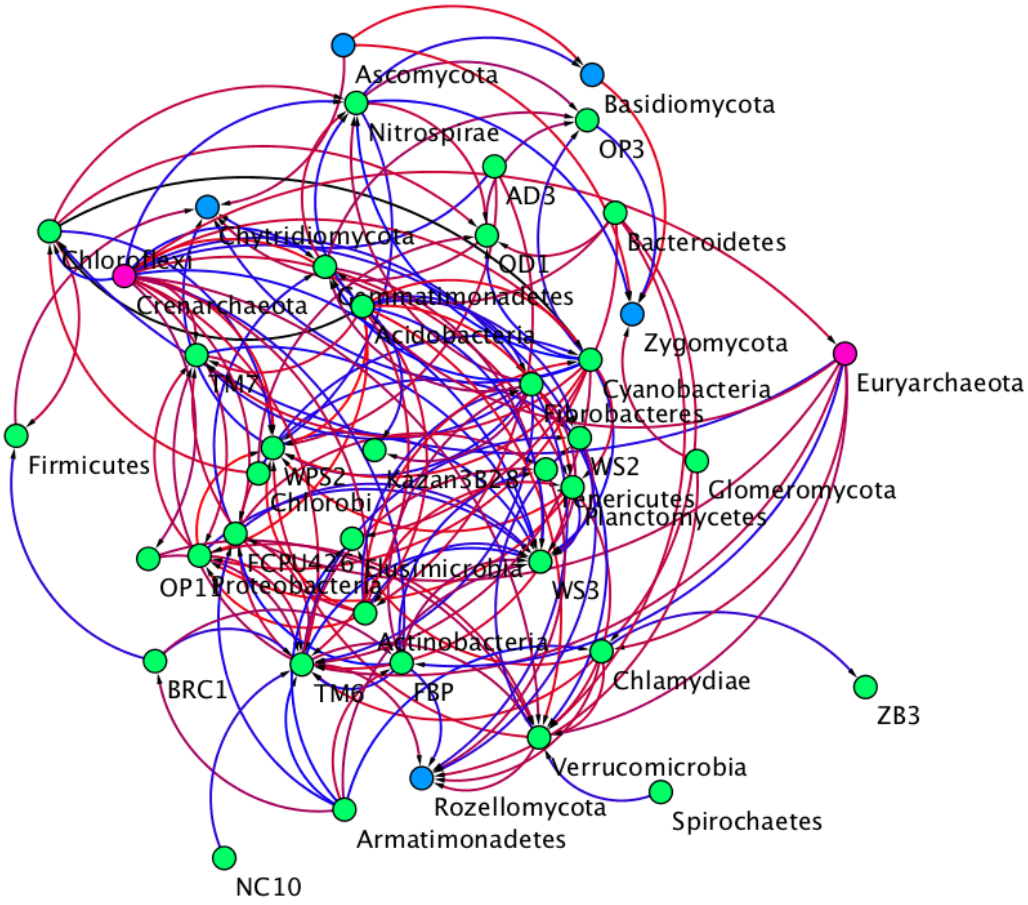

Figure 2-14. Network co-occurrence analysis of archaeal, bacterial, and fungal communities in TB soils. Each dot represents a microbial phylotype (an OTU clustered at 97%): pink dots represent archaea, green dots represent bacteria, blue dots represent fungi. Each connection represents a SparCC correlation with a magnitude >0.6 (positive correlation—red edges) or <−0.6 (negative correlation—blue edges) and statistically significant (P<0.05). Each node was labelled at the phylum level.

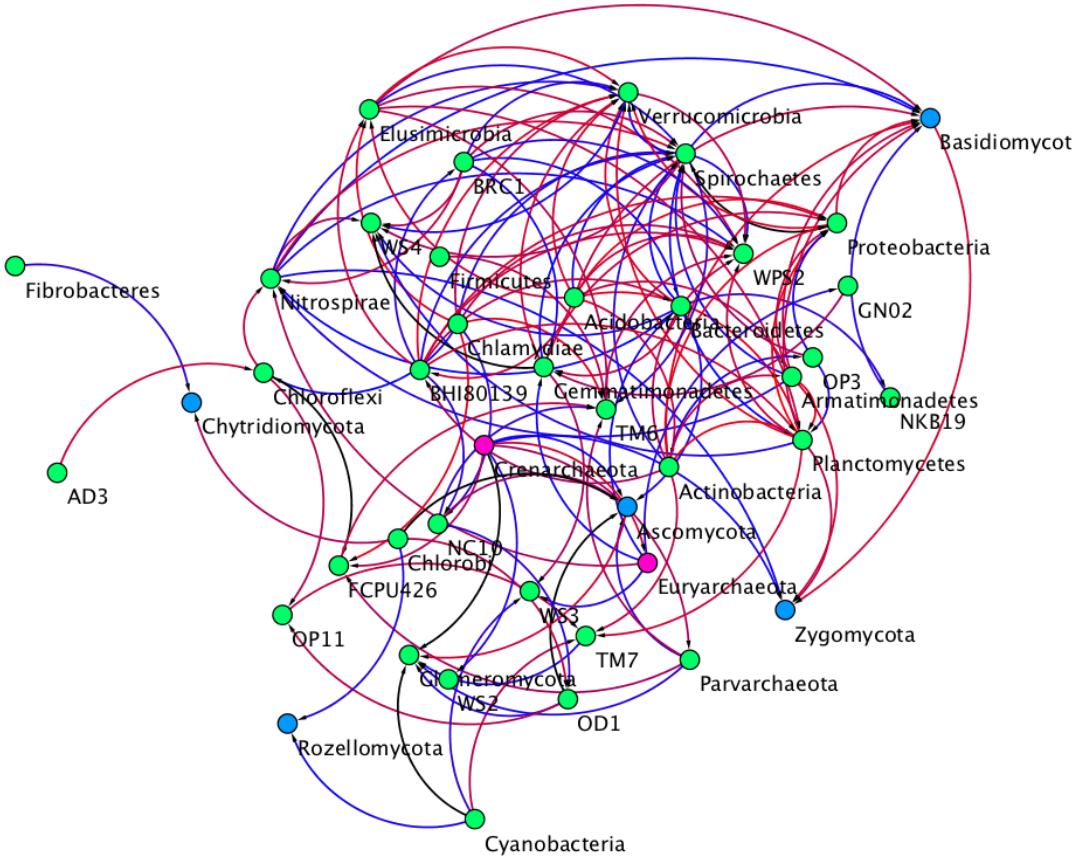

Figure 2-15. Network co-occurrence analysis of archaeal, bacterial, and fungal communities in AB soils. Each dot represents a microbial phylotype (an OTU clustered at 97%): pink dots represent archaea, green dots represent bacteria, blue dots represent fungi. Each connection represents a SparCC correlation with a magnitude >0.6 (positive correlation—red edges) or <−0.6 (negative correlation—blue edges) and statistically significant (P<0.05). Each node was labelled at the phylum level.

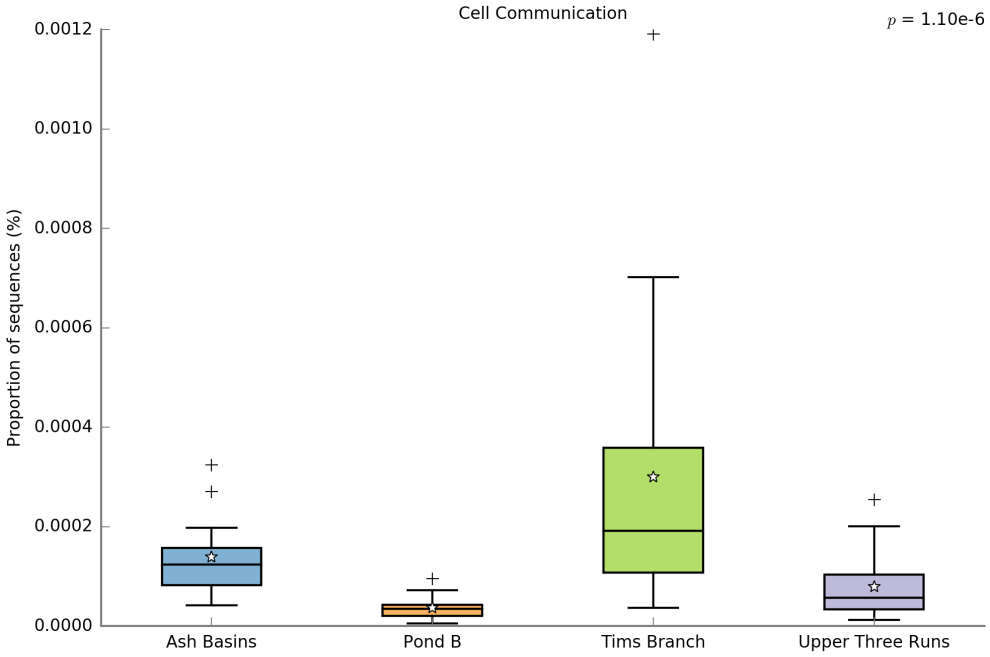

Figure 2-16. Boxplots comparing the the relative abundance of sequences for the KEGG Pathway "Cell Communication" in the soils from the four SRS sites.

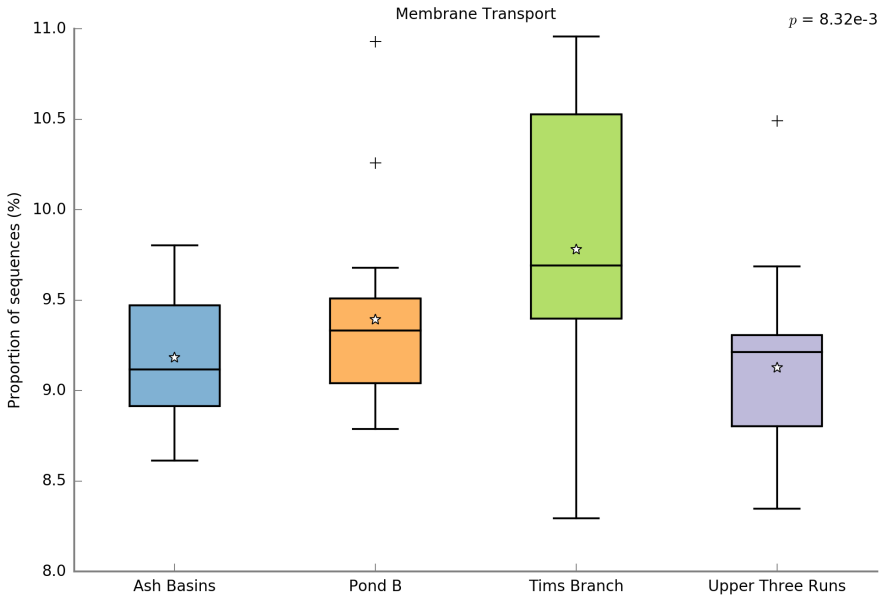

Figure 2-17. Boxplots comparing the the relative abundance of sequences for the KEGG Pathway "Membrane Transport" in the soils from the four SRS sites.

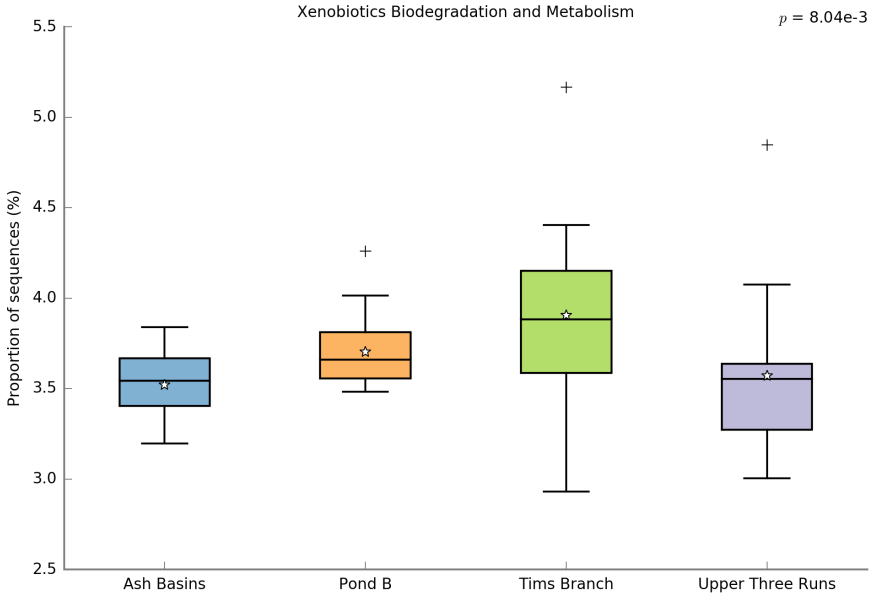

Figure 2-18. Boxplots comparing the the relative abundance of sequences for the KEGG Pathway "Xenobiotics Biodegradation and Metabolism" in the soils from the four SRS sites.

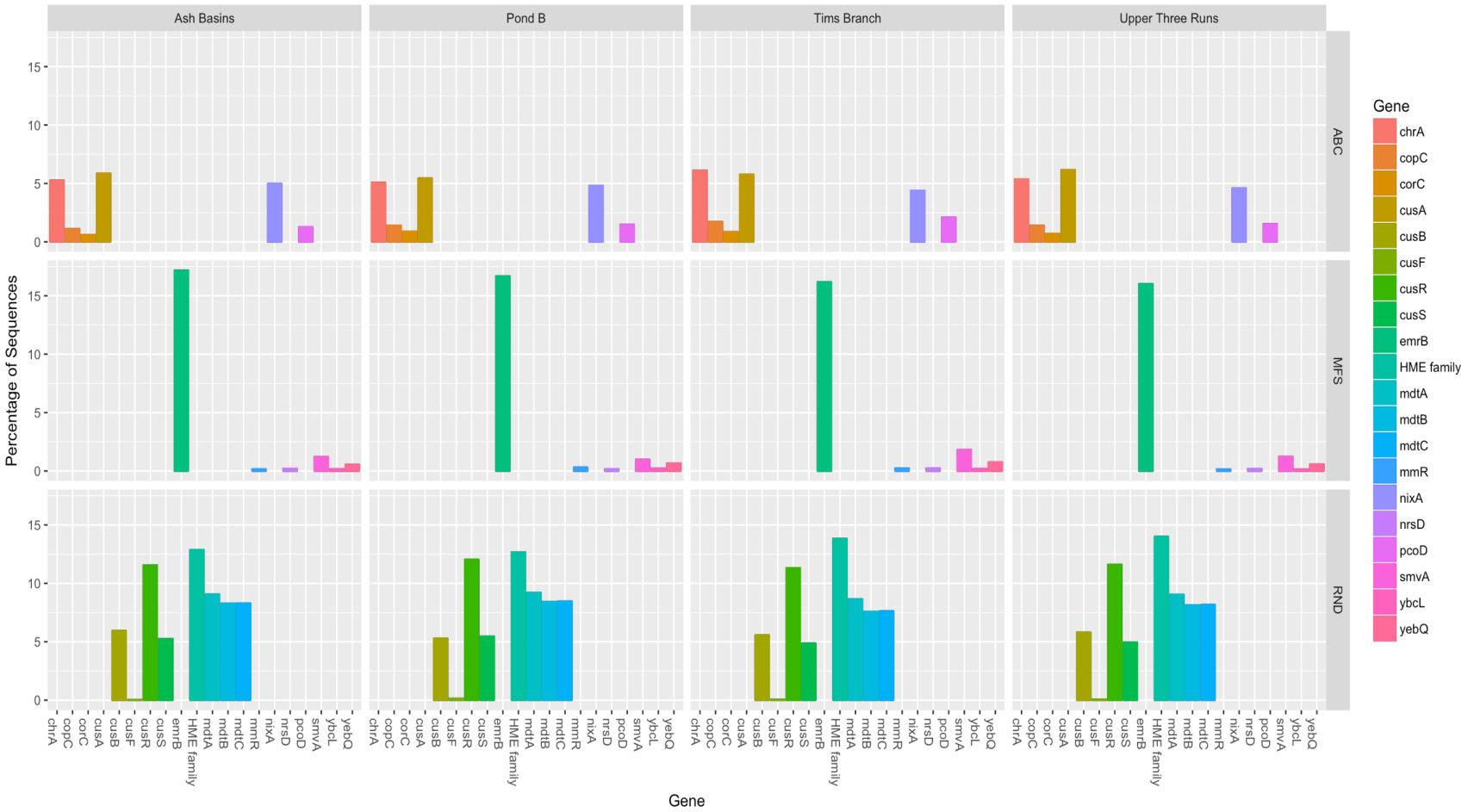
Ash Basins
Pond B
Tims Branch
Upper Three Runs
ABC
MFS
RND
Percentage of Sequences
0
5
10
15
Gene
chrA
copC
corC
cusA
cusB
cusF
cusR
cusS
emrB
HME family
mdtA
mdtB
mdtC
mmR
nixA
nrsD
pcoD
smvA
ybcL
yebQ

Figure 2-19. Relative abundance of top 20 predicted genes detected in soil samples from the four sampled sites. Genes of interest included: “chrA, chromate transporter” (K07240); “copC, copper resistance protein C” (K07156); “corC, magnesium and cobalt transporter” (K06189); “cusA, copper tolerance heavy metal sensor histidine” (K07787); “cusB, copper tolerance heavy metal sensor histidine” (K07798);“cusF, copper tolerance heavy metal sensor histidine” (K07810), “cusR, copper tolerance heavy metal sensor histidine” (K07665); “emrB, multidrug resistance protein” (K03446); “heavy-metal exporter, HME family” (K07239); “mdtA, multidrug efflux pump” (K07799); “mdtB, multidrug efflux pump” (K07788); “mdtC, multidrug efflux pump” (K07789); “mmr, methylenomycin A resistance protein” (K08166); “nixA, high affinity nickel transporter” (K07241); “nrsD; putative nickel transporter” (K07785); “pcoD, copper resistance protein D” (K07245); “smvA, multidrug resistance efflux pump” (K08167); “ybcL, drug effux pump” (K08164); “yebQ, multidrug resistance efflux pump” (K08169).

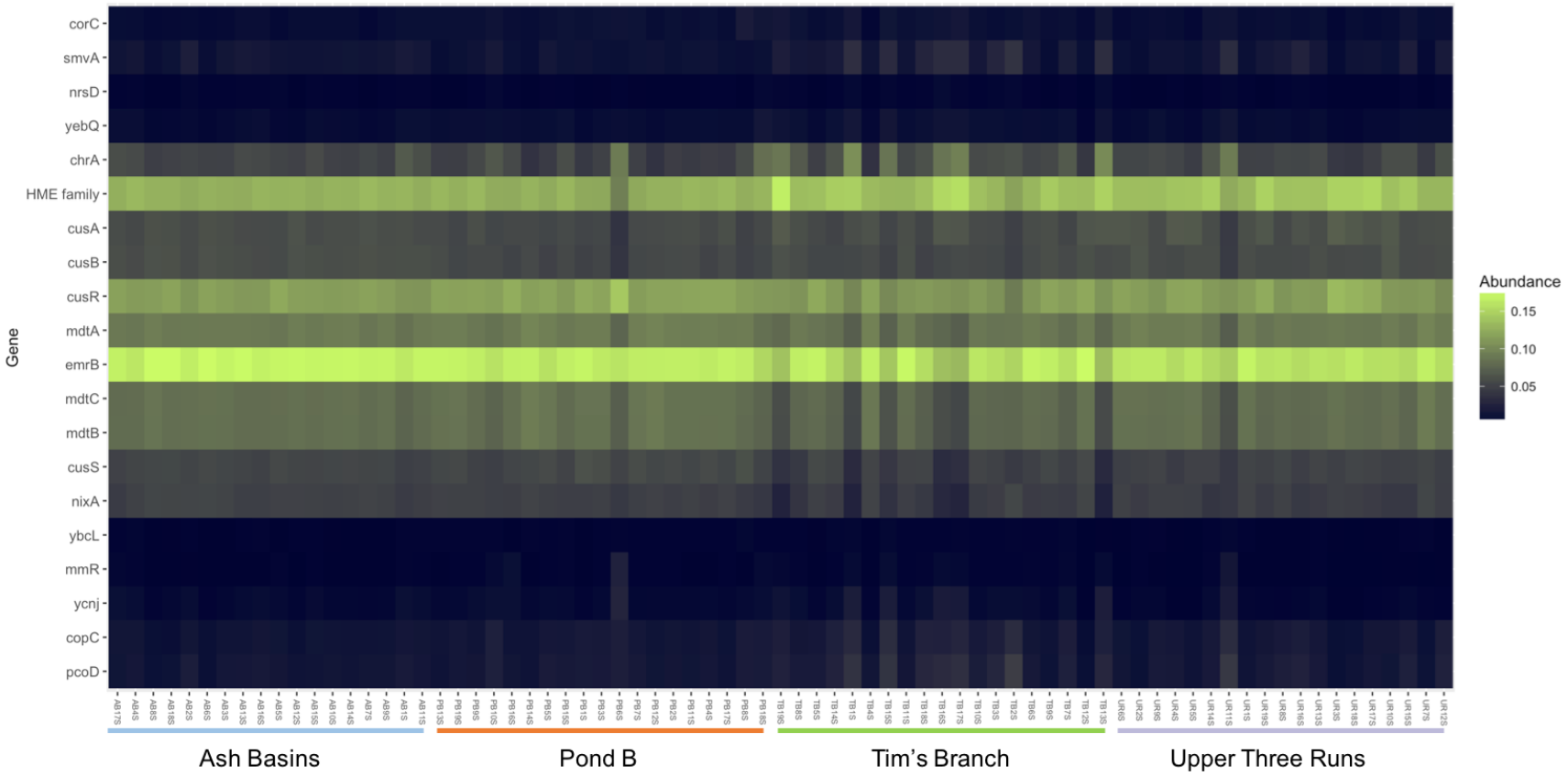

Figure 2-20. Relative abundance of top 20 predicted genes detected in soil samples from the four sampled sites as a heatmap. Genes of interest included: "chrA, chromate transporter" (K07240); "copC, copper resistance protein C" (K07156); "corC, magnesium and

cobalt transporter" (K06189); "cusA, copper tolerance heavy metal sensor histidine" (K07787); "cusB, copper tolerance heavy metal sensor histidine" (K07798);"cusF, copper tolerance heavy metal sensor histidine" (K07810), "cusR, copper tolerance heavy metal sensor histidine" (K07665); "emrB, multidrug resistance protein" (K03446); "heavy-metal exporter, HME family" (K07239); "mdtA, multidrug efflux pump" (K07799); "mdtB, multidrug efflux pump" (K07788); "mdtC, multidrug efflux pump" (K07789); "mmr, methylenomycin A resistance protein" (K08166); "nixA, high affinity nickel transporter" (K07241); "nrsD; putative nickel transporter" (K07785); "pcoD, copper resistance protein D" (K07245); "smvA, multidrug resistance efflux pump" (K08167); "ybcL, drug effux pump" (K08164); "yebQ, multidrug resistance efflux pump" (K08169).

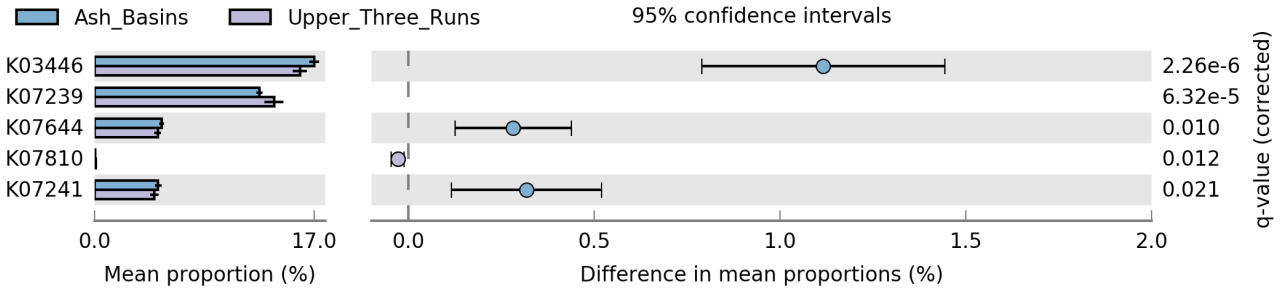

Figure 2-21. Pair-wise comparisons of soils sampled from Ash Basins (blue) and Upper Three Runs (purple) showing the predicted genes with significant differences. Plots are displayed as 95% confidence intervals.

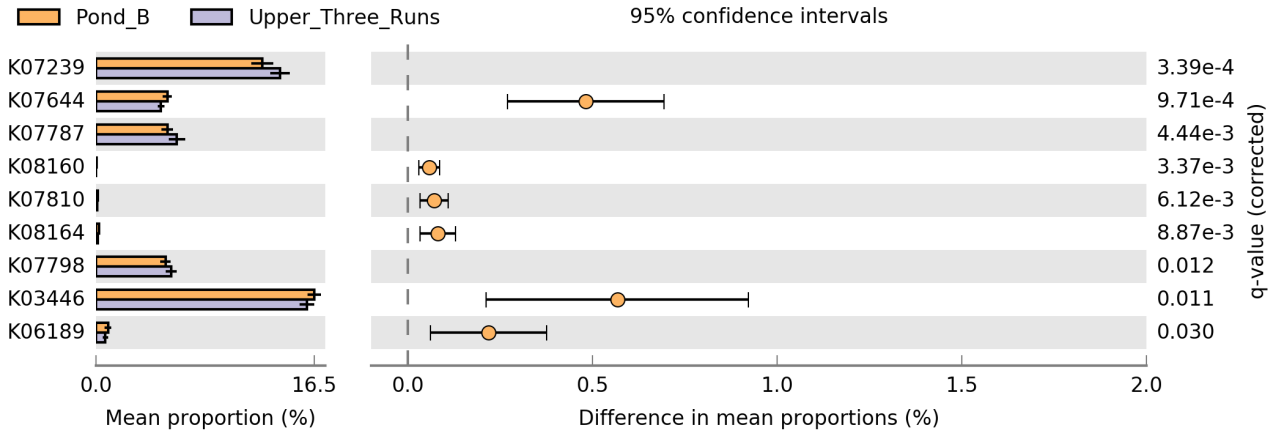

Figure 2-22. Pair-wise comparisons of soils sampled from Pond B (orange) and Upper Three Runs (purple) showing the predicted genes with significant differences. Plots are displayed as 95% confidence intervals.

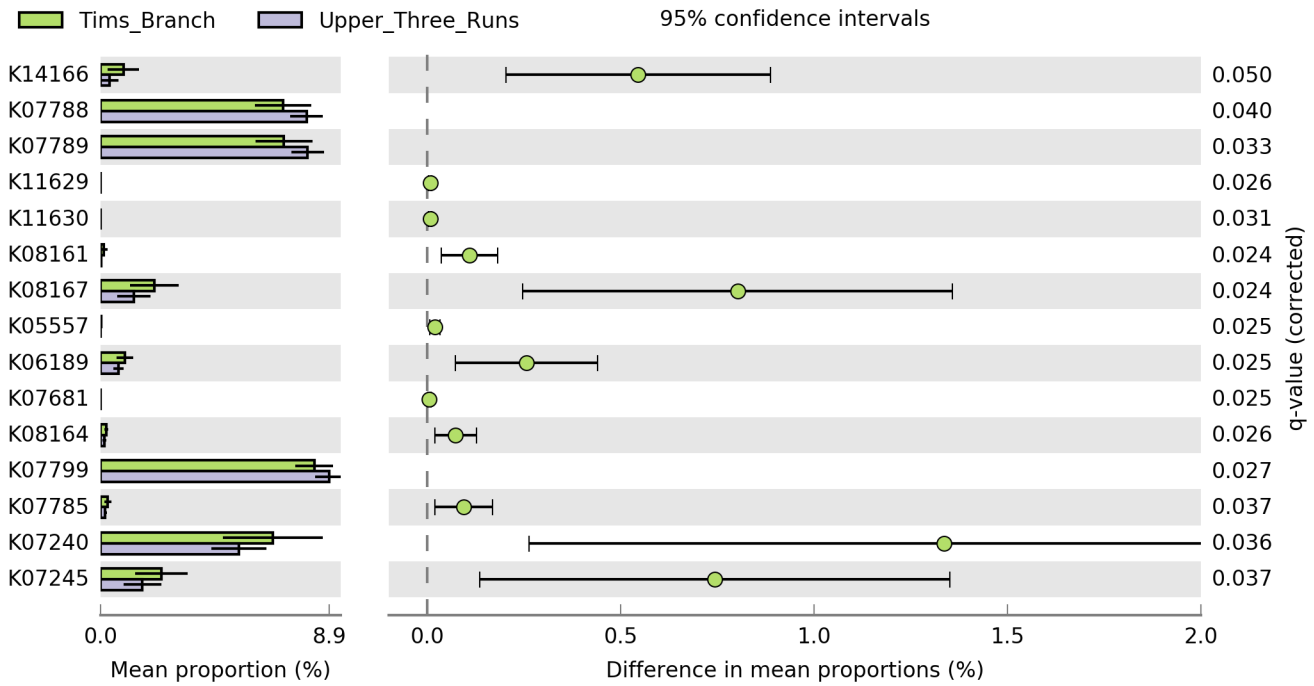

Figure 2-23. Pair-wise comparisons of soils sampled from Tim's Branch (green) and Upper Three Runs (purple) showing the predicted genes with significant differences. Plots are displayed as 95% confidence intervals.

CHAPTER 3

HEAVY METAL CONTAMINATION AT THE SAVANNAH RIVER SITE (SRS) CORRELATES WITH PREDICTED CO-OCCURRENCE OF ANTIBIOTIC AND METAL RESISTANCE GENES IN THE INTESTINAL MICROBIOME OF WILD *PEROMYSCUS GOSSYPINUS*[†]

[†] Thomas, J. C. IV, J. Beasley, J. C. Seaman, J. W. Finger Jr., T. J. Kieran, J V. McArthur, O. E. Rhodes Jr., and T. C. Glenn. Submitting to the ISME Journal: Multidisciplinary Journal of Microbial Ecology.

Abstract

Recent studies have linked heavy-metal exposure with perturbations in the gut microbiota (dysbiosis) of animals. While many of these studies have examined the pathological effect of heavy metals on animals within controlled lab settings, very few have sought to study the intact microbiota of wild animals exposed to sub-lethal levels of persistent environmental metal contamination. Here we utilized 16S rRNA gene sequencing, predictive functional profiling, and network-based analysis to examine the influence of chronic heavy-metal burdens on the gut microbiota of wild cotton mice (*Peromyscus gossypinus*). Mice from sites with elevated heavy metal burden harbored significantly less bacterial diversity than those with less contamination ($P < 0.05$), as well as enriched *Pseudomonas* and deplete *Bacteroidetes*. PERMANOVA of Bray-Curtis dissimilarities revealed associations with the mice intestinal tissue type (large vs small) ($P=0.001$), and the sampling site ($P=0.001$). Predictive functional profiling and network-based analyses revealed significantly higher relative abundance of metal and antibiotic resistance genes in mice from sites with elevated heavy metal contamination, suggesting that such exposures may also encourage both compositional and functional changes in the intestinal microbiota.

Introduction

The gut microbiome: a reservoir for antimicrobial resistance

Given the rapid emergence and spread of antibiotic resistance among bacterial pathogens over the last several decades, coupled with our current understanding of the human microbiome there has been a sizable interest to characterize the antibiotic resistance reservoir (the "resistome") of the human gut microbiome. The gut microbiome presents a densely packed ecosystem, with ample opportunities for the horizontal exchange of genetic material, including antibiotic resistance elements (Schaik, 2015). While, the pre-dominant bacteria are non-pathogenic gut commensals, external factors such as antibiotic use, diet, and other environmental factors have shown strong correlations with microbial dysbiosis—a condition where bacteria shift in an unhealthful direction—and even disease (Phillips et al, 2009; Arthur et al., 2013; Schaik, 2015; Boulangé et al., 2016; Wu et al., 2016). Over time such microbial imbalances can cause the proliferation of potentially harmful microbiota, which may acquire resistance genes from benign commensals (Aarts and Margolles, 2015). In addition, recent findings suggest that antibiotic usage is not the only selection criteria; heavy metals, radiation, and other offensive compounds may also select for resistance through similar or unknown mechanisms (Allen et al., 2010; Seiler and Berendonk, 2012; Chen et., 2015).

Heavy metals can perturb the gut microbiome

Heavy metals (HMs), in particular, have been shown to display a profound influence on gut microbiota and overall host intestinal homeostasis (Breton et al., 2013; Lu et al., 2014; Zhang et al., 2015). In such toxicological studies, laboratory-bred animal models, such as mice, are typically exposed to concentrations of individual HMs.

However, in areas with significant HM pollution (e.g. industrial, mining, or urban areas) the host may be challenged by both the simultaneous and chronic exposure to multiple contaminant stressors (Yu et al., 2011; Zhuang et al., 2014). Hence, studies examining the acute exposure of individual HMs may not accurately represent the exposure of a wild organism including its microbiome as they exist naturally, in a polluted environment.

Specific aims and hypotheses

Thus, we hypothesized that heavy metals (e.g. As, Cr, Co, Cu, Pb, Ni, Sr, Zn) present in soil environments of the mice would exert a significant influence on the diversity and composition of the intestinal microbiota of wild *Peromyscus* in contaminated habitats. In addition, we predicted that mice in contaminated habitats would contain intestinal microbiota with significantly higher abundance of metal and antibiotic resistance elements. To test these hypotheses, we utilized DNA extracts from intestinal samples collected from wild cotton mice inhabiting both contaminated and reference locations to determine the extent which environmental HMs influence the composition and function of the microbiome. Specifically, our study provides further evidence on the role of environmental HMs on the etiology of dysbiosis and the co-selection of antimicrobial and metal resistance (i.e., the "resistome") in the gut microbiome. (Baker-Austin et al., 2006; Stepanauskas et al., 2006; Seiler and Berendonk, 2012; Pal et al., 2015).

Methods

Study areas

The Savannah River Site (SRS) (33º00'N and 81º41W) is an approximately 800-km^2 former nuclear weapons production facility situated along the Savannah River in the upper coastal plain of South Carolina near Aiken, SC**.** The SRS is characterized as having humid, subtropical weather (Garten et al., 2000) (Figure 3-1). Historically, a variety of hazardous materials and wastes were processed, treated, stored, and improperly disposed of on the SRS. In 1989, the site was officially listed on EPA's National Priorities List (NPL) due to chemical (HMs and solvents) and radionuclide contamination of on-site groundwater (Agency for Toxic Substances and Disease Registry, 2007).

In this study, we chose four sampling locations with habitats consisting of mixed hardwood and pine forest; three contaminated areas, and a reference location. The contaminated sites included an area with elevated metal and metalloid concentrations (D-area coal-fly ash basin; AB), an area with only radionuclide contamination (Pond B; PB), and an area with both metals and radionuclide contamination (Tim's Branch; TB) (Figure 3-1). Soils from the D-area ash coal-fly basins are contaminated with coal combustion waste (CCW) containing a range of metals and metalloids such as arsenic (As), chromium (Cr), cadmium (Cd), copper (Cu), iron (Fe), nickel (Ni), selenium (Se), and Zinc (Zn) (Raimondo et al., 1998; Nagle et al., 2001; Agency for Toxic Substances and Disease Registry, 2007; Tannenbaum and Beasley, 2016). Pond B is a reservoir that was originally constructed as a secondary cooling system for nuclear production at R Reactor until it was decommissioned in 1964 (Sugg et al., 1995). Between 1961-1964 R Reactor discharged several radionuclides (e.g. ^{3}H, ^{137}Cs, ^{90}Sr, americium-241, cerium-244, and

plutonium-239, 240) into Pond B as effluents, the vast majority residing in the pond's sediments (Carlton et al., 1992). Tim's Branch is a second-order stream that receives contamination from an eroding former discharge settling pond, Steed Pond (Arey et al., 1999). Steed Pond received up to 44,000 kg of depleted and natural uranium (U), as well as similar quantities of Ni from an aluminum-clad nuclear reactor, between 1954 and 1985 (Arey et al., 1999). TB soils are contaminated with aluminum (Al), Cu, Cr, Zn, lead (Pb), and depleted U (Tannenbaum and Beasley, 2016). Upper Three Runs Creek, a 40-km waterway that empties into the Savannah River, used as the reference location in this study. It lies 8 km away from areas with contamination and is estimated to have one of the highest levels of aquatic insect biodiversity in the world (< 650 species (Voelz and McArthur 2000, Meyer et al., 2007). It is the only major tributary at SRS that has not received any thermal, chemical, or radioactive discharges (Agency for Toxic Substances and Disease Registry, 2007).

Sample Collection and Processing

In this study, we examined the small and large intestinal samples previously collected by Tannenbaum and Beasley (2016). Briefly, 90 wild cotton mice (*Peromyscus gossypinus*) were captured from March to mid-May using randomly placed Sherman live traps (H.B. Sherman Traps, Inc., Tallahassee, FL) baited with black oil sunflower seeds as described in Tannenbaum and Beasley (2016). From Upper Three Runs (UR) there were 23 total (13 males/10 females), Ash Basins (AB) 23 total (15 males/8 females), Pond B (PB) 19 total (11 males/8 females), and Tim's Branch (TB) 25 total (16 males/9 females). Trapping among the study areas was staggered, with traps placed at areas likely to have mouse activity (e.g. along downed trees, etc.) within 10 -15 m of contaminated

water bodies (Tannenbaum and Beasley, 2016). In addition, we also collected approximately 15g of contaminated soil near the GPS points of the Sherman traps using a 70% ethanol-sterilized garden shovel. All samples were placed on ice until eventual storage at -20 °C. Metals were extracted from 0.25g of composited mice tissue (kidneys and livers) and soil samples using the EPA Method 3052 with modifications (Wu et al., 1996) (Supplemental Information). All digestions were analyzed for extractable arsenic (As), cobalt (Co), copper (Cu), chromium (Cr), nickel (Ni), strontium (Sr), uranium (U), and zinc (Zn) using an inductively coupled plasma mass spectrometer (ICP-MS).

DNA isolation, PCR, and Illumina Sequencing of 16S rRNA amplicons

Genomic DNA was extracted from 0.5g of mice intestinal tissues (i.e. small and large) using a MoBio PowerSoil DNA isolation kit (MoBio, Carlsbad, CA, 92010, USA) and purified by a magnetic-based size selection method using SeraMag Speed Beads (Thermo-Fisher Scientific, Asheville, NC, 28804, USA) according to the manufacturer's protocol. PCR libraries were generated using the S-D-Bact-041-b-S-17 (5'-CCTACGGGNGGCWGCAG-3') forward and S-D-Bact-0785-a-A-21 (5'-GACTACHVGGGTATCTAATCC-3') reverse primer pair (Klindworth et., 2012). Modifications to the primer sets (8 forward + 12 reverse) were done according to Taggimatrix protocol, which included fusions with universal 5' iTru sequences containing up to 96 combinations of unique internal tags (Glenn & Faircloth, 2013). DNA from each sample was PCR amplified using the 16S-iTru fusions in 25-µl reactions using the KAPA HiFi Hotstart PCR kit (KAPA Biosystems, Wilmington, MA, 01887, USA). The PCR amplification protocol was as follows: 95°C for 3 minutes, followed by 30 cycles of 95°C for 1 min, 55°C for 30 s, and 72°C for 30 s with a final elongation step

of 72°C for 5 min. PCR was performed using an T100 Thermal Cycler (BioRad, Hercules, CA, 94547, USA) and amplicons were visualized using 1.5% gel electrophoresis. PCR products were purified then quantified using a Qubit Fluorometer (Thermo-Fisher Scientific, Asheville, NC, 28804, USA) set to broad range sensitivity and diluted to a final concentration of 2 ng/µl using sterile nuclease free water. The diluted PCR amplicons were used in a second PCR reaction containing the TruSeq Illumina P5 and P7 Primers. The PCR amplification was the same as above however modified with fewer cycles (14). The quadruple-indexed libraries were purified a final time using the magnetic-bead size selection method and pooled based on the number of desired reads. PCR products were then sent to the Georgia Genomics Facility (http://dna.uga.edu) for sequencing on an Illumina MiSeq using an Illumina PE300 kit (Illumina, San Diego, CA, 92122CA, USA).

De-multiplexing and Quality Filtering

All Fastq conversion and de-multiplexing were conducted using bcl2fastq (Illumina, v1.8.4) and processed to remove low quality reads (FastX toolkit). Paired-end sequencing reads were imported into Geneious v10.0 (Biomatters Limited, NJ, USA), set as paired-reads with an expected insert size of 444 bp and trimmed to remove Illumina adapters using default settings. Paired-end sequencing reads were then merged using the FLASH v1.2.9 plugin (Magoc and Salzberg, 2011). The software package Mr_Demuxy v1.2.0 (https://pypi.python.org/pypi/Mr_Demuxy/1.2.0) was utilized to de-multiplex the merged reads into individual combinatorially tagged FASTQ files. Sequences were filtered based on size (≥ 300 bp) and quality scores (≥Q20).

Mouse intestinal 16S Sequence Analysis

Sequencing reads were imported into the phylogenetic software package QIIME v1.9.1 (MacQiime v1.91 package: http://www.wernerlab.org/software/macqiime, Caporaso et al., 2010) for OTU (Operational Taxonomic Unit) generation, multi-leveled taxonomic classification, and diversity estimates. Briefly, samples were sorted using the *add_qiime_labels.py* script. Afterward, bacterial OTUs were selected using an open reference workflow, with Greengenes v13_8 16S reference database (http://greengenes.secondgenome.com/, DeSantis et al., 2006) and default *uclust* (Edgar, 2010) OTU picking strategy (Supplemental Information). Taxonomy was defined using default settings of ≥ 97% similarity to reference sequences.

Metagenome prediction of HM and antibiotic resistance with PICRUSt and Tax4Fun

The software PICRUSt (Phylogenetic Investigation of Communities by Reconstruction of Unobserved States) (Langille et al., 2013) and Tax4Fun (Aßhauer et al., 20155) were applied to make functional gene content predictions using the Greengenes database v13_5 and Silva119 reference database respectively (Supplemental Information). We were primarily interested in KEGG orthologs corresponding to HM resistance and antibiotic/multi-drug efflux genes, since prior studies have suggested they can be co-selected (Baker-Austin et al., 2006; Pal et al., 2015). A total of 37 KEGG orthologs were selected by manually searching the KEGG database (Table 1).

Network-based analysis

SparCC (available at https://bitbucket.org/yonatanf/sparcc) was utilized to determine co-abundance and co-exclusion networks between K0s. SparCC calculates two-sided pseudo p- values (p values ≤ 0.05 considered significant) based on bootstrapping of 100 repetitions. A network plot was generated, and correlation magnitudes ≥ 0.6 (indicating strong co-abundance relationships) and ≤ -0.6 (indicating strong co-exclusion relationships) were visualized using Cytoscape v3.5.1. In addition, the output from QIIME's *make_otu_network.py* script was utilized to generate a bipartite network, in which sample nodes are connected to KO nodes in a bipartite network. To cluster samples and KOs, we filtered and removed edge weights (number of sequences per OTU) less than 1000, then visualized the network using the stochastic spring-embedded algorithm, as implemented in Cytoscape 3.5.1 (Ley et al., 2012). Edges were colored based on whether the KO was a HM or an antibiotic/multi-drug resistance gene.

Statistical analyses and data visualization

We used linear regression to compare metals present in the soil among different sites using JMP Pro 13 (SAS, Cary, NC USA). Trace elements were log-transformed, when necessary, to meet assumptions of normality. *Post-hoc* multiple comparisons were made using t-tests to further examine site differences in trace elements.

Within-sample (alpha) diversity was evaluated and visualized in QIIME v1.91 and the Phyloseq package using various metrics (Chao1, ACE, Fisher's Alpha, Shannon-Wiener, and Simpson) (McMurdie and Holmes, 2014). Alpha diversity of communities found in mice intestinal tissues was computed using the *core_diversity_analyses.py*

workflow with a sequencing depth set to 15,000 sequences. To test for the significant variation in taxonomic richness across the four sampling sites, we used the non-parametric Kruskal-Wallis test (Kruskal & Wallis, 1952) with the False Discovery Rate (FDR) correction as implemented in the *compare_alpha_diversity.py* script.

We used QIIME v1.91 to test for the significant variation in the frequency of individual OTUs across the four sites, using Kruskal-Wallis test with FDR correction for multiple comparisons, and the Monte Carlo simulated non-parametric t-test for pair-wise comparisons, as implemented in the *group_significance.py* script. Hierarchical clustering based on complete linkage was used to examine the similarity between samples, and similarity of profile analysis (SIMPROF) was used to test the significance of clusters (Clarke et al., 2008). Bray-Curtis distances between samples (beta diversity) were computed and visualized using PRIMER 7.0 software with PERMANOVA+ add-on (Primer-E, United Kingdom; Bray & Curtis, 1957). This dissimilarity matrix was used to generate a non-metric multi-dimensional scaling plot (nMDS) based on 999 permutations, which was followed by canonical analysis of principle coordinates (CAP) for testing our *a priori* hypotheses (e.g. influence of tissue type, sampling location) (Kruskal, 1964; Anderson and Willis, 2003).

Differences in microbial community structure and composition between the four sampling sites were tested using permutational multivariate analysis of variance (PERMANOVA) on log-transformed Bray-Curtis dissimilarity values (Anderson et al., 2005). For the PERMANOVA analysis mice sampling location, sex, and intestinal tissue type were fixed effects. Sex was nested within location, and intestinal tissue type was

nested within sex. We used a type III partial sum of squares design and Monte Carlo sampling permutated 999 times over residuals under a full model.

The final output from the PICRUSt and Tax4Fun workflows was imported into Statistical Analysis of Metagenomic Profiles (STAMP) to examine KEGG pathways and orthologs (KO) (Parks et al., 2014). Multiple comparison analyses were conducted using a Kruskal-Wallis test with the FDR correction (Storey, 2014). Two group comparisons were conducted using a Welch's t-test with FDR correction (Satterthwaite, 1946). Lastly, to compare predicted metagenome data between PICRUSt and Tax4Fun we compared the biom files computed by both using a custom R script to calculate the Spearman correlation between both studies (Supplemental Information) (Myers and Sirois, 2014).

Results

Metal concentrations of soils in *Peromyscus* habitat

The results of HMs analysis in the randomly selected soil samples are presented in Table 3-1. Pairwise comparisons varied depending on the type of HM, however generally, metals such as Sr [AB: up to 176.27 mg/kg (40.43 ± 49.24 mg/kg), TB: up to 37.90 mg/kg (25.05 ± 13.10 mg/kg)), and Co (AB: up to 18.17 mg/kg (4.53 ± 5.10 mg/kg), TB: up to 12.99 mg/kg (5.71 ± 3.38 mg/kg)] were significantly higher ($P < 0.05$) in soil samples from AB and TB, compared to PB and UR (Supplemental Information). All HMs analyzed from mice kidneys and livers were below the minimum detection limit (MDL).

Wild *P. gossypinus* harbors abundant dissimilatory metal-reducing bacteria (DSRB) *Desulfovibrio*, and high heavy-metal concentrations may enrich the opportunistic pathogen *Pseudomonas* spp.

After completing all quality filtering steps, denoising, and chimera removal in Geneious and QIIME, a dataset of 7,712,212 high quality (Q ≥ 20)16S rRNA gene sequences was compiled with an average read of 412.7 ± 29.2. Analyses were performed on rarefied data using an even sampling depth of 15,000 reads per sample. A total of 90,862 OTUs (3,827 ± 2,035 OTUs/sample) were observed spanning 10 bacterial phyla commonly associated with the mammalian gastrointestinal (GI) tract.

We identified a core microbiome consisting of 4 bacterial phyla (i.e. Firmicutes, Proteobacteria, Actinobacteria, and TM7) shared between all the sequences analyzed in the study in the small and large intestines (Figure 3-2). Overall, samples from AB had the highest mean relative abundances of Firmicutes (46.00 ± 0.50 %), Proteobacteria (26.85 ± 0.30 %), and Actinobacteria (10.60 ± 0.20 %). Furthermore, in terms of the major phyla there were significant differences in Bacteroidetes (P=5.81e-9), Proteobacteria (P=2.80e-4), TM7 (P=1.20e-5), Verrucomicrobia (P=1.19e-4), and several others between all intestinal samples (Supplemental Information). Pair-wise group comparisons revealed mice intestinal bacteria from AB had significantly lower abundance of Bacteroidetes, but a higher relative abundance of Proteobacteria compared to mouse intestinal bacteria from both PB and UR ($P < 0.05$), while TB had a significantly lower abundance of TM7, Chlamydiae, and Cyanobacteria compared to PB and UR ($P < 0.05$) (Supplemental Information). At the family level, when examining relative abundance there were several

dominant bacterial families that were observed in the intestinal samples (Figure 3-3). These groups included *Lactobacillaceae* (Firmicutes) (32.00 ± 8.49%), *Desulfovibrionaceae* (δ-Proteobacteria) (10.57 ± 1.95%), *Coriobacteriaceae* (Actinobacteria) (8.34 ± 1.51%), *Pseudomonadaceae* (γ-Proteobacteria) (6.25 ± 6.80%), *Ruminococaceae* (Firmicutes) (5.57 ± 1.17%), *F16* (TM7) (5.45 ± 2.36 %), *S24-7* (Bacteroidetes) (4.90 ± 2.24%), *Lachnospiraceae* (Firmicutes) (3.77 ± 1.30%). Moreover, we examined the top 16 most abundant genera and observed *Lactobacillus* as the most dominant bacterial genus across all intestinal samples. Interestingly, both samples from AB and TB had significantly higher relative abundances of *Pseudomonas* (γ-Proteobacteria) and lower Bacteroidetes compared to UR and PB. In addition, samples from AB had significantly higher relative abundances of *Epulopiscum* (Firmicutes), *Carnobacterium* (Firmicutes), *Adlercreutzia* (Actinobacteria) compared to the other sites ($P < 0.05$) (Supplemental Information).

Intestinal microbiota of *Peromyscus* gossypinus displays reduced species richness in samples from sites with elevated HMs

Generally, intestinal samples from TB and AB mice had the lowest observed diversity, while those from PB and UR had the highest observed diversity across all the diversity metrics (Figure 3-3). In addition, when performing pairwise group comparisons there were significant differences in Chao1 and Faith's phylogenetic diversity (PD) between the mice microbiota from sites with greater HM contamination (AB and TB) and those with lower concentrations (non-parametric test with *compare_alpha_diversity.py*, $P < 0.05$) for all default QIIME diversity metrics (Supplemental Information).

Sampling sites display clear separation of mouse intestinal communities

Unconstrained nMDS plots based on a Bray-Curtis dissimilarity matrix were overlaid with SIMPROF based cluster analysis data to examine overall similarity between sites in multi-dimensional space (Figure 3-4). The nMDS plots indicated that overall the communities displayed between 20 and 40 percent similarity, however, the similarities within-groups showed a high degree of variability. In order, to unravel patterns in multidimensional space that might be masked by high variability and high correlation structure among unrelated variables we also applied canonical analysis of principal coordinates (CAP) (Anderson and Willis, 2003). The results of the CAP constrained ordination demonstrated that both the first squared canonical correlation (σ_1^2= 0.9218) and second squared canonical correlation (σ_1^2= 0.8906) were large, indicating the significance of the CAP model. Both canonical axes showed distinct separation of the samples based primarily by the sampling origin of the mice but also according to the intestinal tissue type (Figure 3-5).

In addition, multivariate analyses based on the Bray-Curtis distances between 16S profiles for the four sites revealed that type of intestinal tissue had a significant effect on the observed OTUs between samples (PERMANOVA, Pseudo-F= 2.6363, P= 0.001). More importantly, the site of origin for the mice had a significant effect on the observed OTUs regardless of the type of intestinal tissue (PERMANOVA, Pseudo-F= 9.3664, P= 0.001) (Table 3-2). Our results, also revealed that the sex of the mice had no significant effect on the clustering of samples (PERMANOVA, Pseudo-F= 1.1628, P= 0.208).

Metagenome prediction and network analysis reveals higher relative abundance of metal and antibiotic resistance in mice intestinal samples from sites with greater HM contamination

We were first interested in how well the metagenome prediction software packages agreed with each other. Tax4Fun is newer, provides more predicted genes, and according to the developers provides greater metagenome prediction accuracy compared to PICRUSt. However, unlike PICRUSt it uses precomputed files from the SILVA SSU Ref NR database instead of Greengenes. Therefore, a spearman correlation was conducted between 16S rRNA KO abundance profiles computed by both PICRUSt and Tax4Fun. Our results, indicated a strong association between the two software packages ($R= 0.78 \pm 0.01$, $P < 0.05$). The median correlation coefficients for each site varied between 0.77 and 0.79 in both small and large intestinal samples (Figure 3-6).

PICRUSt results

The mean weighted nearest sequenced taxon index (NSTI), which measures the prediction accuracy of PICRUSt, of our 171 intestinal samples was 0.15 ± 0.07 (lower values mean a better prediction). We were initially interested in examining the proportion of sequences belonging to pathways that might aid in environments with HM contamination (Table 3-3). Samples from AB and TB had the highest proportion of sequences under the pathway category "Xenobiotics Biodegradation and Metabolism" ($P=3.82e-5$, FDR corrected) and "Membrane Transport" ($P= 1.04e-4$) (Figure 3-6, 3-7). Furthermore, we visualized the relative abundance of predicted genes to examine differences between sampling sites (Figure 3-8, 3-9). We found significant differences in 32 of the 34 selected predicted genes ($P < 0.01$, FDR corrected) between the four sites

which are presented in Table 3-4. Pair-wise comparisons between sites revealed the relative abundance for multiple KOs corresponding to predicted HM and antibiotic resistance genes were significantly higher in mice guts trapped from areas with historic contamination compared to the reference site (Figure 3-10, 3-11, 3-12). In addition, using the PICRUSt script *metagenome_contributions.py* we examined which specific taxa contributing the greatest proportion of predicted resistance KOs. Our results indicated that taxa such as *Pseudomonas* spp. and *Treponema* spp., which were significantly more abundant in intestinal samples from AB and TB, contributed the greatest number of counts (≥1e4) for several predicted HMs and antibiotic genes (Supplemental Information).

Tax4Fun results

Multiple comparisons tests on each sample group inclusive of both small and large intestinal samples revealed significant differences in the majority of KEGG pathways (Table 3-5). Interestingly, pathways such as drug metabolism (K000982; 4.33e-7, FDR corrected), xenobiotic biodegradation and metabolism (K000980; 3.47e-7, FDR corrected), and beta-lactam resistance (K000312; 0.01, FDR corrected) were all significantly higher at AB and TB (Table 3-5). In addition, similarly, to the PICRUSt analyses, we also examined the Tax4Fun predicted metagenome data to look at KOs associated with predicted metal and antibiotic resistance genes. The relative abundance of predicted genes in the mice intestinal tissues was examined between the four sampling sites (Figure 3-13, 3-14, 3-15). Of the 37 selected KOs we found 36 that were significantly different between the sites on the basis of HM contamination ($P < 0.01$, FDR corrected) (Table 3-6). Overall, there was a consistent pattern of higher metal and

antibiotic resistance gene relative abundances from AB and TB across the vast majority of pre-selected KEGG orthologs when compared with PB and UR (Supplemental Information). The Tax4Fun analyses also agreed with PICRUSt, and revealed the most significant KOs included those relating to predicted genes involved in resistances to copper, zinc, cadmium, and antibiotics. Additionally, there were fewer observed significant differences when comparing sites with similar contamination profiles (i.e. AB vs TB; PB vs UR) (Supplemental Information).

Network-based analyses

The network-based SparCC analyses demonstrated that our HM and antibiotic KOs formed four distinct co-abundance/co-exclusion networks (Figure 3-16, 3-17, 3-18, 3-19). Many of the predicted HM and antibiotic genes displayed significant positive correlations ($r \geq 0.60$) with each other across all tissue samples (Tables 3-7, 3-8, 3-9, 3-10). For example, in we observed several HM resistance genes such as K07240 (chrA, chromate transport gene) was strongly correlated ($r \geq 0.60$) with K03446 (emrB, multidrug resistance) across all of the sites. However, the number of shared connections between metals and antibiotics was largely dependent on the sampling location.

Network analysis was also utilized to explore the co-occurrence of predicted heavy metal and antibiotic resistance genes (Figure 3-20). Overall, heavy metal resistance appeared to co-occur across all samples, suggesting to some extent that this trait may be common across bacterial species. However, the site nodes with greater HM contamination (AB, TB, PB) were significantly more connected with KOs corresponding

to heavy metal and antibiotic resistance than the reference site (UR) (G-test: $P \leq 0.05$) (Figure 3-20).

Discussion

Low concentrations of HMs can remain in the intestinal tract for long periods

We conducted a field-based survey on the microbiota of wild *P. gossypinus* in their natural environment, in both undisturbed and HM contaminated areas within the SRS. We examined the extent of metal contamination in mice tissues (livers and kidneys), however we were unable to identify any observable HM accumulation. The literature suggests that the primary exposure route for metals is through oral ingestion of contaminated food and water. Intestinal absorption of HMs can lead to accumulation in target organs, however, most fractions of metals are not absorbed, passing through the intestinal lumen and excreted as feces. Despite this a small proportion of HMs can remain in the intestines, liver, and kidneys up to several years (Zalups and Ahmad, 2003; Breton et al., 2013). Any future studies should strongly consider testing the HM concentrations wild *Peromyscus* feces since we were unable to do so in the current study.

Historic heavy metal contamination at SRS may affect the microbiome of wild animals

Furthermore, we observed elevated HM concentrations in soils from the historically contaminated areas, particularly from AB and TB. Our ICP-MS data revealed HM concentrations that were several orders of magnitude lower than those measured in soils and sediments from the same locations in previous studies, however, this could possibly be attributed to site heterogeneity. For example, mice from AB were trapped in

terrestrial areas downstream of the former CCW discharge route, while mice from TB were trapped within the floodplain of the stream where metal concentrations can vary greatly (Punshon et al., 2003; Snodgrass et al., 2004; Roe et al., 2004; Roe et al., 2006; Hopkins et al., 2006; Unrine et al., 2007; Lance et al., 2012). In the case of Pond B, the majority of its contaminant history is tied to its sediments. In any case, we hypothesized chronic exposure of the host to HMs may affect the composition and shape of the gut community, even if the HMs appeared non-absorbed (Breton et al., 2013). Our results supported this hypothesis, indicating a significantly lower microbial diversity in mice tissue samples from AB and TB, compared with samples from PB and UR. These results starkly contrast with a similar field-based study that reported no significant effect of previous HM contamination on the diversity of wild *Peromyscus* gut microbiota (Coolon et al., 2010). Perhaps, the degree of HM contamination in the remediated ecosystem described by Coolon et al (2010) was too insignificant to cause any perceivable effect on the mice microbiota. Nevertheless, our results do support recent manipulative studies that have validated the deleterious effect of HM exposure on the mouse gut microbiome (Breton et al., 2013; Lu et al., 2014).

Wild *Peromyscus gossypinus* has an intestinal tract dominated by *Lactobacillus* and *Desulfovibrio*, HMs may enrich *Pseudomonas sop* and deplete Bacteriodetes

Interestingly, our study also contrasts with several others that have reported on the gut microbiota of mammals. The literature indicates that mammalian guts, including humans, have two dominant groups, Firmicutes and Bacteroidetes, which represent >70% of the intestinal community (Maurice et al., 2015). While the presence of genus *Lactobacillus* (Firmicutes) in our study confirms the observations of many others, the

relatively low number of OTUs assigned to Bacteroidetes (6.41 ± 0.03%) contrasts with other studies that have reported relatively high abundances (Turnbaugh et al., 2009; Vijay-Kumar et al., 2010; Breton et al., 2013; Weldon et al., 2015; Maurice et al., 2015) (Figure 3-2). Furthermore, a field-based study on two sympatric species of wild *Peromyscus* similarly observed that the dominant representatives of the mice gut microbiota included members from the phyla Firmicutes (Lactobacillaceae, Lachnospiraceae, Ruminococcacae) and Bacteroidetes (Bacteroidales, Porphyromonadaceae) in fecal samples (Baxter et al., 2013). Specifically, the relative abundance of Bacteroidetes has been associated with low-fat diets or feeding behaviors (fasting), while a higher relative proportion of Firmicutes has been associated with obese individuals (Weldon et al., 2015). In our study, *P. gossypinus* were trapped during the spring and summer period when their diet consists primarily of animal material (<68%), including beetles, lepidopterans, spiders, and snails (Calhoun, 1941; Wolfe et al., 1977; Cassola, 2016). A diet rich in protein has been associated with a higher relative abundance of Bacteroidetes, thus their low numbers in *P. gossypinus* are unlikely to be attributed to diet. In fact, a previous study demonstrated that among rumen microflora, Bacteroidetes exhibited the greatest sensitivity to HMs and other trace elements (Forsberg, 1978). Therefore, we hypothesize that the reduced numbers of Bacteroidetes in samples from AB and TB could be directly attributed to exposures of the mice to HMs, and the proliferation of HM resistant bacterial phyla which may occupy the niche of Bacteroidetes.

A similarly interesting observation in our study was that *Proteobacteria* had the second highest relative abundance in all intestinal samples (19.93 ± 0.06 %) (Figure 2). This also contrasts with the available literature on captive and wild murine models that have observed relatively low abundances of *Proteobacteria* (<5%) (Turnbaugh et al., 2009; Vijay-Kumar et al., 2010; Breton et al., 2013; Weldon et al., 2015; Maurice et al., 2015). It has been speculated that a relatively high abundance of *Proteobacteria* could signify a state of microbial dysbiosis (Shin et al., 2015). However, this may depend on the relative abundance of *Proteobacteria* compared to other phyla and, more importantly, the type of genera present. Indeed, it is possible that certain genera of *Proteobacteria* could function as either commensals or pathogens given the right circumstance (Kamada et al., 2013). Furthermore, a closer inspection of OTUs revealed that Desulfovibrio in the class δ-Proteobacteria were dominant taxa in intestinal samples from all of the sites (10.3 ± 0.03%). The genus *Desulfovibrio,* are a group of sulfate-reducing bacteria (SRB), which have been observed in the GI tracts of humans and other animals, as well as a variety of environmental samples (Goldstein et al., 2003). Rey et al. (2013) demonstrated that *Desulfovibrio* benefits from diets low in complex carbohydrates, which prompts the increased utilization of host sulfated glycans. Therefore, we hypothesize, that the relatively large abundance of SRB in *P. gossypinus* is primarily driven by an insect rich diet low in fermentable carbohydrates (Rey et al., 2013). Insects are known to harbor diverse microbiomes dominated by Proteobacteria and Firmicutes (Yun et al., 2014). Moreover, previous studies have revealed that certain microbes may also originate directly from the host environment (Seedorf et al., 2014). In addition to *Desulfovibrio*, all

intestinal samples from AB, and the small intestinal samples from TB also contained a significantly higher relative abundance of *Pseudomonas* in the class λ-Proteobacteria, which is known to contain several opportunistic pathogens (Mei et al., 2012; Mukhopadhya et al., 2012). In hospitals *Pseudomonas* is a major cause of nosocomial infections, especially in immunocompromised patients. It is known to display a remarkable versatility against chemicals including antibiotics, drugs, and HMs, due to its ability to form biofilms (Stewart and Costerton, 2001; Teitzel and Parsek, 2003; Mah et al., 2003, Deredjian et al., 2011).

Predictive functional profiling suggests potential co-selection of antibiotic resistance in guts of mice from HM contaminated environments

Furthermore, we examined NSTI scores to determine PICRUSt's accuracy in predicting metagenomes based on the 16S rRNA gene sequences obtained from the mice intestinal samples (Langille, 2013). Generally, the lower the NSTI, the more accurate the metagenome prediction. As we expected, our results (NSTI = 0.15 ± 0.07) agreed with the mammalian gut microbiome study (NSTI = 0.14 ± 0.06) and provided a reasonable approximation for functional predictions (Muegge et al., 2011). It should be noted, that the latter project's NSTI score may be somewhat illusory due to a comparatively lower sequencing depth (3838 ± 1080) sequences per sample (Muegge et al., 2011). In addition, although Tax4Fun does not calculate a NSTI score, our results revealed that its predictions were strongly correlated with PICRUSt (0.78 ± 0.01, $P < 0.05$), hence for this dataset it is reasonable to assume a similar prediction accuracy.

Finally, our most striking results clearly demonstrated a strong correlation between the soil habitats with higher HM contamination and the co-occurrence of predicted HM and antibiotic resistance genes. For example, we observed that the predicted metagenome of samples from samples from AB, TB, and PB contained a significantly higher relative abundance of metal-resistant genes relating to transporter/sensory proteins of Cu, Ag, Mg, and Co compared to UR (Supplemental Information). A number of previous studies have demonstrated that metal and antibiotic resistance genes can be indirectly co-selected due to the coupling of resistance mechanisms (Baker et al. 2006, Martinez 2012). Consistent with the literature, we observed that samples from AB and TB displayed significantly enriched two-component regulatory systems containing a myriad of genes that encode HM and antibiotic efflux proteins. This observation is supported by the higher relative abundance of *Pseudomonas* spp. in samples from AB and TB, which contributed the greatest number of OTUs linked to HM and antibiotic resistance (Supplemental Information). Further, because it has been consistently shown that antibiotic pre-treatment of intestinal microbiota in murine models can increase the colonization and infection potential of *Pseudomonas* spp. and other pathogens, we hypothesize that a similar mechanism may also exist in mice with chronic HM exposure (Kamada et al., 2013).

Conclusion

In conclusion, through the combination of Illumina-based 16S rRNA amplicon sequencing and predictive functional profiling, we discovered that environmental HM contamination can have biologically relevant effects on the composition, structure and

function of the wild *Peromyscus* intestinal microbiota. We observed a unique intestinal microbiome in *Peromyscus* co-dominated by SRB, as well as putative functional links between key taxa such as *Pseudomonas* spp., and HM driven co-selected antibiotic resistance. These findings provide novel evidence of the influence of HM pollution on the enrichment of the gut "resistome". This is relevant to human health because wildlife are often reservoirs of zoonotic diseases, and exposures to environmental contaminants can create a perfect storm opportunity for the selection and spread of resistant pathogens (Allen et al., 2010). To address these potential public health risks, future studies will be able to more directly examine the longitudinal implications of heavy metal pollution exposure, particularly alterations in gut microbiota composition coupled with the homeostatic responses of *Peromyscus*.

Acknowledgements

We thank our colleagues in the Department of Environmental Health Science, the Georgia Genomics Facility and Savannah River Ecology Laboratory for assistance with sampling and data collection. This research was supported by a contract from the US Department of Energy through Cooperative Agreement number DE-FC09-07SR22506 with the University of Georgia Research Foundation.

Disclaimer

liability or responsibility for the accuracy, completeness, or usefulness of any information, apparatus, product, or process disclosed or represents that its use would not infringe privately owned rights. Reference herein to any specific commercial product, process, or service by trade name, trademark, manufacturer, or otherwise does not necessarily constitute or imply its endorsement, recommendation, or favoring by the United States Government or any agency thereof. The views and opinions of authors expressed herein do not necessarily state or reflect those of the United States Government or any agency thereof.

References

Aarts, H., & Margolles, A. (2015). Antibiotic resistance genes in food and gut (non-pathogenic) bacteria. Bad genes in good bugs. *Frontiers in Microbiology*, *5*. https://doi.org/10.3389/fmicb.2014.00754

Agency for Toxic Substances and Disease Registry. (2007) Evaluation of off-site groundwater and surface water contamination at the Savannah River Site. *https://www.atsdr.cdc.gov/*.

Allen, H., Donato, J., Wang, H., Cloud-Hansen, K., Davies, J., & Handelsman, J. (2010). Call of the wild: antibiotic resistance genes in natural environments. *Nature reviews microbiology*, *8*(4), 251–259.

Anderson, M. J. (2004). DISTLM v. 5: a FORTRAN computer program to calculate a distance-based multivariate analysis for a linear model. *Department of Statistics, University of Auckland, New Zealand*, *10*, 2016.

Anderson, M. J., & Willis, T. J. (2003). Canonical Analysis of Principal Coordinates: A Useful Method of Constrained Ordination for Ecology. *Ecology*, *84*(2), 511–525. https://doi.org/10.1890/0012-9658(2003)084[0511:CAOPCA]2.0.CO;2

Anderson, M. J., R. N. Gorley, and R. K. Clarke. "Permanova." *Permutational multivariate analysis of variance, a computer program. Department of Statistics, University of Auckland* 24 (2005).

Arey, J. S., Seaman, J. C., & Bertsch, P. M. (1999). Immobilization of Uranium in Contaminated Sediments by Hydroxyapatite Addition. *Environmental Science & Technology*, *33*(2), 337–342. https://doi.org/10.1021/es980425+

Arthur, J. C., Gharaibeh, R. Z., Mühlbauer, M., Perez-Chanona, E., Uronis, J. M., McCafferty, J., … Jobin, C. (2014). Microbial genomic analysis reveals the essential role of inflammation in bacteria-induced colorectal cancer. *Nature Communications*, *5*, 4724. https://doi.org/10.1038/ncomms5724

Aßhauer, K. P., Wemheuer, B., Daniel, R., & Meinicke, P. (2015). Tax4Fun: predicting functional profiles from metagenomic 16S rRNA data. *Bioinformatics (Oxford, England)*, *31*(17), 2882–2884. https://doi.org/10.1093/bioinformatics/btv287

Bäckhed, F., Ley, R. E., Sonnenburg, J. L., Peterson, D. A., & Gordon, J. I. (2005). Host-bacterial mutualism in the human intestine. *Science (New York, N.Y.)*, *307*(5717), 1915–1920. https://doi.org/10.1126/science.1104816

Baker-Austin, C., Wright, M. S., Stepanauskas, R., & McArthur, J. V. (2006). Co-selection of antibiotic and metal resistance. *Trends in Microbiology*, *14*(4), 176–182. https://doi.org/10.1016/j.tim.2006.02.006

Boulangé, C. L., Neves, A. L., Chilloux, J., Nicholson, J. K., & Dumas, M.-E. (2016). Impact of the gut microbiota on inflammation, obesity, and metabolic disease. *Genome Medicine*, *8*, 42. https://doi.org/10.1186/s13073-016-0303-2

Bray, J. R., & Curtis, J. T. (1957). An Ordination of the Upland Forest Communities of Southern Wisconsin. *Ecological Monographs*, *27*(4), 325–349. https://doi.org/10.2307/1942268

Breton, J., Massart, S., Vandamme, P., De Brandt, E., Pot, B., & Foligné, B. (2013). Ecotoxicology inside the gut: impact of heavy metals on the mouse microbiome. *BMC Pharmacology and Toxicology*, *14*, 62. https://doi.org/10.1186/2050-6511-14-62

Brown, K., DeCoffe, D., Molcan, E., & Gibson, D. L. (2012). Diet-Induced Dysbiosis of the Intestinal Microbiota and the Effects on Immunity and Disease. *Nutrients*, *4*(8), 1095–1119. https://doi.org/10.3390/nu4081095

Calhoun, J. B. (1941). Distribution and food habits of mammals in the vicinity of the Reelfoot Lake Biological Station. *Journal of the Tennessee Academy of Science*, *16*, 177-185.

Caporaso, J. G., Kuczynski, J., Stombaugh, J., Bittinger, K., Bushman, F. D., Costello, E. K., … Knight, R. (2010). QIIME allows analysis of high-throughput community sequencing data. *Nature Methods*, *7*(5), 335–336. https://doi.org/10.1038/nmeth.f.303

Carlton, W.H., L.R. Bauer, A.G. Evans, L.A. Geary, C.E. Murphy, Jr., J.E. Pinder, and R.N. Strom. (1992) Cesium in the Savannah River Site environment (U). *WSRC-RP-92250*, Westinghouse Savannah River Company, Aiken, SC.

Cassola, F. 2016. *Peromyscus gossypinus*. The IUCN Red List of Threatened Species 2016: e.T42653A22359397. http://dx.doi.org/10.2305/IUCN.UK.2016-3.RLTS.T42653A22359397.en

Chen, S., Li, X., Sun, G., Zhang, Y., Su, J., & Ye, J. (2015). Heavy metal induced antibiotic resistance in bacterium LSJC7. *International Journal of Molecular Sciences*, *16*(10), 23390–23404. https://doi.org/10.3390/ijms161023390

Coolon, J. D., Jones, K. L., Narayanan, S., & Wisely, S. M. (2010). Microbial ecological response of the intestinal flora of *Peromyscus maniculatus* and *P. leucopus* to heavy metal contamination. *Molecular Ecology*, *19*, 67–80. https://doi.org/10.1111/j.1365-294X.2009.04485.x

David, L. A., Maurice, C. F., Carmody, R. N., Gootenberg, D. B., Button, J. E., Wolfe, B. E., … Turnbaugh, P. J. (2014). Diet rapidly and reproducibly alters the human gut microbiome. *Nature*, *505*(7484), 559–563. https://doi.org/10.1038/nature12820

Deredjian, A., Colinon, C., Brothier, E., Favre-Bonté, S., Cournoyer, B., & Nazaret, S. (2011). Antibiotic and metal resistance among hospital and outdoor strains of *Pseudomonas aeruginosa*. *Research in Microbiology*, *162*(7), 689–700. https://doi.org/10.1016/j.resmic.2011.06.007

DeSantis, T. Z., Hugenholtz, P., Larsen, N., Rojas, M., Brodie, E. L., Keller, K., … Andersen, G. L. (2006). Greengenes, a chimera-checked 16S rRNA gene database and workbench compatible with ARB. *Applied and Environmental Microbiology*, *72*(7), 5069–5072. https://doi.org/10.1128/AEM.03006-05

Eckburg, P. B., Bik, E. M., Bernstein, C. N., Purdom, E., Dethlefsen, L., Sargent, M., … Relman, D. A. (2005). Diversity of the human intestinal microbial flora. *Science*, *308*(5728), 1635–1638. https://doi.org/10.1126/science.1110591

Forsberg, C. W. (1978). Effects of heavy metals and other trace elements on the fermentative activity of the rumen microflora and growth of functionally important rumen bacteria. *Canadian Journal of Microbiology*, *24*(3), 298–306.

Fujimura, K. E., Demoor, T., Rauch, M., Faruqi, A. A., Jang, S., Johnson, C. C., … Lynch, S. V. (2014). House dust exposure mediates gut microbiome Lactobacillus enrichment and airway immune defense against allergens and virus infection. *Proceedings of the National Academy of Sciences*, *111*(2), 805–810. https://doi.org/10.1073/pnas.1310750111

Gill, S. R., Pop, M., DeBoy, R. T., Eckburg, P. B., Turnbaugh, P. J., Samuel, B. S., … Nelson, K. E. (2006). Metagenomic analysis of the human distal gut microbiome. *Science*, *312*(5778), 1355–1359. https://doi.org/10.1126/science.1124234

Gorvitovskaia, A., Holmes, S. P., & Huse, S. M. (2016). Interpreting Prevotella and Bacteroides as biomarkers of diet and lifestyle. *Microbiome*, *4*, 15. https://doi.org/10.1186/s40168-016-0160-7

Guinane, C. M., & Cotter, P. D. (2013). Role of the gut microbiota in health and chronic gastrointestinal disease: understanding a hidden metabolic organ. *Therapeutic Advances in Gastroenterology*, *6*(4), 295–308. https://doi.org/10.1177/1756283X13482996

Hill, D. A., & Artis, D. (2010). Intestinal bacteria and the regulation of immune cell homeostasis. *Annual Review of Immunology*, *28*(1), 623–667. https://doi.org/10.1146/annurev-immunol-030409-101330

Hopkins, W. A., DuRant, S. E., Staub, B. P., Rowe, C. L., & Jackson, B. P. (2006). Reproduction, embryonic development, and maternal transfer of contaminants in the amphibian Gastrophryne carolinensis. *Environmental Health Perspectives*, *114*(5), 661–666.

Huse, S. M., Ye, Y., Zhou, Y., & Fodor, A. A. (2012). A core human microbiome as viewed through 16S rRNA sequence clusters. *PLOS ONE*, *7*(6), e34242. https://doi.org/10.1371/journal.pone.0034242

Jovel, J., Patterson, J., Wang, W., Hotte, N., O'Keefe, S., Mitchel, T., … Wong, G. K.-S. (2016). Characterization of the gut microbiome using 16S or shotgun metagenomics. *Frontiers in Microbiology*, *7*. https://doi.org/10.3389/fmicb.2016.00459

Kamada, N., Chen, G. Y., Inohara, N., & Núñez, G. (2013). Control of pathogens and pathobionts by the gut microbiota. *Nature Immunology*, *14*(7), 685–690. https://doi.org/10.1038/ni.2608

Kanehisa, M., Goto, S., Hattori, M., Aoki-Kinoshita, K. F., Itoh, M., Kawashima, S., … Hirakawa, M. (2006). From genomics to chemical genomics: new developments in KEGG. *Nucleic Acids Research*, *34*(suppl 1), D354–D357. https://doi.org/10.1093/nar/gkj102

Kanehisa, M., Goto, S., Sato, Y., Furumichi, M., & Tanabe, M. (2012). KEGG for integration and interpretation of large-scale molecular data sets. *Nucleic Acids Research*, *40*(D1), D109–D114. https://doi.org/10.1093/nar/gkr988

Kinross, J. M., Darzi, A. W., & Nicholson, J. K. (2011). Gut microbiome-host interactions in health and disease. *Genome Medicine*, *3*, 14. https://doi.org/10.1186/gm228

Klindworth, A., Pruesse, E., Schweer, T., Peplies, J., Quast, C., Horn, M., & Glöckner, F. O. (2013). Evaluation of general 16S ribosomal RNA gene PCR primers for classical and next-generation sequencing-based diversity studies. *Nucleic Acids Research*, *41*(1), e1. https://doi.org/10.1093/nar/gks808

Kruskal, W. H., & Wallis, W. A. (1952). Use of ranks in one-criterion variance analysis. *Journal of the American Statistical Association*, *47*(260), 583–621. https://doi.org/10.1080/01621459.1952.10483441

Lance, S. L., Seaman, J. C., Scott D. E., Bryan Jr., A. Lawrence., Singer, J. H. (2012). P-area wetland studies soils and biota. Savannah River Ecology Laboratory. University of Georgia. Drawer E. Aiken, SC 29802.

Langille, M. G. I., Zaneveld, J., Caporaso, J. G., McDonald, D., Knights, D., Reyes, J. A., … Huttenhower, C. (2013). Predictive functional profiling of microbial

communities using 16S rRNA marker gene sequences. *Nature Biotechnology*, *31*(9), 814–821. https://doi.org/10.1038/nbt.2676

Le Chatelier, E., Nielsen, T., Qin, J., Prifti, E., Hildebrand, F., Falony, G., … Pedersen, O. (2013). Richness of human gut microbiome correlates with metabolic markers. *Nature*, *500*(7464), 541–546. https://doi.org/10.1038/nature12506

Legendre, P., & Anderson, M. J. (1999). Distance-based redundancy analysis: testing multispecies responses in multifactorial ecological experiments. *Ecological Monographs*, *69*(1), 1–24. https://doi.org/10.1890/0012-9615(1999)069[0001:DBRATM]2.0.CO;2

Lu, K., Ryan, P. A., Schlieper, K. A., Graffam, M. E., Levine, S., Wishnok, J. S., ... & Fox, J. G. (2014). Arsenic exposure perturbs the gut microbiome and its metabolic profile in mice: an integrated metagenomics and metabolomics analysis. *Environmental Health Perspectives (Online)*, *122*(3), 284.

Magoč, T., & Salzberg, S. L. (2011). FLASH: fast length adjustment of short reads to improve genome assemblies. *Bioinformatics*, *27*(21), 2957–2963. https://doi.org/10.1093/bioinformatics/btr507

Mah, T.-F., Pitts, B., Pellock, B., Walker, G. C., Stewart, P. S., & O'Toole, G. A. (2003). A genetic basis for *Pseudomonas aeruginosa* biofilm antibiotic resistance. *Nature*, *426*(6964), 306–310. https://doi.org/10.1038/nature02122

Martínez, J. L. (2012). Natural antibiotic resistance and contamination by antibiotic resistance determinants: the two ages in the evolution of resistance to antimicrobials. *Frontiers in Microbiology*, *3*. https://doi.org/10.3389/fmicb.2012.00001

Maurice, C. F., CL Knowles, S., Ladau, J., Pollard, K. S., Fenton, A., Pedersen, A. B., & Turnbaugh, P. J. (2015). Marked seasonal variation in the wild mouse gut microbiota. *The ISME Journal*, *9*(11), 2423–2434. https://doi.org/10.1038/ismej.2015.53

McMurdie, P. J., & Holmes, S. (2013). phyloseq: An R package for reproducible interactive analysis and graphics of microbiome census data. *PLOS ONE*, *8*(4), e61217. https://doi.org/10.1371/journal.pone.0061217

Mei, Y., Sun, Y., He, J., Wang, Q., Sun, Y., & Shao, W. (2012). Genome sequences of *Pseudomonas fragi* strains A22 and B25. *Journal of Bacteriology*, *194*(12), 3276–3277. https://doi.org/10.1128/JB.00488-12

Meyer, J. L., Strayer, D. L., Wallace, J. B., Eggert, S. L., Helfman, G. S., & Leonard, N. E. (2007). The contribution of headwater streams to biodiversity in river networks. *JAWRA Journal of the American Water Resources Association*, *43*(1), 86–103. https://doi.org/10.1111/j.1752-1688.2007.00008.x

Muegge, B. D., Kuczynski, J., Knights, D., Clemente, J. C., González, A., Fontana, L., … Gordon, J. I. (2011). Diet drives convergence in gut microbiome functions across mammalian phylogeny and within humans. *Science (New York, N.Y.)*, *332*(6032), 970–974. https://doi.org/10.1126/science.1198719

Mukhopadhya, I., Hansen, R., El-Omar, E. M., & Hold, G. L. (2012). IBD—what role do Proteobacteria play? *Nature Reviews Gastroenterology and Hepatology*, *9*(4), 219–230. https://doi.org/10.1038/nrgastro.2012.14

Myers, L., & Sirois, M. J. (2014). Spearman correlation coefficients, differences between. In *Wiley StatsRef: Statistics Reference Online*. John Wiley & Sons, Ltd. Retrieved from http://onlinelibrary.wiley.com/doi/10.1002/9781118445112.stat02802/abstract

Nagle, R. D., Rowe, C. L., & Congdon, J. D. (n.d.). Accumulation and selective maternal transfer of contaminants in the turtle *Trachemys scripta* associated with coal ash deposition. *Archives of Environmental Contamination and Toxicology*, *40*(4), 531–536. https://doi.org/10.1007/s002440010206

Pal, C., Bengtsson-Palme, J., Kristiansson, E., & Larsson, D. G. J. (2015). Co-occurrence of resistance genes to antibiotics, biocides and metals reveals novel insights into their co-selection potential. *BMC Genomics*, *16*, 964. https://doi.org/10.1186/s12864-015-2153-5

Pal, C., Bengtsson-Palme, J., Kristiansson, E., & Larsson, D. G. J. (2015). Co-occurrence of resistance genes to antibiotics, biocides and metals reveals novel

insights into their co-selection potential. *BMC Genomics*, *16*, 964. https://doi.org/10.1186/s12864-015-2153-5

Parks, D. H., Tyson, G. W., Hugenholtz, P., & BeiK0, R. G. (2014). STAMP: statistical analysis of taxonomic and functional profiles. *Bioinformatics*, *30*(21), 3123–3124. https://doi.org/10.1093/bioinformatics/btu494

Phillips, M. L. (2009). Gut reaction: environmental effects on the human microbiota. *Environmental Health Perspectives*, *117*(5), A198–A205.

Punshon, T., Gaines, K. F., Bertsch, P. M., & Burger, J. (2003). Bioavailability of uranium and nickel to vegetation in a contaminated riparian ecosystem. *Environmental Toxicology and Chemistry*, *22*(5), 1146–1154. https://doi.org/10.1002/etc.5620220525

Purchiaroni, F., Tortora, A., Gabrielli, M., Bertucci, F., Gigante, G., Ianiro, G., … Gasbarrini, A. (2013). The role of intestinal microbiota and the immune system. *European Review for Medical and Pharmacological Sciences*, *17*(3), 323–333.

Qin, J., Li, R., Raes, J., Arumugam, M., Burgdorf, K. S., Manichanh, C., … Wang, J. (2010). A human gut microbial gene catalogue established by metagenomic sequencing. *Nature*, *464*(7285), 59–65. https://doi.org/10.1038/nature08821

Raimondo, S. M., Rowe, C. L., & Congdon, J. D. (1998). Exposure to coal ash impacts swimming performance and predator avoidance in larval bullfrogs (*Rana catesbeiana*). *Journal of Herpetology*, *32*(2), 289–292. https://doi.org/10.2307/1565313

Rey, F. E., Gonzalez, M. D., Cheng, J., Wu, M., Ahern, P. P., & Gordon, J. I. (2013). Metabolic niche of a prominent sulfate-reducing human gut bacterium. *Proceedings of the National Academy of Sciences*, *110*(33), 13582–13587. https://doi.org/10.1073/pnas.1312524110

Roe, J. H., Hopkins, W. A., & Jackson, B. P. (2005). Species- and stage-specific differences in trace element tissue concentrations in amphibians: implications for the disposal of coal-combustion wastes. *Environmental Pollution*, *136*(2), 353–363. https://doi.org/10.1016/j.envpol.2004.11.019

Roe, J. H., Hopkins, W. A., DuRant, S. E., & Unrine, J. M. (2006). Effects of competition and coal-combustion wastes on recruitment and life history characteristics of salamanders in temporary wetlands. *Aquatic Toxicology*, *79*(2), 176–184. https://doi.org/10.1016/j.aquatox.2006.06.007

Satterthwaite, F. E. (1946). An Approximate Distribution of Estimates of Variance Components. *Biometrics Bulletin*, *2*(6), 110–114. https://doi.org/10.2307/3002019

Schaik, W. van. (2015). The human gut resistome. *Phil. Trans. R. Soc. B*, *370*(1670), 20140087. https://doi.org/10.1098/rstb.2014.0087

Seedorf, H., Griffin, N. W., Ridaura, V. K., Reyes, A., Cheng, J., Rey, F. E., … Gordon, J. I. (2014). Bacteria from diverse habitats colonize and compete in the mouse gut. *Cell*, *159*(2), 253–266. https://doi.org/10.1016/j.cell.2014.09.008

Seiler, C., & Berendonk, T. U. (2012). Heavy metal driven co-selection of antibiotic resistance in soil and water bodies impacted by agriculture and aquaculture. *Frontiers in Microbiology*, *3*. https://doi.org/10.3389/fmicb.2012.00399

Shin, N.-R., Whon, T. W., & Bae, J.-W. (2015). Proteobacteria: microbial signature of dysbiosis in gut microbiota. *Trends in Biotechnology*, *33*(9), 496–503. https://doi.org/10.1016/j.tibtech.2015.06.011

Snodgrass, J. W., Hopkins, W. A., Broughton, J., Gwinn, D., Baionno, J. A., & Burger, J. (2004). Species-specific responses of developing anurans to coal combustion wastes. *Aquatic Toxicology (Amsterdam, Netherlands)*, *66*(2), 171–182. https://doi.org/10.1016/j.aquatox.2003.09.002

Sommer, F., & Bäckhed, F. (2013). The gut microbiota — masters of host development and physiology. *Nature Reviews Microbiology*, *11*(4), 227–238. https://doi.org/10.1038/nrmicro2974

Stepanauskas, R., Glenn, T. C., Jagoe, C. H., Tuckfield, R. C., Lindell, A. H., King, C. J., & McArthur, J. V. (2006). Coselection for microbial resistance to metals and antibiotics in freshwater microcosms. *Environmental Microbiology*, *8*(9), 1510–1514. https://doi.org/10.1111/j.1462-2920.2006.01091.x

Stewart, P. S., & William Costerton, J. (2001). Antibiotic resistance of bacteria in biofilms. *The Lancet*, *358*(9276), 135–138. https://doi.org/10.1016/S0140-6736(01)05321-1

Storey, J. D. (2011). False Discovery Rate. In M. Lovric (Ed.), *International Encyclopedia of Statistical Science* (pp. 504–508). Springer Berlin Heidelberg. https://doi.org/10.1007/978-3-642-04898-2_248

Sugg, D. W., Chesser, R. K., Brooks, J. A., & Grasman, B. T. (1995). The association of DNA damage to concentrations of mercury and radiocesium in largemouth bass. *Environmental Toxicology and Chemistry*, *14*(4), 661–668. https://doi.org/10.1002/etc.5620140414

Tannenbaum, L. V., & Beasley, J. C. (2016). Validating mammalian resistance to stressor-mediated reproductive impact using rodent sperm analysis. *Ecotoxicology (London, England)*, *25*(3), 584–593. https://doi.org/10.1007/s10646-016-1617-y

Teitzel, G. M., & Parsek, M. R. (2003). Heavy metal resistance of biofilm and planktonic *Pseudomonas aeruginosa*. *Applied and Environmental Microbiology*, *69*(4), 2313–2320. https://doi.org/10.1128/AEM.69.4.2313-2320.2003

Turnbaugh, P. J., Ridaura, V. K., Faith, J. J., Rey, F. E., Knight, R., & Gordon, J. I. (2009). The effect of diet on the human gut microbiome: a metagenomic analysis in humanized gnotobiotic mice. *Science Translational Medicine*, *1*(6), 6ra14-6ra14. https://doi.org/10.1126/scitranslmed.3000322

Unrine, J. M., Hopkins, W. A., Romanek, C. S., & Jackson, B. P. (2007). Bioaccumulation of trace elements in omnivorous amphibian larvae: Implications for amphibian health and contaminant transport. *Environmental Pollution*, *149*(2), 182–192. https://doi.org/10.1016/j.envpol.2007.01.039

Vijay-Kumar, M., Aitken, J. D., Carvalho, F. A., Cullender, T. C., Mwangi, S., Srinivasan, S., … Gewirtz, A. T. (2010). Metabolic syndrome and altered gut microbiota in mice lacking toll-like receptor 5. *Science*, *328*(5975), 228–231. https://doi.org/10.1126/science.1179721

Voelz, N. J., & McArthur, J. V. (2000). An exploration of factors influencing lotic insect species richness. *Biodiversity & Conservation*, *9*(11), 1543–1570. https://doi.org/10.1023/A:1008984802844

Wang, W.-L., Xu, S.-Y., Ren, Z.-G., Tao, L., Jiang, J.-W., & Zheng, S.-S. (2015). Application of metagenomics in the human gut microbiome. *World Journal of Gastroenterology : WJG*, *21*(3), 803–814. https://doi.org/10.3748/wjg.v21.i3.803

Weldon, L., Abolins, S., Lenzi, L., Bourne, C., Riley, E. M., & Viney, M. (2015). The Gut Microbiota of Wild Mice. *PLOS ONE*, *10*(8), e0134643. https://doi.org/10.1371/journal.pone.0134643

Wolfe, J. L., & Linzey, A. V. (1977). *Peromyscus gossypinus*. *Mammalian Species*, (70), 1–5. https://doi.org/10.2307/3503898

Wu, G., Zhang, C., Wang, J., Zhang, F., Wang, R., Shen, J., … Zhang, M. (2016). Diminution of the gut resistome after a gut microbiota-targeted dietary intervention in obese children. *Scientific Reports*, *6*, 24030. https://doi.org/10.1038/srep24030

Wu, S., Zhao, Y.-H., Feng, X., & Wittmeier, A. (1996). Application of inductively coupled plasma mass spectrometry for total metal determination in silicon-containing solid samples using the microwave-assisted nitric acid–hydrofluoric acid–hydrogen peroxide–boric acid digestion system, *11*(4), 287–296. https://doi.org/10.1039/JA9961100287

Yassour, M., Vatanen, T., Siljander, H., Hämäläinen, A.-M., Härkönen, T., Ryhänen, S. J., … Xavier, R. J. (2016). Natural history of the infant gut microbiome and impact of antibiotic treatment on bacterial strain diversity and stability. *Science Translational Medicine*, *8*(343), 343ra81-343ra81. https://doi.org/10.1126/scitranslmed.aad0917

Yu, X.-D., Yan, C.-H., Shen, X.-M., Tian, Y., Cao, L.-L., Yu, X.-G., … Liu, J.-X. (2011). Prenatal exposure to multiple toxic heavy metals and neonatal neurobehavioral development in Shanghai, China. *Neurotoxicology and Teratology*, *33*(4), 437–443. https://doi.org/10.1016/j.ntt.2011.05.010

Yun, Ji-Hyun, Seong Woon Roh, Tae Woong Whon, Mi-Ja Jung, Min-Soo Kim, Doo-Sang Park, Changmann Yoon, et al. "Insect Gut Bacterial Diversity Determined by Environmental Habitat, Diet, Developmental Stage, and Phylogeny of Host." *Applied and Environmental Microbiology* 80, no. 17 (September 2014): 5254–64. doi:10.1128/AEM.01226-14.

Zhang, S., Jin, Y., Zeng, Z., Liu, Z., & Fu, Z. (2015). Subchronic exposure of mice to cadmium perturbs their hepatic energy metabolism and gut microbiome. *Chemical Research in Toxicology*, *28*(10), 2000–2009. https://doi.org/10.1021/acs.chemrestox.5b00237

Zhuang, P., Lu, H., Li, Z., Zou, B., & McBride, M. B. (2014). Multiple exposure and effects assessment of heavy metals in the population near mining area in South China. *PLOS ONE*, *9*(4), e94484. https://doi.org/10.1371/journal.pone.0094484

Tables

Table 3-1. Means and standard deviations for heavy metal concentrations and edaphic factors in SRS soils. The soils were collected in the same areas the mice were trapped.

HM (mg/kg) or edaphic factor	UR		AB		TB		PB	
	Mean	Stdev	Mean	Stdev	Mean	Stdev	Mean	Stdev
Cr 53	17.418	10.830	25.746	22.358	19.283	10.630	12.302	6.419
Co 59	2.742	1.267	4.553	5.099	5.707	3.375	1.522	0.388
Ni 60	6.644	4.430	9.753	11.641	8.987	6.414	5.317	3.951
Cu 63	7.489	5.921	11.654	16.183	7.230	3.539	4.217	2.601
Zn 66	21.995	14.370	25.074	23.550	20.767	10.892	11.639	3.441
As 75	26.633	2.482	27.325	4.881	25.987	1.590	24.798	1.645
Sr 88	14.464	9.333	40.343	49.245	25.051	13.099	5.920	2.946
Pb 208	21.480	14.750	16.422	11.031	18.587	9.102	7.740	4.879
U 238	1.611	0.878	2.108	1.381	6.285	13.773	1.029	0.306
Phosphorus (mg/g)	0.007	0.000	0.021	0.001	0.011	0.001	0.003	0.000
pH	3.983	0.031	4.273	0.042	4.337	0.006	4.377	0.025
Moisture (g)	22.000	0.000	8.333	0.577	7.000	0.000	29.333	0.577
Carbon (mg/g)	12.667	0.866	5.800	0.358	11.377	1.851	3.107	0.430
Nitrogen (mg/g)	0.477	0.038	0.313	0.021	0.580	0.104	0.113	0.015
C:N Ratio	26.784	0.467	18.572	0.005	19.683	0.519	27.823	0.152

Table 3-2. Effects of main factors and their interactions assessed by PERMANOVA. Main factors represent site (Lo) (Ash Basins, Pond B, Tim's Branch, Upper Three Runs), intestinal tissue type (In) (small, large), sex of mice (Se)(male, female). Values in table represent the F-ratio (F), the level of significance, $P < 0.05$).

Source	df	SS	MS	Pseudo-F	P(perm)	Unique perms	P (Monte Carlo Test)
Location of site (Lo)	3	18760	6253.3	9.3664	**0.001**	999	**0.001**
Sex of mice (Lo)	4	3105.4	776.35	1.1628	0.208	996	0.215
Intestinal tissue type (Se(Lo))	8	14081	1760.1	2.6363	**0.001**	999	**0.001**

Table 3-3. KEGG Pathways with significant differences between bacterial communities within mice intestinal tissues sampled from the four sampling sites as inferred by PICRUSt.

Observation Ids	p-values	p-values (corrected)	Effect size
Metabolism of Cofactors and Vitamins	7.54E-07	2.79E-05	0.153006254
Xenobiotics Biodegradation and Metabolism	2.07E-06	3.82E-05	0.192236399
Signaling Molecules and Interaction	4.14E-06	3.83E-05	0.173412231
Replication and Repair	7.71E-06	4.07E-05	0.131940968
Energy Metabolism	7.59E-06	4.68E-05	0.164263359
Metabolism of Terpenoids and Polyketides	4.11E-06	5.07E-05	0.16144162
Infectious Diseases	7.04E-06	5.21E-05	0.160282712
Nucleotide Metabolism	2.09E-05	9.67E-05	0.116063653
Membrane Transport	2.54E-05	0.00010427	0.135466641
Excretory System	3.32E-05	0.000122949	0.093236207
Cell Growth and Death	4.68E-05	0.000157336	0.143152815
Lipid Metabolism	0.000104378	0.000321832	0.155004995
Translation	0.000244346	0.000695446	0.127180846
Enzyme Families	0.000333578	0.000881599	0.116714234
Circulatory System	0.000570265	0.001406653	0.111520213
Folding, Sorting and Degradation	0.000638613	0.001476793	0.111085937
Signal Transduction	0.000741115	0.001613015	0.108020381
Transcription	0.000811291	0.001667654	0.078714177
Endocrine System	0.000939361	0.001829282	0.091576074
Metabolic Diseases	0.001952725	0.003440515	0.113569706
Cardiovascular Diseases	0.001866106	0.003452296	0.063985593
Neurodegenerative Diseases	0.003286014	0.005526477	0.080671856

Immune System Diseases	0.004144026	0.006666477	0.082028021
Metabolism of Other Amino Acids	0.004772626	0.007357798	0.103378325
Environmental Adaptation	0.007074292	0.010469951	0.065987916
Glycan Biosynthesis and Metabolism	0.012092519	0.017208585	0.06155232
Digestive System	0.023520808	0.032232218	0.064277917
Amino Acid Metabolism	0.027454806	0.036279566	0.063123784

Table 3-4. Selected antibiotic and metal resistance KEGG Orthologs (KOs) with significant differences between bacterial communities in mice intestinal tissues from the four sampling sites as inferred by PICRUSt.

KO	Superfamily	Family	Gene	Type	Significance ($p < 0.05$)
K03446	MFS	DHA2	emrB	antibiotic	7.88E-06
K05557	MFS	DHA2	actVA1	antibiotic	1.43E-06
K06189	ABC	CorC	corC	metal	4.06E-05
K07156	ABC	CopC	copC	metal	2.34E-03
K07239	RND	HME	HME family	metal	3.63E-07
K07240	ABC	CHR	chrA	metal	1.12E-02
K07241	ABC	NIX	nixA	metal	1.23E-03
K07245	ABC	PCO	pcoD	metal	2.58E-03
K07644	RND	OmpR	cusS	metal	7.23E-05
K07664	RND	OmpR	baeR	antibiotic	5.49E-02
K07665	RND	OmpR	cusR	metal	2.50E-03
K07681	RND	NarL	vraS	antibiotic	2.30E-06
K07694	RND	NarL	vraR	antibiotic	2.36E-02
K07785	MFS	NRE	nrsD	metal	2.41E-02
K07786	MFS	DHA2	emrY	antibiotic	4.12E-01
K07787	ABC	OmpR	cusA	metal	5.89E-04
K07788	RND	MDT	mdtB	antibiotic	5.87E-04
K07789	RND	MDT	mdtC	antibiotic	5.55E-04
K07796	RND	OmpR	cusC	metal	7.83E-03
K07798	RND	OmpR	cusB	metal	1.71E-06
K07799	RND	MDT	mdtA	antibiotic	2.42E-03
K07803	RND	NtrC	zraP	metal	3.75E-03
K07810	RND	OmpR	cusF	metal	3.25E-06
K08160	MFS	DHA1	mdfA	antibiotic	1.61E-05
K08161	MFS	DHA1	mdtG	antibiotic	2.11E-03
K08162	MFS	DHA1	mdtH	antibiotic	2.87E-01
K08163	MFS	DHA1	mdtL	antibiotic	6.30E-01
K08164	MFS	DHA1	ybcL	antibiotic	3.59E-03
K08166	MFS	DHA2	mmR	antibiotic	5.19E-04
K08167	MFS	DHA2	smvA	antibiotic	1.72E-04
K08168	MFS	DHA2	tetB	antibiotic	5.37E-07
K08169	MFS	DHA2	yebQ	antibiotic	9.31E-04
K11629	RND	OmpR	bceS	antibiotic	2.46E-06
K11630	RND	OmpR	bceR	antibiotic	2.87E-06
K14166	ABC	NosL	Ycnj	antibiotic	1.54E-04

Table 3-5. KEGG Pathways with significant differences between bacterial communities within mice intestinal tissues sampled from the four sampling sites as inferred by Tax4Fun.

Observation Ids	p-values	p-values (corrected)	Effect size
ko00770; Pantothenate and CoA biosynthesis	1.43E-11	4.05E-09	0.273479022
ko00250; Alanine, aspartate and glutamate metabolism	6.79E-11	4.82E-09	0.259556701
ko00510; N-Glycan biosynthesis	5.68E-11	5.38E-09	0.261165685
ko00620; Pyruvate metabolism	1.15E-10	6.53E-09	0.254793229
ko00730; Thiamine metabolism	5.30E-11	7.53E-09	0.26178353
ko03040; Spliceosome	2.59E-10	1.05E-08	0.247403206
ko05146; Amoebiasis	2.29E-10	1.09E-08	0.248497315
ko00430; Taurine and hypotaurine metabolism	4.49E-10	1.27E-08	0.242330734
ko00500; Starch and sucrose metabolism	3.68E-10	1.30E-08	0.24416721
ko00660; C5-Branched dibasic acid metabolism	4.33E-10	1.37E-08	0.242661884
ko05014; Amyotrophic lateral sclerosis (ALS)	1.01E-09	2.61E-08	0.234780961
ko04725; Cholinergic synapse	1.38E-09	3.03E-08	0.231838737
ko04370; VEGF signaling pathway	1.37E-09	3.24E-08	0.231944937
ko00253; Tetracycline biosynthesis	3.74E-09	7.60E-08	0.222449102
ko05410; Hypertrophic cardiomyopathy (HCM)	4.12E-09	7.79E-08	0.221551722
ko03060; Protein export	8.04E-09	1.43E-07	0.215154275
ko00564; Glycerophospholipid metabolism	1.03E-08	1.63E-07	0.212749017
ko05120; Epithelial cell signaling in Helicobacter pylori infection	1.01E-08	1.68E-07	0.212978134
ko00520; Amino sugar and nucleotide sugar metabolism	2.42E-08	3.62E-07	0.204501172
ko00051; Fructose and mannose metabolism	4.95E-08	6.11E-07	0.197498687
ko00380; Tryptophan metabolism	4.37E-08	6.21E-07	0.198708809
ko04724; Glutamatergic synapse	4.88E-08	6.30E-07	0.197626302
ko05016; Huntingtons disease	4.79E-08	6.48E-07	0.197810776
ko00980; Metabolism of xenobiotics by cytochrome P450	5.67E-08	6.71E-07	0.196159087

ko00072; Synthesis and degradation of ketone bodies	6.82E-08	7.45E-07	0.194330465
ko00982; Drug metabolism - cytochrome P450	6.72E-08	7.64E-07	0.194471828
ko00020; Citrate cycle (TCA cycle)	8.53E-08	8.36E-07	0.192114468
ko00590; Arachidonic acid metabolism	8.44E-08	8.56E-07	0.192227294
ko01040; Biosynthesis of unsaturated fatty acids	8.21E-08	8.63E-07	0.19249959
ko00400; Phenylalanine, tyrosine and tryptophan biosynthesis	1.02E-07	9.03E-07	0.190364833
ko04940; Type I diabetes mellitus	1.01E-07	9.27E-07	0.190421069
ko00310; Lysine degradation	9.86E-08	9.33E-07	0.190684935
ko00240; Pyrimidine metabolism	1.15E-07	9.90E-07	0.189146262
ko00130; Ubiquinone and other terpenoid-quinone biosynthesis	1.24E-07	1.00E-06	0.188436097
ko00627; Aminobenzoate degradation	1.30E-07	1.02E-06	0.187962437
ko00640; Propanoate metabolism	1.23E-07	1.03E-06	0.188492229
ko00053; Ascorbate and aldarate metabolism	1.55E-07	1.19E-06	0.186202281
ko00920; Sulfur metabolism	1.60E-07	1.20E-06	0.185854518
ko00760; Nicotinate and nicotinamide metabolism	1.65E-07	1.20E-06	0.185550873
ko00523; Polyketide sugar unit biosynthesis	1.88E-07	1.33E-06	0.184245222
ko00860; Porphyrin and chlorophyll metabolism	2.30E-07	1.56E-06	0.182211891
ko00601; Glycosphingolipid biosynthesis - lacto and neolacto series	2.26E-07	1.57E-06	0.182385723
ko00361; Chlorocyclohexane and chlorobenzene degradation	2.47E-07	1.63E-06	0.181493258
ko00950; Isoquinoline alkaloid biosynthesis	3.35E-07	2.16E-06	0.178427741
ko04727; GABAergic synapse	3.56E-07	2.20E-06	0.177815482
ko00643; Styrene degradation	3.53E-07	2.23E-06	0.177910806
ko00626; Naphthalene degradation	3.70E-07	2.24E-06	0.17742009
ko00440; Phosphonate and phosphinate metabolism	3.84E-07	2.27E-06	0.177050192
ko05204; Chemical carcinogenesis	4.10E-07	2.37E-06	0.176396371
ko03440; Homologous recombination	4.57E-07	2.54E-06	0.175289909
ko05111; Vibrio cholerae pathogenic cycle	4.52E-07	2.57E-06	0.175390751

ko00532; Glycosaminoglycan biosynthesis - chondroitin sulfate	5.41E-07	2.90E-06	0.173582847
ko03008; Ribosome biogenesis in eukaryotes	5.36E-07	2.93E-06	0.17367529
ko01055; Biosynthesis of vancomycin group antibiotics	5.70E-07	3.00E-06	0.17303958
ko04122; Sulfur relay system	6.32E-07	3.26E-06	0.171991367
ko00903; Limonene and pinene degradation	6.94E-07	3.52E-06	0.17103847
ko00592; alpha-Linolenic acid metabolism	7.52E-07	3.75E-06	0.170222071
ko04260; Cardiac muscle contraction	8.08E-07	3.96E-06	0.169483282
ko00480; Glutathione metabolism	8.72E-07	4.20E-06	0.168710604
ko05110; Vibrio cholerae infection	9.54E-07	4.52E-06	0.167781027
ko03050; Proteasome	1.26E-06	5.78E-06	0.164913659
ko04020; Calcium signaling pathway	1.24E-06	5.78E-06	0.165070635
ko00331; Clavulanic acid biosynthesis	1.39E-06	6.29E-06	0.163882473
ko00280; Valine, leucine and isoleucine degradation	1.50E-06	6.66E-06	0.163116444
ko04910; Insulin signaling pathway	1.59E-06	6.96E-06	0.162512668
ko04146; Peroxisome	1.62E-06	6.96E-06	0.162350595
ko00364; Fluorobenzoate degradation	1.74E-06	7.39E-06	0.161572798
ko04721; Synaptic vesicle cycle	2.17E-06	8.91E-06	0.159333371
ko04962; Vasopressin-regulated water reabsorption	2.17E-06	9.04E-06	0.159333371
ko00624; Polycyclic aromatic hydrocarbon degradation	2.24E-06	9.07E-06	0.158998047
ko05131; Shigellosis	2.33E-06	9.33E-06	0.158562567
ko04080; Neuroactive ligand-receptor interaction	2.44E-06	9.50E-06	0.15808796
ko05133; Pertussis	2.41E-06	9.52E-06	0.158206514
ko00622; Xylene degradation	3.17E-06	1.20E-05	0.155364801
ko05012; Parkinsons disease	3.14E-06	1.21E-05	0.155454621
ko00363; Bisphenol degradation	3.34E-06	1.25E-05	0.154817048
ko00521; Streptomycin biosynthesis	3.44E-06	1.27E-05	0.154513365
ko00232; Caffeine metabolism	3.50E-06	1.28E-05	0.154326433
ko05034; Alcoholism	3.57E-06	1.29E-05	0.154112281
ko05142; Chagas disease (American trypanosomiasis)	3.72E-06	1.29E-05	0.153707726
ko03010; Ribosome	3.78E-06	1.29E-05	0.153529481

ko00196; Photosynthesis - antenna proteins	3.66E-06	1.30E-05	0.1538676
ko00062; Fatty acid elongation	3.71E-06	1.30E-05	0.153717512
ko00785; Lipoic acid metabolism	3.92E-06	1.33E-05	0.153139831
ko00061; Fatty acid biosynthesis	3.99E-06	1.33E-05	0.152953334
ko05020; Prion diseases	4.28E-06	1.41E-05	0.152224791
ko04141; Protein processing in endoplasmic reticulum	4.45E-06	1.45E-05	0.1518145
ko00930; Caprolactam degradation	5.14E-06	1.66E-05	0.150313954
ko00983; Drug metabolism - other enzymes	5.95E-06	1.90E-05	0.148772511
ko00472; D-Arginine and D-ornithine metabolism	6.80E-06	2.14E-05	0.147367478
ko01057; Biosynthesis of type II polyketide products	7.27E-06	2.27E-05	0.146660932
ko05143; African trypanosomiasis	7.56E-06	2.33E-05	0.146237049
ko00071; Fatty acid metabolism	7.66E-06	2.34E-05	0.146103597
ko00330; Arginine and proline metabolism	7.85E-06	2.37E-05	0.145842533
ko05203; Viral carcinogenesis	8.82E-06	2.64E-05	0.144607037
ko00195; Photosynthesis	9.23E-06	2.73E-05	0.144125732
ko00281; Geraniol degradation	9.62E-06	2.82E-05	0.143687791
ko00565; Ether lipid metabolism	1.08E-05	3.13E-05	0.142452088
ko04666; Fc gamma R-mediated phagocytosis	1.14E-05	3.26E-05	0.141914148
ko03070; Bacterial secretion system	1.20E-05	3.36E-05	0.141381279
ko00830; Retinol metabolism	1.20E-05	3.39E-05	0.141384665
ko05130; Pathogenic Escherichia coli infection	1.23E-05	3.43E-05	0.141062105
ko04612; Antigen processing and presentation	1.33E-05	3.64E-05	0.140227161
ko04914; Progesterone-mediated oocyte maturation	1.33E-05	3.67E-05	0.140227161
ko00642; Ethylbenzene degradation	1.37E-05	3.69E-05	0.139963215
ko00621; Dioxin degradation	1.38E-05	3.71E-05	0.139823255
ko00190; Oxidative phosphorylation	1.45E-05	3.84E-05	0.13933779
ko04912; GnRH signaling pathway	1.49E-05	3.85E-05	0.139036048
ko04144; Endocytosis	1.49E-05	3.87E-05	0.139063073
ko05215; Prostate cancer	1.47E-05	3.88E-05	0.139145851
ko00901; Indole alkaloid biosynthesis	1.61E-05	4.11E-05	0.138226176
ko05200; Pathways in cancer	1.77E-05	4.48E-05	0.137205201

ko03022; Basal transcription factors	2.17E-05	5.47E-05	0.1349879
ko00630; Glyoxylate and dicarboxylate metabolism	2.56E-05	6.38E-05	0.133226651
ko05219; Bladder cancer	2.79E-05	6.90E-05	0.132297956
ko00311; Penicillin and cephalosporin biosynthesis	2.92E-05	7.16E-05	0.131802702
ko00945; Stilbenoid, diarylheptanoid and gingerol biosynthesis	3.07E-05	7.45E-05	0.131274277
ko00740; Riboflavin metabolism	3.14E-05	7.55E-05	0.131038393
ko05152; Tuberculosis	3.24E-05	7.73E-05	0.13069777
ko05150; Staphylococcus aureus infection	4.11E-05	9.74E-05	0.128107956
ko00906; Carotenoid biosynthesis	4.39E-05	0.000103128	0.127392386
ko00260; Glycine, serine and threonine metabolism	4.47E-05	0.000104141	0.127196814
ko00625; Chloroalkane and chloroalkene degradation	4.54E-05	0.000104838	0.127035738
ko04626; Plant-pathogen interaction	5.24E-05	0.000119917	0.125485961
ko05032; Morphine addiction	7.91E-05	0.000179759	0.120975283
ko00780; Biotin metabolism	0.00010787	0.000243135	0.117568475
ko05134; Legionellosis	0.000128445	0.000284986	0.115642043
ko03015; mRNA surveillance pathway	0.000128083	0.000286422	0.115673187
ko05340; Primary immunodeficiency	0.000133459	0.000293816	0.115218689
ko00650; Butanoate metabolism	0.000135303	0.000295585	0.115066915
ko00100; Steroid biosynthesis	0.000136744	0.000296453	0.114949724
ko00360; Phenylalanine metabolism	0.000140597	0.000302496	0.11464228
ko01053; Biosynthesis of siderophore group nonribosomal peptides	0.000144117	0.000307738	0.114368517
ko00970; Aminoacyl-tRNA biosynthesis	0.000154193	0.000326797	0.113619763
ko00030; Pentose phosphate pathway	0.00018183	0.000382517	0.111789558
ko05164; Influenza A	0.000193705	0.000404502	0.111085887
ko03420; Nucleotide excision repair	0.00022755	0.000471709	0.109291286
ko00290; Valine, leucine and isoleucine biosynthesis	0.000277685	0.000571468	0.107065273

ko04070; Phosphatidylinositol signaling system	0.000285402	0.000583124	0.106758214
ko00362; Benzoate degradation	0.000288973	0.000586203	0.106618877
ko02010; ABC transporters	0.000293644	0.000591453	0.106439167
ko04726; Serotonergic synapse	0.000302359	0.000604718	0.106111222
ko00540; Lipopolysaccharide biosynthesis	0.000312372	0.000620375	0.105745711
ko00471; D-Glutamine and D-glutamate metabolism	0.000318395	0.000627945	0.10553137
ko00909; Sesquiterpenoid and triterpenoid biosynthesis	0.000329042	0.000644468	0.105162002
ko00591; Linoleic acid metabolism	0.000342966	0.000667139	0.104696289
ko05322; Systemic lupus erythematosus	0.000352548	0.000676511	0.104386446
ko05145; Toxoplasmosis	0.000351835	0.000679736	0.104409221
ko00680; Methane metabolism	0.000375005	0.000714774	0.103691579
ko00750; Vitamin B6 metabolism	0.000380943	0.000716476	0.103514664
ko00965; Betalain biosynthesis	0.00037845	0.000716533	0.103588591
ko03030; DNA replication	0.000387992	0.000724933	0.103308137
ko00563; Glycosylphosphatidylinositol(GPI)-anchor biosynthesis	0.000469342	0.000871197	0.101160037
ko00900; Terpenoid backbone biosynthesis	0.000514542	0.000948896	0.100119729
ko00300; Lysine biosynthesis	0.000525793	0.000963388	0.099874756
ko00940; Phenylpropanoid biosynthesis	0.000534348	0.000972788	0.099691875
ko00340; Histidine metabolism	0.000579821	0.001048847	0.098765708
ko04916; Melanogenesis	0.00062713	0.001127246	0.097874911
ko05010; Alzheimers disease	0.000654709	0.001169417	0.097385576
ko03430; Mismatch repair	0.000776254	0.001377851	0.095445499
ko04514; Cell adhesion molecules (CAMs)	0.000783416	0.001381927	0.095340685
ko00908; Zeatin biosynthesis	0.000808757	0.001417821	0.094977239
ko04011; MAPK signaling pathway - yeast	0.000819315	0.001427519	0.094829096
ko00670; One carbon pool by folate	0.000893445	0.001547186	0.09383886
ko00790; Folate biosynthesis	0.00092554	0.001593051	0.093434906
ko05030; Cocaine addiction	0.000998179	0.001697503	0.092569183
ko05031; Amphetamine addiction	0.000998179	0.001707729	0.092569183
ko00603; Glycosphingolipid biosynthesis - globo series	0.001027433	0.001736851	0.092237869
ko00010; Glycolysis / Gluconeogenesis	0.001181361	0.001985246	0.090634006

ko02060; Phosphotransferase system (PTS)	0.001346759	0.00224988	0.089124574
ko00550; Peptidoglycan biosynthesis	0.001368688	0.002273142	0.088938247
ko04728; Dopaminergic synapse	0.001379625	0.002277986	0.088846402
ko04978; Mineral absorption	0.00143576	0.002356969	0.088385977
ko00944; Flavone and flavonol biosynthesis	0.001445748	0.002359727	0.088305898
ko04973; Carbohydrate digestion and absorption	0.001853422	0.00300784	0.08542932
ko00600; Sphingolipid metabolism	0.001916092	0.003074408	0.085043119
ko00350; Tyrosine metabolism	0.001914049	0.00308858	0.085055514
ko00473; D-Alanine metabolism	0.0019909	0.003176491	0.084598003
ko04330; Notch signaling pathway	0.002013136	0.003194026	0.084468845
ko04115; p53 signaling pathway	0.002332544	0.003639793	0.082753557
ko04310; Wnt signaling pathway	0.002322068	0.003643466	0.082806064
ko05220; Chronic myeloid leukemia	0.002322068	0.003663707	0.082806064
ko03450; Non-homologous end-joining	0.002390575	0.003689801	0.082466802
ko04113; Meiosis - yeast	0.002377642	0.003689893	0.082530114
ko04064; NF-kappa B signaling pathway	0.002466393	0.003765891	0.082102253
ko05140; Leishmaniasis	0.002466393	0.003786247	0.082102253
ko05412; Arrhythmogenic right ventricular cardiomyopathy (ARVC)	0.002535302	0.003829924	0.081780318
ko05414; Dilated cardiomyopathy	0.002535302	0.003850405	0.081780318
ko04810; Regulation of actin cytoskeleton	0.002565374	0.003854847	0.0816425
ko03320; PPAR signaling pathway	0.002592359	0.003874895	0.081520165
ko04976; Bile secretion	0.002986358	0.004440448	0.079863366
ko05416; Viral myocarditis	0.003012335	0.004455745	0.079761782
ko05168; Herpes simplex infection	0.003040172	0.004473621	0.079653867
ko05210; Colorectal cancer	0.003078446	0.004506592	0.079507063
ko00410; beta-Alanine metabolism	0.003346885	0.004874438	0.078524984
ko04960; Aldosterone-regulated sodium reabsorption	0.003584104	0.005140836	0.077719233
ko04970; Salivary secretion	0.003584104	0.005166932	0.077719233
ko04971; Gastric acid secretion	0.003584104	0.005193294	0.077719233
ko00710; Carbon fixation in photosynthetic organisms	0.003774121	0.005386183	0.077110571
ko00312; beta-Lactam resistance	0.003907288	0.005548349	0.076701608
ko04610; Complement and coagulation cascades	0.003959198	0.00559409	0.076545872

ko04961; Endocrine and other factor-regulated calcium reabsorption	0.005700357	0.008014363	0.072226026
ko00140; Steroid hormone biosynthesis	0.005941158	0.008271024	0.071733301
ko05169; Epstein-Barr virus infection	0.005925735	0.008290191	0.071764271
ko00460; Cyanoamino acid metabolism	0.006063514	0.008400186	0.071490357
ko05100; Bacterial invasion of epithelial cells	0.006102485	0.008413135	0.071413982
ko00040; Pentose and glucuronate interconversions	0.007843741	0.010761462	0.068411992
ko05222; Small cell lung cancer	0.008097758	0.011056555	0.068029489
ko04972; Pancreatic secretion	0.008235271	0.011190512	0.067827272
ko00052; Galactose metabolism	0.008556477	0.011571617	0.067367461
ko04920; Adipocytokine signaling pathway	0.00932362	0.012549327	0.066333973
ko00401; Novobiocin biosynthesis	0.010034453	0.01344238	0.065447768
ko00351; DDT degradation	0.010088603	0.013451471	0.065382786
ko00120; Primary bile acid biosynthesis	0.010625215	0.014100752	0.064756588
ko00561; Glycerolipid metabolism	0.011819946	0.015613324	0.063466275
ko03020; RNA polymerase	0.012895014	0.016954555	0.062409376
ko04723; Retrograde endocannabinoid signaling	0.013726814	0.017965047	0.061648861
ko04145; Phagosome	0.014249693	0.01856382	0.061193398
ko04614; Renin-angiotensin system	0.015788391	0.020474444	0.059941631
ko00910; Nitrogen metabolism	0.016087517	0.020767522	0.059712108
ko00984; Steroid degradation	0.016529394	0.021241393	0.059380521
ko00121; Secondary bile acid biosynthesis	0.016791506	0.021481025	0.059187873
ko00791; Atrazine degradation	0.016898365	0.021520788	0.05911017
ko04622; RIG-I-like receptor signaling pathway	0.018462804	0.023408198	0.058024109
ko04621; NOD-like receptor signaling pathway	0.019909406	0.025130095	0.057096536
ko00450; Selenocompound metabolism	0.022022137	0.027673836	0.055853
ko04623; Cytosolic DNA-sensing pathway	0.02290393	0.028655138	0.055367864
ko00623; Toluene degradation	0.024843395	0.030945281	0.054361519
ko00943; Isoflavonoid biosynthesis	0.026336085	0.032661346	0.053637492
ko00562; Inositol phosphate metabolism	0.026556765	0.032791832	0.053533834

ko05212; Pancreatic cancer	0.026873541	0.033039332	0.053386485
ko04150; mTOR signaling pathway	0.027923926	0.034182737	0.052909634
ko03018; RNA degradation	0.028767619	0.035064393	0.052539009
ko02020; Two-component system	0.035461119	0.043038281	0.049923668
ko00720; Carbon fixation pathways in prokaryotes	0.036961045	0.044667816	0.049403419
ko05160; Hepatitis C	0.037472262	0.04490347	0.049230743
ko05162; Measles	0.037472262	0.045093739	0.049230743
ko00941; Flavonoid biosynthesis	0.039635137	0.04729571	0.048524434
ko00511; Other glycan degradation	0.042539786	0.050549369	0.047632135
ko00770; Pantothenate and CoA biosynthesis	1.43E-11	4.05E-09	0.273479022
ko00250; Alanine, aspartate and glutamate metabolism	6.79E-11	4.82E-09	0.259556701
ko00510; N-Glycan biosynthesis	5.68E-11	5.38E-09	0.261165685
ko00620; Pyruvate metabolism	1.15E-10	6.53E-09	0.254793229
ko00730; Thiamine metabolism	5.30E-11	7.53E-09	0.26178353
ko03040; Spliceosome	2.59E-10	1.05E-08	0.247403206
ko05146; Amoebiasis	2.29E-10	1.09E-08	0.248497315
ko00430; Taurine and hypotaurine metabolism	4.49E-10	1.27E-08	0.242330734

Table 3-6. Selected antibiotic and metal resistance KEGG Orthologs (KOs) with significant differences between bacterial communities in mice intestinal tissues sampled from the four sampling sites as inferred by Tax4Fun.

Observation Ids	p-values	p-values (corrected)	Effect size
K07797; multidrug resistance protein K	3.83E-11	3.55E-10	0.176250821
K07786; MFS transporter, multidrug resistance protein Y	4.97E-11	3.68E-10	0.168037261
K08163; MFS transporter, DHA1 family, multidrug resistance protein	3.38E-11	4.16E-10	0.179321221
K08160; MFS transporter, DHA1 family, multidrug/chloramphenicol efflux transport protein	3.10E-11	5.74E-10	0.193085332
K08162; MFS transporter, DHA1 family, multidrug resistance protein	2.49E-11	9.20E-10	0.178004189
K07664; two-component system, OmpR family, response regulator BaeR	1.91E-09	1.18E-08	0.258153177
K16267; zinc and cadmium transporter	6.99E-09	3.69E-08	0.173035234
K07665; two-component system, OmpR family, copper resistance phosphate regulon response regulator CusR	2.45E-08	1.13E-07	0.208481514
K07810; Cu(I)/Ag(I) efflux system periplasmic protein CusF	3.48E-08	1.43E-07	0.190271404
K07798; Cu(I)/Ag(I) efflux system membrane protein CusB/SilB	1.77E-07	6.56E-07	0.163649502
K07796; Cu(I)/Ag(I) efflux system outer membrane protein CusC/SilC	2.41E-07	8.10E-07	0.168270212
K07245; putative copper resistance protein D	4.42E-07	1.36E-06	0.185150906

K07789; RND superfamily, multidrug transport protein MdtC	3.53E-06	9.32E-06	0.134842646
K07788; RND superfamily, multidrug transport protein MdtB	3.46E-06	9.86E-06	0.133969795
K07787; Cu(I)/Ag(I) efflux system membrane protein CusA/SilA	6.01E-06	1.48E-05	0.13190116
K11629; two-component system, OmpR family, bacitracin resistance sensor histidine kinase BceS [EC:2.7.13.3]	1.57E-05	3.64E-05	0.138586881
K08167; MFS transporter, DHA2 family, methyl viologen resistance protein SmvA	1.82E-05	3.96E-05	0.089395932
K08166; MFS transporter, DHA2 family, methylenomycin A resistance protein	2.99E-05	6.15E-05	0.127755129
K07785; MFS transporter, NRE family, putaive nickel resistance protein	5.09E-05	9.90E-05	0.144690132
K05557; MFS transporter, DHA2 family, integral membrane protein	6.87E-05	0.000127163	0.029739317
K07644; two-component system, OmpR family, heavy metal sensor histidine kinase CusS [EC:2.7.13.3]	0.000110392	0.000194501	0.139972061
K07240; chromate transporter	0.000125044	0.000210302	0.133050847
K07241; high-affinity nickel-transport protein	0.000145061	0.000233359	0.116755365
K08164; MFS transporter, DHA1 family, chloramphenicol resistance protein	0.000307385	0.000473885	0.108192288
K03446; MFS transporter, DHA2 family, multidrug resistance protein B	0.000476039	0.000704538	0.101727982

K07239; heavy-metal exporter, HME family	0.000579084	0.000824081	0.062864761
K08170; MFS transporter, DHA2 family, multidrug resistance protein	0.000779206	0.001067801	0.102618343
K07681; two-component system, NarL family, vancomycin resistance sensor histidine kinase VraS [EC:2.7.13.3]	0.000936291	0.001237241	0.104100642
K11630; two-component system, OmpR family, bacitracin resistance response regulator BceR	0.001240455	0.001582649	0.087750655
K07694; two-component system, NarL family, vancomycin resistance associated response regulator VraR	0.001705006	0.002102841	0.096728507
K07799; putative multidrug efflux transporter MdtA	0.003345489	0.003993002	0.062280244
K08161; MFS transporter, DHA1 family, multidrug resistance protein	0.006440018	0.00744627	0.077359097
K16264; cobalt-zinc-cadmium efflux system protein	0.009762481	0.010945812	0.068569596
K08169; MFS transporter, DHA2 family, multidrug resistance protein	0.015978013	0.016891042	0.017519901
K08168; MFS transporter, DHA2 family, metal-tetracycline-proton antiporter	0.015754004	0.017144063	0.064783051
K06189; magnesium and cobalt transporter	0.030768344	0.03162302	0.037265598
K07803; zinc resistance-associated protein	0.063458123	0.063458123	0.026081603
K07797; multidrug resistance protein K	3.83E-11	3.55E-10	0.176250821

Table 3-7. Significant SparCC correlations between PICRUSt predicted genes in UR intestinal tissues.

OTU 1	OTU 2	corr	pval
K06189	K07789	0.986	0.000
K07796	K07803	0.983	0.000
K07789	K07796	0.979	0.000
K07789	K07803	0.978	0.000
K06189	K07803	0.978	0.000
K06189	K07796	0.975	0.000
K07238	K07240	0.929	0.000
K07156	K07644	0.905	0.000
K07803	K07810	0.884	0.000
K07244	K07664	0.877	0.000
K07796	K07810	0.821	0.000
K06189	K07810	0.792	0.000
K07665	K07799	0.785	0.000
K07789	K07810	0.783	0.000
K07244	K07644	0.774	0.000
K07156	K07244	0.771	0.000
K07243	K11629	0.749	0.000
K07644	K08168	0.705	0.000
K07156	K07664	0.702	0.000
K07644	K07664	0.695	0.000
K07156	K08168	0.686	0.000
K03446	K07238	0.669	0.000
K07664	K08167	0.662	0.000
K07799	K08168	0.642	0.000
K03446	K07772	0.629	0.000
K03446	K07240	0.629	0.000
K07244	K08167	0.627	0.000
K07644	K08167	0.625	0.000
K07238	K07772	0.616	0.000
K07156	K08167	0.607	0.000
K03446	K07803	0.606	0.000
K07665	K07788	0.588	0.000
K07240	K07772	0.576	0.000
K07240	K07681	0.575	0.000
K07788	K07799	0.559	0.000
K03446	K06189	0.554	0.000
K03446	K07796	0.553	0.000
K07238	K07810	0.551	0.000
K03446	K07789	0.524	0.000

K03446	K07810	0.523	0.000
K07664	K07788	0.505	0.000
K07243	K07787	0.503	0.000
K07244	K08168	0.490	0.000
K07244	K07788	0.488	0.000
K07665	K08168	0.480	0.000
K07644	K07799	0.466	0.000
K07156	K07799	0.466	0.000
K07787	K11629	0.446	0.000
K07238	K07803	0.437	0.000
K07238	K07681	0.427	0.000
K07664	K07799	0.425	0.010
K07241	K07788	0.420	0.000
K03446	K07681	0.413	0.010
K07244	K07810	-0.404	0.000
K03446	K07156	-0.406	0.010
K07244	K07772	-0.409	0.010
K07644	K07772	-0.428	0.010
K07665	K07810	-0.437	0.000
K07240	K07244	-0.440	0.010
K03446	K11629	-0.441	0.000
K07156	K07772	-0.446	0.000
K07156	K07810	-0.448	0.000
K03446	K07644	-0.471	0.000
K07238	K07799	-0.474	0.000
K03446	K07243	-0.482	0.000
K07810	K08168	-0.482	0.000
K03446	K07787	-0.486	0.000
K07644	K07810	-0.497	0.000
K07238	K07244	-0.501	0.000
K03446	K08168	-0.509	0.000
K07799	K07810	-0.534	0.000
K07240	K08168	-0.549	0.000
K07788	K07810	-0.559	0.000
K07156	K07240	-0.564	0.000
K07240	K07644	-0.584	0.000
K07238	K08168	-0.605	0.000
K07156	K07238	-0.607	0.000
K07238	K07644	-0.629	0.000

Table 3-8. Significant SparCC correlations between PICRUSt predicted genes in PB intestinal tissues.

OTU 1	OTU 2	corr	pval
K07789	K07796	0.994	0.000
K07789	K07803	0.979	0.000
K07796	K07803	0.978	0.000
K07243	K11629	0.955	0.000
K07787	K11629	0.950	0.000
K07238	K07240	0.950	0.000
K06189	K07803	0.943	0.000
K07243	K07787	0.940	0.000
K06189	K07789	0.927	0.000
K07156	K07644	0.925	0.000
K06189	K07796	0.921	0.000
K07664	K08167	0.846	0.000
K07803	K07810	0.828	0.000
K07244	K07644	0.823	0.000
K07644	K07664	0.815	0.000
K06189	K07810	0.794	0.000
K07244	K07664	0.790	0.000
K07239	K07799	0.760	0.000
K07156	K07664	0.759	0.000
K03446	K07803	0.754	0.000
K03446	K07796	0.735	0.000
K03446	K07789	0.734	0.000
K07238	K07772	0.733	0.000
K07644	K08167	0.724	0.000
K07789	K07810	0.715	0.000
K07796	K07810	0.709	0.000
K07156	K08167	0.707	0.000
K07664	K07788	0.705	0.000
K07156	K07244	0.692	0.000
K07244	K08167	0.687	0.000
K07240	K07772	0.683	0.000
K03446	K07238	0.676	0.000
K07239	K07664	0.674	0.000
K07238	K07810	0.657	0.000
K03446	K07240	0.657	0.000
K07239	K07788	0.645	0.000
K07681	K07796	0.644	0.000
K03446	K06189	0.642	0.010
K07681	K07789	0.635	0.000

K07239	K07644	0.591	0.000
K03446	K07810	0.589	0.000
K07681	K07803	0.572	0.000
K07239	K07244	0.565	0.000
K03446	K07772	0.552	0.000
K06189	K07681	0.549	0.000
K11630	K14166	0.540	0.000
K07644	K07788	0.538	0.000
K07240	K07810	0.533	0.000
K07238	K07803	0.530	0.000
K06189	K07238	0.527	0.000
K07772	K07810	0.524	0.000
K07156	K07788	0.523	0.010
K03446	K07681	0.521	0.010
K07788	K08167	0.509	0.000
K07244	K07788	0.506	0.000
K07694	K14166	0.493	0.000
K07694	K11630	0.492	0.000
K07156	K07239	0.452	0.000
K07788	K07799	0.444	0.000
K07238	K07789	0.439	0.010
K07238	K07796	0.435	0.020
K07241	K07788	0.435	0.020
K07772	K07803	0.430	0.000
K07240	K07803	0.429	0.020
K07240	K07644	-0.406	0.010
K07238	K07644	-0.408	0.030
K07238	K07788	-0.419	0.010
K07665	K07681	-0.427	0.020
K03446	K07244	-0.429	0.000
K07681	K14166	-0.433	0.000
K07239	K07240	-0.434	0.000
K07772	K08168	-0.444	0.000
K07156	K07810	-0.445	0.010
K07240	K07799	-0.445	0.000
K07788	K07810	-0.463	0.000
K06189	K07799	-0.473	0.000
K07644	K07772	-0.482	0.000
K07244	K07772	-0.484	0.010
K07681	K11630	-0.485	0.000
K07238	K07244	-0.486	0.000
K07681	K08168	-0.496	0.000
K03446	K08168	-0.519	0.000
K07240	K07244	-0.526	0.000
K07238	K07239	-0.541	0.000

K07799	K07810	-0.552	0.010
K07664	K07810	-0.556	0.000
K07238	K07799	-0.584	0.000
K07644	K07810	-0.598	0.000
K07244	K07810	-0.630	0.000
K03446	K07665	-0.658	0.000
K07239	K07810	-0.706	0.000

Table 3-9. Significant SparCC correlations between PICRUSt predicted genes in TB intestinal tissues.

OTU 1	OTU 2	corr	pval
K07789	K07796	0.990	0.000
K07156	K07644	0.970	0.000
K07156	K07244	0.962	0.000
K07244	K07644	0.956	0.000
K07796	K07803	0.956	0.000
K07789	K07803	0.955	0.000
K06189	K07796	0.953	0.000
K06189	K07789	0.950	0.000
K07244	K07664	0.935	0.000
K06189	K07803	0.929	0.000
K07644	K07664	0.910	0.000
K07156	K07664	0.908	0.000
K07788	K08167	0.896	0.000
K07244	K08167	0.893	0.000
K07238	K07240	0.891	0.000
K07644	K08167	0.886	0.000
K07156	K08167	0.882	0.000
K07664	K08167	0.870	0.000
K07239	K07788	0.854	0.000
K07239	K08167	0.820	0.000
K07244	K07788	0.816	0.000
K07156	K07788	0.806	0.000
K07664	K07788	0.802	0.000
K07644	K07788	0.801	0.000
K03446	K07796	0.783	0.000
K07239	K07644	0.775	0.000
K03446	K07789	0.768	0.000
K03446	K07803	0.766	0.000
K07156	K07239	0.763	0.000
K07239	K07244	0.763	0.000
K07238	K07810	0.756	0.000
K07664	K07681	0.748	0.000
K03446	K06189	0.740	0.000
K07239	K07664	0.708	0.000
K07244	K07681	0.700	0.000
K07772	K07810	0.678	0.000
K07240	K07772	0.677	0.000
K07156	K07681	0.663	0.000
K07644	K07681	0.656	0.000

K07239	K07799	0.648	0.000
K07240	K07810	0.641	0.000
K07238	K07772	0.634	0.000
K07243	K11629	0.606	0.000
K07803	K07810	0.578	0.000
K03446	K07240	0.550	0.000
K07681	K07788	0.536	0.000
K07681	K08167	0.532	0.000
K03446	K07681	0.512	0.000
K06189	K07238	0.511	0.000
K07238	K07803	0.508	0.000
K07239	K07681	0.504	0.000
K07788	K07799	0.499	0.000
K07799	K08168	0.487	0.000
K07665	K07799	0.476	0.000
K07240	K07803	0.464	0.000
K07787	K11629	0.463	0.000
K06189	K07240	0.462	0.000
K07243	K07787	0.447	0.000
K07681	K07796	0.446	0.010
K07681	K07789	0.444	0.000
K07238	K07796	0.437	0.000
K06189	K07810	0.431	0.010
K06189	K07681	0.423	0.000
K07799	K08167	0.421	0.010
K07238	K07789	0.418	0.010
K07799	K07810	-0.400	0.000
K07788	K11326	-0.413	0.000
K07240	K08168	-0.429	0.000
K07681	K11630	-0.435	0.000
K07681	K14166	-0.439	0.000
K07239	K07772	-0.442	0.000
K07240	K07799	-0.458	0.000
K07244	K07772	-0.460	0.000
K07238	K08168	-0.462	0.000
K07664	K07772	-0.462	0.000
K06189	K07241	-0.465	0.000
K07156	K07772	-0.473	0.000
K07644	K07772	-0.486	0.000
K07240	K08167	-0.499	0.000
K07240	K07665	-0.501	0.000
K07772	K07788	-0.513	0.000
K07238	K07788	-0.538	0.000
K07238	K07665	-0.559	0.000
K07238	K07239	-0.576	0.000

K07244	K07810	-0.580	0.000
K07772	K08167	-0.584	0.000
K07664	K07810	-0.599	0.000
K07238	K08167	-0.604	0.000
K07156	K07810	-0.611	0.000
K07644	K07810	-0.616	0.000
K07238	K07799	-0.649	0.000
K07239	K07810	-0.685	0.000
K07788	K07810	-0.706	0.000
K07810	K08167	-0.764	0.000

Table 3-10. Significant SparCC correlations between PICRUSt predicted genes in AB intestinal tissues.

OTU 1	OTU 2	corr	pval
K07789	K07796	0.990	0.000
K07156	K07644	0.971	0.000
K07156	K07244	0.960	0.000
K07244	K07644	0.956	0.000
K07796	K07803	0.954	0.000
K06189	K07796	0.953	0.000
K06189	K07789	0.951	0.000
K07789	K07803	0.951	0.000
K07244	K07664	0.934	0.000
K06189	K07803	0.925	0.000
K07644	K07664	0.909	0.000
K07156	K07664	0.906	0.000
K07244	K08167	0.894	0.000
K07238	K07240	0.892	0.000
K07788	K08167	0.891	0.000
K07644	K08167	0.889	0.000
K07156	K08167	0.888	0.000
K07664	K08167	0.872	0.000
K07239	K07788	0.853	0.000
K07239	K08167	0.819	0.000
K07244	K07788	0.810	0.000
K07644	K07788	0.808	0.000
K07156	K07788	0.807	0.000
K07664	K07788	0.799	0.000
K07239	K07644	0.784	0.000
K07239	K07244	0.767	0.000
K07156	K07239	0.766	0.000
K03446	K07796	0.764	0.000
K03446	K07803	0.764	0.000
K07664	K07681	0.751	0.000
K07238	K07810	0.751	0.000
K03446	K07789	0.748	0.000
K03446	K06189	0.740	0.000
K07239	K07664	0.711	0.000
K07244	K07681	0.699	0.000
K07772	K07810	0.680	0.000
K07240	K07772	0.679	0.000
K07156	K07681	0.662	0.000
K07644	K07681	0.657	0.000

K07239	K07799	0.643	0.000
K07240	K07810	0.637	0.000
K07238	K07772	0.629	0.000
K07243	K11629	0.609	0.000
K07803	K07810	0.565	0.000
K03446	K07240	0.549	0.000
K07681	K07788	0.537	0.010
K07681	K08167	0.533	0.000
K07243	K07787	0.515	0.000
K03446	K07681	0.507	0.000
K07239	K07681	0.506	0.000
K07788	K07799	0.503	0.000
K06189	K07238	0.503	0.000
K07238	K07803	0.491	0.000
K07665	K07799	0.468	0.000
K07799	K08168	0.463	0.000
K06189	K07240	0.453	0.000
K07787	K11629	0.451	0.000
K07240	K07803	0.449	0.000
K07681	K07796	0.439	0.000
K07681	K07789	0.433	0.000
K07238	K07796	0.429	0.000
K06189	K07681	0.429	0.000
K07799	K08167	0.424	0.010
K07238	K07789	0.420	0.000
K06189	K07810	0.408	0.000
K07238	K07644	-0.402	0.000
K07240	K07788	-0.402	0.020
K07799	K07810	-0.409	0.000
K07681	K14166	-0.410	0.000
K07788	K11326	-0.410	0.000
K07681	K07694	-0.415	0.000
K07239	K11326	-0.416	0.000
K03446	K07243	-0.418	0.000
K06189	K07241	-0.432	0.000
K07239	K07772	-0.438	0.000
K07244	K07772	-0.444	0.000
K07240	K08168	-0.444	0.000
K07240	K07665	-0.445	0.000
K07664	K07772	-0.446	0.000
K07238	K08168	-0.475	0.000
K07240	K07799	-0.477	0.000
K07644	K07772	-0.479	0.000
K07156	K07772	-0.480	0.000
K07238	K07665	-0.506	0.000

K07240	K08167	-0.507	0.000
K07772	K07788	-0.510	0.000
K07238	K07788	-0.535	0.000
K07238	K07239	-0.562	0.000
K07244	K07810	-0.590	0.000
K07772	K08167	-0.598	0.000
K07238	K08167	-0.603	0.000
K07664	K07810	-0.606	0.000
K07156	K07810	-0.613	0.000
K07644	K07810	-0.635	0.000
K07238	K07799	-0.655	0.000
K07239	K07810	-0.711	0.000
K07788	K07810	-0.721	0.000
K07810	K08167	-0.774	0.000
K07238	K07799	-0.655	0.000
K07239	K07810	-0.711	0.000

Figures

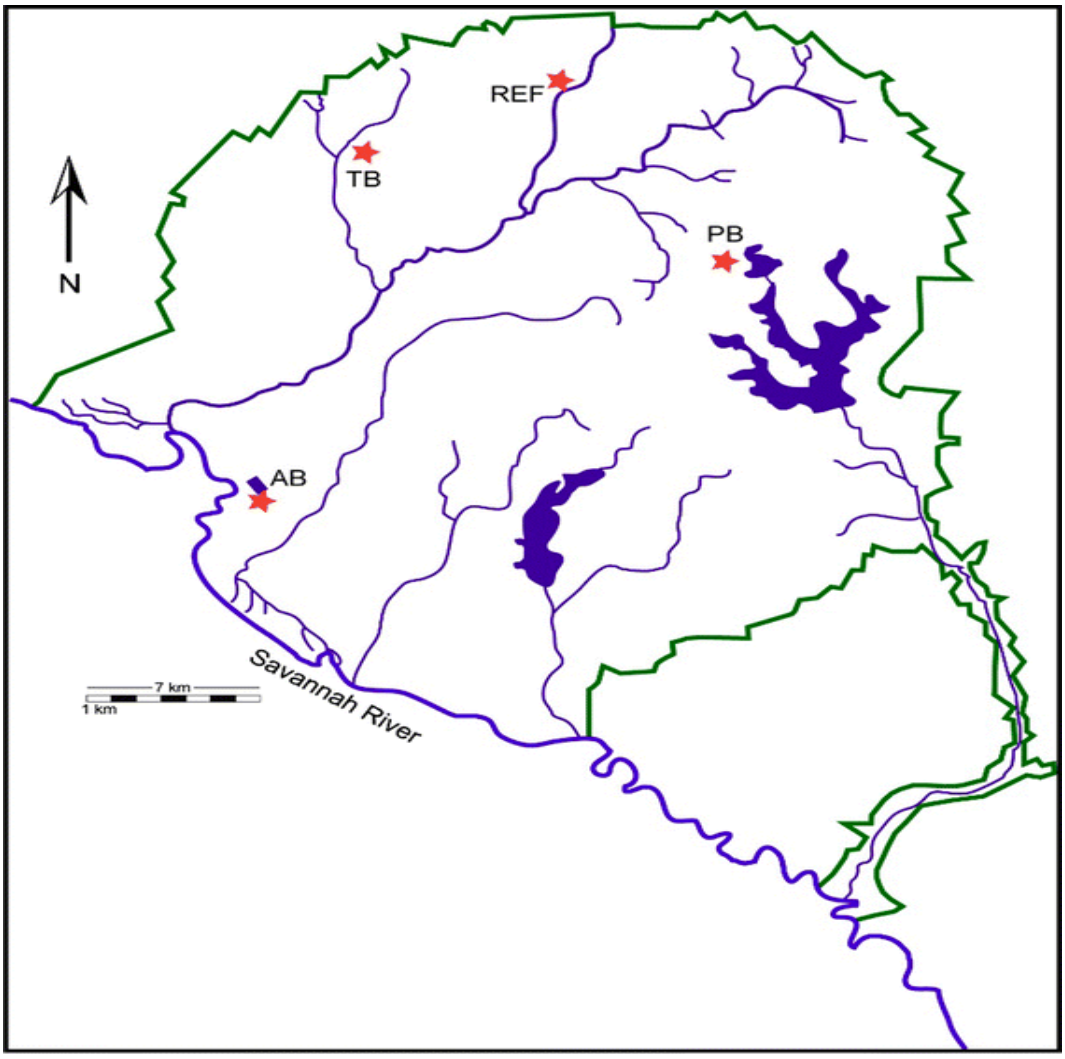

Figure 3-1. Map of the Savannah River Site, South Carolina, USA, depicting the distribution of the reference location (REF) and contaminated study areas, ash basin (AB), Pond B (PB), and Tim's Branch (TB) sampled for small mammals in spring 2014 (Tannebaum and Beasley, 2016).

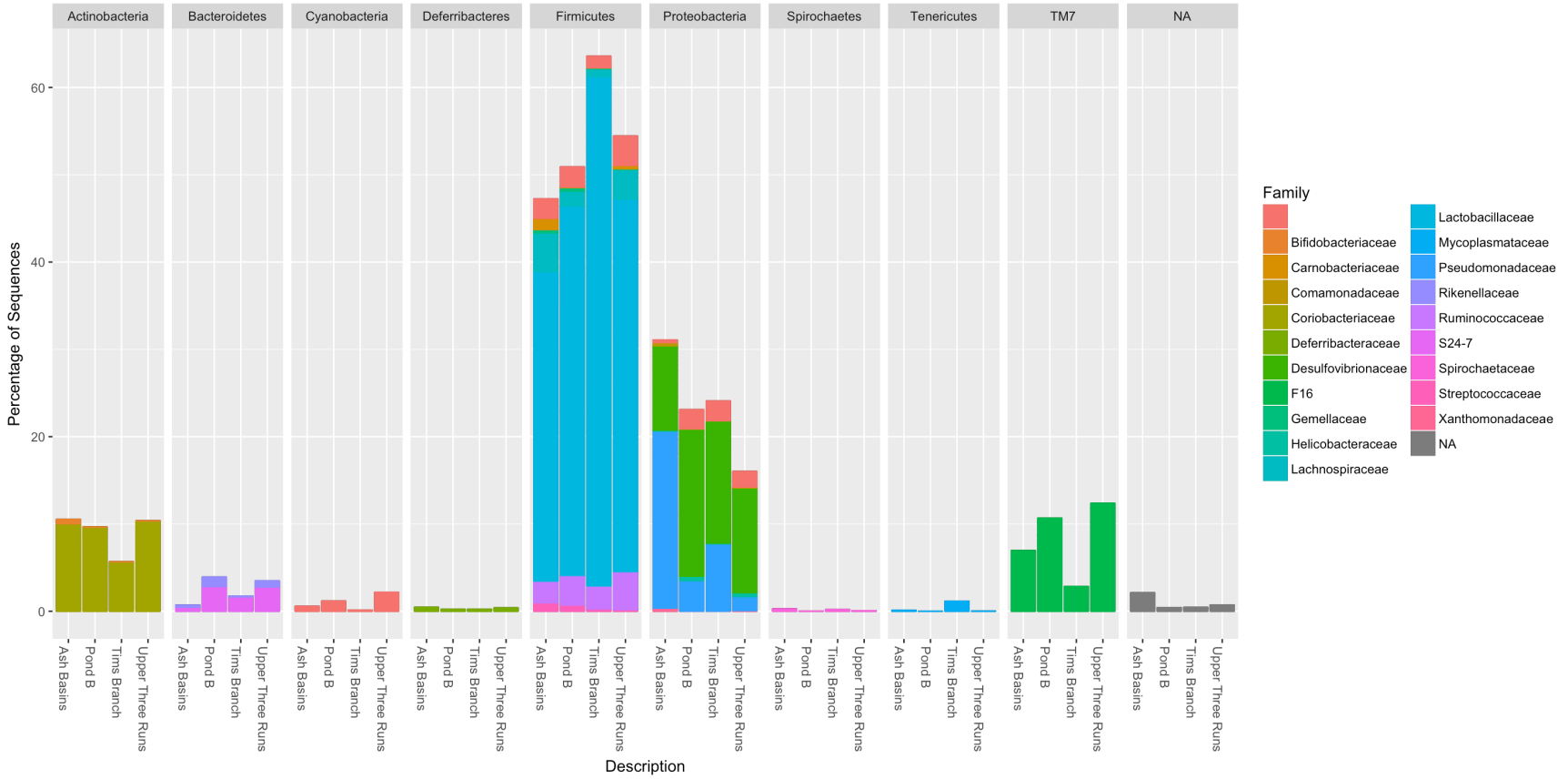

Figure 3-2. The relative abundance at the level of Phylum and corresponding families representing the 9 most abundant OTUs (clustered at 97% similarity) in mice instestinal tissues samples. Phyla are further expanded into respective families.

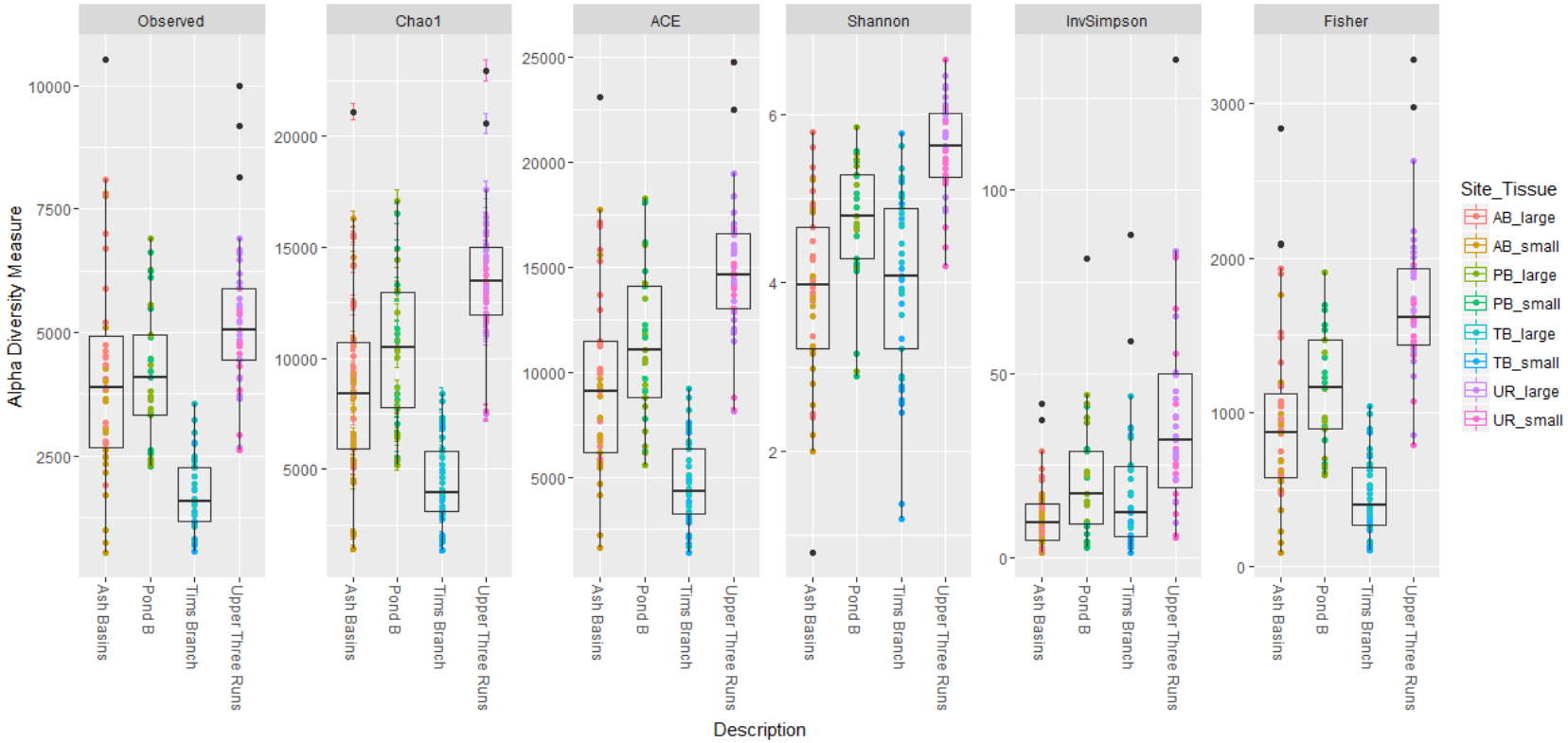

Figure 3-3. Alpha diversity measures for the four sampling sites (defined either by the number of bacterial OTUs observed or by Chao1, ACE, Shannon, Inverse Simpson, and Fisher diversity measures).

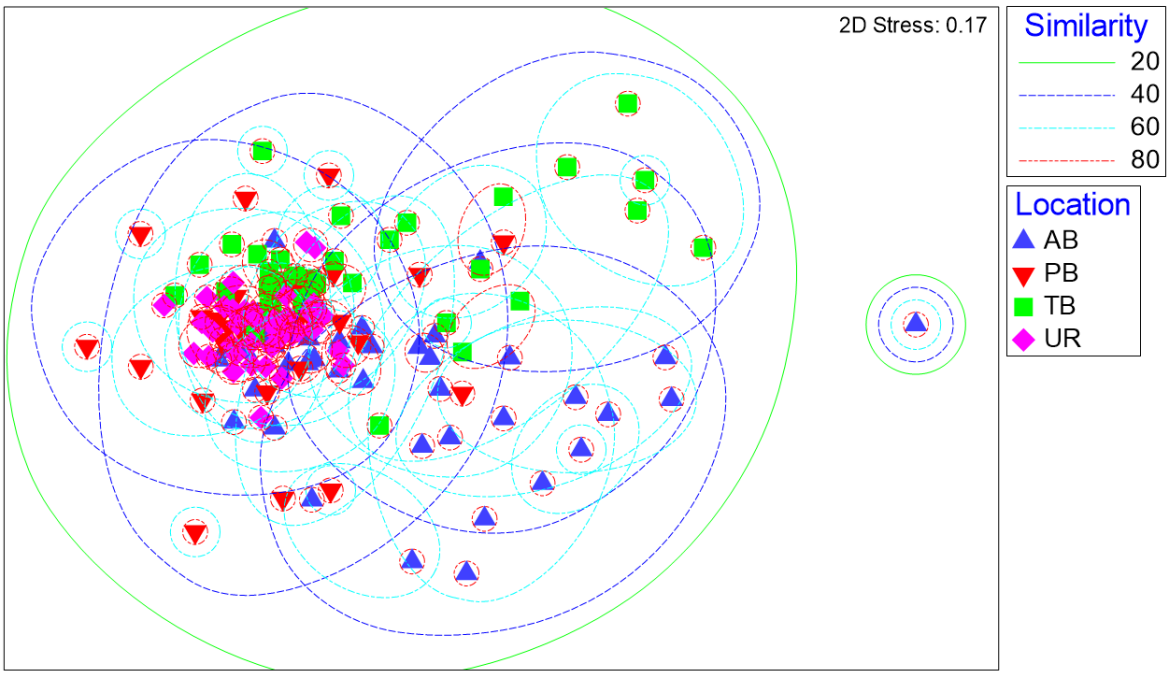

Figure 3-4. Non-metric multi-dimensional scaling plot of OTU frequency after log-transformation, which reduces the influence of the most abundant OTUs. Dashed lines represent percent similarity of clusters using SIMPROF: green lines 20%, dashed blue lines 40%, dashed cyan lines 60%, dashed red lines 80%. Blue triangles represent soils from Ash Basins (AB); Red upside down triangles represent Pond B (PB) soils; Green squares represent Tim's Branch (TB) soils; pink diamonds represent Upper Three Runs (UR) soils. Stress value is 0.13.

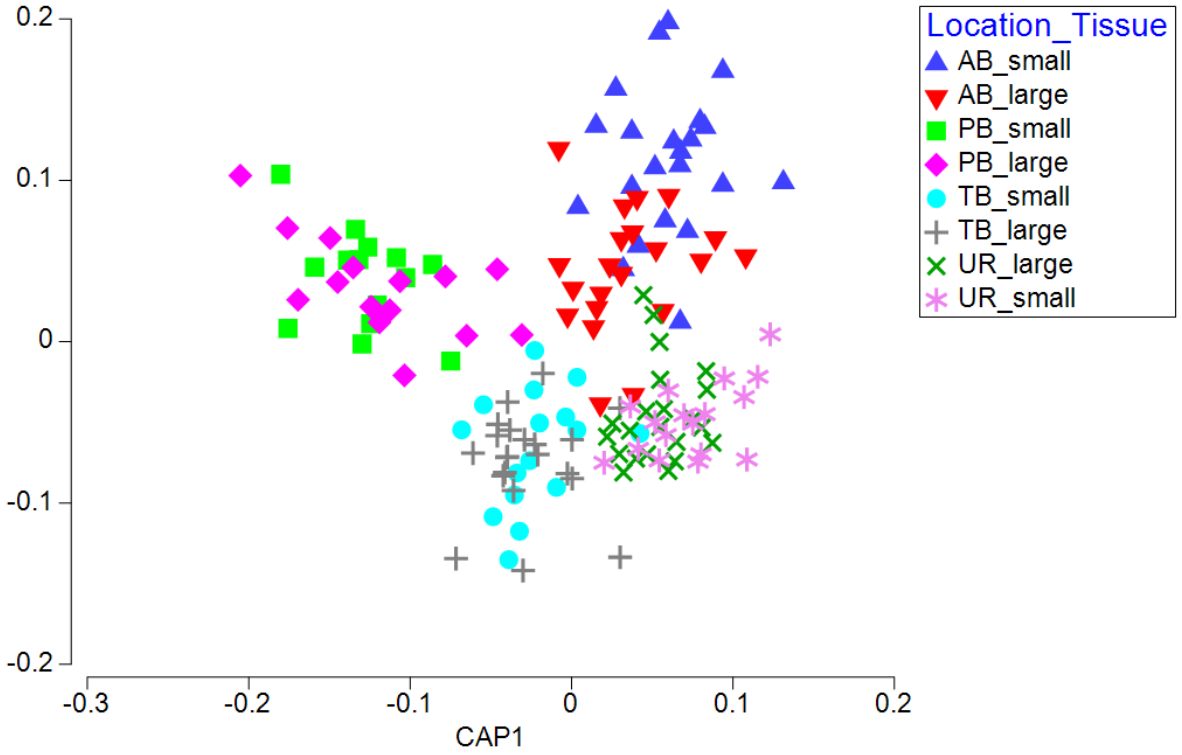

Figure 3-5. Canonical analysis of principal coordinates based on a Bray–Curtis dissimilarity matrix of log-transformed OTU frequencies. Blue triangles represent small intestines, Ash Basins; Red upside down triangles represent large intestines, Ash Basins; Green squares represent small intestines, Pond B; pink diamonds represent large intestines, Pond B; cyan circles represent small intestines, Tim's Branch; grey pluses represent large intestines, Tim's Branch; green exes represent large intestines, Upper Three Runs; pink asterisks represent small intestines, Upper Three Runs.

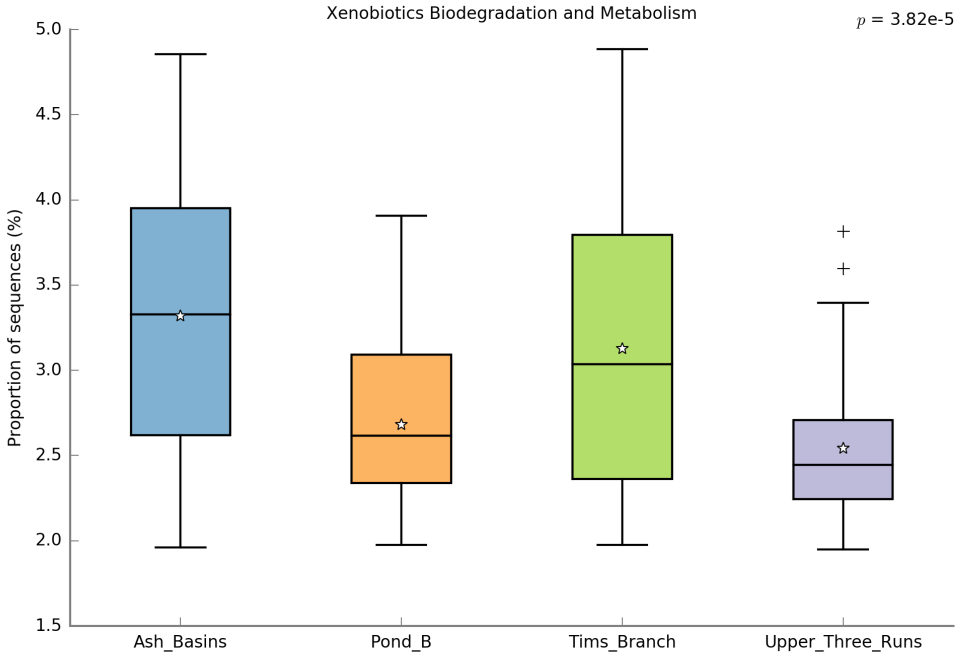

Figure 3-6. Relative abundance of sequences for the KEGG Pathway "Xenobiotics Biodegration and Metabolism".

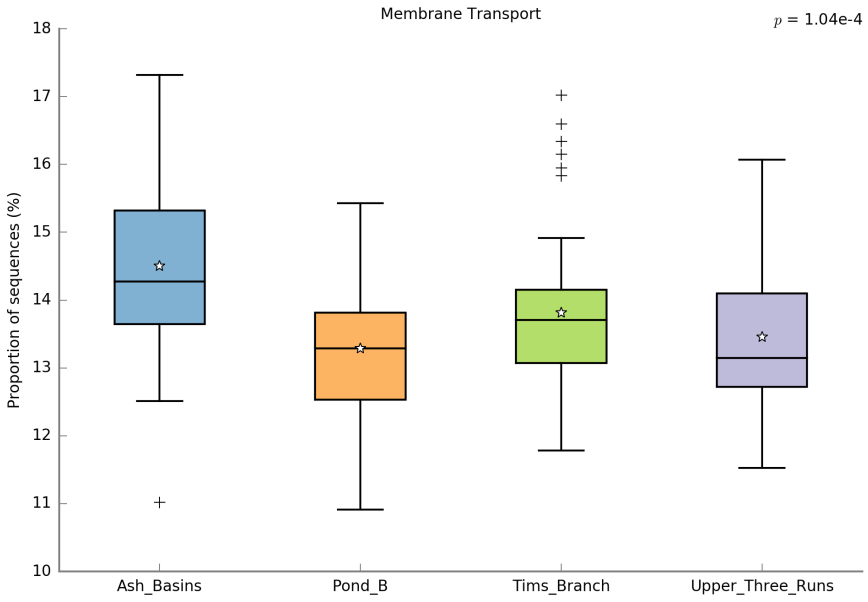

Figure 3-7. Relative abundance of sequences for the KEGG Pathway "Membrane Transport".

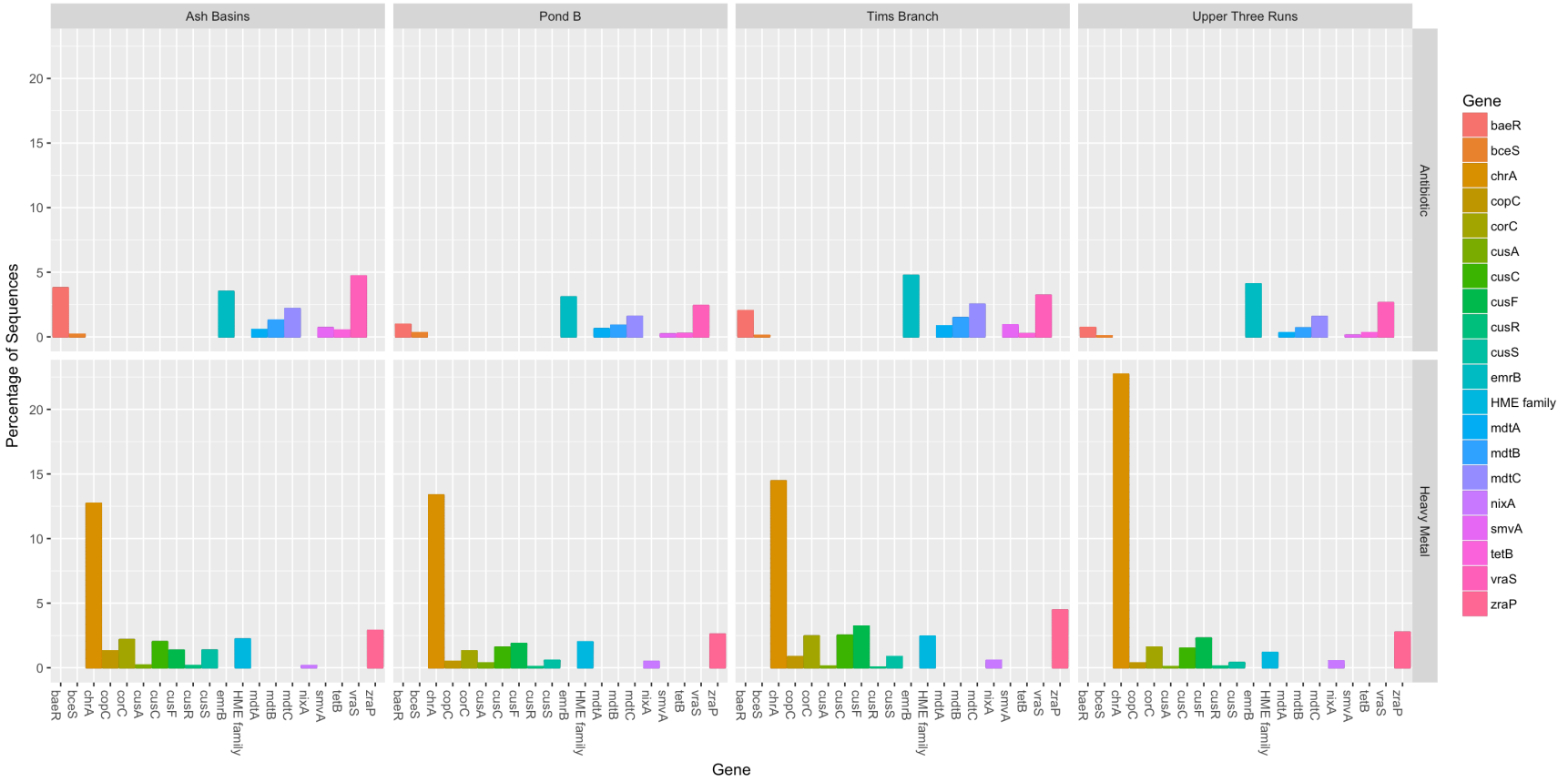

Figure 3-8. Relative abundance of top 20 predicted genes detected in mice intestinal samples. Genes of interest included: "baeR, multidrug resistance efflux pump" (K07664); "chrA, chromate transporter" (K07240); "copC, copper resistance protein C" (K07156);

“corC, magnesium and cobalt transporter” (K06189); “cusA, copper tolerance heavy metal sensor histidine” (K07787); “cusF, copper tolerance heavy metal sensor histidine” (K07810), “cusR, copper tolerance heavy metal sensor histidine” (K07665); “emrB, multidrug resistance protein” (K03446); “heavy-metal exporter, HME family” (K07239); “mdtA, multidrug efflux pump” (K07799); “mdtB, multidrug efflux pump” (K07788); “mdtC, multidrug efflux pump” (K07789 “nixA, high affinity nickel transporter” (K07241); “smvA, multidrug resistance efflux pump” (K08168); “tetB, metal-tetracycline-proton antiporter ”; “vraS, vancomycin resistance sensor” (K07681); “zraP, zinc resistance-associated protein” (K07803); “zupT; zinc transporter” (K07238).

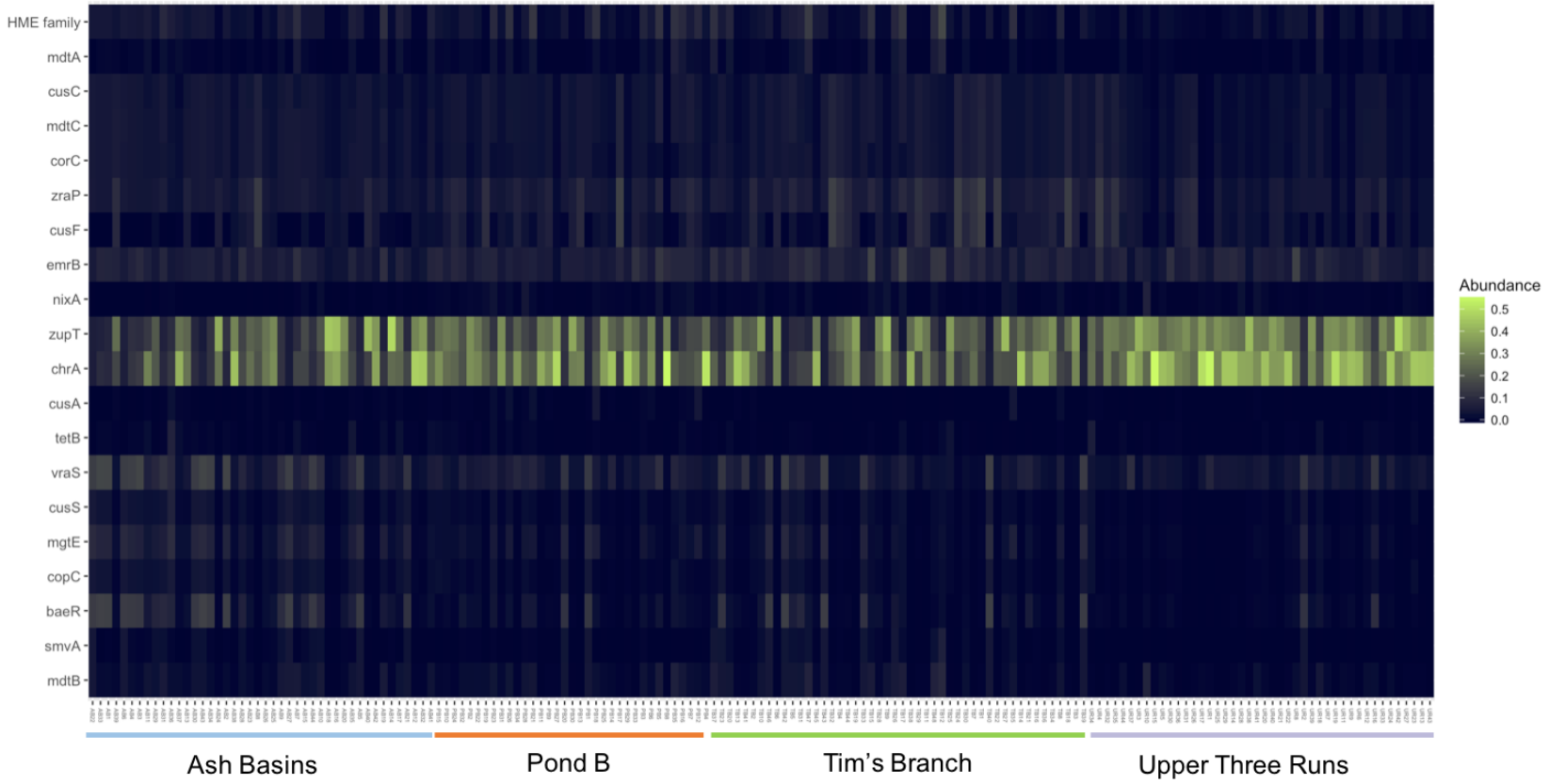

Figure 3-9. Relative abundance of top 20 predicted genes detected in mice intestinal samples visualized as a heatmap. Genes of interest included: "baeR, multidrug resistance efflux pump" (K07664); "chrA, chromate transporter" (K07240); "copC, copper resistance protein C" (K07156); "corC, magnesium and cobalt transporter" (K06189); "cusA, copper tolerance heavy metal sensor

histidine" (K07787); "cusF, copper tolerance heavy metal sensor histidine" (K07810), "cusR, copper tolerance heavy metal sensor histidine" (K07665); "emrB, multidrug resistance protein" (K03446); "heavy-metal exporter, HME family" (K07239); "mdtA, multidrug efflux pump" (K07799); "mdtB, multidrug efflux pump" (K07788); "mdtC, multidrug efflux pump" (K07789 "nixA, high affinity nickel transporter" (K07241); "smvA, multidrug resistance efflux pump" (K08168); "tetB, metal-tetracycline-proton antiporter "; "vraS, vancomycin resistance sensor" (K07681); "zraP, zinc resistance-associated protein" (K07803); "zupT; zinc transporter" (K07238).

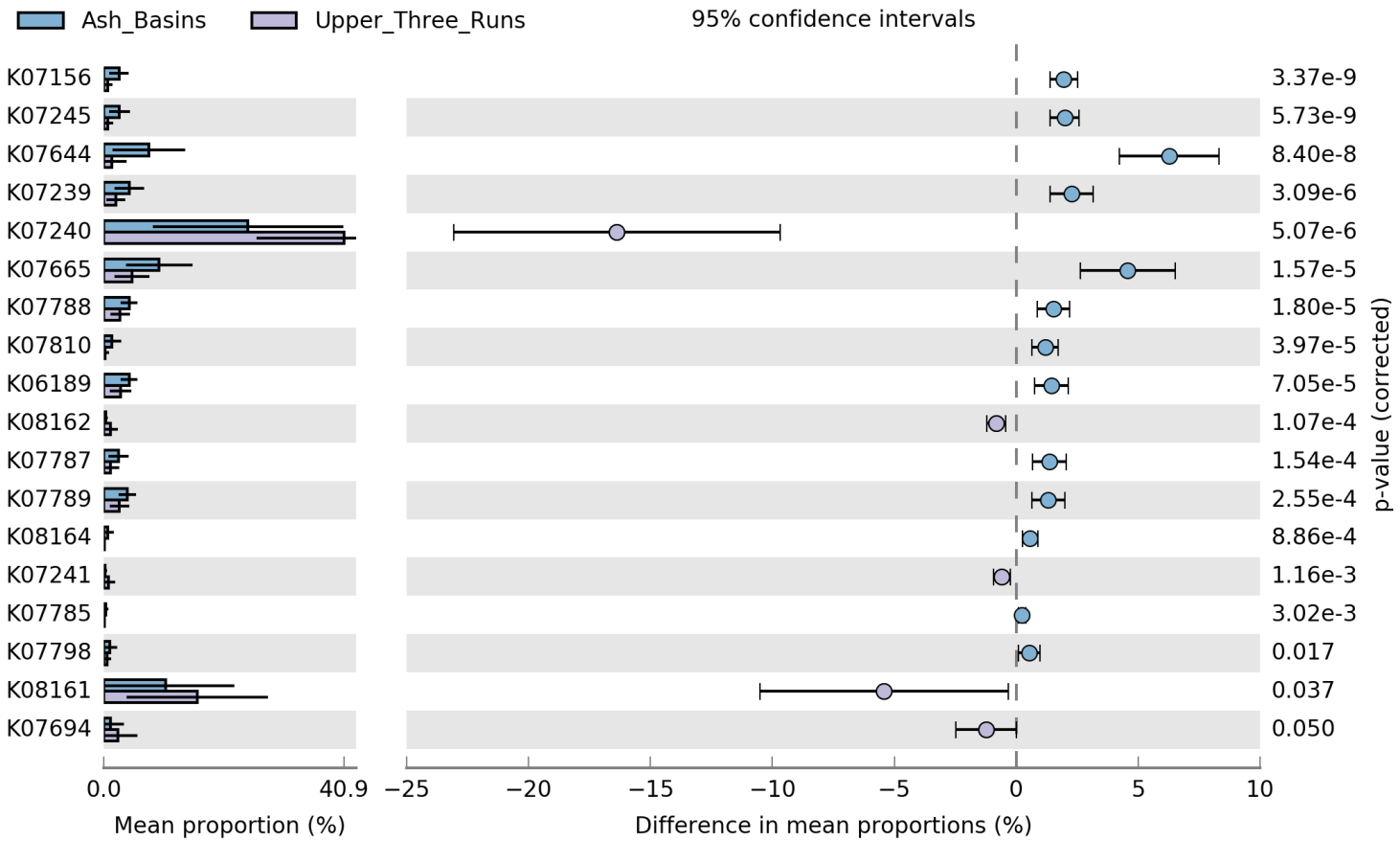

Figure 3-10. Pair-wise comparisons between Ash Basins and Upper Three Runs with 95% confidence intervals using PICRUSt predicted metagenome.

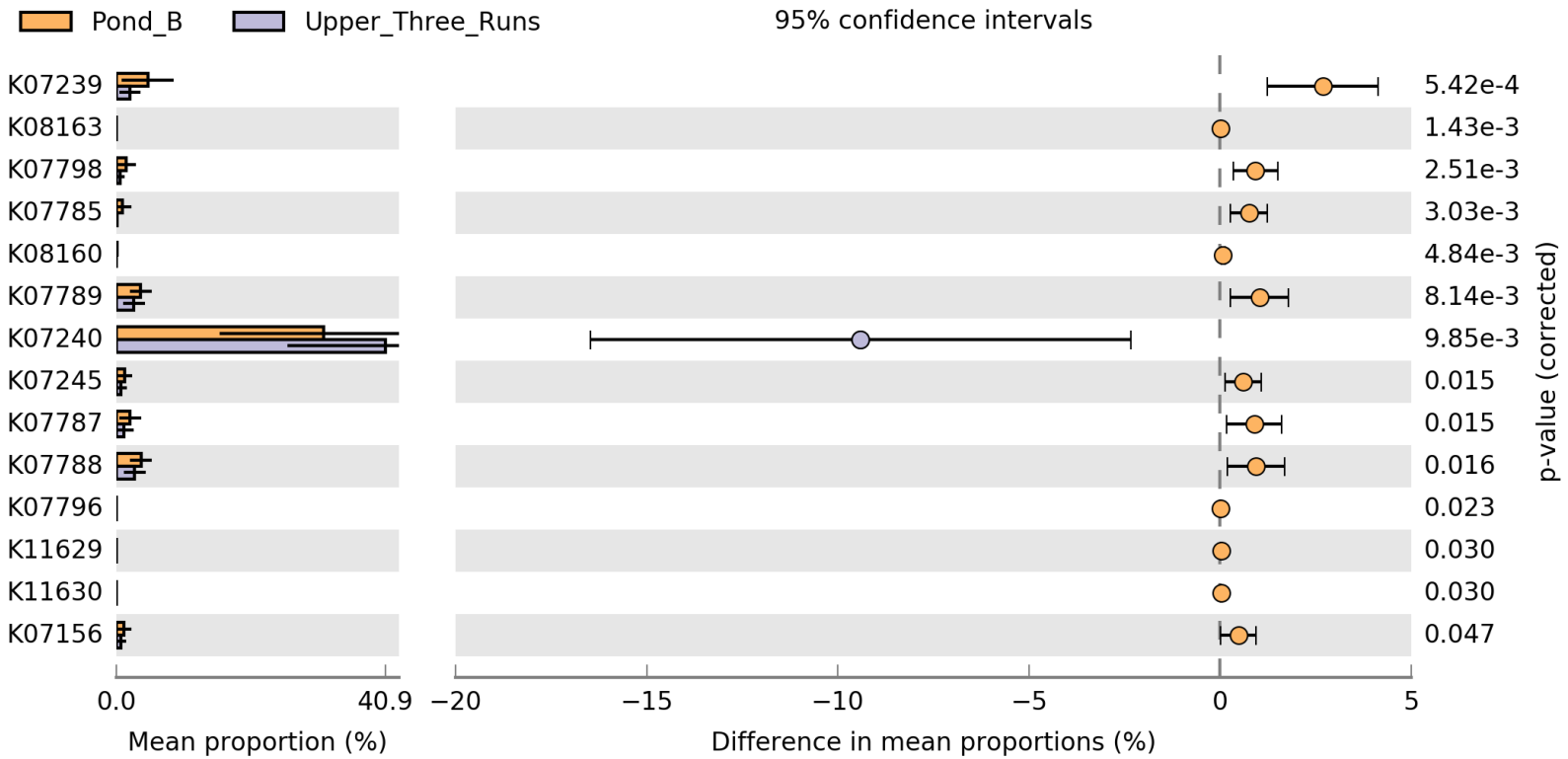

Figure 3-11. Pair-wise comparisons between Pond B and Upper Three Runs with 95% confidence intervals using PICRUSt predicted metagenome.

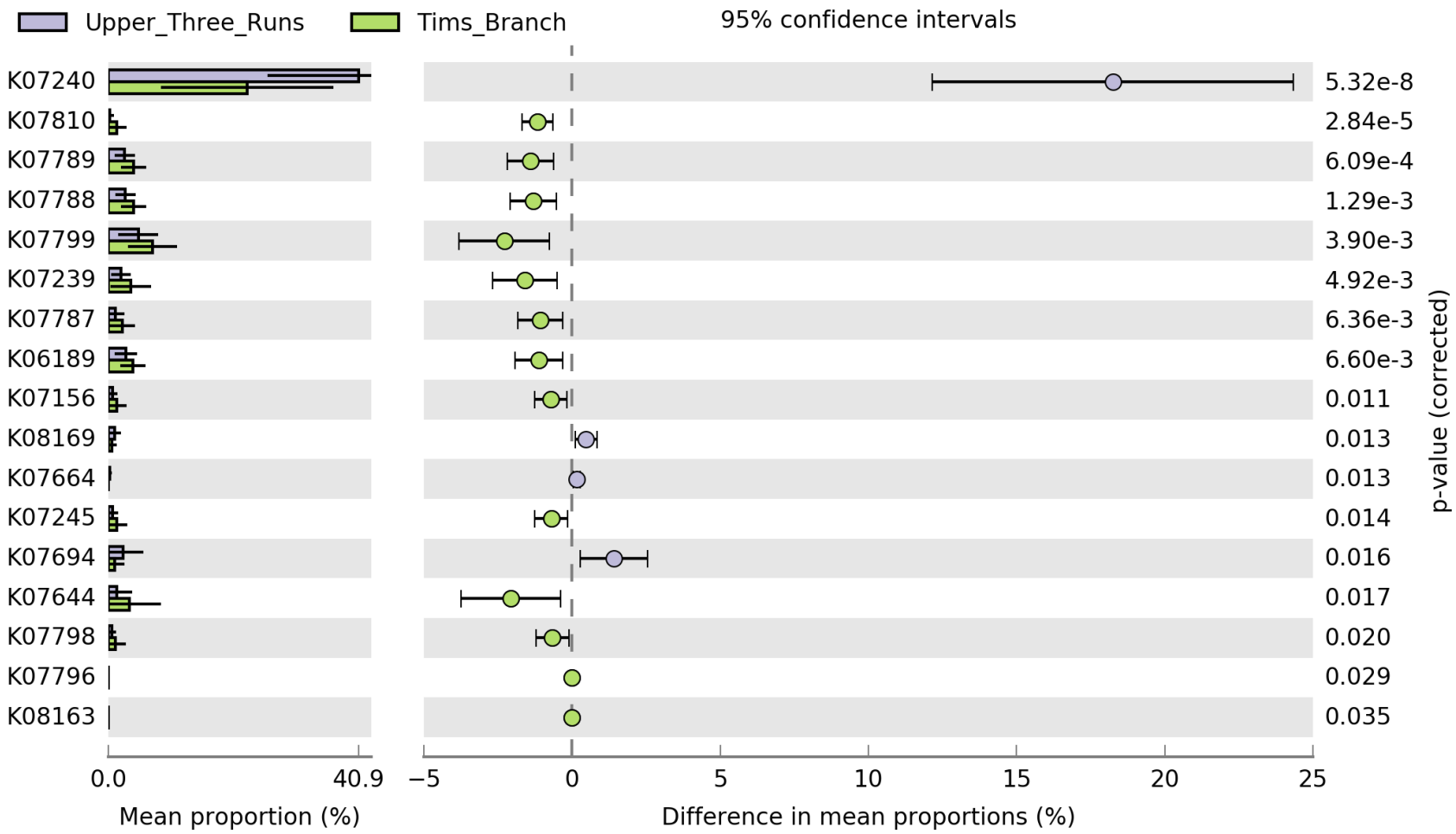

Figure 3-12. Pair-wise comparisons between Tim's Branch and Upper Three Runs with 95% confidence intervals using PICRUSt predicted metagenome.

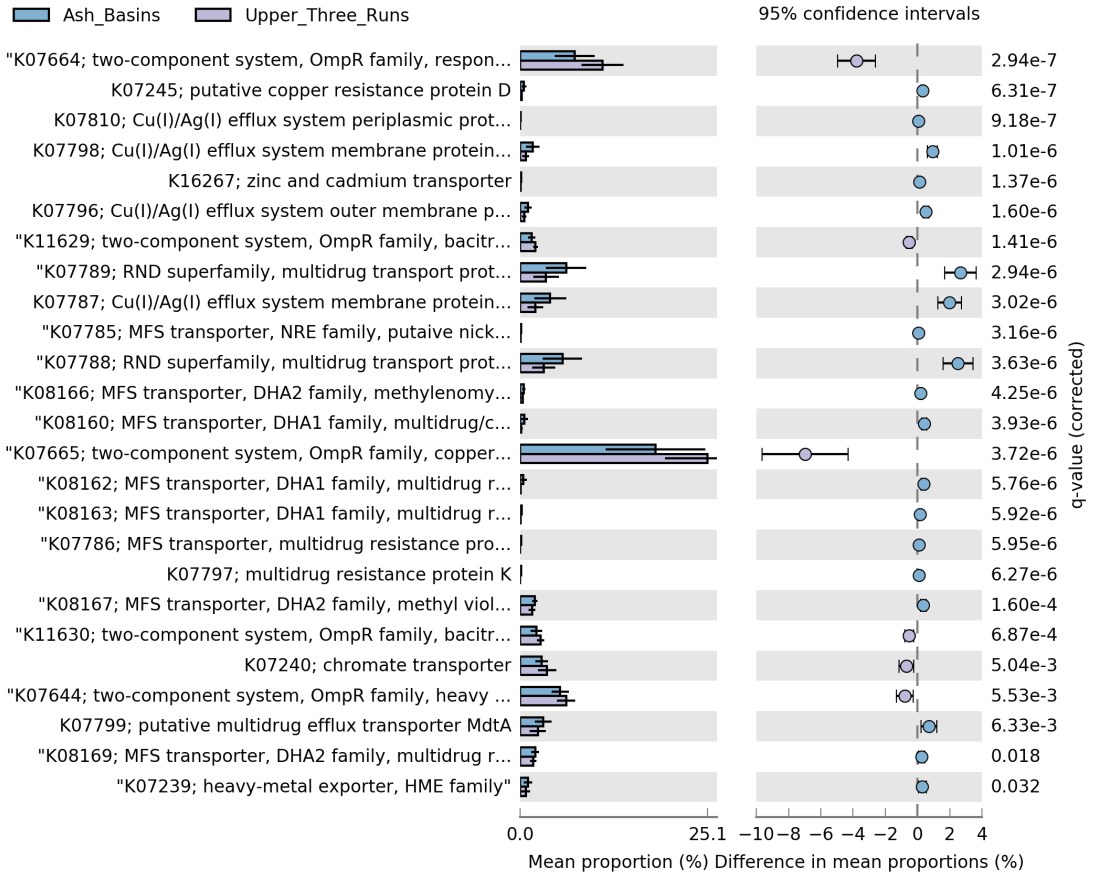

Figure 3-13. Pair-wise comparisons between Ash Basins and Upper Three Runs with 95% confidence intervals using Tax4Fun predicted metagenome.

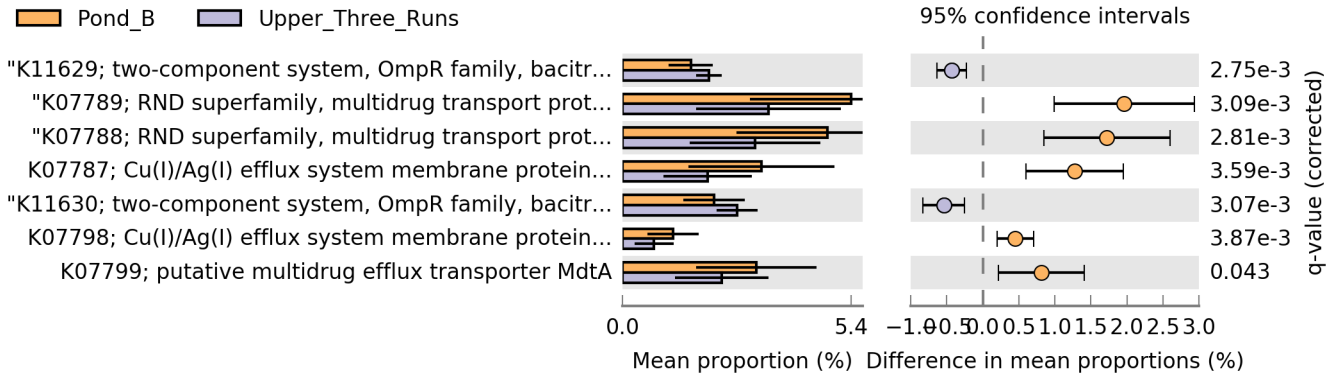

Figure 3-14. Pair-wise comparisons between Pond B and Upper Three Runs with 95% confidence intervals using Tax4Fun predicted metagenome.

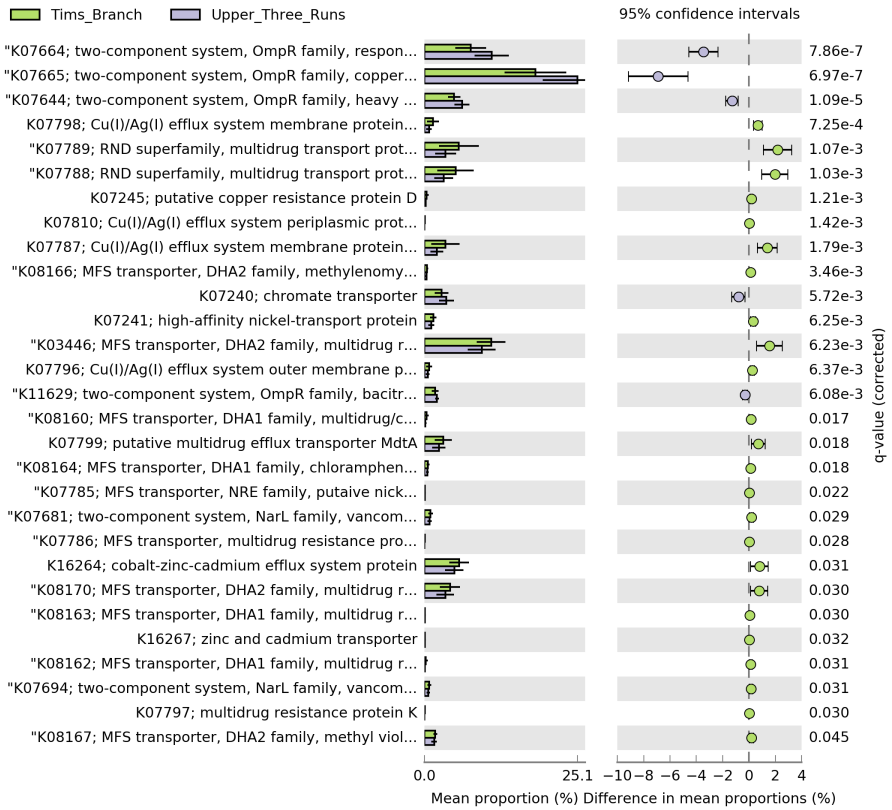

Figure 3-15. Pair-wise comparisons between Ash Basins and Upper Three Runs with 95% confidence intervals using Tax4Fun predicted metagenome.

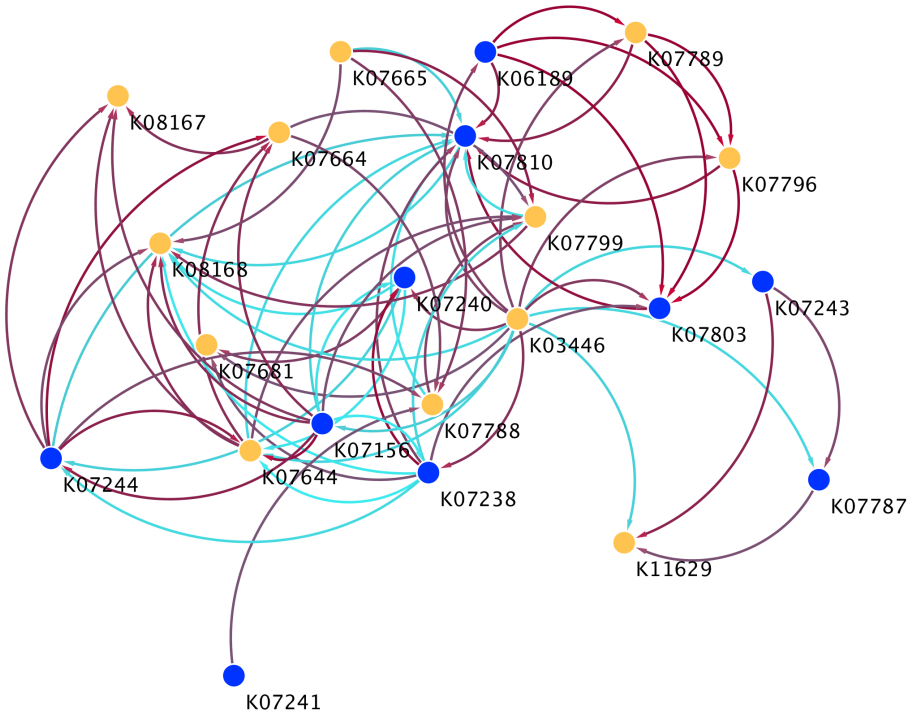

Figure 3-16. Network co-occurrence analysis of predicted HM and antibiotic resistance genes at UR. Each dot represents a PICRUSt predicted HM or antibiotic gene inferred from 16S rRNA gene sequence data: blue dots represent HM genes, yellow-orange dots respresent antibiotic resistance genes. Each connection represents a SparCC correlation with a magnitude >0.6 (positive correlation—red edges) or <−0.6 (negative correlation—light blue edges) and statistically significant ($P < 0.05$).

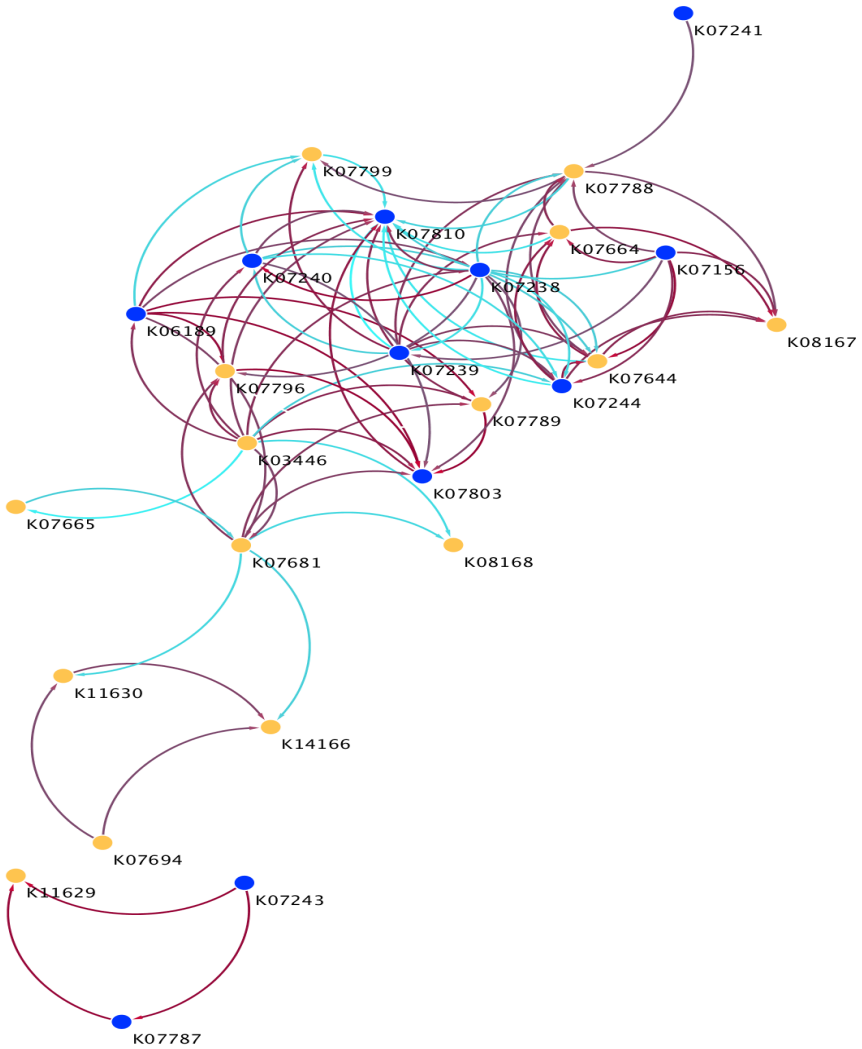
K07241
K07799
K07788
K07810
K07664
K07156
K07240
K07238
K06189
K08167
K07239
K07644
K07796
K07244
K07789
K03446
K07803
K07665
K07681
K08168
K11630
K14166
K07694
K11629
K07243
K07787

Figure 3-17. Network co-occurrence analysis of predicted HM and antibiotic resistance genes at PB. Each dot represents a PICRUSt predicted HM or antibiotic gene inferred from 16S rRNA gene sequence data: blue dots represent HM genes, yellow-orange dots respresent antibiotic resistance genes. Each connection represents a SparCC correlation with a magnitude >0.6 (positive correlation—red edges) or <−0.6 (negative correlation—light blue edges) and statistically significant ($P < 0.05$).

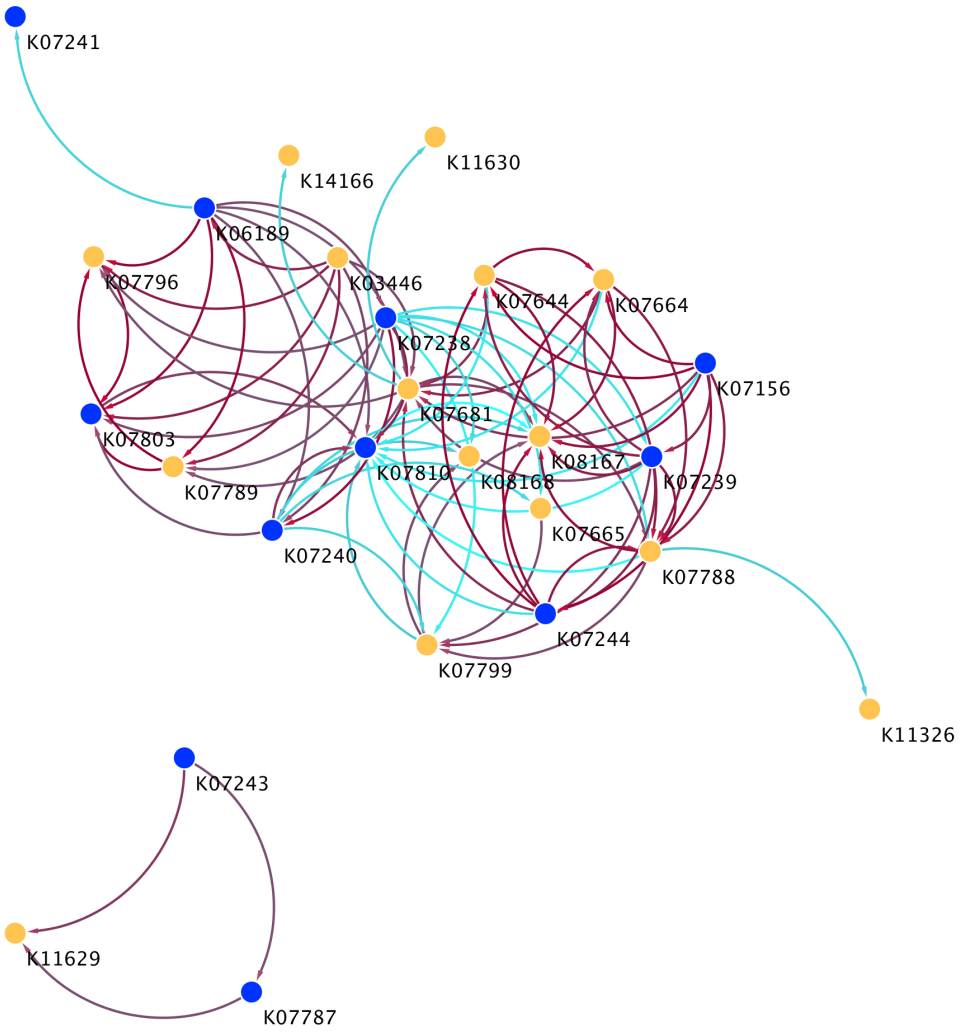
K07241
K14166
K11630
K06189
K07796
K03446
K07644
K07664
K07238
K07156
K07681
K07803
K08167
K07810
K08168
K07239
K07789
K07665
K07240
K07788
K07244
K07799
K11326
K07243
K11629
K07787

Figure 3-18. Network co-occurrence analysis of predicted HM and antibiotic resistance genes at TB. Each dot represents a PICRUSt predicted HM or antibiotic gene inferred from 16S rRNA gene sequence data: blue dots represent HM genes, yellow-orange dots respresent antibiotic resistance genes. Each connection represents a SparCC correlation with a magnitude >0.6 (positive correlation—red edges) or <−0.6 (negative correlation—light blue edges) and statistically significant ($P < 0.05$).

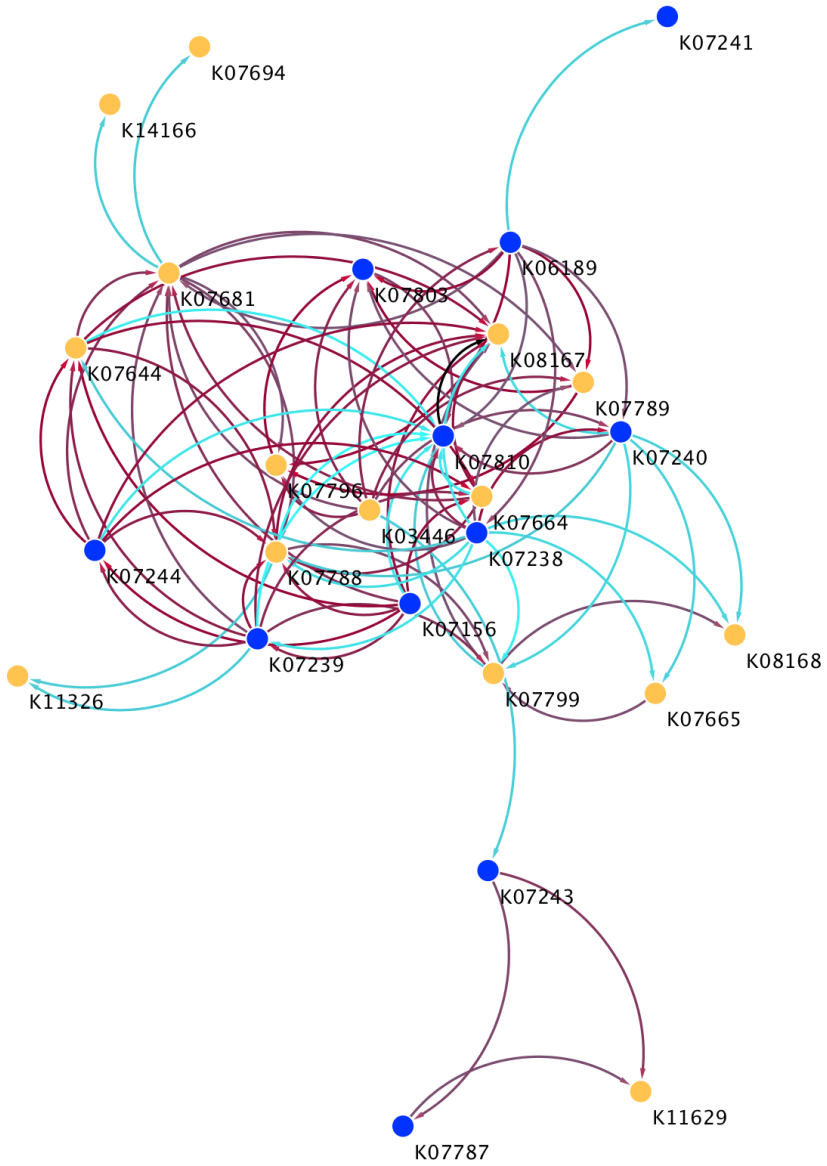
K07241
K07694
K14166
K06189
K07681
K07803
K08167
K07644
K07789
K07810
K07240
K07796
K07664
K03446
K07238
K07244
K07788
K07156
K08168
K07239
K07799
K11326
K07665
K07243
K11629
K07787

Figure 3-19. Network co-occurrence analysis of predicted HM and antibiotic resistance genes at AB. Each dot represents a PICRUSt predicted HM or antibiotic gene inferred from 16S rRNA gene sequence data: blue dots represent HM genes, yellow-orange dots respresent antibiotic resistance genes. Each connection represents a SparCC correlation with a magnitude >0.6 (positive correlation—red edges) or <−0.6 (negative correlation—light blue edges) and statistically significant ($P < 0.05$).

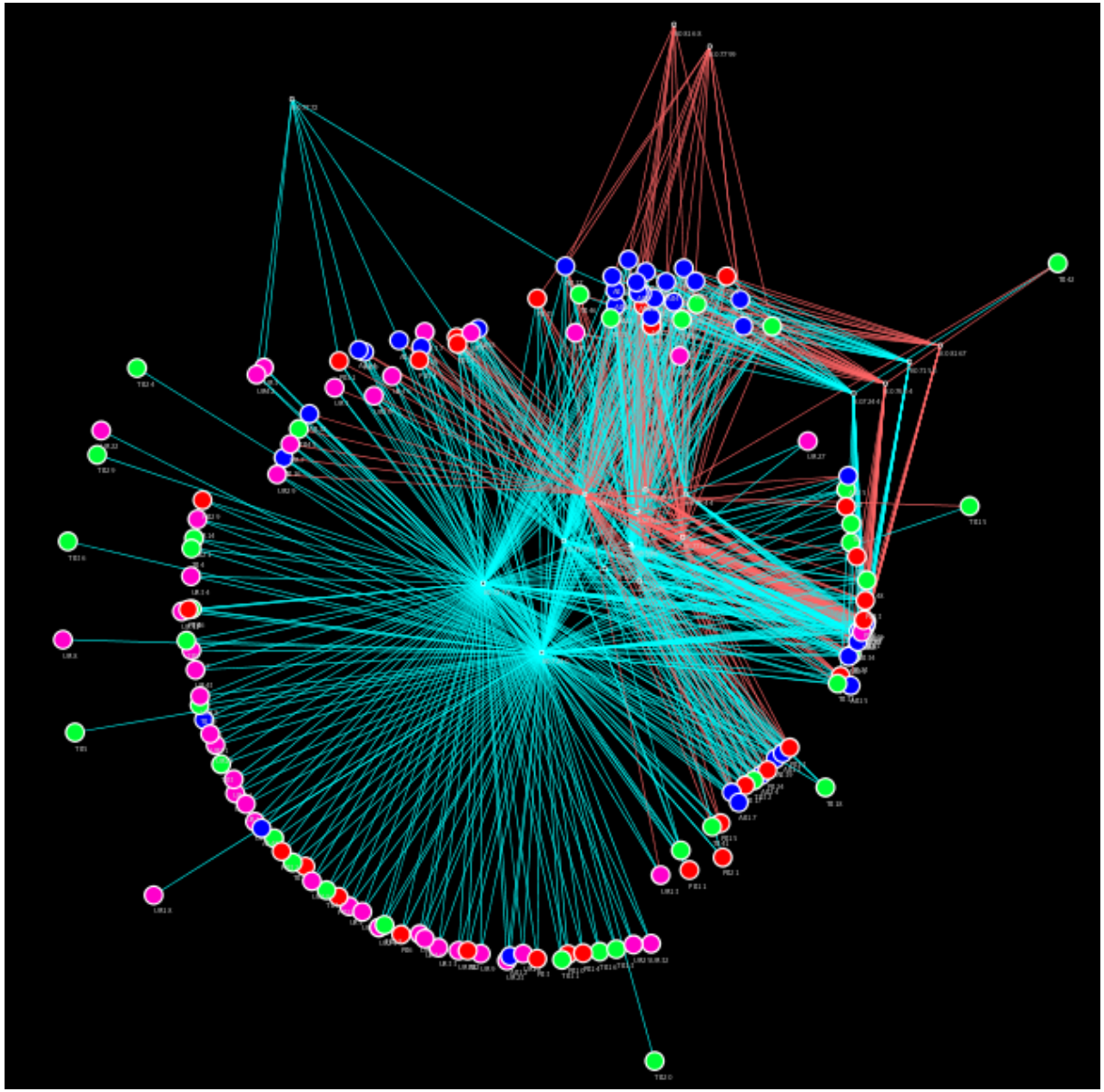

Figure 3-20. Network analysis of the co-occcurence of PICRUSts HM and antibiotic genes by site. The connecting edges are colored by the type of gene (small dots where edges originate): Cyan represents HMs while orange edges represent antibiotic resistance genes. Site nodes are consistently colored according to site type: Pink (TB), Blue (AB), Red (PB), Green (TB).

CHAPTER 4

THE GUT RESISTOME OF CAPTIVE *PEROMYSCUS LEUCOPUS*

[†] Thomas, J. C. IV, J. C. Seaman, J V. McArthur, V. Kaza, H. Kiaris, O. E. Rhodes Jr., and T. C. Glenn. The gut resistome of captive *Peromyscus leucopus*. In preparation for Microbiome.

Abstract

The emergence and spread of antimicrobial resistant (AMR) organisms is one of the most significant global health threats of the 21st century. In order, to deal with the rapidly increasing spread of antimicrobial resistance, it is important to identify reservoirs (e.g. the gut microbiome) known to harbor many opportunistic human pathogens. In this study, we examined the effects of heavy metal exposure on the co-selection of metal and antibiotic resistance bacteria in the cecal contents of white-footed mice (*Peromyscus leucopus*). We examined this using a latin-square design where mice were separately fed heavy metals (low and high dosage) and ciprofloxacin for 4 weeks. We observed significant accumulation of cobalt in livers and kidneys ($P < 0.05$). Using 16S rRNA gene sequencing, and predictive functional profiling we demonstrated that heavy metals significantly depleted several 'protective' genera observed in the control and ciprofloxacin treatment such as *Lachnospiraceae*, while enriching others such as *Lactobacillus* and *Flexispira*. Further, low dose heavy metal exposures significantly increased species richness ($P < 0.05$). Finally, predictive functional profiling revealed significantly higher relative abundance of predicted genes corresponding to metal and antibiotic resistance in the high dose heavy metal treatment compared to either the control or antibiotic treatment. Together, our results illustrate the potential for the co-selection of AMR resistant organisms in the gut microbiome.

Introduction

Chronic heavy metal exposure can alter the gut microbiome

Described as a "hidden" metabolic organ within the gastrointestinal epithelium, the gut microbiome encodes 100-fold more unique genes than the human genome (Gill et al., 2006; Kinross et al., 2011; Guinane and Cotter, 2013). This collection of microbes plays a fundamental role in harvesting energy and nutrients from food, such as short-chain fatty acids (SCFA) and amino acids (Krajmalnik-Brown et al., 2012). In addition, gut microbiota function in concert with specialized intestinal epithelial cells (IECs) through an intricate system of "cross-talk" through the mucosal component of the gut. This dynamic immune-microbial dialogue allows the regulation of the immune system while providing a pro-inflammatory control within the intestinal lumen (Hill and Artis, 2010; Cahenzli et al., 2013; Purchiaroni et al., 2013). However, host exposure to heavy metals (HMs), subsequently followed by intestinal absorption and accumulation of HMs has been associated with both perturbations in the microbial ecosystem and the occurrence of various inflammatory diseases.

Heavy metal contamination has been associated with microbial dysbiosis

Chronic HM exposure can have profound detrimental effects on host health including heightened oxidative stress, inflammation of internal organs, and genotoxicity. Heavy metal exposures can also alter the structure and diversity of gut microbiota, leading to the reduction in "protective bacteria" and the proliferation of potentially harmful microbiota. Such perturbations are strongly associated with microbial dysbiosis—a condition where bacteria communities shift in an unhealthful direction—and even disease (Phillips et al, 2009; Arthur et al., 2013; Schaik, 2015; Boulangé et al., 2016; Wu et al., 2016).

Heavy metals can affect microbial functional diversity and co-select antibiotic resistance

Furthermore, HMs can not only alter the microbial ecology of the host gut but also severely impact microbial physiology, basal gene expression, and even metabolic profiles (Lu et al., 2014). Recent studies have demonstrated that widespread HM contamination in the environment, typically from farming, industry, and other human activities, may facilitate the proliferation of antibiotic resistance strains via co-selection of antibiotic resistance genes (ARGs) (Di Cesare et al., 2016). Heavy metal resistance systems (HMRGs) are the most well-known examples of ARG selection mechanisms, since they can indirectly support the proliferation and maintenance of AMR using similar resistance mechanisms such as increasing efflux pump activity and reorganization of the cell membrane (Di Cesare et al., 2016; Munita and Arias, 2016).

Horizontal gene exchange and antimicrobial resistance

Resistance to toxic compounds such as HMs and antibiotics produced by other microbes in the environment are commonly the result of resistance determinants (chromosomal or plasmid-encoded genes) located on mobile genetic elements (MGEs) (e.g. transposons, integrons, and gene cassettes). Mobile resistance elements can efficiently disseminate within a microbial population via several horizontal gene transfer (HGT) mechanisms, regardless of the genetic relatedness between species (Domingues et al., 2012). For instance, MGEs such as integrons can capture multiple gene cassettes, and form tandem arrays of genetically linked resistance genes. These tandem arrays, such as multidrug resistance (MDR) systems are commonly manifested as co-resistance, in which multiple genes responsible for two or more resistances are adjacent to one another on a MGE. Heavy metal and antibiotic resistance mechanisms can also be coupled physiologically, in a selection process termed cross-resistance.

The gut as potential reservoir of antimicrobial resistance

Given the considerable number of microbial species within the human gut and their shared ecology, there are numerous opportunities for exchange of genetic material between pathogens and commensals, in addition to the co-selection of ARGs following host exposure to HMs. Mounting evidence suggests that exposures to HMs can be associated with the occurrence of a myriad of inflammatory diseases, metabolic syndromes, and microbial dysbiosis. However, it is unclear how HM exposure may affect the reservoir of antimicrobial resistance (AMR) elements (the resistome) of the gastrointestinal (GI) tract, particularly regarding the co-occurrence of ARGs and MRGs. A multitude of prior studies have demonstrated that ARGs and MRGs, including clinically relevant pathogens, are ubiquitous in a range of environments. Consequently, the spread of AMR in clinically relevant pathogens has emerged as a major global health crisis that has only accelerated due to inappropriate use of antibiotic drugs, and pollution of the environment with antibiotic drugs and heavy metals. Here we aimed to 1) experimentally determine how environmentally relevant exposures to a suite of HMs might affect the composition, structure, and diversity of microbiota associated with the GI tract of *Peromyscus leucopus*; 2) explore patterns of ARG and MRG co-occurrence, and 3) evaluate the interaction between alterations in host microbiota and host inflammatory response.

Methods

Animals

Forty-eight male *Peromyscus leucopus* mice derived from the University of South Carolina (USC) *Peromyscus* genetic stock center, aged six to seven months were randomly assigned in a 4 x 4 Latin square experiment. All mice cages were contained within a standard

animal laboratory with a 12h light–dark cycle and were fed with a custom AIN-93M diet (Envigo, Madison, Wisconsin USA). Treatments consisted of 1) TD.160615 (Control), 2) TD.160616, low dose (1X) heavy metals (HMs), 3) TD. 160617, high dose (5X) HMs, 4) TD.160618, Ciprofloxacin. The composition of the diets is presented in Table 4-1. Diets were stored at room temperature until used. All animal care procedures were approved by the Institutional Animal Care and Use Committee of South Carolina University prior to initiation of the experiment (AUP-237-101170-121916).

Mice were fed and watered ad libitum. Fresh feces were collected by gently massaging the mice rectal wall over a sterilized conical tube within one hour of feeding. Initial feces collection took place on the third day of feeding to allow for acclimation, then on the seventh day, and every following week for four weeks. At the completion of the exposure experiments all mice were asphyxiated by placing them in a standard glass desiccator contained within a chemical fume hood with the cover on for 30 seconds. After mice were euthanized they were weighed, and a retro-orbital bleed was used to collect blood. Finally, the entire small intestines (duodenum, jejunum, ileum), cecum, large intestines, liver, kidney, visceral fat, brain, were weighed and immediately frozen on dry ice. All samples were stored at −80°C until DNA extraction.

ICP-MS Metals analysis

Heavy metals were extracted from 0.25g of freeze dried mouse tissue (combined kidneys and livers), and fecal pellets using the EPA Method 3052 with modifications (Wu et al., 1996) (Supplemental Information). All digestions were analyzed for extractable arsenic (As), cobalt (Co), copper (Cu), chromium (Cr), nickel (Ni), strontium (Sr), uranium (U), and zinc (Zn) using an inductively coupled plasma mass spectrometer (ICP-MS).

We used a latin square analysis of variance (ANOVA) to compare metals present in the gut tissue samples using the R package version 3.33. All post-hoc multiple comparisons were made using TukeyHSD to further examine differences in trace elements.

DNA isolation, PCR amplification, and Illumina Sequencing of 16S rRNA amplicons

DNA was independently extracted from small intestines (duodenum, jejunum), cecum, and large intestines using a Biospec 96 minibeater (Biospec Products, Bartlesville, OK), and ZymoBiomics-96 DNA isolation kit (Zymo Research, Tustin, CA, USA). However, for this dissertation chapter, only the sequence data from the cecum and large intestines were analyzed. Purified genomic DNA was obtained by a magnetic-based size selection method using SeraMag Speed Beads (Thermo-Fisher Scientific, Asheville, NC, 28804, USA) according to the manufacturer's protocol. PCR libraries were generated using the S-D-Bact-041-b-S-17 (5'-CCTACGGGNGGCWGCAG-3') forward and S-D-Bact-0785-a-A-21 (5'-GACTACHVGGGTATCTAATCC-3') reverse primer pair (Klindworth et., 2012). Modifications to the primer sets (8 forward + 12 reverse) were done according to Taggimatrix protocol, which included fusions with universal 5' iTru sequences containing up to 96 combinations of unique internal tags (Glenn et al., 2016). DNA from each sample was PCR amplified using the 16S-iTru fusions in 25-µl reactions using the KAPA HiFi Hotstart PCR kit (KAPA Biosystems, Wilmington, MA, 01887, USA). The PCR amplification protocol was as follows: 95°C for 3 minutes, followed by 30 cycles of 95°C for 1 min, 55°C for 30 s, and 72°C for 30 s with a final elongation step of 72°C for 5 min. PCR was performed using a T100 Thermal Cycler (BioRad, Hercules, CA, 9454, USA) and amplicons were visualized using 1.5% gel electrophoresis. PCR products were purified then quantified using a Qubit Fluorometer (Thermo-Fisher Scientific, Asheville, NC, 28804, USA) set to broad range sensitivity and diluted

to a final concentration of 2 ng/μl using sterile nuclease free water. The diluted PCR amplicons were used in a second PCR reaction containing the TruSeq Illumina P5 and P7 Primers. The PCR amplification was the same as above however modified with fewer cycles (14). The quadruple-indexed libraries were purified a final time using the magnetic-bead size selection method and pooled based on the number of desired reads. PCR products were then sent to the Georgia Genomics Facility (http://dna.uga.edu) for sequencing on an Illumina MiSeq using an Illumina PE300 kit (Illumina, San Diego, CA, 92122, USA).

De-multiplexing and Quality Filtering

All Fastq conversion and de-multiplexing were conducted using bcl2fastq (Illumina, v1.8.4) and processed to remove low quality reads (FastX toolkit). Paired-end sequencing reads were imported into Geneious v10.0 (Biomatters Limited, NJ, USA), set as paired-reads with an expected insert size of 444 bp and trimmed to remove Illumina adapters using default settings. Paired-end sequencing reads were then merged using the FLASH v1.2.9 plugin (Magoc and Salzberg, 2011). The software package Mr_Demuxy v1.2.0 (https://pypi.python.org/pypi/Mr_Demuxy/1.2.0) was utilized to de-multiplex the merged reads into individual combinatorially tagged FASTQ files. Sequences were filtered based on size (≥ 300 bp) and quality scores (≥Q20).

Intestinal 16S Sequence Analysis

Sequencing reads were imported into the phylogenetic software package QIIME v1.9.1 (MacQiime v1.91 package: http://www.wernerlab.org/software/macqiime, Caporaso et al., 2010) for OTU (Operational Taxonomic Unit) generation, multi-leveled taxonomic classification, and diversity estimates. Briefly, samples were sorted using the *add_qiime_labels.py* script.

Afterward, bacterial OTUs were selected using an open reference workflow, with Greengenes v13_8 16S reference database (http://greengenes.secondgenome.com/, DeSantis et al., 2006) and default *uclust* (Edgar, 2010) OTU picking strategy (Supplemental Information). Taxonomy was defined using default settings of ≥ 97% similarity to reference sequences.

Metagenome prediction of HM and antibiotic resistance with PICRUSt

The software PICRUSt (Phylogenetic Investigation of Communities by Reconstruction of Unobserved States) (Langille et al., 2013) were applied to make functional gene content predictions using the Greengenes database v13_5 database respectively. We were primarily interested in KEGG orthologs corresponding to HM resistance and antibiotic/multi-drug efflux genes, since prior studies have suggested they can be co-selected (Baker-Austin et al., 2006; Pal et al., 2015). A total of 19 KEGG orthologs were selected by manually searching the KEGG database (Table 4-2).

Statistical analyses and data visualization

Within-sample (alpha) diversity was evaluated and visualized in QIIME v1.91 and the Phyloseq package using various metrics (Chao1, ACE, Fisher's Alpha, Shannon-Wiener, and Simpson) (McMurdie and Holmes, 2014). Alpha diversity of communities found in mice intestinal tissues were computed using the *core_diversity_analyses.py* workflow with a sequencing depth set to 5,000 sequences. To test for the significant variation in taxonomic richness across the four treatments, we used the non-parametric Kruskal-Wallis test (Kruskal & Wallis, 1952) with the False Discovery Rate (FDR) correction as implemented in the *compare_alpha_diversity.py* script.

For the cecum and large intestinal samples we used QIIME v1.91 and MetaCoMET to explore and visualize the core microbiome (Wang et al., 2016). The software package QIIME

v1.91 was also used to test for the significant variation in the frequency of individual OTUs across the four treatments, using a G-test of independence test with FDR correction for multiple comparisons, and the Monte Carlo simulated non-parametric T-test for pair-wise comparisons, as implemented in the *group_significance.py* script. Hierarchical clustering based on complete linkage was used to examine the similarity between samples, and similarity of profile analysis (SIMPROF) was used to test the significance of clusters (Clarke et al., 2008). Bray-Curtis distances between samples (beta diversity) were computed and visualized using PRIMER 7.0 software with PERMANOVA+ add-on (Primer-E, United Kingdom; Bray & Curtis, 1957). This dissimilarity matrix was used to generate a non-metric multi-dimensional scaling plot (nMDS) based on 999 permutations, which was followed by canonical analysis of principle coordinates (CAP) for testing our *a priori* hypotheses (e.g. influence of tissue type, sampling location) (Kruskal, 1964; Anderson and Willis, 2003).

In order, to determine statistically significant differences in OTU abundances between cecum and large intestines samples we utilized the DeSeq2 package (using a Wald test with FDR correction for multiple comparisons) on our non-rarefied OTU table. The significant OTUs ($P \leq 0.01$) were visualized with R version 3.3.3 and R packages ggplot2 (Wickham, 2009), vegan (Oksanen et al., 2007), and phyloseq (McMurdie and Holmes, 2013). We performed these analyses for all treatment groups (Ciprofloxacin, Low Dose, and High Dose) and compared the log2 fold change with the Control.

Differences in microbial community structure and composition between tissues were tested using permutational multivariate analysis of variance (PERMANOVA) on log-transformed Bray-Curtis dissimilarity values (Anderson et al., 2005). For the PERMANOVA analysis cage number, row, treatment, and intestinal tissue region were fixed effects. Differences

among rows and columns (our blocking factors) were tested by permuting cages among both. Differences among intestinal tissues were tested by permutating treatments within rows and columns. We used a type III partial sum of squares design and Monte Carlo sampling permutated 999 times over residuals under a full model.

The final output from the PICRUSt workflow was imported into Statistical Analysis of Metagenomic Profiles (STAMP) to examine KEGG orthologs (KO) and pathways (Kaneshisa and Goto, 2000; Parks et al., 2014). Multiple comparison analyses were conducted using a Kruskal-Wallis test. Two group comparisons were conducted using a Welch's T-test (Satterthwaite, 1946).

Results

ICP-MS heavy metals analysis of tissues

The results of our ICP-MS analysis on the composited tissue (livers and kidney) and pooled fecal samples are presented in Table 4-3. Our latin-square analysis of variance (ANOVA) indicated that the concentration of cobalt ($P < 0.001$) differed significantly between our four treatment groups (Table 4-3). TukeyHSD post-hoc comparisons indicated that the differences in the accumulation of cobalt in the composited tissues was significant ($P < 0.05$) when comparing the control and ciprofloxacin treatments with either of the metal (low and high) treatments (Table 4-4). In addition, we also explored heavy metal accumulation in pooled fecal samples from each treatment with respect to the time point they were collected on (Day 0, Day 21) (Figure 4-1).

Microbial community composition and structure in mice cecum

After completing all quality filtering steps, denoising, and chimera removal in Geneious and QIIME, a dataset of 505,790 high quality (Q ≥ 20)16S rRNA gene sequences was compiled with an average read of 416.5 ± 11.0. Analyses were performed on rarefied data using an even sampling depth of 5,000 reads per sample. A total of 27,527 OTUs (1,927 ± 710 OTUs/sample) were observed spanning 10 bacterial phyla commonly associated with the mammalian gastrointestinal (GI) tracts (Figure 4-2).

We identified a core microbiome consisting of 6 bacterial phyla (i.e. Firmicutes, Bacteroidetes, Proteobacteria, Actinobacteria, TM7, Deferribacteres) and 2,352 shared OTUs between all the sequences analyzed in the study (Figure 4-3). Within these phyla, we detected several re-occuring OTUs: Firmicutes (*Lactobacillus*, *Streptococcus*, *Ruminococcus*), Bacteroidetes (*Parabacteroides*, *Odoribacter*), Proteobacteria (*Flexispira*), Actinobacteria (*Aldercreutzia*), TM7 (*F16*), and Deferribacteres (*Mucispirillum*). In addition, we calculated the relative abundance between the most abundant phyla: Firmicutes (60.00% ± 3.00 %), Bacteroidetes (19.00% ± 4.00 %), Proteobacteria (8.00% ± 1.00 %), TM7 (2.00% ± 1.00 %). At the level of family, the relative abundance of the predominant taxa between treatments were: Lactobacillaceae (22.00% ± 5.00 %), Turibacteraceae (16.00% ± 3.00 %), S24-7 (16.00% ± 3.00 %), Lachnospiraceae (3.00% ± 1.00 %), Helicobacteraceae (3.00% ± 1.00 %) and Ruminococcaceae (3.00% ± 1.00 %). A G-test of independence (implemented in Qiime 1.91) indicated that there were significant differences in many of these taxa in the cecum samples when comparing the four treatment groups ($P < 0.001$).

Differential abundance testing between control and treatments in mice cecum

Furthermore, in the DESeq2 analysis, the abundances of several bacterial families and genera were detected to be significant different between the Control and Low Dose HM groups ($P < 0.001$). For instance, *Coprococcus* (Lachnospiraceae), *Fusobacterium (*Fusobacteriaceae), and *Bacteriodes acidifaciens* were significantly more abundant in the Control group compared to the Low Dose group ($P < 0.001$) (Figure 4-4) (Table 4-5). The Low Dose group had a significantly higher abundance of F16 (TM7), and Flexispira ($P < 0.001$) (Figure 4-4) (Table 4-5). When comparing the differences between the Control and the High Dose groups we noticed significantly higher abundances of Fusobacterium, *Treponema* spp., *Dorea* spp. (Lachnospiraceae), Mogibacteriaceae in the Control group ($P < 0.001$) (Figure 4-5) (Table 4-6). Similarly, to the Low Dose group the High Dose group had significantly higher abundance of Flexispira ($P < 0.001$) (Figure 4-5) (Table 4-6). In addition, several OTUs that clustered with similar families and genera appeared to vary in differential abundance. For example, both the Low and High dose had OTUs that clustered with *Coriobacteriacae*, but had fewer representatives than the Control group. In our evaluation of the differential abundance of the Control group with the Ciprofloxacin group, we found that S24-7 (Bacteroidales) displayed a significantly higher abundance in Ciprofloxacin group compared to the Control ($P < 0.001$); while the Control had significantly higher abundances of *Desulfovibrio*, *Coriobacteriaceae*, *Rikenallaceae*, and *Lactobacillus* ($P < 0.001$) (Figure 4-6)(Table 4-7).

Microbial community composition and structure in large intestines

Our large intestines dataset of consisted of 428,087 high quality ($Q \geq 20$) 16S rRNA gene sequences with an average read of 416.7 ± 10.5. Analyses were performed on rarefied data using

an even sampling depth of 5,000 reads per sample. A total of 27,527 OTUs (1,903 ± 608 OTUs/sample) were observed spanning 10 bacterial phyla commonly associated with the mammalian gastrointestinal (GI) tracts (Figure 4-7).

The large intestines displayed many of the same taxa observed in the mice cecum but in different abundances. Among treatments we identified a core microbiome consisting of 7 bacterial phyla (i.e. Firmicutes, Bacteroidetes, Proteobacteria, Actinobacteria, TM7, Deferribacteres) and 1,915 OTUs shared between all the sequences analyzed in the study (Figure 4-8). Within these phyla, we detected several re-occuring OTUs: Firmicutes (*Lactobacillus*, *Streptococcus*, *Turibacter*, *Ruminococcus*), Bacteroidetes (*Parabacteroides*, *Odoribacter, Bacteroides, Prevotella*), Proteobacteria (*Flexispira*), Actinobacteria (*Aldercreutzia*), and TM7 (*F16*), Deferribacteres (*Mucispirillum*), and Verrucomicrobiaceae (*Akkermansia*). The relative abundance between the most abundant phyla were as follows: Firmicutes (49.01% ± 6.10 %), Bacteroidetes (28.73% ± 3.83 %), Proteobacteria (7.21% ± 2.88 %), TM7 (3.04% ± 0.92 %). At the level of family, the relative abundances of the predominant taxa between treatments were: *S24-7* (Bacteroidetes) (24.37% ± 2.71 %), *Lactobacillaceae* (15.82% ± 4.94 %), Turibacteraceae (13.22% ± 5.06 %), *Clostridiales* (8.12% ± 0.58 %), Lachnospiraceae (4.58% ± 1.09 %), Ruminococcaceae (4.17% ± 0.36 %), Helicobacteraceae (3.88% ± 2.45 %) and F16 (TM7) (3.01% ± 0.92 %). A G-test of independence (implemented in Qiime 1.91) indicated that there were significant differences in many of these taxa in the large intestine samples when comparing our four treatment groups ($P < 0.001$).

Differential abundance testing between control and treatments in large intestines

Our DESeq2 analysis for the large intestines displayed many similar patterns to our cecum samples. Genera such as *Desulfovibrio*, *Dorea*, *Helicobacter*, and *Fusobacterium* ($P < 0.001$) were significantly higher in the Control group; while *Flexispira* and *Oscillospira* were significantly higher in the Low Dose treatment when performing pair-wise comparisons ($P < 0.001$) (Figure 4-9) (Table 4-8). When comparing the High Dose treatment with the Control we noticed significantly higher abundances of *Ruminococcus*, *Allobaculum*, *Helicobacter*, *Turibacter*, *Oscillospira*, *Desulfovibrio*, and *Fusobacterium* within the Control group ($P < 0.001$) (Figure 4-10) (Table 4-9). We also observed significantly higher abundances of *Sphingomonas* and *Flexispira* in the High Dose treatment (Figure 4-11) (Table 4-9). Finally, we compared the Ciprofloxacin treatment and the Control group and observed a significantly higher abundance of *Desulfovibro* in the Control; but a higher abundance of *Prevolella* in the Ciprofloxacin treatment ($P < 0.001$) (Figure 4-12) (Table 4-10).

HM exposure in cecum and large intestines does not significantly increases bacterial species richness over control

Generally, cecum samples within the Ciprofloxacin and Control treatment displayed the lowest diversity, followed by the High dose, while those from the Low dose appeared to have the highest diversity across all diversity metrics (Figure 4-13). In addition, when performing pairwise group comparisons there were significant differences in microbial diversity when comparing both the low (Chao1: $P= 0.024$) and ciprofloxacin treatments (Chao1: $P= 0.006$; Faith's phylogenetic diversity (PD): $P= 0.012$) to the control (non-parametric test with *compare_alpha_diversity.py*, $P < 0.05$) (Supplemental Information). We did not detect significant differences in microbial diversity between the high HM treatment and the other

treatments, or the ciprofloxacin treatment when compared to the low HM treatment. Within the large intestine we observed significant differences in microbial diversity between the low HM treatment and ciprofloxacin treatment (Chao1: P= 0.024) (Figure 4-14), however we did not detect further significant differences between treatment groups when performing pairwise comparisons using either Chao1 or PD (Supplemental Information).

Beta-diversity analyses of cecum and large intestinal samples

We initially utilized an unconstrained non-metric multidimensional (nMDS) plot based on a double square root transformed Bray-Curtis dissimilarity matrix to explore differences in the large intestinal community based on treatments. We overlaid the nMDS plots with SIMPROF based cluster analysis data to examine overall similarity between treatments in multi-dimensional space (Figure 4-15; Figure 4-16). The nMDS plots for the cecum samples indicated that overall similarity between bacterial communities within the treatments was approximately 60%. Marginal PERMANOVA tests and CAP ordination indicated significant differences microbial composition among the treatments (Pseudo-F= 2.6526, P = 0.001) (Figure 4-17) (Table 4-11). However, pairwise PERMANOVA indicated that the Low and High treatment groups displayed no differences in microbial composition (P = 0.043) (Table 4-12).

In the large intestines nMDS analyses indicated that overall the communities displayed between 50 and 60 percent similarity among the four treatments (Figure 4-18). Marginal PERMANOVA tests and CAP ordination indicated significant differences in microbial composition among the treatments (Psuedo-F= 2.8322, P = 0.001) (Figure 4-19) (Table 4-13). Interestingly, our pairwise PERMANOVA tests indicated that were no differences in microbial composition between the Ciprofloxacin and Control groups, but every other comparison was significant (Table 4-14).

Predicted antibiotic resistance between treatments in cecum and large intestines

The mean weighted nearest sequenced taxon index (NSTI), which measures the prediction accuracy of PICRUSt, of our 44 cecum samples was 0.14 ± 0.02. In the cecum samples, we found 11 out of 19 KEGG features that were significantly different between the four treatment groups (Table 4-3). Predicted genes such as K06189 (corC, magnesium and cobalt transporter), K07787 (cusA, copper/silver efflux system), K03446 (emr, multidrug resistance), and several others were found to display significant differences in relative abundance. Interestingly, pairwise comparisons between the Control and Low Dose group in mice cecum indicated that K07239 (HME family, heavy metal exporter) was significantly higher in the Control. No significant differences were observed between the Control and High Dose. In addition, only one predicted gene, K07238 (zupT, zinc transporter) was found to be significantly higher in the Ciprofloxacin group when compared with the Control.

The mean weighted nearest sequenced taxon index (NSTI), which measures the prediction accuracy of PICRUSt, of our 38 large intestines samples was 0.17 ± 0.04. The large intestines revealed several key differences when compared to the cecum. We found 10 out of 18 KEGG features that were significantly different between the four treatment groups (Table 4-3). These included genes corresponding to heavy metal and antibiotic resistance such as K06189 (corC, cobalt and magnesium transport), K03446 (emrB, multidrug resistance), K01467 (ampC, beta-lactam resistance), K09687 (antibiotic transport system), and several others (Table 4-3). Between the Control and Low Dose groups we only detected differences in K06189 (magnesium and cobalt transporter) (Figure 4-20). We detected higher numbers of predicted genes corresponding to antibiotic resistance in the High treatment compared to the Control, including K01467 (ampC, beta-lactam resistance), K03446 (emrB, multidrug resistance), and K03543

(emrA, multidrug efflux) (Figure 4-21). Interestingly, the High treatment also had significantly higher abundance of predicted genes corresponding to K01467 (ampC, beta-lactam resistance) compared to the Ciprofloxacin treatment (Figure 4-22). Pairwise comparisons between the Control and Ciprofloxacin group revealed higher abundances of predicted genes corresponding to K05595 (multiple antibiotic resistance), K08218 (beta-lactam resistance), and K03446 (multidrug resistance) in the Ciprofloxacin treatment (Figure 4-23).

Because, the large intestines appeared to display the potential co-selection of antimicrobial resistance, particularly in the High Dose compared to the cecum, we investigated the taxa that contributed to the significantly higher relative abundance of predicted resistance genes. Using PICRUSt's *metagenome_contributions.py* script we found that *Lactobacillus* contributed the greatest number of predicted resistance genes per sample. Other bacterial taxa that contributed to predicted resistance genes included several OTUs corresponding to *Turibacter*, *Flexispira*, S24-7, *Clostridia*, *Streptococcus*, *Enterobacteriaceae*, *Bacteroides* and *Sphingomonas*.

Discussion

In this study, captive *Peromyscus leucopus* underwent 4 weeks of continuous exposure to several heavy metals (low and high dose) or ciprofloxacin (1 ppm) administered in their food. Heavy metals were selected that mimicked contaminated soils from the Savannah River Site (SRS). Our results indicated significant accumulation of cobalt, when comparing the control and antibiotic treatments with either of the heavy metal treatments ($P < 0.05$). Previous studies on cobalt have indicated that chronic cobalt exposure can lead to tissue and cellular toxicity (Vengellur and LaPres, 2004).

In addition, we used Illumina-based 16S rRNA gene sequencing and predictive functional profiling to study the impact of heavy metal exposure on the *Peromyscus* gut microbiome and its resistome. We showed that exposure to heavy metals or ciprofloxacin had no significant impact on microbial diversity compared to the control, as illustrated in Figure 4-11, despite both heavy metal groups possessing more overall OTUs. This contrasts with other studies that suggest heavy metal exposure can reduce normal phylogenetic diversity (Lu et al., 2014). Several metals including zinc are known to be important co-factors for commensals and opportunistic gut pathogens. Therefore, the effect of heavy metals on the gut microbiome structure and diversity is likely dependent on the concentration and the type of HMs in the gut microenvironment.

We also demonstrated that heavy metal exposure can deplete certain 'normal' mice gut microbiota such as *Desulfovibrio*, *Dorea*, *Helicobacter*, *Lachnospiraceae*, and *Fusobacterium*. Members of the *Lachnospiraceae* family, in particular, are thought to provide a protective effect in the intestinal lumen through production of anti-inflammatory short chain fatty acids (SCFAs) (Pérez-Cobas et al., 2015). Reduction in these bacteria is concomitant with a predisposition to colitis (Breton et al., 2013; Nakanishe et al., 2015). In addition, we demonstrated that heavy metals can also significantly increase taxa such as *Flexispira, Turicibacter, Sphingomonas, F16,* and certain *Lactobacillus* species. Members of the genus *Helicobacter* including *Flexispira* have been isolated from a wide range of host species and have been associated with diarrhea, hepatitis, and atrophic gastritis (Iten et al., 2001). The genus *Turicibacter* has been demonstrated to increase in proportion in the gut following exposure to heavy metals (Breton et al., 2016). The genus *Sphingomonas* has been reported as a minor nosocomial pathogens, with high genetic plasticity (Ryan and Adley, 2010; Vaz-Moreira et al., 2011). The bacteria F16 in the TM7 bacterial division has been reported to possess an atypical resistance to streptomycin and play an

essential role as a promoter of inflammation in the early stages of inflammatory bowel disease (IBD) (Kuehbacher et al., 2008). Interestingly, we found that while certain members within the same genus, such as *Lactobacillus*, may decrease others may see an increase in differential abundance with respect to heavy metal exposure. Unfortunately, our 16S rRNA analyses provided limited resolution at the species level so we were unable to discern the precise sensitivities of very closely related organisms. In any case, these results highlighted the potential for heavy metals to produce minor yet significant perturbations in microbial community structure and composition.

Finally, our data also suggest that at high exposures, heavy metals can indirectly co-select antibiotic resistance, particularly in the large intestines. Several predicted antibiotic and multi-drug resistance genes were found to be enriched in the high HM treatment even when compared to the antibiotic treatments. Perhaps, most strikingly is that the most abundant species in the Peromyscus cecum and large intestines, *Lactobacillus*, contributed the greatest number of predicted genes associated with antibiotic resistance, especially (K09647, antibiotic transport) and (K01467, beta-lactam resistance). This suggests that not only does a sizeable portion of the gut microbiome already possess intrinsic antibiotic resistance, but that heavy metals can enrich the resistance phenotype. Furthermore, because antibiotic resistance determinants are carried on mobile genetic elements, the gut microbiome constitutes a large reservoir of antimicrobial resistance (Gueimonde et al., 2013).

Conclusion

To our knowledge, there are very few microbiome focused studies that have examined the influence of multiple heavy metals on the gut microbiome using murine models. Our present

observations provide further evidence that heavy metals can cause alterations in the structure of the cecal microbiome of captive *Peromyscus leucopus*. In addition, our results also suggest that heavy metal ingestion can indirectly co-select antibiotic resistance. Given the global concurrent issues of metal pollution and increasingly antibiotic resistant pathogens, identifying potential reservoirs of antimicrobial resistance is of key importance. Further studies are needed to more directly assess the impact of heavy metals on the gut microbiome, determine the degree to which high dose exposures modulate the enrichment of the resistome, and assess the risk toward human health.

Acknowledgements

We thank our colleagues in the Department of Environmental Health Science, the Georgia Genomics Facility, University of South Carolina Peromyscus Genetic Stock Center, and Savannah River Ecology Laboratory for assistance with sampling and data collection. This research was supported by a contract from the US Department of Energy through Cooperative Agreement number DE-FC09-07SR22506 with the University of Georgia Research Foundation.

Disclaimer

recommendation, or favoring by the United States Government or any agency thereof. The views and opinions of authors expressed herein do not necessarily state or reflect those of the United States Government or any agency thereof.

References

Anderson, Marti J. "Permutational Multivariate Analysis of Variance." *Department of Statistics, University of Auckland, Auckland* 26 (2005): 32–46.

Arthur, Janelle C., Raad Z. Gharaibeh, Marcus Mühlbauer, Ernesto Perez-Chanona, Joshua M. Uronis, Jonathan McCafferty, Anthony A. Fodor, and Christian Jobin. "Microbial Genomic Analysis Reveals the Essential Role of Inflammation in Bacteria-Induced Colorectal Cancer." *Nature Communications* 5 (September 3, 2014): 4724. doi:10.1038/ncomms5724.

Baker-Austin, Craig, Meredith S. Wright, Ramunas Stepanauskas, and J.V. McArthur. "Co-Selection of Antibiotic and Metal Resistance." *Trends in Microbiology* 14, no. 4 (April 2006): 176–82. doi:10.1016/j.tim.2006.02.006.

Baumgard, Lance H., Benjamin A. Corl, Debra A. Dwyer, A. Saebø, and Dale E. Bauman. "Identification of the Conjugated Linoleic Acid Isomer That Inhibits Milk Fat Synthesis." *American Journal of Physiology - Regulatory, Integrative and Comparative Physiology* 278, no. 1 (January 1, 2000): R179–84.

Betts, Kellyn S. "A Study in Balance: How Microbiomes Are Changing the Shape of Environmental Health." *Environmental Health Perspectives* 119, no. 8 (August 2011): a340–46. doi:10.1289/ehp.119-a340.

Bonder, Marc J., Sanne Abeln, Egija Zaura, and Bernd W. Brandt. "Comparing Clustering and Pre-Processing in Taxonomy Analysis." *Bioinformatics* 28, no. 22 (November 15, 2012): 2891–97. doi:10.1093/bioinformatics/bts552.

Boulangé, Claire L., Ana Luisa Neves, Julien Chilloux, Jeremy K. Nicholson, and Marc-Emmanuel Dumas. "Impact of the Gut Microbiota on Inflammation, Obesity, and Metabolic Disease." *Genome Medicine* 8 (2016): 42. doi:10.1186/s13073-016-0303-2.

Breton, Jérôme, Catherine Daniel, Cécile Vignal, Mathilde Body-Malapel, Anne Garat, Coline Plé, and Benoît Foligné. “Does Oral Exposure to Cadmium and Lead Mediate Susceptibility to Colitis? The Dark-and-Bright Sides of Heavy Metals in Gut Ecology.” *Scientific Reports* 6 (January 11, 2016): srep19200. doi:10.1038/srep19200.

Cahenzli, Julia, Maria L Balmer, and Kathy D McCoy. “Microbial–immune Cross-Talk and Regulation of the Immune System.” *Immunology* 138, no. 1 (January 2013): 12–22. doi:10.1111/j.1365-2567.2012.03624.x.

Cesare, Andrea Di, Ester Eckert, and Gianluca Corno. “Co-Selection of Antibiotic and Heavy Metal Resistance in Freshwater Bacteria.” *Journal of Limnology* 75, no. s2 (April 13, 2016). http://www.jlimnol.it/index.php/jlimnol/article/view/jlimnol.2016.1198.

DeSantis, T. Z., P. Hugenholtz, N. Larsen, M. Rojas, E. L. Brodie, K. Keller, T. Huber, D. Dalevi, P. Hu, and G. L. Andersen. “Greengenes, a Chimera-Checked 16S rRNA Gene Database and Workbench Compatible with ARB.” *Applied and Environmental Microbiology* 72, no. 7 (July 2006): 5069–72. doi:10.1128/AEM.03006-05.

Domingues, Sara, Gabriela J. da Silva, and Kaare M. Nielsen. “Integrons.” *Mobile Genetic Elements* 2, no. 5 (September 1, 2012): 211–23. doi:10.4161/mge.22967.

Gill, Steven R., Mihai Pop, Robert T. DeBoy, Paul B. Eckburg, Peter J. Turnbaugh, Buck S. Samuel, Jeffrey I. Gordon, David A. Relman, Claire M. Fraser-Liggett, and Karen E. Nelson. “Metagenomic Analysis of the Human Distal Gut Microbiome.” *Science* 312, no. 5778 (June 2, 2006): 1355–59. doi:10.1126/science.1124234.

Gloor, Gregory B., Ruben Hummelen, Jean M. Macklaim, Russell J. Dickson, Andrew D. Fernandes, Roderick MacPhee, and Gregor Reid. “Microbiome Profiling by Illumina

Sequencing of Combinatorial Sequence-Tagged PCR Products." *PloS One* 5, no. 10 (October 26, 2010): e15406. doi:10.1371/journal.pone.0015406.

Gu, Shenghua, Dandan Chen, Jin-Na Zhang, Xiaoman Lv, Kun Wang, Li-Ping Duan, Yong Nie, and Xiao-Lei Wu. "Bacterial Community Mapping of the Mouse Gastrointestinal Tract." *PLOS ONE* 8, no. 10 (October 7, 2013): e74957. doi:10.1371/journal.pone.0074957.

Gueimonde, Miguel, Borja Sánchez, Clara G. de los Reyes-Gavilán, and Abelardo Margolles. "Antibiotic Resistance in Probiotic Bacteria." *Frontiers in Microbiology* 4 (July 18, 2013). doi:10.3389/fmicb.2013.00202.

Guinane, Caitriona M., and Paul D. Cotter. "Role of the Gut Microbiota in Health and Chronic Gastrointestinal Disease: Understanding a Hidden Metabolic Organ." *Therapeutic Advances in Gastroenterology* 6, no. 4 (July 2013): 295–308. doi:10.1177/1756283X13482996.

Hamilton, Matthew J., Alexa R. Weingarden, Tatsuya Unno, Alexander Khoruts, and Michael J. Sadowsky. "High-Throughput DNA Sequence Analysis Reveals Stable Engraftment of Gut Microbiota Following Transplantation of Previously Frozen Fecal Bacteria." *Gut Microbes* 4, no. 2 (January 1, 2013): 125–35. doi:10.4161/gmic.23571.

Hill, David A., and David Artis. "Intestinal Bacteria and the Regulation of Immune Cell Homeostasis." *Annual Review of Immunology* 28, no. 1 (2010): 623–67. doi:10.1146/annurev-immunol-030409-101330.

Hudson, Corey M., Zachary W. Bent, Robert J. Meagher, and Kelly P. Williams. "Resistance Determinants and Mobile Genetic Elements of an NDM-1-Encoding Klebsiella Pneumoniae Strain." *PLOS ONE* 9, no. 6 (June 6, 2014): e99209. doi:10.1371/journal.pone.0099209.

Iten, Anne, Susanne Graf, Martin Egger, Martin Täuber, and Joerg Graf. “Helicobacter Sp. Flexispira Bacteremia in an Immunocompetent Young Adult.” *Journal of Clinical Microbiology* 39, no. 5 (May 2001): 1716–20. doi:10.1128/JCM.39.5.1716-1720.2001.

Jackson, Matthew A., Jordana T. Bell, Tim D. Spector, and Claire J. Steves. “A Heritability-Based Comparison of Methods Used to Cluster 16S rRNA Gene Sequences into Operational Taxonomic Units.” *PeerJ* 4 (August 30, 2016). doi:10.7717/peerj.2341.

Jones, Ryan Thomas, Leticia Gonzales Sanchez, and Noah Fierer. “A Cross-Taxon Analysis of Insect-Associated Bacterial Diversity.” *PLOS ONE* 8, no. 4 (April 16, 2013): e61218. doi:10.1371/journal.pone.0061218.

Jousselin, E., A.-L. Clamens, M. Galan, M. Bernard, S. Maman, B. Gschloessl, G. Duport, A. S. Meseguer, F. Calevro, and A. Coeur d’acier. “Assessment of a 16S rRNA Amplicon Illumina Sequencing Procedure for Studying the Microbiome of a Symbiont-Rich Aphid Genus.” *Molecular Ecology Resources* 16, no. 3 (May 1, 2016): 628–40. doi:10.1111/1755-0998.12478.

Kanehisa, Minoru, and Susumu Goto. “KEGG: Kyoto Encyclopedia of Genes and Genomes.” *Nucleic Acids Research* 28, no. 1 (January 1, 2000): 27–30. doi:10.1093/nar/28.1.27.

Kanehisa, Minoru, Susumu Goto, Masahiro Hattori, Kiyoko F. Aoki-Kinoshita, Masumi Itoh, Shuichi Kawashima, Toshiaki Katayama, Michihiro Araki, and Mika Hirakawa. “From Genomics to Chemical Genomics: New Developments in KEGG.” *Nucleic Acids Research* 34, no. suppl 1 (January 1, 2006): D354–57. doi:10.1093/nar/gkj102.

Kinross, James M., Ara W. Darzi, and Jeremy K. Nicholson. “Gut Microbiome-Host Interactions in Health and Disease.” *Genome Medicine* 3 (2011): 14. doi:10.1186/gm228.

Krajmalnik-Brown, Rosa, Zehra-Esra Ilhan, Dae-Wook Kang, and John K. DiBaise. "Effects of Gut Microbes on Nutrient Absorption and Energy Regulation." *Nutrition in Clinical Practice : Official Publication of the American Society for Parenteral and Enteral Nutrition* 27, no. 2 (April 2012): 201–14. doi:10.1177/0884533611436116.

Kruskal, William H., and W. Allen Wallis. "Use of Ranks in One-Criterion Variance Analysis." *Journal of the American Statistical Association* 47, no. 260 (December 1, 1952): 583–621. doi:10.1080/01621459.1952.10483441.

Kuehbacher, Tanja, Ateequr Rehman, Patricia Lepage, Stephan Hellmig, Ulrich R. Fölsch, Stefan Schreiber, and Stephan J. Ott. "Intestinal TM7 Bacterial Phylogenies in Active Inflammatory Bowel Disease." *Journal of Medical Microbiology* 57, no. 12 (2008): 1569–76. doi:10.1099/jmm.0.47719-0.

Langille, Morgan G. I., Jesse Zaneveld, J. Gregory Caporaso, Daniel McDonald, Dan Knights, Joshua A. Reyes, Jose C. Clemente, et al. "Predictive Functional Profiling of Microbial Communities Using 16S rRNA Marker Gene Sequences." *Nature Biotechnology* 31, no. 9 (2013): 814–21. doi:10.1038/nbt.2676.

Love, Michael I, Wolfgang Huber, and Simon Anders. "Moderated Estimation of Fold Change and Dispersion for RNA-Seq Data with DESeq2." *Genome Biology* 15, no. 12 (2014). doi:10.1186/s13059-014-0550-8.

Mcmurdie, Paul J., and Susan Holmes. "Phyloseq: a bioconductor package for handling and analysis of high-throughput phylogenetic sequence data." *Pacific Symposium on Biocomputing. Pacific Symposium on Biocomputing*, 2012, 235–46.

Nies, Dietrich H. "Efflux-Mediated Heavy Metal Resistance in Prokaryotes." *FEMS Microbiology Reviews* 27, no. 2–3 (June 1, 2003): 313–39. doi:10.1016/S0168-6445(03)00048-2.

Oksanen, Jari, Roeland Kindt, Pierre Legendre, Bob O'Hara, M. Henry H. Stevens, Maintainer Jari Oksanen, and MASS Suggests. "The Vegan Package." *Community Ecology Package* 10 (2007): 631–37.

Pal, Chandan, Johan Bengtsson-Palme, Erik Kristiansson, and D. G. Joakim Larsson. "Co-Occurrence of Resistance Genes to Antibiotics, Biocides and Metals Reveals Novel Insights into Their Co-Selection Potential." *BMC Genomics* 16 (November 17, 2015): 964. doi:10.1186/s12864-015-2153-5.

Partridge, Sally R., Guy Tsafnat, Enrico Coiera, and Jonathan R. Iredell. "Gene Cassettes and Cassette Arrays in Mobile Resistance Integrons." *FEMS Microbiology Reviews* 33, no. 4 (July 2009): 757–84. doi:10.1111/j.1574-6976.2009.00175.x.

Pérez-Cobas, Ana Elena, Andrés Moya, María José Gosalbes, and Amparo Latorre. "Colonization Resistance of the Gut Microbiota against Clostridium Difficile." *Antibiotics* 4, no. 3 (August 7, 2015): 337–57. doi:10.3390/antibiotics4030337.

Pini, Francesco, Marco Galardini, Marco Bazzicalupo, and Alessio Mengoni. "Plant-Bacteria Association and Symbiosis: Are There Common Genomic Traits in Alphaproteobacteria?" *Genes* 2, no. 4 (November 29, 2011): 1017–32. doi:10.3390/genes2041017.

Purchiaroni, F., A. Tortora, M. Gabrielli, F. Bertucci, G. Gigante, G. Ianiro, V. Ojetti, E. Scarpellini, and A. Gasbarrini. "The Role of Intestinal Microbiota and the Immune System." *European Review for Medical and Pharmacological Sciences* 17, no. 3 (February 2013): 323–33.

Ryan, M. P., and C. C. Adley. “Sphingomonas Paucimobilis: A Persistent Gram-Negative Nosocomial Infectious Organism.” *Journal of Hospital Infection* 75, no. 3 (July 1, 2010): 153–57. doi:10.1016/j.jhin.2010.03.007.

Schaik, Willem van. “The Human Gut Resistome.” *Phil. Trans. R. Soc. B* 370, no. 1670 (June 5, 2015): 20140087. doi:10.1098/rstb.2014.0087.

Schmieder, Robert, and Robert Edwards. “Fast Identification and Removal of Sequence Contamination from Genomic and Metagenomic Datasets.” *PLOS ONE* 6, no. 3 (March 9, 2011): e17288. doi:10.1371/journal.pone.0017288.

Seiler, Claudia, and Thomas U. Berendonk. “Heavy Metal Driven Co-Selection of Antibiotic Resistance in Soil and Water Bodies Impacted by Agriculture and Aquaculture.” *Frontiers in Microbiology* 3 (December 14, 2012). doi:10.3389/fmicb.2012.00399.

Vaz-Moreira, Ivone, Olga C. Nunes, and Célia M. Manaia. “Diversity and Antibiotic Resistance Patterns of Sphingomonadaceae Isolates from Drinking Water.” *Applied and Environmental Microbiology* 77, no. 16 (August 15, 2011): 5697–5706. doi:10.1128/AEM.00579-11.

Vengellur, A., & LaPres, J. J. (2004). The Role of Hypoxia Inducible Factor 1α in Cobalt Chloride Induced Cell Death in Mouse Embryonic Fibroblasts. *Toxicological Sciences*, *82*(2), 638–646. https://doi.org/10.1093/toxsci/kfh278

Walujkar, Sandeep A., Dhiraj P. Dhotre, Nachiket P. Marathe, Parimal S. Lawate, Renu S. Bharadwaj, and Yogesh S. Shouche. “Characterization of Bacterial Community Shift in Human Ulcerative Colitis Patients Revealed by Illumina Based 16S rRNA Gene Amplicon Sequencing.” *Gut Pathogens* 6 (2014): 22. doi:10.1186/1757-4749-6-22.

Wang, Yi, Ling Xu, Yong Q. Gu, and Devin Coleman-Derr. "MetaCoMET: A Web Platform for Discovery and Visualization of the Core Microbiome." *Bioinformatics* 32, no. 22 (November 15, 2016): 3469–70. doi:10.1093/bioinformatics/btw507.

Wexler, Hannah M. "Bacteroides: The Good, the Bad, and the Nitty-Gritty." *Clinical Microbiology Reviews* 20, no. 4 (October 1, 2007): 593–621. doi:10.1128/CMR.00008-07.

Wickham, Hadley. *ggplot2: Elegant Graphics for Data Analysis*. Springer, 2016.

Wu, Guojun, Chenhong Zhang, Jing Wang, Feng Zhang, Ruirui Wang, Jian Shen, Linghua Wang, et al. "Diminution of the Gut Resistome after a Gut Microbiota-Targeted Dietary Intervention in Obese Children." *Scientific Reports* 6 (April 5, 2016): 24030. doi:10.1038/srep24030.

Xie, Guoxiang, Xiaoning Wang, Ping Liu, Runmin Wei, Wenlian Chen, Cynthia Rajani, Brenda Y. Hernandez, et al. "Distinctly Altered Gut Microbiota in the Progression of Liver Disease." *Oncotarget* 7, no. 15 (March 29, 2016): 19355–66. doi:10.18632/oncotarget.8466.

Yatsunenko, Tanya, Federico E. Rey, Mark J. Manary, Indi Trehan, Maria Gloria Dominguez-Bello, Monica Contreras, Magda Magris, et al. "Human Gut Microbiome Viewed across Age and Geography." *Nature* 486, no. 7402 (June 14, 2012): 222–27. doi:10.1038/nature11053.

Zhang, Yanming, Peifeng Ji, Jinfeng Wang, and Fangqing Zhao. "RiboFR-Seq: A Novel Approach to Linking 16S rRNA Amplicon Profiles to Metagenomes." *Nucleic Acids Research* 44, no. 10 (June 2, 2016): e99–e99. doi:10.1093/nar/gkw165.

Tables

Table 4-1. Concentrations (mg/kg) of heavy metals and antibiotics added to custom mouse diet based on AIN-93M.

Metal or Antibiotic	Control	Low Dose	High Dose	Cipro
Co	-	4.252	21.26	-
Cr	-	24.87	124.35	-
Cu	-	10.72	53.6	-
Ni	-	10.38	51.9	-
Sr	-	21.49	107.45	-
Zn	-	24.38	121.9	-
Cipro	-	-	-	1

Table 4-2. Selected KEGG Ortholog/Genes surveyed and their level of significance.

KO	Superfamily	Family	Gene	Type	Significance ($p < 0.05$)
K06189	ABC	CorC	corC	metal	**0.007**
K03446	MFS	DHA2	emrB	antibiotic	**0.008**
K01467	ABC	CopC	copC	metal	**0.009**
K07787	RND	HME	HME family	metal	**0.009**
K07239	ABC	CHR	chrA	metal	**0.015**
K09687	ABC	NIX	nixA	metal	**0.015**
K03543	ABC	PCO	pcoD	metal	**0.023**
K05595	RND	OmpR	cusS	metal	**0.034**
K07803	RND	OmpR	baeR	antibiotic	**0.041**
K07644	RND	OmpR	cusR	metal	**0.047**
K07644	RND	NarL	vraS	antibiotic	0.053
K07664	RND	NarL	vraR	antibiotic	0.065
K07576	MFS	NRE	nrsD	metal	0.108
K07156	MFS	DHA2	emrY	antibiotic	0.111
K07245	ABC	OmpR	cusA	metal	0.152
K07243	RND	MDT	mdtB	antibiotic	0.276
K07241	RND	MDT	mdtC	antibiotic	0.281
K07240	RND	OmpR	cusC	metal	0.417
K07238	RND	OmpR	cusB	metal	0.053

Table 4-3. Latin square ANOVA summary for the factor "Treatment". The differences in mean concentrations of heavy metals in livers and kidneys.

	Sum Sq	Mean Sq	F value	Pr(>F)
Cr	183.830	61.277	1.198	0.329
Co	107.403	35.801	171.753	**0.000**
Ni	85.860	28.622	1.264	0.306
Cu	5.095	1.699	0.337	0.799
Zn	307.300	102.432	0.959	0.426
Sr	5.601	1.867	1.611	0.209

Table 4-4. TukeyHSD post-hoc comparisons for the factor "Treatment".

		Cipro-Control	High-Control	Low-Control	High-Cipro	Low-Cipro	Low-High
Mass	diff	1.573	2.329	-1.738	0.757	-3.311	-4.068
	p-value	0.625	0.297	0.547	0.936	**0.074**	**0.020**
Cr	diff	5.249	1.181	0.773	-4.068	-4.476	-0.409
	p-value	0.332	0.980	0.994	0.550	0.470	0.999
Cobalt	diff	0.089	3.692	2.301	3.603	2.211	-1.391
	p-value	0.968	**0.000**	**0.000**	**0.000**	**0.000**	**0.000**
Ni	diff	3.564	0.612	0.594	-2.952	-2.970	-0.017
	p-value	0.315	0.990	0.991	0.477	0.472	1.000
Cu	diff	0.232	-0.607	0.210	-0.839	-0.022	0.817
	p-value	0.995	0.920	0.996	0.817	1.000	0.828
Zn	diff	4.705	-2.315	2.475	-7.020	-2.230	4.790
	p-value	0.712	0.952	0.943	0.399	0.957	0.700
Sr	diff	0.065	0.876	0.509	0.811	0.443	-0.367
	p-value	0.999	0.248	0.688	0.310	0.770	0.854

Table 4-5. Log2 Fold Change showing differential abundance of bacterial taxa between Control (Grey colored) and Low Dose in cecum.

Mean	log2FC	stat	padj	Phylum	Class	Order	Family
22.173	3.068	6.698	0.000	Proteobacteria	Deltaproteobacteria	Desulfovibrionales	Desulfovibrionaceae
1.493	2.868	3.956	0.007	Proteobacteria	Epsilonproteobacteria	Campylobacterales	Helicobacteraceae
2.263	2.585	3.502	0.025	Proteobacteria	Deltaproteobacteria	Desulfovibrionales	Desulfovibrionaceae
3.773	2.425	3.338	0.032	Proteobacteria	Alphaproteobacteria	Rickettsiales	
1.979	2.213	3.192	0.046	Bacteroidetes	Bacteroidia	Bacteroidales	S24-7
5.891	2.124	3.555	0.024	Firmicutes	Clostridia	Clostridiales	
3.239	1.996	3.358	0.032	Actinobacteria	Coriobacteriia	Coriobacteriales	Coriobacteriaceae
17.060	1.920	3.642	0.020	Proteobacteria	Alphaproteobacteria	Rickettsiales	
13.237	1.837	5.606	0.000	Proteobacteria	Epsilonproteobacteria	Campylobacterales	Helicobacteraceae
4.925	1.818	3.198	0.046	Firmicutes	Bacilli	Turicibacterales	Turicibacteraceae
5.408	1.789	3.800	0.012	Proteobacteria	Epsilonproteobacteria	Campylobacterales	Helicobacteraceae
9.748	1.650	3.620	0.020	Firmicutes	Clostridia	Clostridiales	
6.951	1.340	3.360	0.032	TM7	TM7-3	CW040	F16
19.919	-1.264	-3.677	0.018	Bacteroidetes	Bacteroidia	Bacteroidales	Bacteroidaceae
12.070	-1.405	-3.319	0.034	Bacteroidetes	Bacteroidia	Bacteroidales	S24-7
4.625	-1.438	-3.191	0.046	Bacteroidetes	Bacteroidia	Bacteroidales	S24-7
8.034	-1.535	-3.448	0.027	Firmicutes	Clostridia	Clostridiales	Lachnospiraceae
6.076	-1.612	-3.428	0.027	Firmicutes	Clostridia	Clostridiales	[Mogibacteriaceae]
1.777	-2.075	-3.240	0.042	Bacteroidetes	Bacteroidia	Bacteroidales	S24-7
31.663	-2.210	-5.544	0.000	Bacteroidetes	Bacteroidia	Bacteroidales	S24-7
5.709	-2.417	-3.538	0.024	Bacteroidetes	Bacteroidia	Bacteroidales	S24-7
1.370	-2.518	-3.373	0.032	Firmicutes	Clostridia	Clostridiales	
11.290	-2.549	-3.435	0.027	Firmicutes	Bacilli	Lactobacillales	Lactobacillaceae
17.421	-2.648	-3.554	0.024	Firmicutes	Bacilli	Lactobacillales	Lactobacillaceae

22.612	-2.670	-4.324	0.002	Bacteroidetes	Bacteroidia	Bacteroidales	S24-7
12.500	-2.872	-4.610	0.001	Firmicutes	Bacilli	Lactobacillales	Lactobacillaceae
31.081	-2.902	-4.296	0.002	Proteobacteria	Deltaproteobacteria	Desulfovibrionales	Desulfovibrionaceae
4.334	-3.094	-5.606	0.000	Proteobacteria	Epsilonproteobacteria	Campylobacterales	Helicobacteraceae
1.410	-3.263	-4.106	0.004	Firmicutes	Clostridia	Clostridiales	
1.863	-3.266	-3.455	0.027	Fusobacteria	Fusobacteriia	Fusobacteriales	Fusobacteriaceae
2.334	-3.322	-4.649	0.001	Actinobacteria	Coriobacteriia	Coriobacteriales	Coriobacteriaceae
5.602	-3.379	-5.127	0.000	Proteobacteria	Deltaproteobacteria	Desulfovibrionales	Desulfovibrionaceae
6.553	-3.421	-3.438	0.027	Fusobacteria	Fusobacteriia	Fusobacteriales	Fusobacteriaceae
27.018	-3.875	-5.290	0.000	Actinobacteria	Coriobacteriia	Coriobacteriales	Coriobacteriaceae
Mean	log2FC	stat	padj	Phylum	Class	Order	Family
22.173	3.068	6.698	0.000	Proteobacteria	Deltaproteobacteria	Desulfovibrionales	Desulfovibrionaceae
1.493	2.868	3.956	0.007	Proteobacteria	Epsilonproteobacteria	Campylobacterales	Helicobacteraceae
2.263	2.585	3.502	0.025	Proteobacteria	Deltaproteobacteria	Desulfovibrionales	Desulfovibrionaceae
3.773	2.425	3.338	0.032	Proteobacteria	Alphaproteobacteria	Rickettsiales	
1.979	2.213	3.192	0.046	Bacteroidetes	Bacteroidia	Bacteroidales	S24-7
5.891	2.124	3.555	0.024	Firmicutes	Clostridia	Clostridiales	
3.239	1.996	3.358	0.032	Actinobacteria	Coriobacteriia	Coriobacteriales	Coriobacteriaceae
17.060	1.920	3.642	0.020	Proteobacteria	Alphaproteobacteria	Rickettsiales	

Table 4-6. Log2 Fold Change showing differential abundance of bacterial taxa between Control (Grey colored) and High Dose in cecum.

Mean	log2FC	stat	padj	Phylum	Class	Order	Family
1.887	3.305	3.930	0.004	Actinobacteria	Coriobacteriia	Coriobacteriales	Coriobacteriaceae
7.318	2.992	4.118	0.003	Firmicutes	Clostridia	Clostridiales	Clostridiaceae
9.770	2.899	3.920	0.004	Bacteroidetes	Bacteroidia	Bacteroidales	S24-7
2.557	2.897	3.592	0.010	Bacteroidetes	Bacteroidia	Bacteroidales	S24-7
2.433	2.663	3.265	0.026	Bacteroidetes	Bacteroidia	Bacteroidales	S24-7
3.617	2.516	3.128	0.040	Proteobacteria	Alphaproteobacteria	Rickettsiales	
22.215	2.500	3.948	0.004	Proteobacteria	Alphaproteobacteria	Rickettsiales	
62.472	2.356	3.910	0.004	Bacteroidetes	Bacteroidia	Bacteroidales	S24-7
6.801	2.291	3.980	0.004	Proteobacteria	Epsilonproteobacteria	Campylobacterales	Helicobacteraceae
8.221	2.281	3.294	0.024	Firmicutes	Bacilli	Lactobacillales	Lactobacillaceae
12.230	2.176	4.232	0.002	Firmicutes	Clostridia	Clostridiales	
89.469	2.131	3.494	0.013	Firmicutes	Clostridia	Clostridiales	
34.176	1.928	3.160	0.036	Bacteroidetes	Bacteroidia	Bacteroidales	S24-7
9.594	1.913	3.797	0.006	Proteobacteria	Deltaproteobacteria	Desulfovibrionales	Desulfovibrionaceae
8.746	1.623	3.068	0.048	Firmicutes	Clostridia	Clostridiales	
19.783	1.608	3.911	0.004	Firmicutes	Bacilli	Lactobacillales	Lactobacillaceae
10.746	1.593	3.209	0.032	Proteobacteria	Epsilonproteobacteria	Campylobacterales	Helicobacteraceae
16.308	-1.672	-3.802	0.006	Firmicutes	Clostridia	Clostridiales	Lachnospiraceae
32.737	-1.851	-3.934	0.004	Bacteroidetes	Bacteroidia	Bacteroidales	S24-7
85.157	-1.996	-3.918	0.004	Firmicutes	Clostridia	Clostridiales	
12.166	-2.092	-3.516	0.013	Bacteroidetes	Bacteroidia	Bacteroidales	S24-7
12.840	-2.185	-3.438	0.015	Firmicutes	Bacilli	Lactobacillales	Lactobacillaceae
5.273	-2.537	-4.290	0.002	Firmicutes	Clostridia	Clostridiales	[Mogibacteriaceae]
2.396	-2.900	-3.579	0.011	Actinobacteria	Coriobacteriia	Coriobacteriales	Coriobacteriaceae
3.073	-3.038	-3.598	0.010	Firmicutes	Clostridia	Clostridiales	Ruminococcaceae

1.451	-3.122	-3.498	0.013	Firmicutes	Clostridia	Clostridiales	Lachnospiraceae
2.154	-3.278	-3.670	0.009	Firmicutes	Bacilli	Turicibacterales	Turicibacteraceae
2.101	-3.520	-3.771	0.006	Firmicutes	Bacilli	Lactobacillales	Lactobacillaceae
2.812	-3.548	-3.968	0.004	Firmicutes	Clostridia	Clostridiales	
1.943	-3.552	-3.497	0.013	Fusobacteria	Fusobacteriia	Fusobacteriales	Fusobacteriaceae
3.419	-3.646	-4.090	0.003	Proteobacteria	Gammaproteobacteria	Enterobacteriales	Enterobacteriaceae
3.481	-3.773	-3.975	0.004	Firmicutes	Clostridia	Clostridiales	Lachnospiraceae
4.694	-3.790	-4.762	0.000	Firmicutes	Clostridia	Clostridiales	Lachnospiraceae
6.425	-3.940	-3.494	0.013	Fusobacteria	Fusobacteriia	Fusobacteriales	Fusobacteriaceae
2.771	-3.994	-4.147	0.002	Firmicutes	Clostridia	Clostridiales	Lachnospiraceae
2.565	-4.057	-4.234	0.002	Firmicutes	Clostridia	Clostridiales	Lachnospiraceae
2.555	-4.096	-4.187	0.002	Spirochaetes	Spirochaetes	Spirochaetales	Spirochaetaceae
5.052	-4.113	-5.486	0.000	Firmicutes	Bacilli	Lactobacillales	Lactobacillaceae
2.231	-4.209	-4.998	0.000	Actinobacteria	Coriobacteriia	Coriobacteriales	Coriobacteriaceae
15.437	-4.231	-5.952	0.000	Firmicutes	Bacilli	Lactobacillales	Lactobacillaceae
26.677	-4.662	-5.059	0.000	Actinobacteria	Coriobacteriia	Coriobacteriales	Coriobacteriaceae
6.027	-4.849	-5.563	0.000	Firmicutes	Bacilli	Lactobacillales	Lactobacillaceae
15.824	-5.241	-7.063	0.000	Firmicutes	Bacilli	Turicibacterales	Turicibacteraceae
20.741	-5.298	-7.126	0.000	Firmicutes	Bacilli	Lactobacillales	Lactobacillaceae
9.871	-5.659	-6.789	0.000	Firmicutes	Bacilli	Lactobacillales	Lactobacillaceae

Table 4-7. Log2 Fold Change showing differential abundance of bacterial taxa between Ciprofloxacin (Grey colored) and Control in cecum.

Mean	log2FC	stat	padj	Phylum	Class	Order	Family
19.539	3.660	5.762	0.000	Proteobacteria	Deltaproteobacteria	Desulfovibrionales	Desulfovibrionaceae
20.312	3.544	4.781	0.005	Actinobacteria	Coriobacteriia	Coriobacteriales	Coriobacteriaceae
8.709	3.170	6.163	0.000	Bacteroidetes	Bacteroidia	Bacteroidales	Rikenellaceae
2.569	2.929	4.655	0.007	Firmicutes	Bacilli	Lactobacillales	Lactobacillaceae
41.767	-1.721	-4.965	0.002	Bacteroidetes	Bacteroidia	Bacteroidales	S24-7

Table 4-8. Log2 Fold Change showing differential abundance of bacterial taxa between Control (Grey colored) and Low Dose in large intestines.

Mean	log2FC	stat	padj	Phylum	Class	Order	Family
2.572	3.281	4.266	0.003	Bacteroidetes	Bacteroidia	Bacteroidales	S24-7
3.005	3.224	4.874	0.000	Bacteroidetes	Bacteroidia	Bacteroidales	S24-7
1.989	3.116	4.219	0.003	Firmicutes	Clostridia	Clostridiales	Peptococcaceae
3.026	3.023	4.168	0.003	Firmicutes	Bacilli	Lactobacillales	Lactobacillaceae
38.986	2.678	5.515	0.000	Proteobacteria	Deltaproteobacteria	Desulfovibrionales	Desulfovibrionaceae
1.330	2.574	3.372	0.037	Bacteroidetes	Bacteroidia	Bacteroidales	S24-7
2.525	2.255	3.470	0.031	Bacteroidetes	Bacteroidia	Bacteroidales	S24-7
1.546	2.239	3.261	0.045	Proteobacteria	Epsilonproteobacteria	Campylobacterales	Helicobacteraceae
2.494	2.200	3.259	0.045	Firmicutes	Bacilli	Lactobacillales	Lactobacillaceae
6.341	2.139	4.776	0.001	Proteobacteria	Epsilonproteobacteria	Campylobacterales	Helicobacteraceae
56.929	2.106	4.415	0.002	Firmicutes	Clostridia	Clostridiales	
10.210	2.091	3.315	0.042	Proteobacteria	Alphaproteobacteria	Rickettsiales	
63.635	2.056	3.788	0.012	Bacteroidetes	Bacteroidia	Bacteroidales	S24-7
6.648	1.966	4.470	0.002	Firmicutes	Clostridia	Clostridiales	
96.881	1.788	3.381	0.037	Proteobacteria	Epsilonproteobacteria	Campylobacterales	Helicobacteraceae
12.328	1.708	3.317	0.042	Firmicutes	Clostridia	Clostridiales	Ruminococcaceae
8.911	1.646	4.161	0.003	Bacteroidetes	Bacteroidia	Bacteroidales	Rikenellaceae
9.058	1.576	3.730	0.014	Firmicutes	Clostridia	Clostridiales	
38.906	1.112	3.962	0.007	Firmicutes	Bacilli	Lactobacillales	Lactobacillaceae
43.165	-1.319	-4.177	0.003	Bacteroidetes	Bacteroidia	Bacteroidales	S24-7
8.395	-1.348	-3.467	0.031	Firmicutes	Clostridia	Clostridiales	Lachnospiraceae
1.203	-2.332	-3.290	0.043	Cyanobacteria	4C0d-2	YS2	
5.669	-2.424	-3.427	0.034	Firmicutes	Erysipelotrichi	Erysipelotrichales	Erysipelotrichaceae
1.813	-2.697	-3.423	0.034	Firmicutes	Clostridia	Clostridiales	Lachnospiraceae

4.284	-2.852	-3.737	0.014	Proteobacteria	Deltaproteobacteria	Desulfovibrionales	Desulfovibrionaceae
1.657	-2.973	-4.064	0.005	Firmicutes	Clostridia	Clostridiales	
11.867	-3.017	-4.514	0.002	Bacteroidetes	Bacteroidia	Bacteroidales	S24-7
1.983	-3.036	-3.552	0.026	Bacteroidetes	Bacteroidia	Bacteroidales	S24-7
4.766	-4.391	-5.196	0.000	Fusobacteria	Fusobacteriia	Fusobacteriales	Fusobacteriaceae

Table 4-9. Log2 Fold Change showing differential abundance of bacterial taxa between Control (Grey colored) and HighDose in large intestines.

Mean	log2FC	stat	padj	Phylum	Class	Order	Family
4.963	4.062	5.526	0.000	Bacteroidetes	Bacteroidia	Bacteroidales	S24-7
3.750	3.593	4.611	0.000	Firmicutes	Bacilli	Lactobacillales	Lactobacillaceae
182.628	2.778	4.022	0.004	Proteobacteria	Epsilonproteobacteria	Campylobacterales	Helicobacteraceae
1.277	2.724	3.255	0.029	Firmicutes	Bacilli	Lactobacillales	Lactobacillaceae
74.843	2.687	4.862	0.000	Firmicutes	Clostridia	Clostridiales	
1.814	2.658	3.325	0.024	Bacteroidetes	Bacteroidia	Bacteroidales	S24-7
2.483	2.632	3.129	0.040	Proteobacteria	Alphaproteobacteria	Sphingomonadales	Sphingomonadaceae
4.625	2.559	3.704	0.009	Bacteroidetes	Bacteroidia	Bacteroidales	S24-7
8.511	2.494	4.211	0.002	Bacteroidetes	Bacteroidia	Bacteroidales	S24-7
2.255	2.452	3.392	0.021	Firmicutes	Clostridia	Clostridiales	
6.528	2.434	3.447	0.019	Firmicutes	Clostridia	Clostridiales	Clostridiaceae
2.608	2.404	3.328	0.024	Bacteroidetes	Bacteroidia	Bacteroidales	S24-7
14.951	2.280	3.895	0.006	Bacteroidetes	Bacteroidia	Bacteroidales	S24-7
6.359	2.235	3.780	0.008	Proteobacteria	Epsilonproteobacteria	Campylobacterales	Helicobacteraceae
90.980	2.221	3.875	0.006	Bacteroidetes	Bacteroidia	Bacteroidales	S24-7
7.355	2.178	3.824	0.007	Firmicutes	Clostridia	Clostridiales	
12.450	2.112	5.078	0.000	Firmicutes	Bacilli	Lactobacillales	Lactobacillaceae
29.277	1.947	4.088	0.004	Bacteroidetes	Bacteroidia	Bacteroidales	S24-7
10.162	1.860	3.456	0.018	Firmicutes	Clostridia	Clostridiales	
9.169	1.799	3.183	0.036	Bacteroidetes	Bacteroidia	Bacteroidales	Rikenellaceae
17.597	1.755	3.366	0.023	Bacteroidetes	Bacteroidia	Bacteroidales	Rikenellaceae
18.478	1.681	3.170	0.036	Proteobacteria	Deltaproteobacteria	Desulfovibrionales	Desulfovibrionaceae
34.855	1.062	3.729	0.009	Firmicutes	Bacilli	Lactobacillales	Lactobacillaceae
14.864	-1.167	-3.096	0.044	Firmicutes	Clostridia	Clostridiales	Lachnospiraceae

40.090	-1.349	-3.160	0.037	Bacteroidetes	Bacteroidia	Bacteroidales	S24-7
78.347	-1.793	-3.679	0.009	Firmicutes	Clostridia	Clostridiales	
11.937	-2.086	-3.838	0.007	Firmicutes	Clostridia	Clostridiales	Lachnospiraceae
4.070	-2.116	-3.172	0.036	Firmicutes	Clostridia	Clostridiales	
27.540	-2.158	-3.332	0.024	Firmicutes	Erysipelotrichi	Erysipelotrichales	Erysipelotrichaceae
3.760	-2.340	-3.913	0.006	Firmicutes	Clostridia	Clostridiales	
3.726	-2.416	-3.545	0.015	Firmicutes	Clostridia	Clostridiales	[Mogibacteriaceae]
1.779	-2.550	-3.327	0.024	Proteobacteria	Epsilonproteobacteria	Campylobacterales	Helicobacteraceae
2.996	-2.587	-4.164	0.003	Firmicutes	Bacilli	Turicibacterales	Turicibacteraceae
2.215	-2.642	-3.417	0.020	Firmicutes	Bacilli	Turicibacterales	Turicibacteraceae
0.851	-2.672	-3.240	0.030	Bacteroidetes	Bacteroidia	Bacteroidales	S24-7
28.562	-2.819	-3.749	0.008	Proteobacteria	Epsilonproteobacteria	Campylobacterales	Helicobacteraceae
6.430	-2.903	-3.158	0.037	Actinobacteria	Coriobacteriia	Coriobacteriales	Coriobacteriaceae
1.347	-3.107	-3.517	0.015	Proteobacteria	Epsilonproteobacteria	Campylobacterales	Helicobacteraceae
1.447	-3.158	-4.102	0.004	Proteobacteria	Epsilonproteobacteria	Campylobacterales	Helicobacteraceae
2.174	-3.183	-3.571	0.014	Bacteroidetes	Bacteroidia	Bacteroidales	S24-7
1.961	-3.193	-3.325	0.024	Bacteroidetes	Bacteroidia	Bacteroidales	S24-7
2.167	-3.357	-3.865	0.006	Firmicutes	Clostridia	Clostridiales	Ruminococcaceae
1.398	-3.379	-3.808	0.007	Firmicutes	Clostridia	Clostridiales	
3.181	-3.412	-3.934	0.006	Proteobacteria	Deltaproteobacteria	Desulfovibrionales	Desulfovibrionaceae
19.639	-3.571	-5.755	0.000	Proteobacteria	Deltaproteobacteria	Desulfovibrionales	Desulfovibrionaceae
2.931	-3.788	-4.826	0.000	Firmicutes	Bacilli	Lactobacillales	Lactobacillaceae
3.442	-4.168	-4.805	0.000	Proteobacteria	Gammaproteobacteria	Enterobacteriales	Enterobacteriaceae
4.677	-4.566	-4.986	0.000	Fusobacteria	Fusobacteriia	Fusobacteriales	Fusobacteriaceae

Table 4-10. Log2 Fold Change showing differential abundance of bacterial taxa between Ciprofloxacin (Grey colored) and Control in large intestines.

Mean	log2FC	stat	padj	Phylum	Class	Order	Family
4.449	3.557	4.371	0.022	Firmicutes	Clostridia	Clostridiales	Ruminococcaceae
12.775	3.388	6.341	0.000	Proteobacteria	Deltaproteobacteria	Desulfovibrionales	Desulfovibrionaceae
21.233	3.323	7.467	0.000	Proteobacteria	Deltaproteobacteria	Desulfovibrionales	Desulfovibrionaceae
5.194	3.208	5.408	0.000	Bacteroidetes	Bacteroidia	Bacteroidales	S24-7
19.248	-2.459	-5.180	0.001	Bacteroidetes	Bacteroidia	Bacteroidales	S24-7
69.708	-2.846	-5.013	0.001	Bacteroidetes	Bacteroidia	Bacteroidales	[Paraprevotellaceae]

Table 4-11. PERMANOVA analyses exploring effect of treatment on cecum microbiota.

Source	df	SS	MS	Pseudo-F	P(perm)	Unique perms	P(MC)
Treatment	3	2353.7	784.58	2.6526	0.001	994	0.001
Res	39	11535	295.78				
Total	42	13889					

Table 4-12. Pairwise PERMANOVA tests on cecum microbiota subjected to treatments.

Groups	t	P(perm)	Unique perms	P(MC)
Control, Low	1.6985	0.001	996	0.001
Control, Cipro	1.389	0.002	990	0.043
Control, High	1.6315	0.001	996	0.003
Low, Cipro	1.9055	0.001	997	0.001
Low, High	1.2002	0.04	997	0.114
Cipro, High	1.8443	0.001	999	0.002

Table 4-13. PERMANOVA analyses exploring effect of treatment on large intestine microbiota.

Source	df	SS	MS	Pseudo-F	P(perm)	Unique perms	P(MC)
Treatment	3	2958.1	986.04	2.8332	0.001	997	0.001
Res	33	11485	348.03				
Total	36	14443					

Table 4-14. Pairwise PERMANOVA tests on large intestine microbiota subjected to treatments.

Groups	t	P(perm)	Unique perms	P(MC)
Low, Control	1.6882	0.001	995	0.005
Low, High	1.654	0.002	999	0.016
Low, Cipro	1.6615	0.001	987	0.009
Control, High	1.8615	0.001	988	0.002
Control, Cipro	1.3154	0.009	924	0.082
High, Cipro	1.7914	0.005	971	0.01

Figures

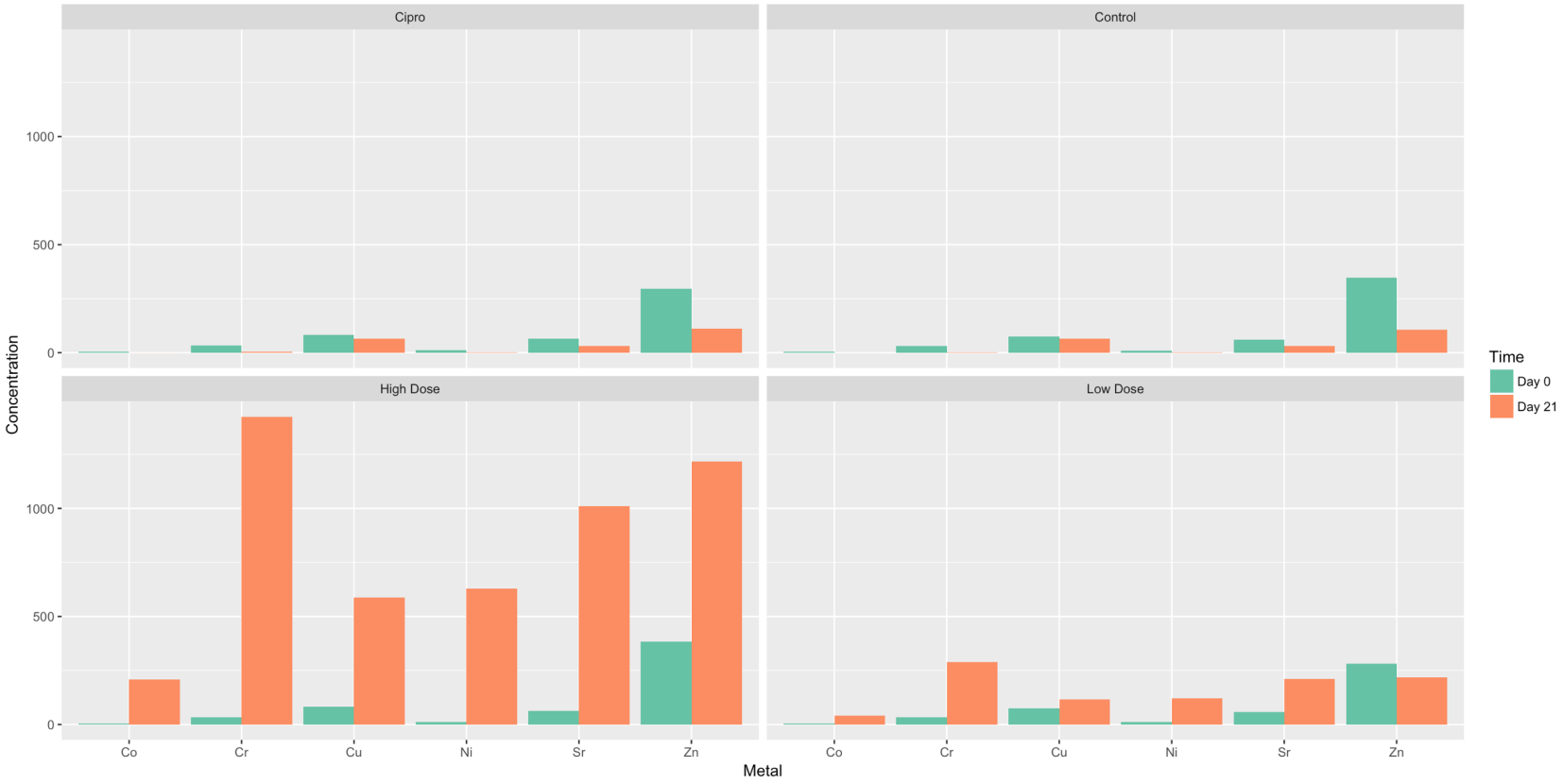

Figure 4-1. Heavy metals analysis in mice fecal samples by treatment: 1) Ciprofloxacin, 2) Control, 3) High heavy metals dose, 4) Low heavy metals dose. Bar are colored by the time in which they were collected: green (Day 0) and orange (Day 21).

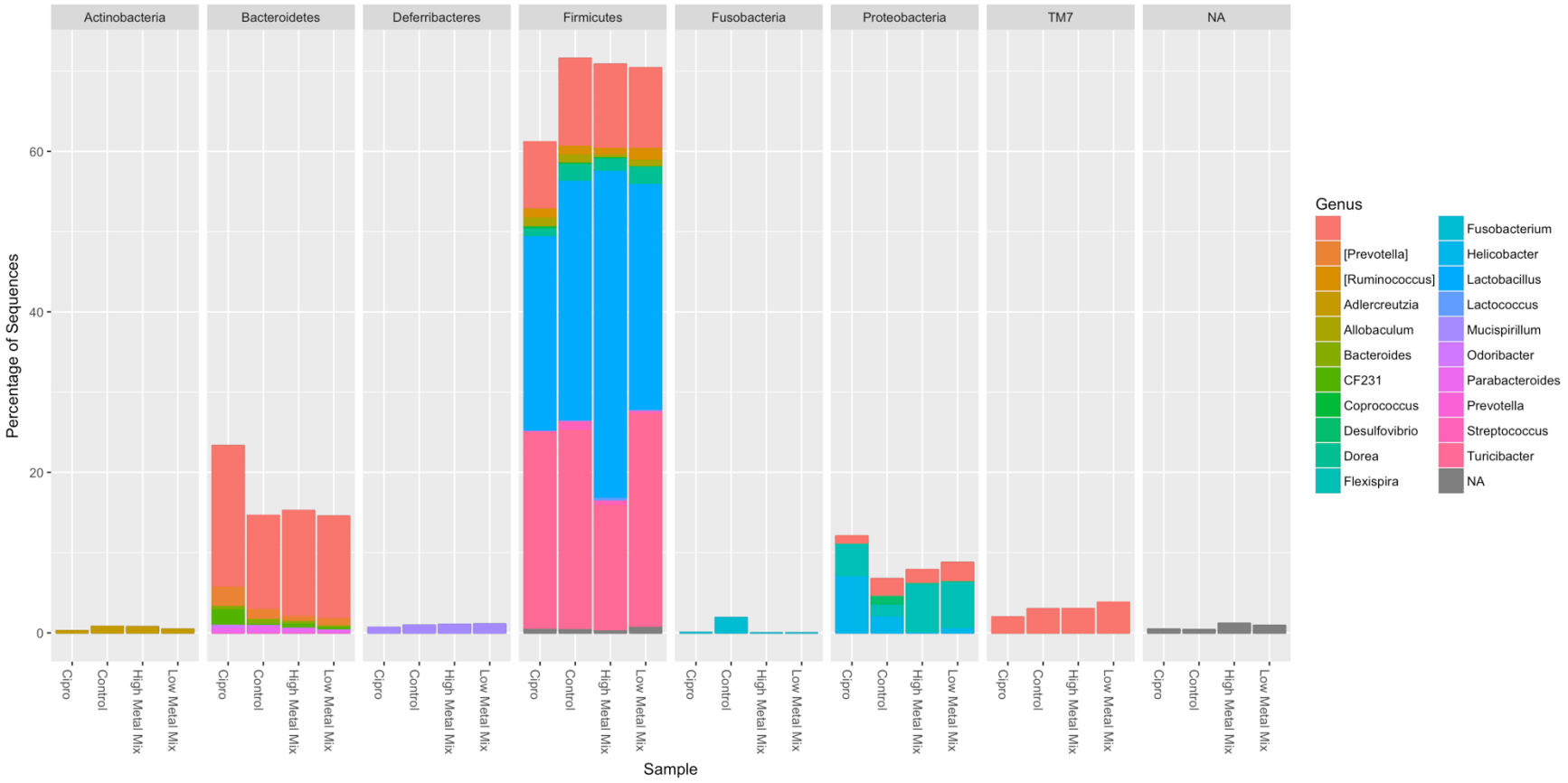

Figure 4-2. The relative abundance at the level of Phylum and corresponding genera representing the 7 most abundant OTUs (clustered at 97% similarity) in cecum samples.

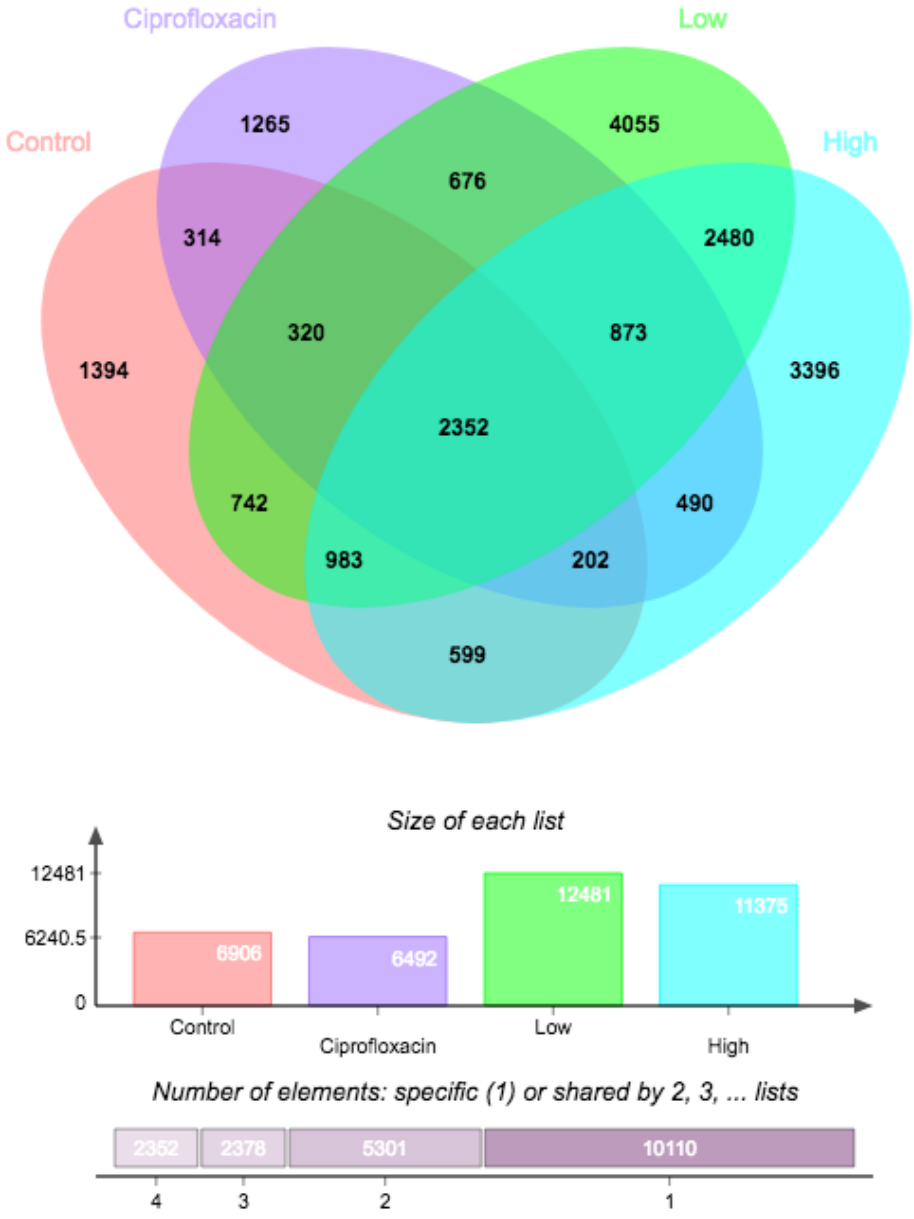

Figure 4-3. A Venn diagram showing the number of shared and unique OTUs between treatments in mouse cecum. Control treatment is colored red, Ciprofloxacin treatment is colored purple, Low Dose heavy metal treatment is colored green, High Dose heavy metal treatment is colored cyan.

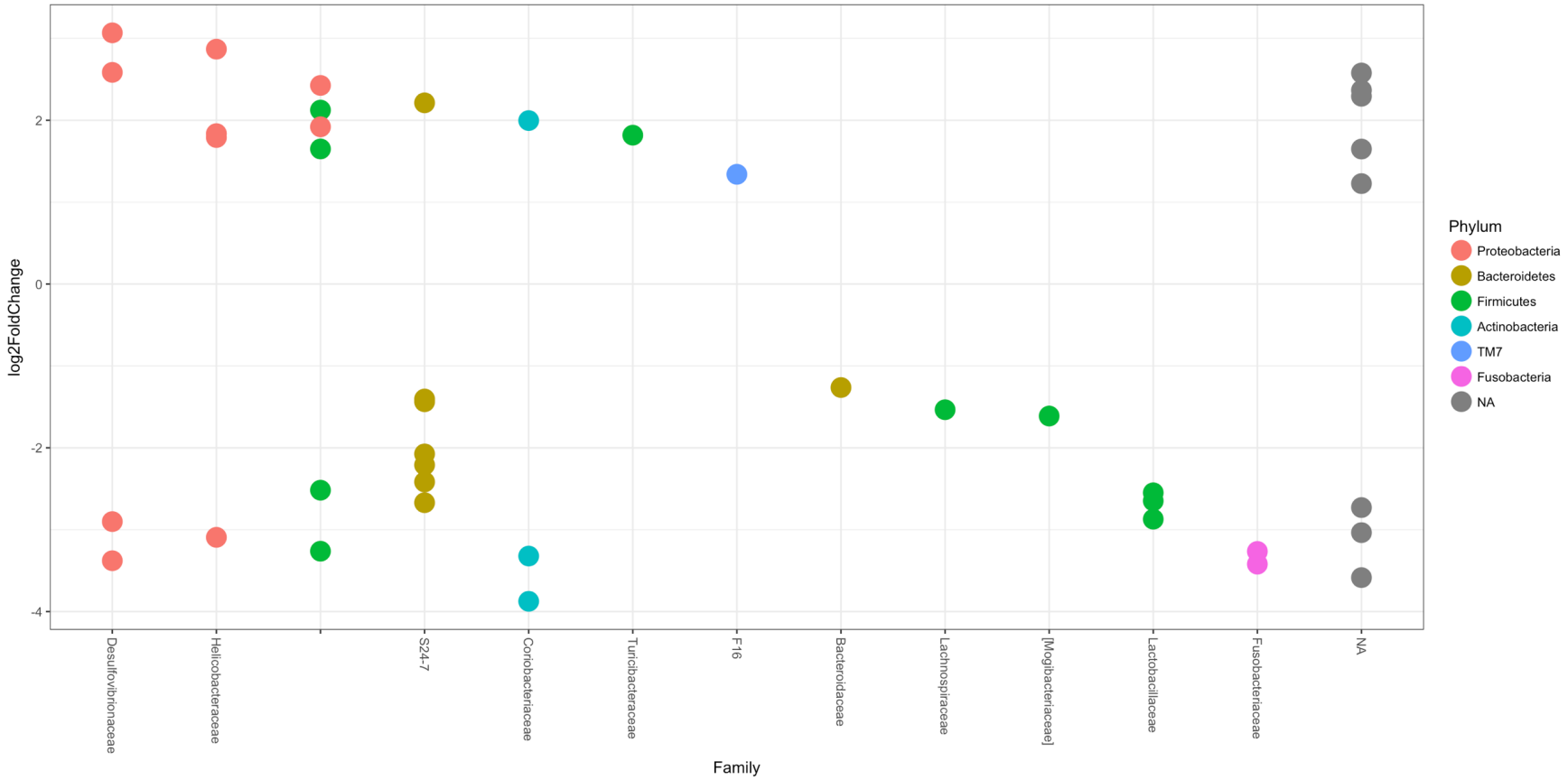

Figure 4-4. DeSeq2 results showing the differential abundance of bacterial families between the Control (bottom row) and Low Dose (upper row) in cecum. Bacterial OTUs appear as circles colored based on their respective phyla.

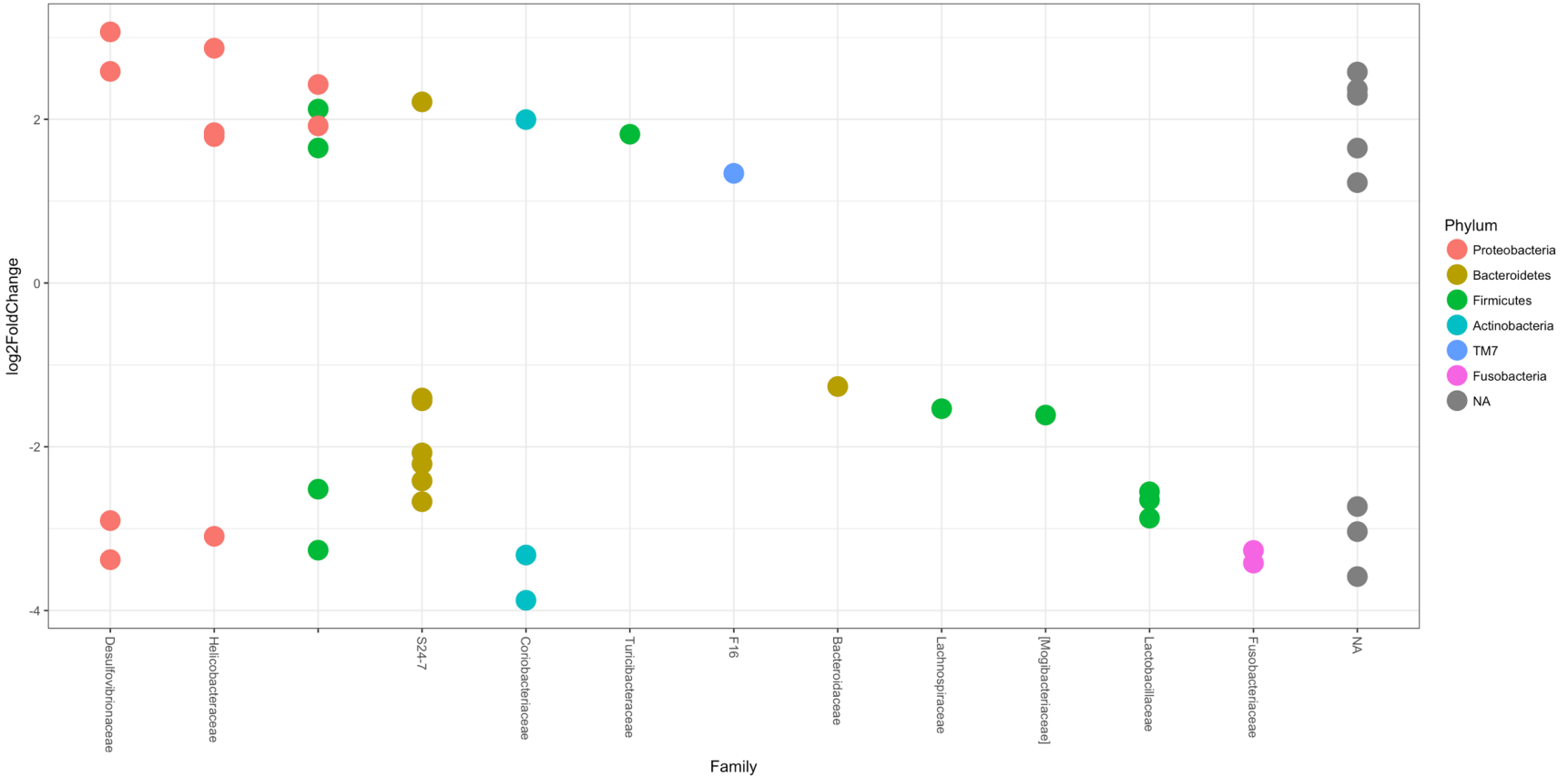

Figure 4-5. DeSeq2 results showing the differential abundance of bacterial families between the Control (bottom row) and High Dose (upper row) in cecum. Bacterial OTUs appear as circles colored based on their respective phyla.

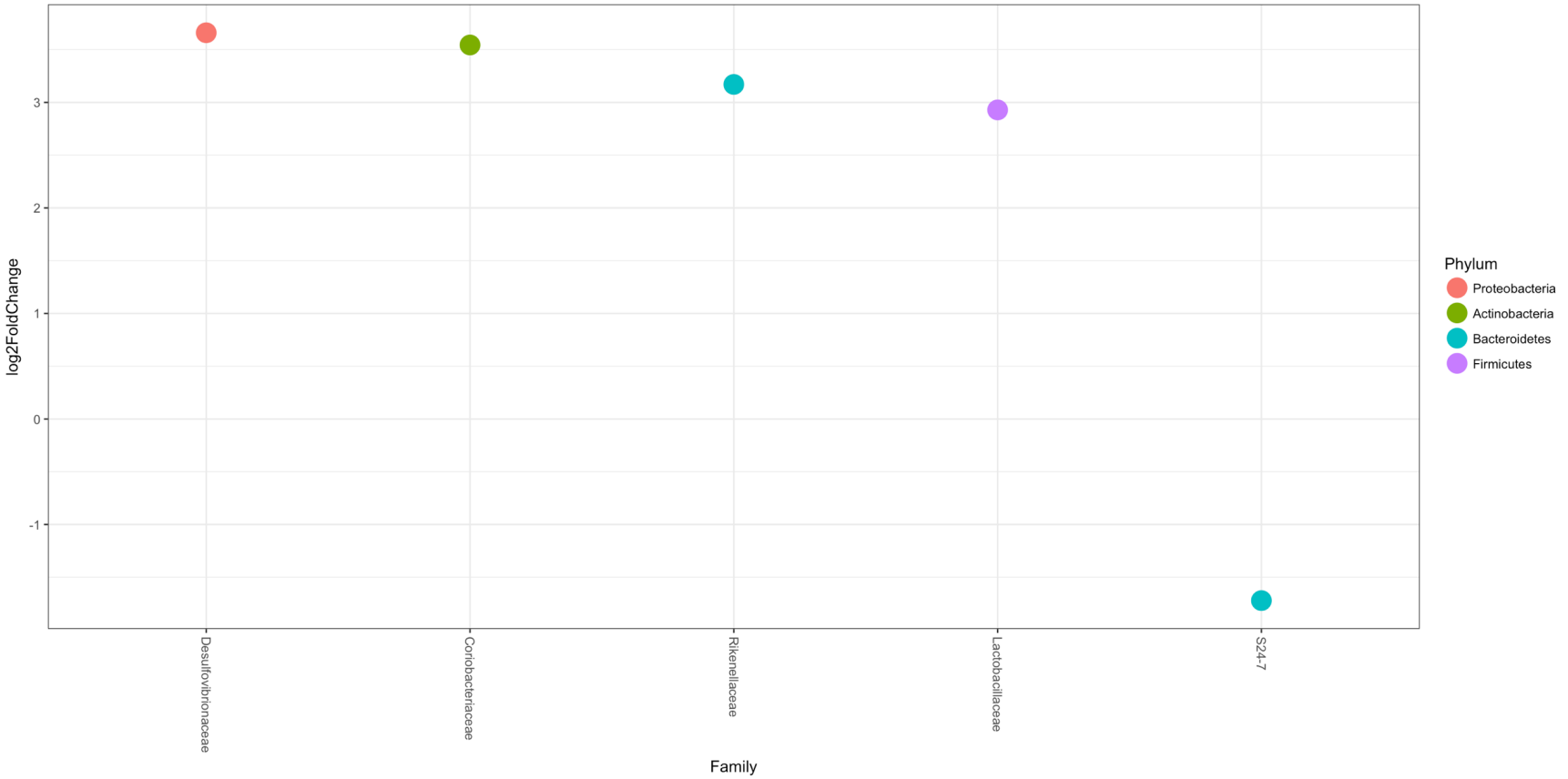

Figure 4-6. DeSeq2 results showing the differential abundance of bacterial families between the Control (all points above 0) and Ciprofloxacin Dose (all points below 0) in mice cecum. Bacterial OTUs appear as circles colored based on their respective phyla.

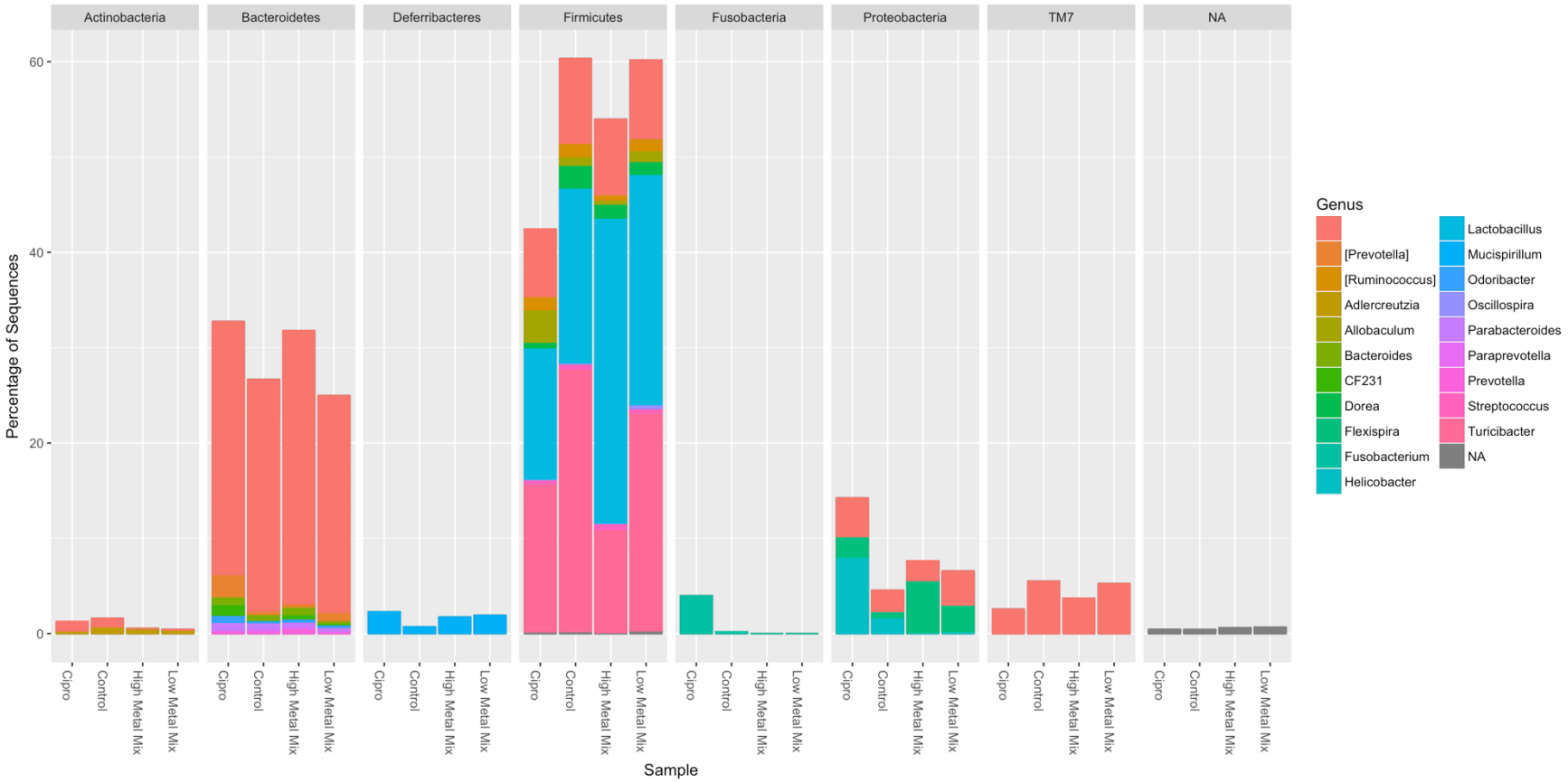

Figure 4-7. The relative abundance at the level of Phylum and corresponding genera representing the 7 most abundant OTUs (clustered at 97% similarity) in mice large intestinal samples.

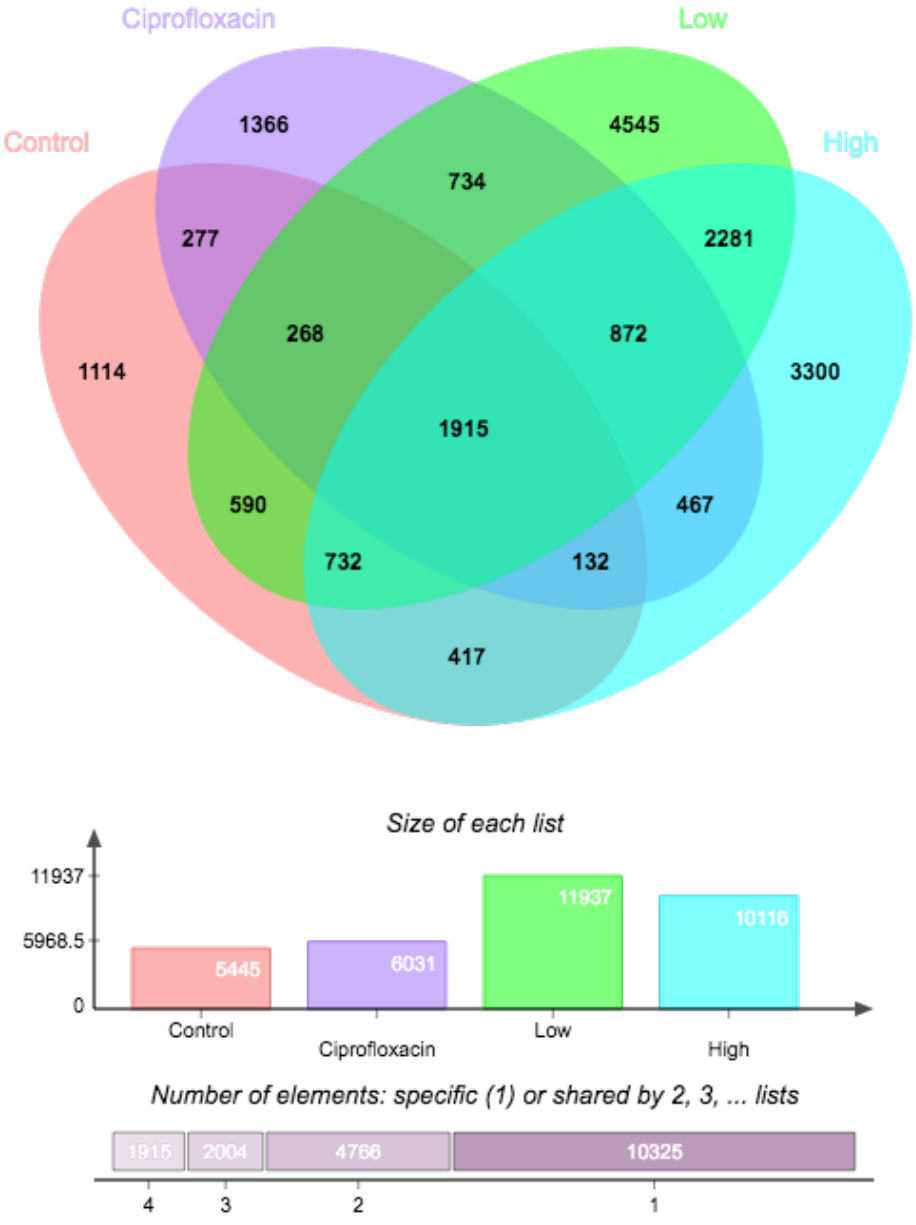

Figure 4-8. A Venn diagram showing the number of shared and unique OTUs between treatment in mice large intestines. Control treatment is colored red, Ciprofloxacin treatment is colored

purple, Low Dose heavy metal treatment is colored green, High Dose heavy metal treatment is colored cyan.

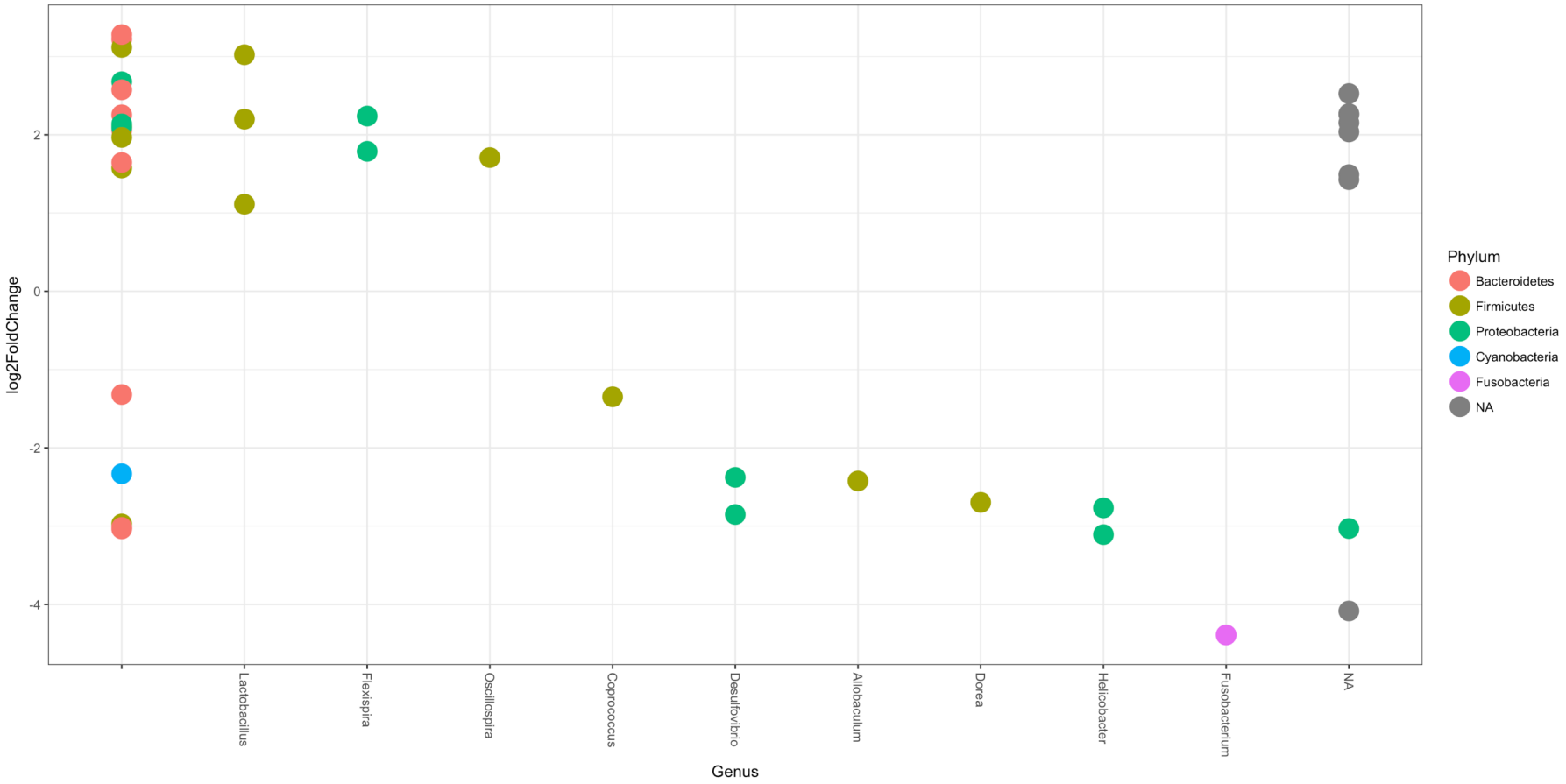

Figure 4-9. DeSeq2 results showing the differential abundance of bacterial families between the Control (all points below 0) and Low Dose (all points above 0) in large intestines. Bacterial OTUs appear as circles colored based on their respective phyla.

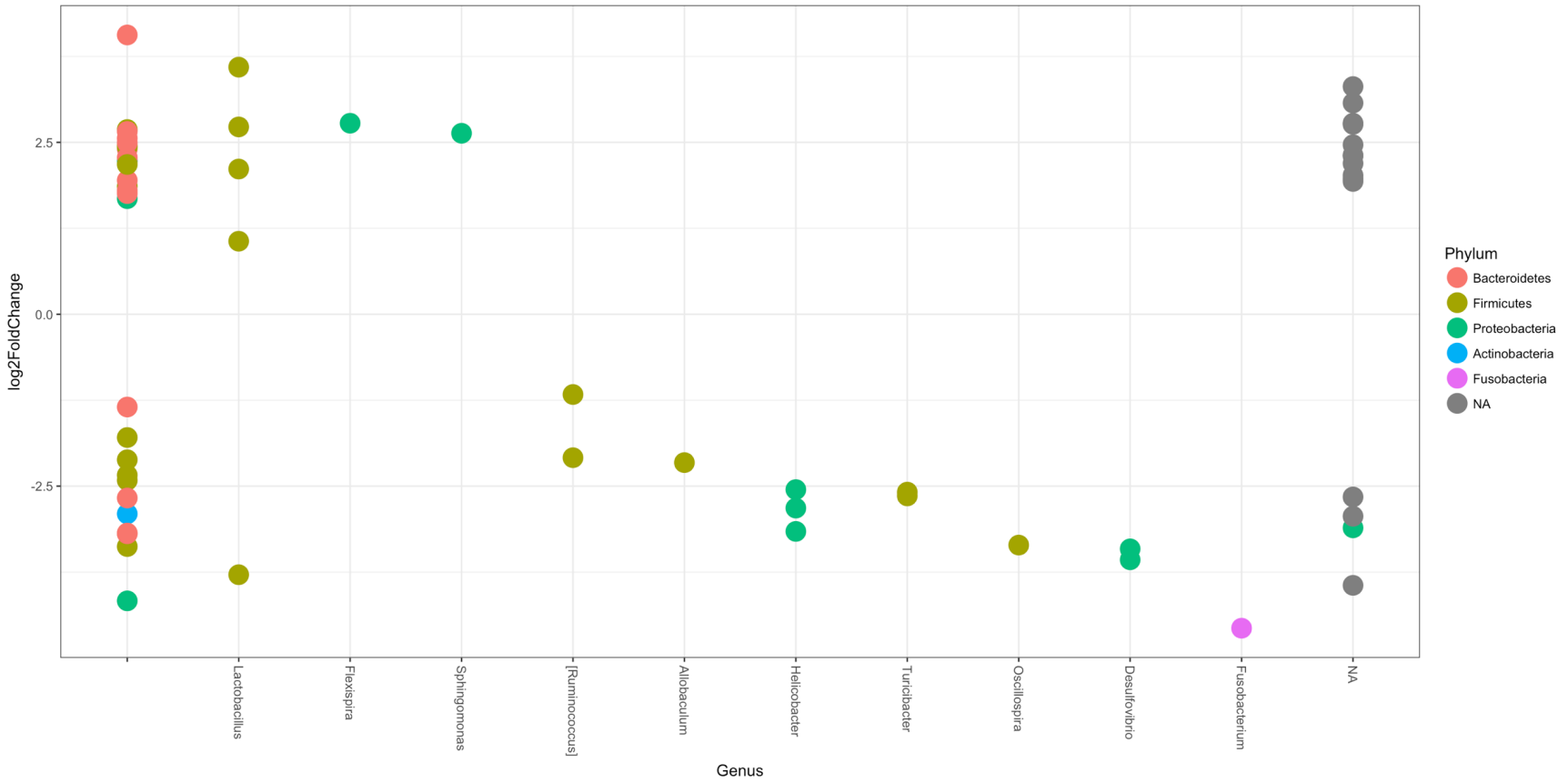

Figure 4-10. DeSeq2 results showing the differential abundance of bacterial families between the Control (all points below 0) and High Dose (all points above 0) in large intestines. Bacterial OTUs appear as circles colored based on their respective phyla.

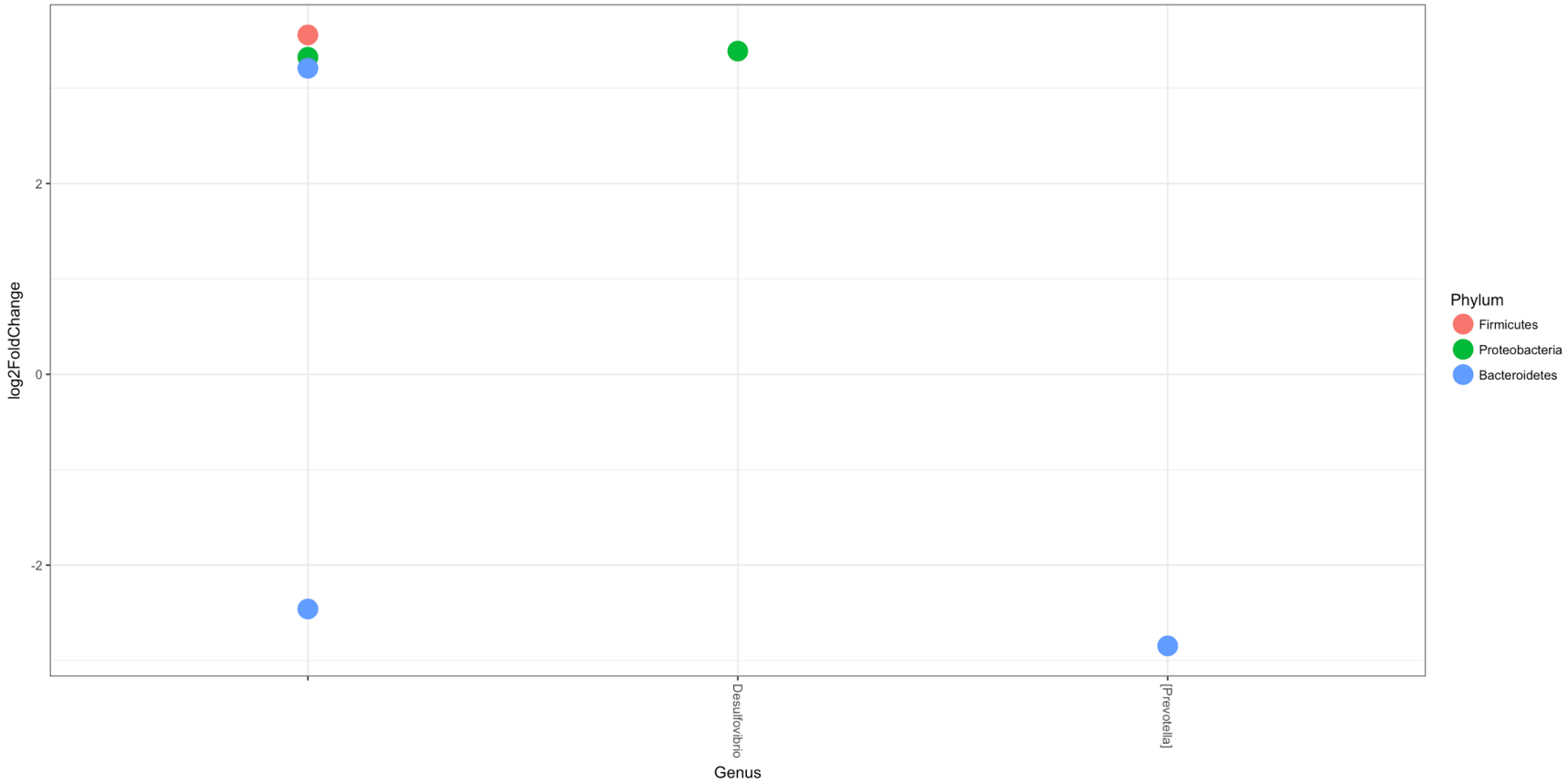

Figure 4-11. DeSeq2 results showing the differential abundance of bacterial families between the Control (all point above 0) and Ciprofloxacin Dose (all points below 0) in large intestines. Bacterial OTUs appear as circles colored based on their respective phyla

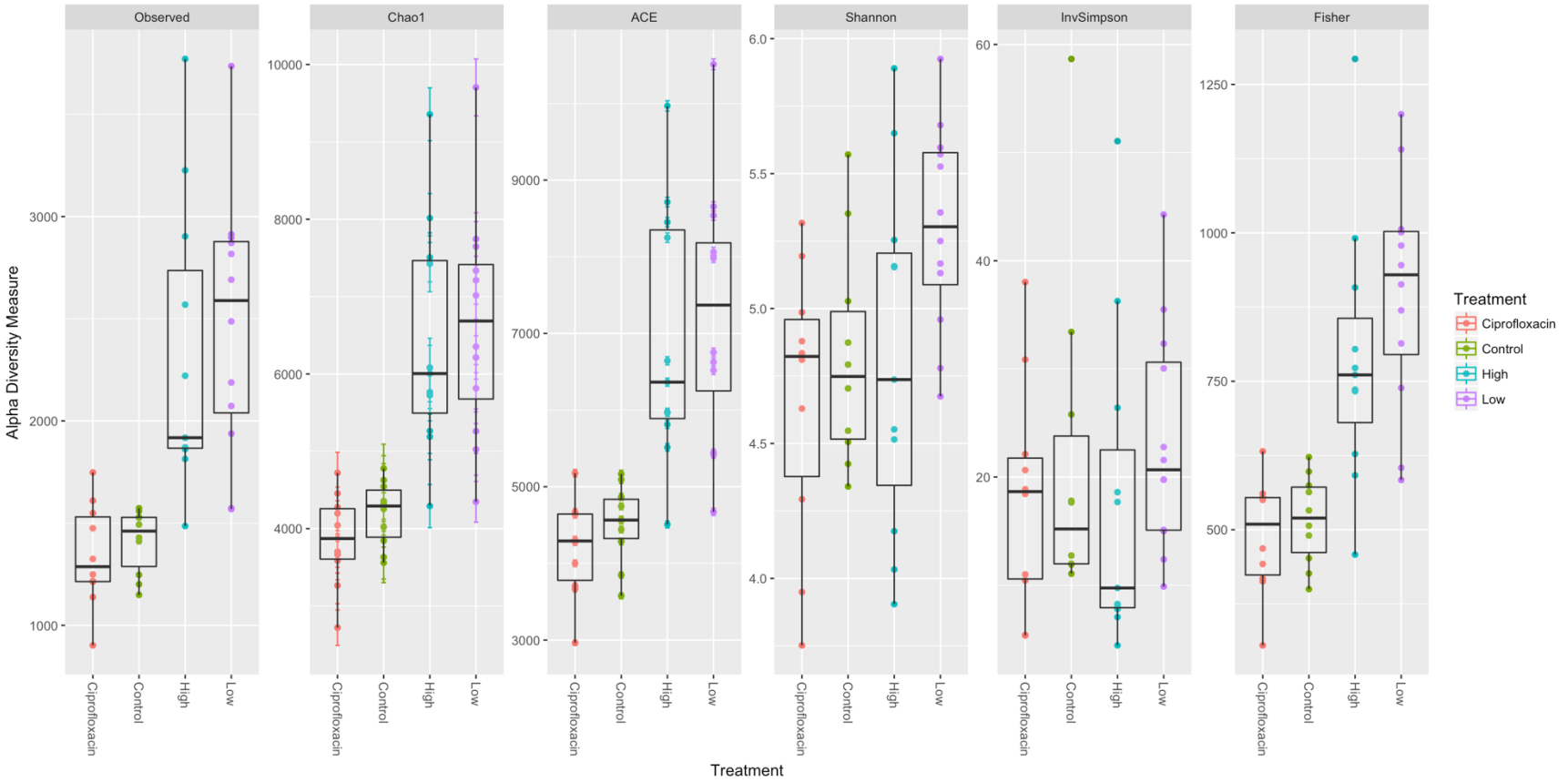

Figure 4-12. Alpha diversity measures for the four treatments in cecum (defined either by the number of bacterial OTUs observed or by Chao1, ACE, Shannon, Inverse Simpson, and Fisher diversity measures).

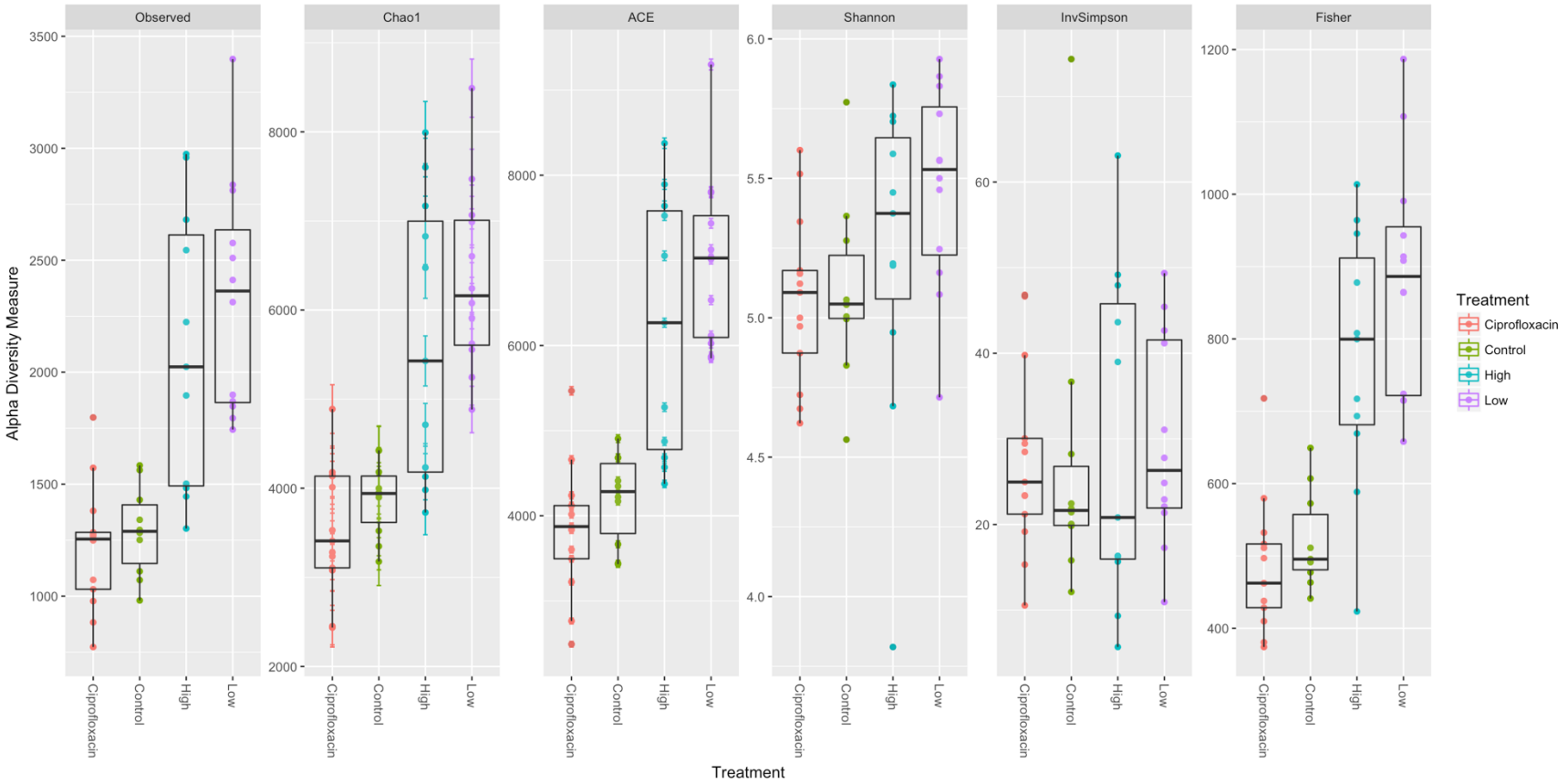

Figure 4-13. Alpha diversity measures for the four treatments in large intestines (defined either by the number of bacterial OTUs observed or by Chao1, ACE, Shannon, Inverse Simpson, and Fisher diversity measures)

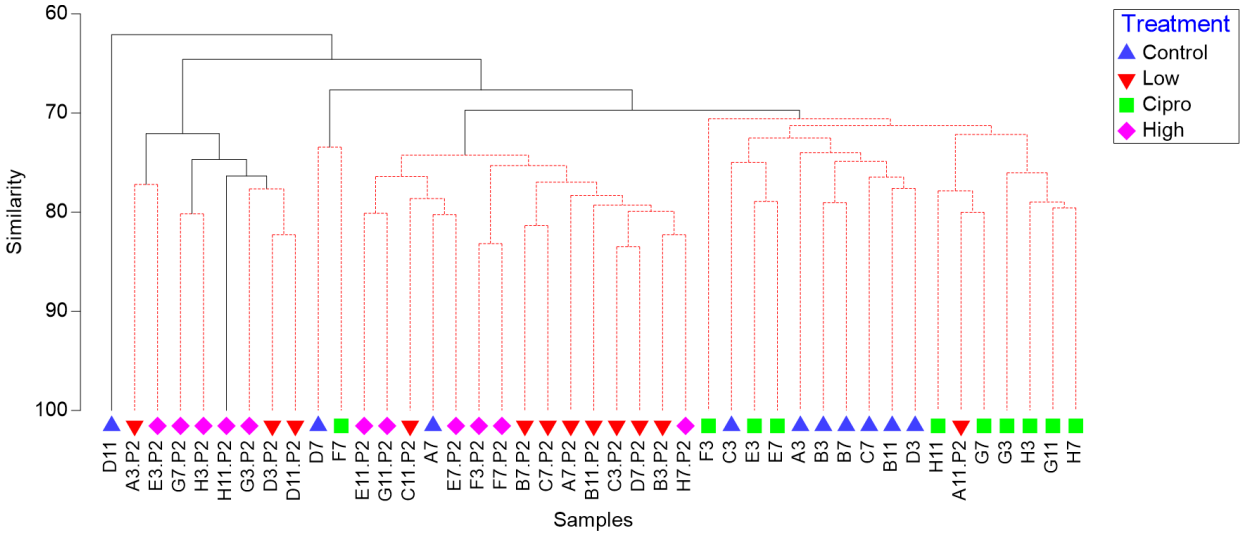

Figure 4-14. Dendogram from complete-linkage clustering of bacterial OTU frequencies in cecum. Red dotted branches represent nodes with significant dissimilarities based on SIMPROF analysis ($p < 0.05$)

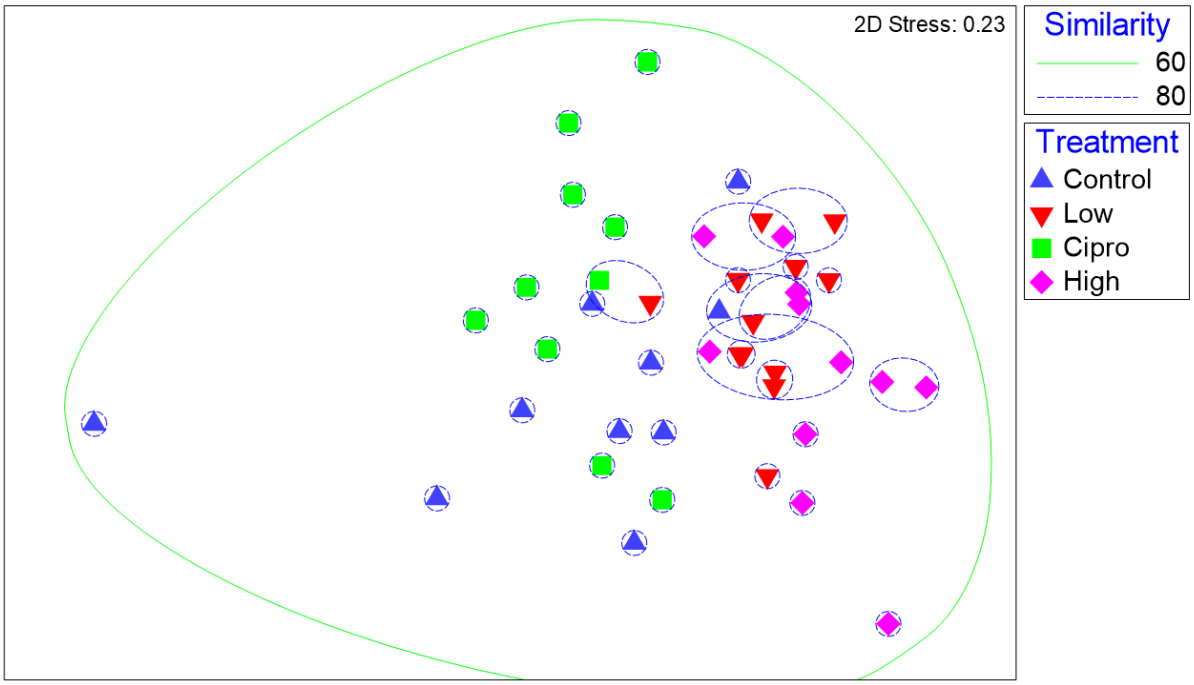

Figure 4-15. Non-metric multi-dimensional scaling plot of bacterial OTU frequencies in cecum after fourth root transformation, which reduces the influence of the most abundant OTUs. Dashed lines represent percent similarity of clusters using SIMPROF: green lines 60%, dashed blue lines 80. Blue triangles represent samples from Low dose treatment; Red upside down triangles represent the Control; Green squares represent the Ciprofloxacin treatment; pink diamonds represent the High dose treatment. Stress value is 0.16.

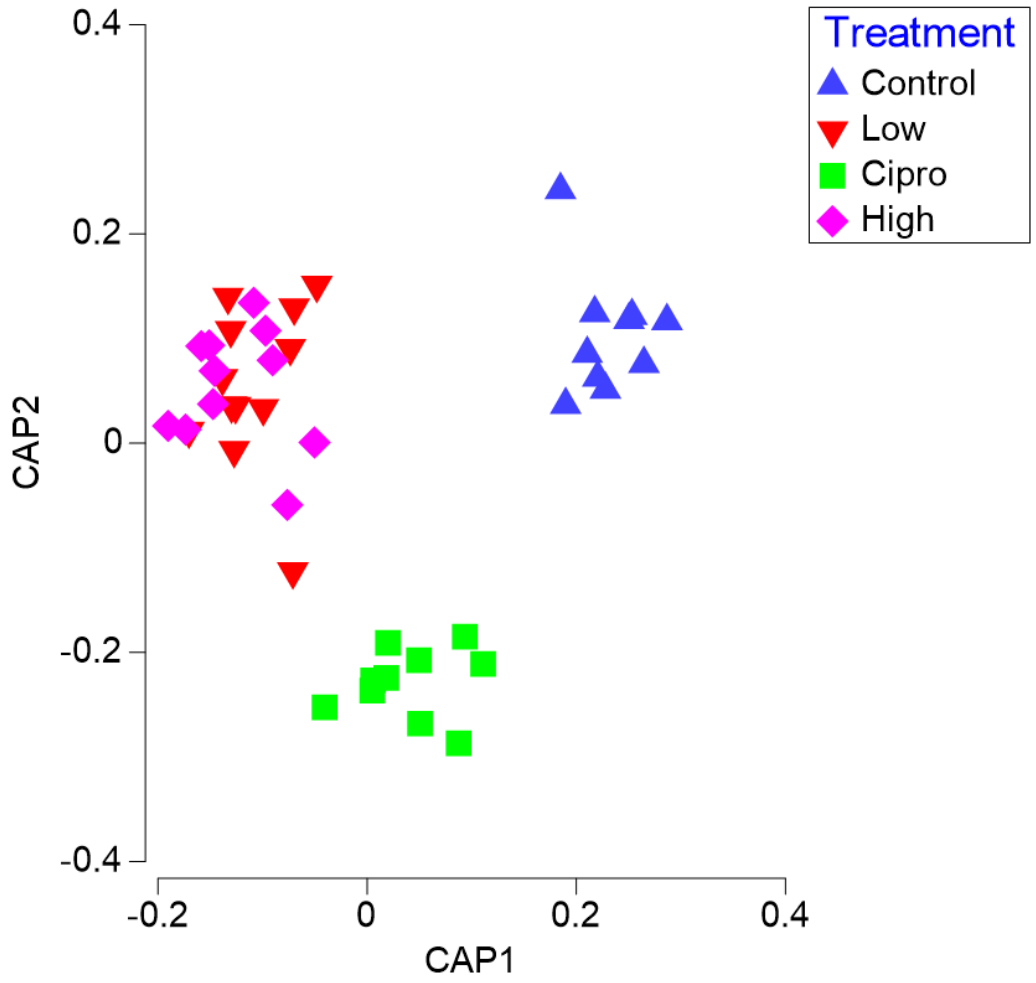

Figure 4-16. Canonical analysis of principal coordinates based on a Bray–Curtis dissimilarity matrix of fourth root transformed bacterial OTU frequencies in cecum. Blue triangles represent the Low dose; Red upside down triangles represent the Control; Green squares represent the Ciprofloxacin treatment; pink diamonds represent the High dose treatment

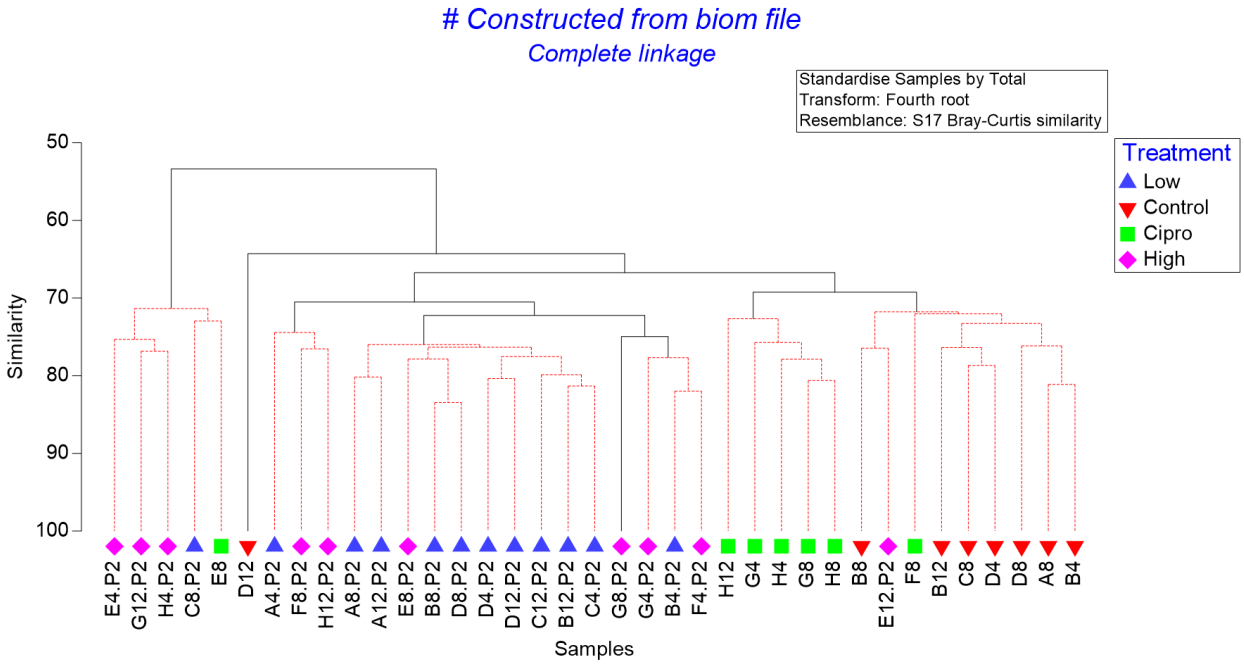

Figure 4-17. Dendogram from complete-linkage clustering of bacterial OTU frequencies in large intestines. Red dotted branches represent nodes with significant dissimilarities based on SIMPROF analysis ($p < 0.05$).

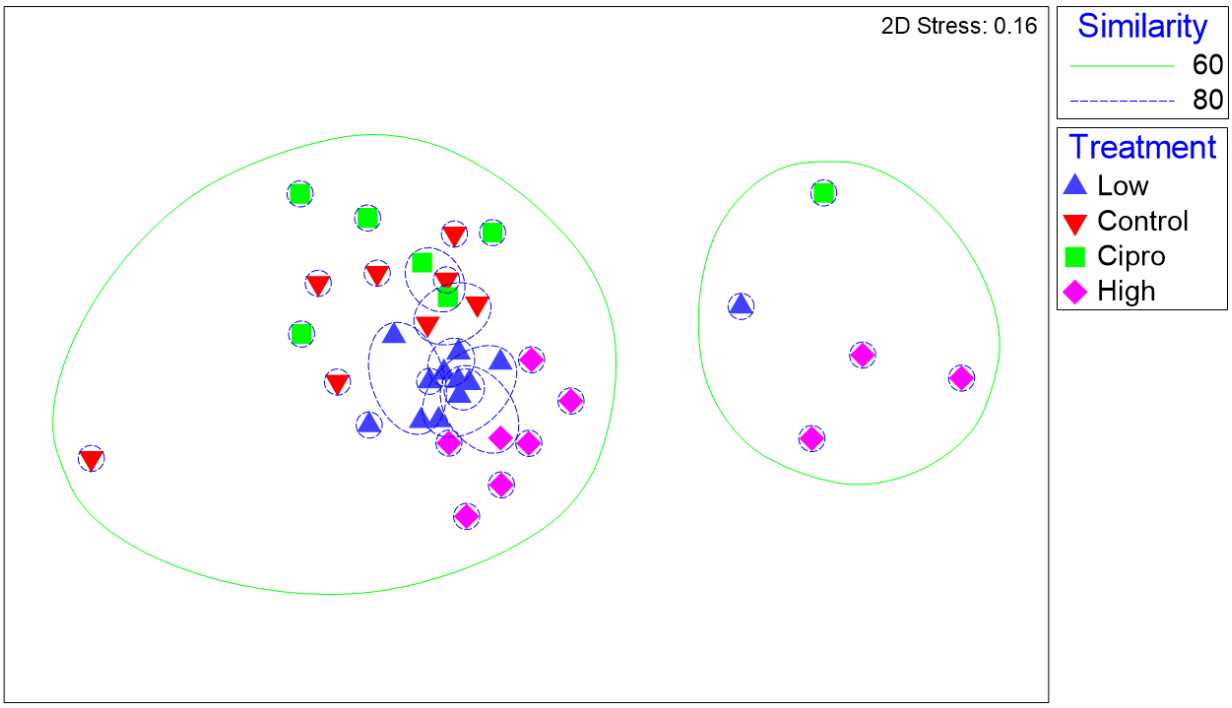

Figure 4-18. Non-metric multi-dimensional scaling plot of bacterial OTU frequencies of large intestines after fourth root transformation, which reduces the influence of the most abundant OTUs. Dashed lines represent percent similarity of clusters using SIMPROF: green lines 60%, dashed blue lines 80. Blue triangles represent samples from Low dose treatment; Red upside down triangles represent the Control; Green squares represent the Ciprofloxacin treatment; pink diamonds represent the High dose treatment. Stress value is 0.16.

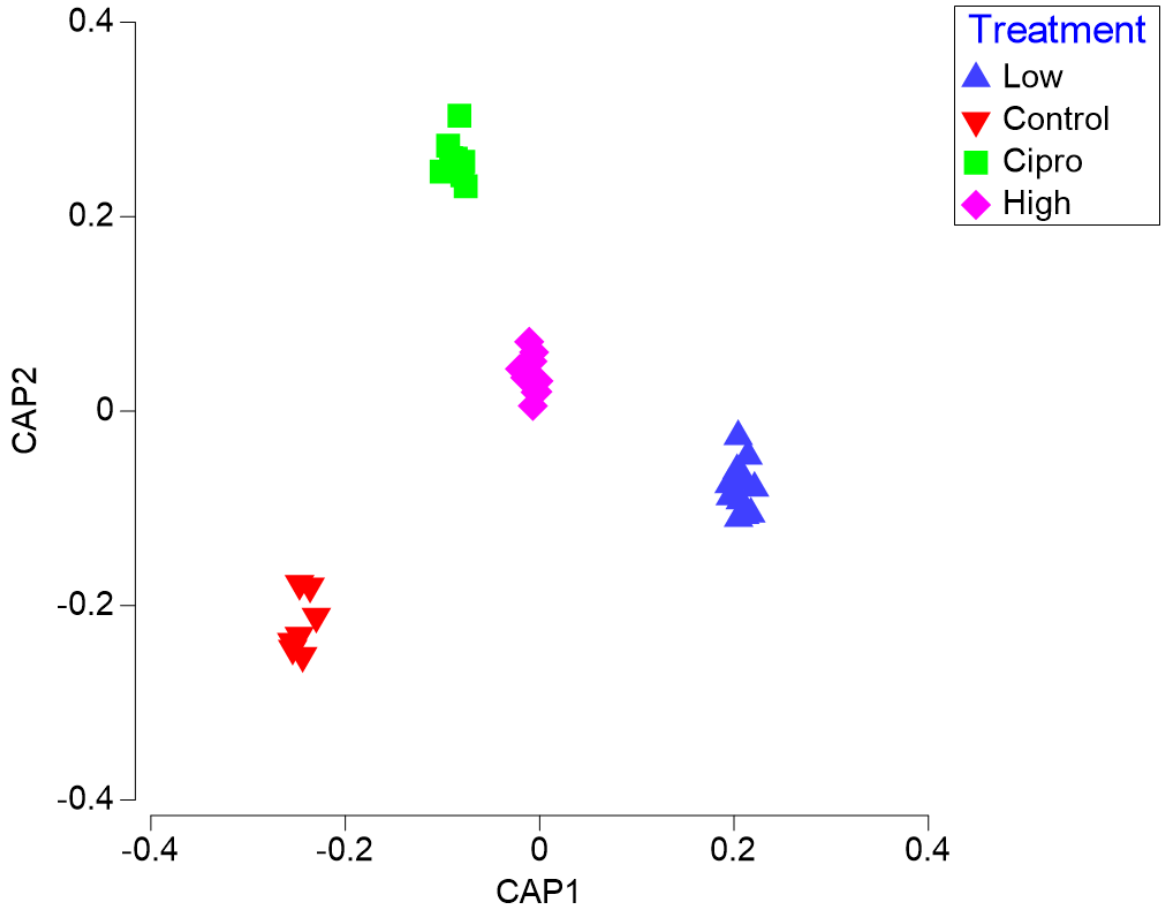

Figure 4-19. Canonical analysis of principal coordinates based on a Bray–Curtis dissimilarity matrix of fourth root transformed bacterial OTU frequencies in large intestines. Blue triangles represent the Low dose; Red upside down triangles represent the Control; Green squares represent the Ciprofloxacin treatment; pink diamonds represent the High dose treatment.

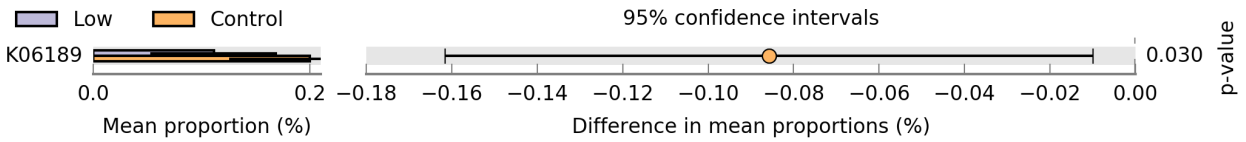

Figure 4-20. Pair-wise comparisons between Low Dose (purple) and Control (orange) with 95% confidence intervals of large intestines.

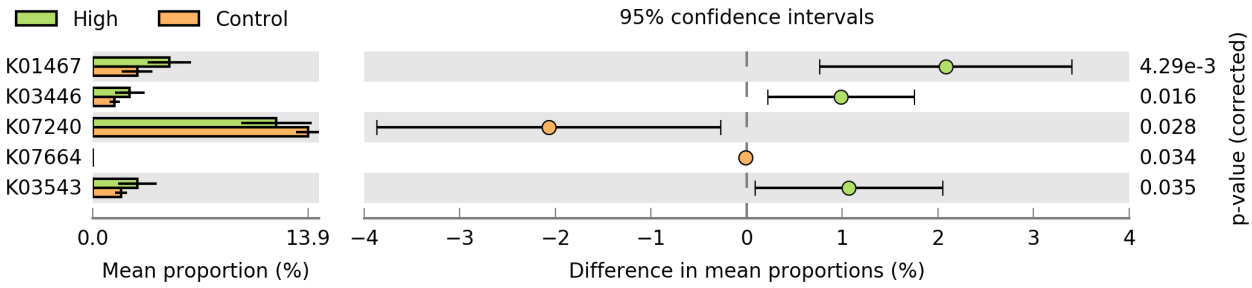

Figure 4-21. Pair-wise comparisons between High Dose (purple) and Control (orange) with 95% confidence intervals of large intestines.

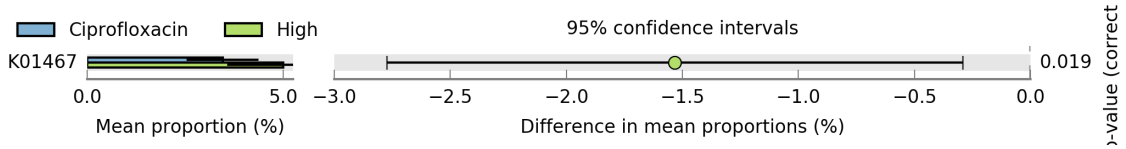

Figure 4-22. Pair-wise comparisons between Ciprofloxacin (blue) and High (green) with 95% confidence intervals of large intestines.

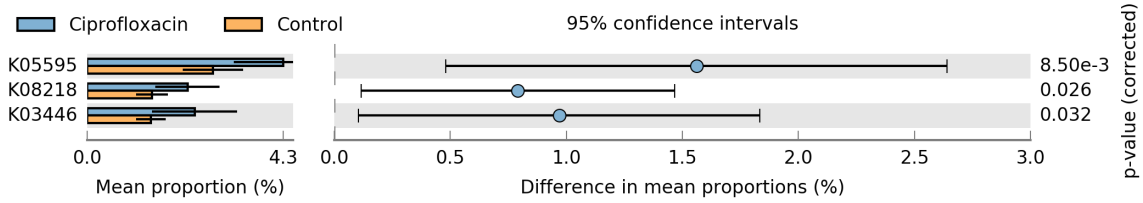

Figure 4-23. Pair-wise comparisons between Ciprofloxacin (blue) and Control (orange) with 95% confidence intervals of large intestines.

CHAPTER 5

Conclusions

Over hundreds of million years, microorganisms have evolved a myriad of strategies to overcome various environmental (e.g. heavy metals, radiation) and biological insults (i.e. antibiotics). Recent evidence has confirmed that antibiotic resistance, in particular, is consistent with an ancient origin, and that bacteria have been engaged in an evolutionary "arms race" since the first bacteria evolved on Earth. Moreover, the environment itself has been a reservoir of antibiotic resistance genes long before the clinical use of antimicrobial drugs. The mobilization of these genes in the all-encompassing environmental resistome, and the conditions that facilitate their acquisition by pathogens is a one of the most pressing global health concerns of the modern era.

Furthermore, human activities have increasingly altered and contaminated the biosphere, and in doing so provided bacteria new opportunities for antimicrobial resistance selection and mobilization. For instance, as mentioned previously, antibiotic usage is not the only mechanism of selection that promotes developing antimicrobial resistance—heavy metals and even radiation can indirectly co-select antimicrobial resistant bacteria. Taken together, the result is as Gaze et al. (2013) surmised, "a perfect storm of opportunity for bacterial human pathogens to exploit millions of years of evolution, uncounted microbial generations, and modern human activity."

In this dissertation, I reviewed essential research in the field of microbial ecology/microbiome research pertaining to the influence of the heavy metals on biological organisms, the role of heavy metals in shaping antimicrobial resistance within bacteria, and the genetic mechanisms that enables resistance (Chapter 1). I investigated how heavy metals affect microbial community structure, diversity, and co-abundance in the environment and the animals that inhabit them (Chapter 2 and Chapter 3). I also examined the potential for heavy metals to indirectly co-select antibiotic resistance, and potential links between heavy metal contamination and the enrichment of the soil and gut resistome.

Specifically, I examined microbiota associated with the soil environments collected from heavy metal contaminated areas at the Savannah River Site (SRS) (Chapter 2). I then examined the gut microbiota of wild *Peromyscus* chronically exposed to hotspots of heavy metal contamination. In both studies, I utilized a combination of 16S rRNA gene sequencing, predictive functional profiling, and network based analysis that provided novel insights into the influence of heavy metal contamination on soil habitats and the wild *Peromyscus* microbiome. Very few studies have examined the soil microbiota at SRS, and those that did were conducted before the advent of next generation sequencing (NGS) technique. Therefore, many of the previous surveys of soil microbiota lacked sufficient coverage to properly assess microbial structure and diversity. In the soils, I explored microbial community structure and diversity of soil archaea, bacteria, and fungi; examined patterns of microbial co-abundance and co-exclusion; and also examined the co-occurrence of heavy metal and antibiotic resistance (Chapter 2). I demonstrated that heavy metals can differentially affect bacterial and fungal diversity,

and that predicted resistance determinants are common in uncontaminated soils; but enriched in areas with contamination.

In Chapter 3, I conducted novel research which provided new insights into the wild *Peromyscus gossypinus* microbiome. To my knowledge, this mammalian species has never had its gut microbiota examined. Further, until recently there have been very few studies that has examined the resistome of wild *Peromyscus* in contaminated environments using next-generation sequencing. I identified a core microbiome dominated by *Lactobacillus* and *Desulfovibrio*, and demonstrated that not only do mice from contaminated areas harbor significantly reduced species richness but also enriched patterns of antimicrobial resistance.

Finally, in Chapter 4 I subjected captive-bred *Peromyscus leucopus* to a 4-week heavy metal and antibiotic exposure challenge. I found that heavy metals can cause minor but significant alterations in gut microbiota. Differential abundance testing also illustrated that certain microbiota such as *Flexispira*, F16 (TM7), and certain OTUs of *Lactobacillus* are not only tolerant to heavy metal exposure in the gut; but they also display heightened antimicrobial resistance.

In conclusion, the primary aims of this dissertation were to provide exploratory evidence that heavy metals can 1) influence the structure and diversity of microbial communities, and 2) that they can indirectly co-select antimicrobial resistance. The use of Illumina-based sequencing provided a highly reproducible, reasonably accurate, and cost-effective way to profile microbial communities in a range of environments. Predictive functional profiling allowed me to infer antimicrobial resistance, which can be later confirmed with shotgun sequence or sequence capture metagenomics. Network analysis,

also allowed me to see how microbial communities organize spatio-temporally and how antimicrobial resistance co-occurs across communities. Together, all of these techniques allowed me to provide important groundwork for examining important ecological questions and confronting the public health challenges of the 21st century.